



National Library
of Canada

Bibliothèque nationale
du Canada

Canadian Theses Service Service des thèses canadiennes

Ottawa, Canada
K1A 0N4

NOTICE

The quality of this microform is heavily dependent upon the quality of the original thesis submitted for microfilming. Every effort has been made to ensure the highest quality of reproduction possible.

If pages are missing, contact the university which granted the degree.

Some pages may have indistinct print especially if the original pages were typed with a poor typewriter ribbon or if the university sent us an inferior photocopy.

Reproduction in full or in part of this microform is governed by the Canadian Copyright Act, R.S.C. 1970, c. C-30, and subsequent amendments.

AVIS

La qualité de cette microforme dépend grandement de la qualité de la thèse soumise au microfilmage. Nous avons tout fait pour assurer une qualité supérieure de reproduction.

S'il manque des pages, veuillez communiquer avec l'université qui a conféré le grade.

La qualité d'impression de certaines pages peut laisser à désirer, surtout si les pages originales ont été dactylographiées à l'aide d'un ruban usé ou si l'université nous a fait parvenir une photocopie de qualité inférieure.

La reproduction, même partielle, de cette microforme est soumise à la Loi canadienne sur le droit d'auteur, SRC 1970, c. C-30, et ses amendements subséquents.

Permission has been granted to the National Library of Canada to microfilm this thesis and to lend or sell copies of the film.

The author (copyright owner) has reserved other publication rights, and neither the thesis nor extensive extracts from it may be printed or otherwise reproduced without his/her written permission.

L'autorisation a été accordée à la Bibliothèque nationale du Canada de microfilmer cette thèse et de prêter ou de vendre des exemplaires du film.

L'auteur (titulaire du droit d'auteur) se réserve les autres droits de publication; ni la thèse ni de longs extraits de celle-ci ne doivent être imprimés ou autrement reproduits sans son autorisation écrite.

ISBN 0-315-53827-9

Finite-Element Simulation of Ram Pipe Bending

by

Vinhson Ba Nguyen

Thesis submitted to the School of Graduate Studies
as partial fulfillment of the requirements
for the degree of M.A.Sc. in
Mechanical Engineering

UNIVERSITY OF OTTAWA

© Vinhson B. Nguyen, Ottawa, Canada, 1988.

ABSTRACT

The present study is concerned with the simulation of the ram-pipe bending process using the finite element method (FEM). Investigated are springback, ovalization, and growth of plastic zones in the pipe bend. Residual stresses are also calculated for certain parts of the pipe. Simulation is restricted to bends of small angles.

A nonlinear FEM program is developed, utilizing the Updated Lagrangian Jaumann Stress-Rate Formulation. The solution is carried out with the modified Newton-Raphson method and the Profile Solver technique. The formulation of the elbow element developed earlier in [3] - [5] is extended to model a forming problem (ram pipe bending). To check the accuracy of the program, a number of piping problems are solved, covering both elastic and nonelastic phenomena. Present FEM calculations have been found to be in good agreement with available experimental data and other numerical results.

The above FEM program is then used to obtain the results for the ram-pipe problem. The FEM results are compared with those calculated using an elastic-plastic beam theory. Satisfactory agreements have been obtained between the two sets of results. To further investigate the maximum ovalization of the cross section due to local deformation, ADINA shell-element predictions are also given. A number of charts of practical interest are presented for typical sizes of pipe bends formed by ram benders.

ACKNOWLEDGEMENT

The author wishes to express his gratitude to Dr. D. Redekop for his continuous encouragement, invaluable suggestions, and patient guidance throughout the research.

Special thanks to the author's parents for their moral support and encouragement during the study.

The financial support received from the University of Ottawa, and the Natural Sciences and Engineering Research Council of Canada is gratefully acknowledged.

Contents

Abstract	ii
Acknowledgement	iii
Table of Contents	iv
List of Figures	v
List of Tables	vi
Nomenclature	vii
1 Introduction	1
1.1 Finite-Element Modelling in Metal Forming	1
1.2 Overview Of Sheet Metal Forming	2
1.3 Techniques of Pipe Bending	4
1.4 Outline of Present Investigation	6
2 Literature Survey	8
2.1 Background of FEM in Metal Forming	8
2.2 Previous FEM Work on Sheet Metal Forming	10
2.3 Previous Analytical Work on Pipe Bending Processes	14
2.4 Previous Work on Elbow Element	16
3 Finite Element Modelling	19
3.1 General	19

3.2	Finite Element Method	20
3.3	Review of Elbow Element Formulation	23
3.3.1	Beam Behaviour	24
3.3.2	von Karman's Description of Ovalization	30
3.4	Extension of Elbow Element's Capability	33
4	Comparison of FENSA (Finite Element Nonlinear Static Analysis)	
	Results with Available Data	36
4.1	Introduction	36
4.2	Elastic Bending of a Straight Pipe	36
4.3	Elastic In-Plane Bending of a Flanged 90 ⁰ -Pipe Bend	38
4.4	Elastic-Plastic Bending of a Straight Pipe	43
4.5	Elastic-Plastic Bending of a 180 ⁰ U-Bend	48
4.6	Elastic-Plastic Bending of a 90 ⁰ -Elbow with Tangent Pipes	52
4.7	Summary of Comparison	60
5	Ram Pipe Bending	63
5.1	Introduction	63
5.2	Simulation Using Elastic-Plastic Beam Theory (EPBT)	63
5.3	Simulation Using Program FENSA	73
5.4	Comparison of EPBT and FENSA Results	74
5.5	Computed Results for Practical Cases	77
5.6	Remarks	79
6	Conclusions	89
	Bibliography	92
A	Transformation	100
B	Summaries	103

B.1	Updated Lagrangian Formulation with Jaumann Stress Rate	103
B.2	Modified Newton-Raphson Method	106
C	Computer Software	109
C.1	Computer Program for EPBT	109
C.2	Flowchart of Program FENSA	114
C.3	Listing of Program FENSA	116
D	ADINA Shell-Element Results	157

List of Figures

1.1	Some typical processes of Sheet Metal Forming	2
1.2	Cold pipe bending processes	5
3.1	Schematic view of ram bending	20
3.2	Simply supported beam	20
3.3	Discretization of a 3-D continuous body	21
3.4	Geometry of the pipe elbow element	24
3.5	Updating of the curvature of an elbow element	35
4.1	Cantilever beam under a concentrated load	37
4.2	Geometry and modelling of a flanged 90° elbow	39
4.3	Predicted circumferential stresses at $\theta = 45^\circ$ and at outside surface for $R = 0.250\text{ m}$	40
4.4	Predicted longitudinal stresses at $\theta = 45^\circ$ and at outside surface for $R = 0.250\text{ m}$	40
4.5	Predicted circumferential stresses at $\theta = 45^\circ$ and at outside surface for $R = 0.375\text{ m}$	40
4.6	Predicted longitudinal stresses at $\theta = 45^\circ$ and at outside surface for $R = 0.375\text{ m}$	40
4.7	Predicted flexibility factors of flanged elbows	42
4.8	Predicted diameter change factors of flanged elbows	42
4.9	Thin-walled straight pipe under pure bending	44

4.10	Bilinear representation of uniaxial tensile stress-strain curve	45
4.11	Predicted moment-curvature results for straight pipes under pure bending	45
4.12	Comparison of FENSA and theoretical results for the longitudinal stresses in the middle surface of the pipe wall at various loadings	46
4.13	Predicted circumferential stresses in the middle surface of pipe wall at various loadings	47
4.14	Geometry and finite element modelling of a 180° U-bend under opening moment	50
4.15	Multilinear approximation of uniaxial tensile stress-strain curve	50
4.16	Predicted moment-deflection results for 180° U-bend under opening mo- ment	51
4.17	Comparison of FENSA and experimental results for outer axial strains at symmetry plane and at $\Delta D = 76$ mm	51
4.18	Comparison of FENSA and experimental results for hoop strains at symmetry plane and at $\Delta D = 76$ mm	51
4.19	Geometry and FEM modelling of a 90° -elbow structure	53
4.20	Multilinear approximation of uniaxial tensile stress-strain curve	54
4.21	Comparison of FENSA and experimental moment-end displacement re- sults	54
4.22	Comparison of FENSA and experimental moment-end rotation results .	54
4.23	Comparison of FENSA and experimental moment-hoop strain results (inner surface)	54
4.24	Predicted changes in cross-sectional mean radius around the elbow cir- cumference and along the elbow length at $M/M_y = 1.00$	56
4.25	Predicted changes in cross-sectional mean radius around the elbow cir- cumference and along the elbow length at $M/M_y = 1.69$	56
4.26	Predicted changes in cross-sectional mean radius around the elbow cir- cumference and along the elbow length at $M/M_y = 2.16$	57

4.27	Predicted changes in cross-sectional mean radius around the elbow circumference and along the elbow length at $M/M_y = 2.40$	57
4.28	Growth of plastic zones on the outside surface	58
4.29	Growth of plastic zones on the inside surface	58
4.30	Growth of plastic zones through the wall thickness	59
5.1	Elastic-plastic flexure of beam of annular cross section	65
5.2	Simply supported beam under a symmetrical two-point loading	70
5.3	Bending moment diagram of the beam for $W = W_y$	71
5.4	Models of ram pipe bending	74
5.5	Moment-curvature results calculated by a beam-theory method	80
5.6	Comparison of theoretical and numerical load-deflection results for ram pipe bending	80
5.7	Variation of maximum changes in cross-sectional mean radius along pipe length predicted by FENSA	81
5.8	Predicted growth of plastic zones towards the centre of pipe due to increasing loading	81
5.9	Predicted residual circumferential and longitudinal stresses at the plane of symmetry and on the outside surface	82
5.10	Predicted residual circumferential and longitudinal stresses at the plane of symmetry and on the inside surface	82
5.11	Predicted final rotation per unit length of bent pipe for $L/r_m = 10$ and $c/r_m = 2$	83
5.12	Predicted final rotation per unit length of bent pipe for $L/r_m = 12$ and $c/r_m = 2$	83
5.13	Predicted final rotation per unit length of bent pipe for $L/r_m = 14$ and $c/r_m = 2$	84
5.14	Predicted final rotation per unit length of bent pipe for $L/r_m = 16$ and $c/r_m = 2$	84

5.15	Predicted final rotation per unit length of bent pipe for $L/r_m = 18$ and $c/r_m = 2$	85
5.16	Predicted final rotation per unit length of bent pipe for $L/r_m = 20$ and $c/r_m = 2$	85
5.17	Predicted final rotation per unit length of bent pipe for $L/r_m = 10$ and $c/h = 20$	86
5.18	Predicted final rotation per unit length of bent pipe for $L/r_m = 12$ and $c/h = 20$	86
5.19	Predicted final rotation per unit length of bent pipe for $L/r_m = 14$ and $c/h = 20$	87
5.20	Predicted final rotation per unit length of bent pipe for $L/r_m = 16$ and $c/h = 20$	87
5.21	Predicted final rotation per unit length of bent pipe for $L/r_m = 18$ and $c/h = 20$	88
5.22	Predicted final rotation per unit length of bent pipe for $L/r_m = 20$ and $c/h = 20$	88
B.1	Full Newton-Raphson method	107
B.2	Modified Newton-Raphson method	108

List of Tables

3.1	Number of ovalization shape functions to be used	31
4.1	Comparison of FENSA and beam-theory results for end deflection and rotation	37
4.2	Convergence rate of solution	42
4.3	Comparison of collapse loads for a 90° elbow	59

Nomenclature

A_1	half the total area of the plastic zones
A_2	half the total area of the elastic zones
b	distance from one end of a beam to the nearest elastic-plastic boundary
c	width of a ram (in ram benders)
c_i^k	i th ovalization displacement at nodal point k
d	$2r_2$
D	$2R$
e	E/E_T
E	Young's modulus
E_T	strain-hardening modulus
f_γ	flexibility factor
f_d	diameter change factor
h	wall thickness of a pipe
h_k	interpolation function at nodal point k
H^*	strain-hardening constant
I	moment of inertia of a cross section
k	non-dimensional curvature, defined as $\frac{\kappa}{\kappa_y}$
L	length of a straight beam or pipe
m	non-dimensional applied moment, defined as $\frac{M}{M_y}$
M	applied bending moment
r	isoparametric coordinate (along the element length)

r	r_1/r_2
r_m	mean radius of cross section
r_1, r_2	inside radius and outside radius of cross section, respectively
r_1^k	outside radius of cross section at nodal point k
R	radius of curvature
s	isoparametric coordinate (toward the center of curvature)
S_{ij}	components of the deviatoric stress tensor
t	isoparametric coordinate (orthogonal to the r - and s - directions)
u_i	displacement at nodal point k in the x_i direction
v	end vertical displacement
w_ξ, w_ζ	circumferential and radial displacements of the middle surface of pipe wall, respectively
W	applied concentrated load
W_y	applied concentrated load at first yielding
x	coordinate measured from one end of a pipe (or beam)
x_i	Cartesian coordinates, $i = 1, 2, 3$
y	vertical Cartesian coordinate
z	distance from the neutral axis to the elastic-plastic boundary
η	pipe-wall local coordinate (along the center line)
δ	deflection
γ	end rotation
$\gamma_{\xi\eta}$	shear strain in the $\xi\eta$ -plane
$\gamma_{\eta\zeta}$	shear strain in the $\eta\zeta$ -plane
$\gamma_{\zeta\xi}$	shear strain in the $\zeta\xi$ -plane
$\epsilon_{\xi\xi}$	hoop (circumferential) strain
$\epsilon_{\eta\eta}$	longitudinal strain

$\epsilon_{\zeta\zeta}$	radial strain
ϵ_{ij}	components of the strain tensor
κ	curvature
κ_y	curvature at first yielding
λ	pipe geometric parameter
ν	Poisson's ratio
θ	positional angle (along a pipe bend)
θ_i^k	rotation at nodal point k about the x_i -axis
ρ	polar coordinate in the radial direction
σ_y	uniaxial yield stress (proportional limit)
${}^t\sigma_y$	uniaxial yield stress at time t
$\sigma_{\xi\xi}$	hoop (circumferential) stress
$\sigma_{\eta\eta}$	longitudinal stress
σ_{ij}	component of a stress tensor
${}^t\tau_{ij}$	components of the Cauchy stress tensor, referred to time t
ϕ	positional angle (around the cross-section periphery) measured from the intrados
ξ	pipe-wall local coordinate (in the hoop direction)
ζ	pipe-wall local coordinate (in the radial direction)
tB_L	linear strain-displacement transformation matrix at time t
${}^tB_{NL}$	nonlinear strain-displacement transformation matrix at time t
\hat{B}_{OV}	strain-displacement transformation matrix for ovalization
C^E	linear stress-strain matrix
${}^tC^{EP}$	instantaneous elastic-plastic stress-strain matrix
${}_{t+\Delta t}^{t+\Delta t}F^{(i-1)}$	vector of nodal point forces equivalent to element stresses at time $t + \Delta t$ and in iteration $(i - 1)$
J	Jacobian transformation matrix

${}^t\mathbf{K}_L$	linear strain incremental stiffness matrix
${}^t\mathbf{K}_{NL}$	nonlinear strain incremental stiffness matrix
P, Q	transformation matrices for second-order tensors
${}^t\mathbf{q}$	vector containing deviatoric stress components at time t
${}^{t+\Delta t}\mathbf{R}$	vector of externally applied nodal point loads at time $t + \Delta t$
$\Delta\mathbf{U}^{(i)}$	vector of increments in nodal point displacements in iteration i
$\mathbf{V}_s^k, \mathbf{V}_t^k$	unit vectors at nodal point k in the s - and t -directions, respectively

Chapter 1

Introduction

1.1 Finite-Element Modelling in Metal Forming

Metal forming is an essential part of modern industry. It is required in the manufacture of a variety of goods, ranging from customer products to automobiles, aircrafts, ships, etc.. A substantial part of metal forming is still an art, depending on the skills and knowledge of individual artisans and tradesmen. Therefore, it is generally believed that to achieve significant improvements in efficiency, the field will have to be brought onto a scientific basis.

With the development of fast and powerful digital computers in recent years, the Finite Element Method (FEM) has made valuable contributions to metal forming analyses. The method has the capability to overcome complexities arising from geometric and material nonlinearities, as well as friction at the material-tool interface. A number of sheet metal processes have already been simulated by the FEM, thus avoiding much of experimental work. It is possible that the nonlinear FEM will replace most of sheet metal experimentation in the future in the same way that the linear FEM has substituted experimentation in design.

1.2 Overview Of Sheet Metal Forming

Sheet metal forming is one of the two broad categories [1] of metal forming. This category is characterized by significant changes in the shape of the workpiece but not in the cross section. Although sheet metal forming is important in many branches of industry, it has received relatively little attention compared with the other category, bulk forming [2]. Four sheet metal forming processes that have been given extensive FEM research are: deep drawing, stretch forming, hydraulic bulging, and brake bending (Figure 1.1).

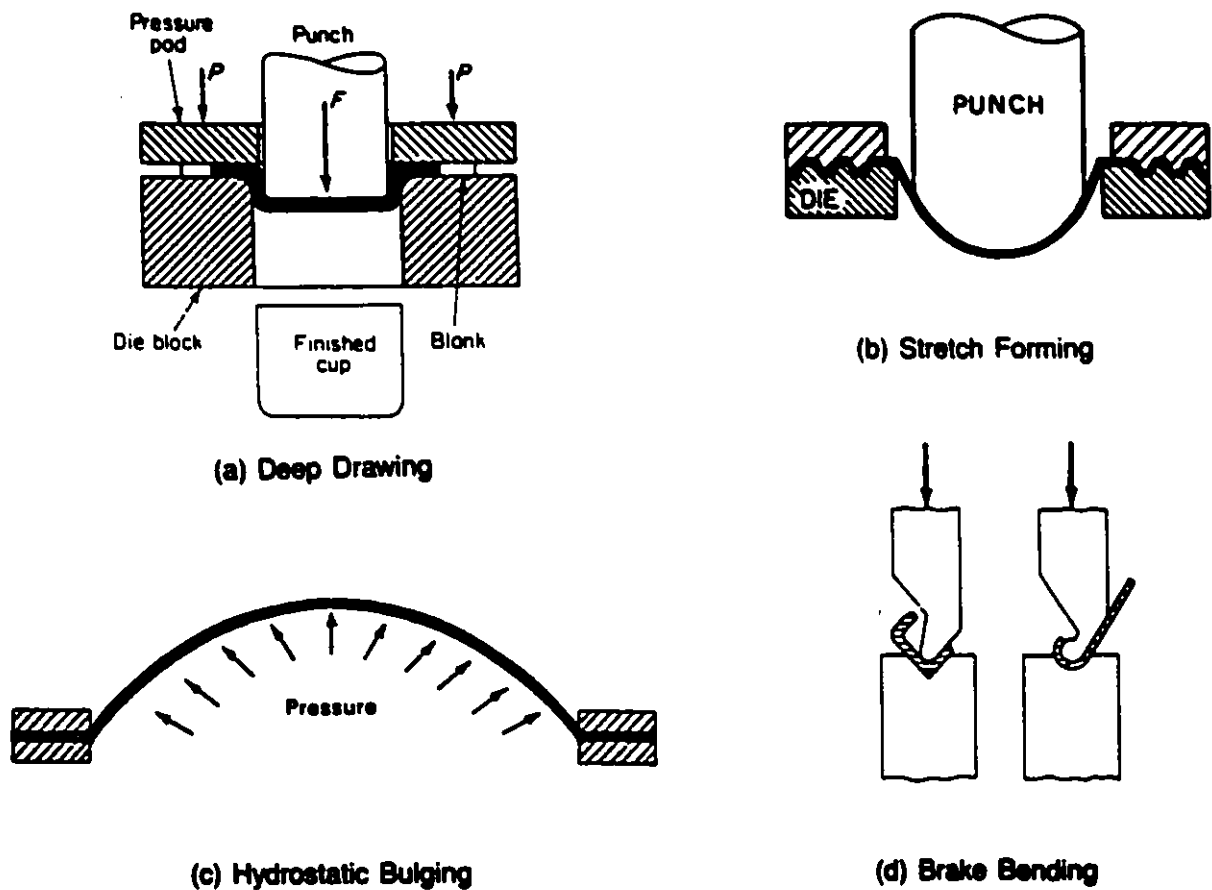


Figure 1.1: Some typical processes of Sheet Metal Forming.

Deep drawing is one of the most common metal working processes. Typical parts produced from this process are beverage cans, containers of all shapes and sizes, sinks, and automobile panels. This process involves a flat sheet of metal being drawn into a cylindrical or box shape by means of a punch pushing the sheet into a die cavity.

Stretch forming is another major process for producing aerospace and automotive parts, e.g. rocket or aircraft-wing skin panels, car-door panels, roofs, or the like. In stretch forming, a sheet of metal is clamped at its edges and a male tool with or without a female backup is pushed into the blank to produce the desired shape. The sheet is stretched just to the elastic limit, and then the stress is slightly raised into the plastic range for permanent set.

Hydraulic bulging is a less common process used for the production of shallow-recessed sheet metal parts as well as for the expansion of tubular parts. Recently, it has been used for testing the ductility of sheet metal. In this test, a blank of metal (of circular shape mostly) is clamped at its periphery and then bulged by hydraulic pressure. Because no friction is involved, the bulging problem is relatively easy to analyze. It is, however, still unclear at present how the results of such a test can be applied to commercial shallow-recessed parts formed by other methods such as punch-and-die forming.

Brake bending is a forming process widely used for the production of linear sections such as angles, channels, or hats from flat sheets and straight plates. There are two types of brake bending; in air bending, the workpiece is supported only at the outer edges; and in press bending, the workpiece is forced into a female die cavity. Air bending is preferred over press bending and usually used for metals with springback problems. Although brake bending is a rather simple process, it also presents technical problems, such as the limitations of bendability, the deviation in the bend angle due to springback, shape accuracies, and so on.

1.3 Techniques of Pipe Bending

Pipe and tube bending is also one of sheet metal forming processes, which has been ignored in some previous classifications. The process is important for many industrial applications such as tubes, pipelines, boilers, heat exchangers, etc.. In recent years, bending technology has become increasingly complex and diversified; equipment for pipe bending now ranges from a simple manual machine for non-critical work to a fully computerized bender for mass production and various design specifications. Relatively little information is as yet available concerning practical and theoretical aspects of the process. Six main types of bending being used today are: ram bending, rotary draw bending, compression bending, coiling, induction bending, and internal roll bending (Figure 1.2).

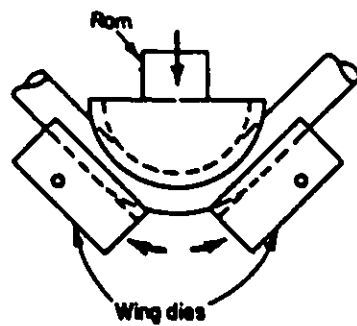
Ram bending is one of the oldest and simplest methods of pipe bending. In this process, a hydraulic ram pushes against the centre of a pipe supported at each of its ends by a pair of wing dies. These dies play the role of a pivot in constraining and guiding the bend. For ordinary work, ram bending is ideal because it is fast and simple. However, there are limitations to using this method in terms of ovality of the cross section and minimum bend radii achievable.

Rotary draw bending is widely used because of its versatility and accuracy, particularly for tight radii and thin-walled tubes. The operation is carried out with the pipe clamped tightly against a form block at the front end of the bend while a pressure bar at the other end guides and constrains the pipe. The form block and clamp rotate together, pulling the pipe around the form block. A mandrel is usually inserted into the pipe to reduce cross-sectional flattening and prevent collapse during the bending action.

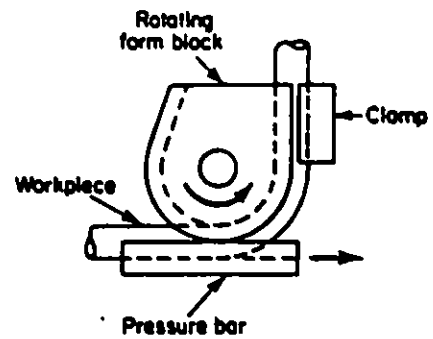
Compression bending, on the other hand, has a working principle basically opposite to that of draw bending. The form block and clamp are stationary, rigidly holding the trailing end of the pipe while the pressure bar moves around the periphery of the

form block. One main advantage of this technique is that it can make a series of bends in various planes with almost no straight portion between consecutive bends.

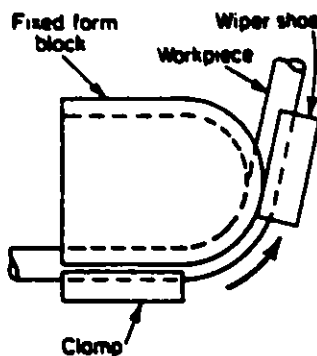
Coiling is a relatively simple process usually carried out with a machine having three rolls. These rolls are often adjustable for various pipe dimensions and wall thicknesses, and their relative positions determine the curvature of the formed coil. Coiling becomes impractical if more than one bend is needed, or if the forming of extremely tight coils with given ovality tolerances is required.



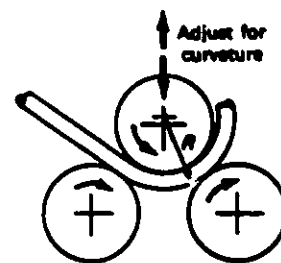
(a) Ram (Press) Bending



(b) Draw Bending



(c) Compression Bending



(d) Coiling

Figure 1.2: Cold pipe bending processes.

In induction bending, the pipe is heated in a narrow annular zone which moves continuously over the length of the bend. Bending only takes place in this zone with the temperature measured and maintained at a pre-determined value by a computer. An advantage of induction bending is that it requires no forming tools and is very flexible with regard to geometric dimensions and desired bend radii. Nevertheless, there are still some limitations on the process; for example, bending of non-ferrous materials or thin-walled pipes cannot as yet be done by this method.

In internal roll bending, pressure is applied to the inside of the pipe by a rolling head rotated within the pipe itself. Benders based on this technique cover an area of pipe bending that is not handled by either cold or induction bending. The main advantage is that almost any desired radius, within a certain minimum-maximum range of the equipment, can be produced by internal roll bending, including thin-walled pipes and non-ferrous materials.

1.4 Outline of Present Investigation

The present study is concerned mainly with ram pipe bending. Attention is given to the simulation of the process using the Finite Element Method (FEM), and the study is carried out with two main objectives:

1. To extend the elbow finite element proposed by Bathe and Almeida [3] - [6]. In this study, modifications of the formulation of the element are made that allow the element to be used to model structures having continuously changing curvature as a result of plastic deformations. A nonlinear FEM program is developed using the Updated Lagrangian Jaumann Stress-Rate Formulation. The solution is carried out using the Profile Solution Solver, and then iterated with the modified Newton-Raphson technique. A number of elastic and elasto-plastic piping problems are solved to check the accuracy of the program.

2. To obtain practical information on ram bending for different values of the pipe parameters. Investigated are changes in ovality of the cross section of pipe bends of different angles formed from straight pipes, growth of plastic zones in the pipe, possible buckling, and springback due to bending action. The FEM results are compared with those obtained from the elastic-plastic beam theory. The ADINA shell-element results are also obtained for the maximum ovalization of the pipe cross section due to local deformation. A number of charts of practical value are presented.

Chapter 2

Literature Survey

2.1 Background of FEM in Metal Forming

The use of the Finite Element Method (FEM) dates back to the early 1960's when the method, then known as the Structural Stiffness Method, was developed by civil engineers for solving linear elastic structural problems.

As the computer technology progressed in the 1960's, the FEM received greater attention and quickly gained popularity in industry. The number of research papers published on the subject increased dramatically [7], and at the same time the method was extended to many other fields of Science and Engineering, such as Nonlinear Dynamics, Fluid Mechanics, Metal Forming, Electro-Magnetism, ect.. A number of books about the technique were written, covering in detail the various capabilities. Typical ones were those by Zienkiewicz [8] and more recently by Bathe [9].

In the field of metal forming, applications of the FEM began when Yamada et al. [11] introduced the closed form of the plasticity method in the incremental stiffness approach, based on the Prandtl-Reuss equations (Elasto-Plastic analysis). Alternative procedures, such as the "initial stress" method by Zienkiewicz et al. [12] and the weighted stress rate-strain rate technique by Marcal et al. [13] for the elastic-plastic transition elements, were also introduced to reduce computational efforts. Although

these works marked advances in the field, it was realized that the formulations developed were restricted to small-strain problems only. Such a restriction is not realistic since most forming processes, by their nature, generate very large plastic deformations.

The foundation of large-strain analyses had been established in the 1950's by Hill [14,15]. It was not until 1970, however, before Hibbitt et al. [16] introduced the first complete finite element large strain code using a Total Lagrangian Formulation (TLF). In this formulation, the reference state is the original undeformed configuration. One year later, Hofmeister et al. [17] proposed an alternate approach, the Updated Lagrangian Formulation (ULF) in which reference is made to the current state under consideration. The ULF method is more appealing to researchers than the TLF method because of its relative simplicity. Using ULF, there is no need for the so-called "initial displacement matrix" and available small-strain programs can be easily extended to handle large-strain situations. Furthermore, configuration-dependent problems and treatment of contact boundary conditions are easier with ULF.

More recently, a number of other formulations dealing successfully with large plastic deformations have also been presented. The Rigid-Plastic formulation was introduced by Kobayashi and his collaborators. It is based on the idealization that elastic deformations can be ignored in comparison with the large plastic strains, thus simplifying the solution procedure. Zienkiewicz et al. [18] made the first attempt to apply the flow formulation derived from Fluid Mechanics to study the large plastic deformation of sheets of metal, particularly axisymmetric deep drawing and stretch forming. Such problems have also been solved by Wang and Wenner [19], and subsequently by Rebelo and Kobayashi [20] using the Elasto-Viscoplastic and Rigid-Viscoplastic formulations, respectively.

All of the above-mentioned formulations have by no means exhausted the list of FEM techniques used in the field of sheet metal forming. Hughes [7] has given a comprehensive survey on current trends of FEM research with a strong emphasis on practical applications. His work has led to a review by Kobayashi [21] on theoretical

aspects of various FEM approaches, including coupled analyses of heat transfer and metal flow. Meanwhile, the condensed review of Wifi [22] has identified difficulties in the large-strain Elasto-Plastic FEM analysis of forming processes. Recently, Gadala and Oravas [23] have provided a survey on the FEM solution techniques for nonlinear continuum mechanics problems. Cheng and Kikuchi [24] have focussed attention on FEM solutions of large-strain Elasto-Plastic deformations, including those involving unilateral contact and friction.

2.2 Previous FEM Work on Sheet Metal Forming

As briefly mentioned in Art. 1.2, most FEM work that has been done in this field is on deep drawing, stretch forming, bulging and brake bending. Not only is FEM analysis relatively economical, but also the method has successfully been used to solve a number of forming problems of such a complex nature that a theoretical or experimental analysis had long been considered inadequate or impossible.

Research on deep drawing can be traced back to the very early experimental works of Woo [25] – [27]. The topic, however, seemed to be abandoned until Wifi [28] provided complete TLF solutions to deep drawing and stretch forming of a circular blank using a hemispherical punch. His study was focussed on the bending action under tension at the die profile, that had been disregarded in previous works, and on boundary conditions, which are usually unknown beforehand. The problems solved in the study turned out to be computationally time consuming.

Later, Wifi and Yamada [29] introduced a general self-correcting technique to reduce errors due to the performance of finite elements, particularly of plate and shell types, and nonlinearities of large deformations. Andersen [30] analyzed the deep drawing problem with both hemispherical and flat-headed punches using ULF, coupled with a direct Euler procedure to minimize computer time. Because the displacements computed in the thickness direction varied linearly, a shell-theory method was employed for

the analysis, as had been done earlier by Wang and Budianski [31]. Honnor and Wood [32], on the other hand, solved the same problem with a linear Mindlin axisymmetric shell element using the Eulerian formulation which, though less well-known than TLF and ULF, proved to be the most efficient for this highly nonlinear problem.

The first use of the Rigid-Plastic model was by Kobayashi and Kim [33]. They developed a membrane shell theory model from the variational formulation and then verified it by analyzing problems of deep drawing, stretch forming, and hydrostatic bulging. The model was found to handle sheet metal forming problems with efficiency and gave reasonable accuracy although its validity still required further investigation. Following the work of [33], Gotoh and Ishisé [34] – [35] used the Rigid-Plastic approach to predict the deformed shape of the flange region in a deep drawing process with a fourth-degree yield function. The prediction obtained was in good agreement with experimental data, and it was found that numerical analysis, based on the quadratic yield function only, gives inaccurate results, particularly for the earing development.

From another viewpoint, Zienkiewicz et al. [36] reasoned that when plastic deformations are so large that the elastic strains are negligible, the problem becomes that of an incompressible viscous non-Newtonian flow with prescribed boundary friction, strain hardening as well as elastic springback and thermal effects. In addition, when the process involves thin sheets of metal, simplifications on this approach can be made [37] and the deformation of sheets of arbitrary shapes can be analyzed with the general viscous shell element [38]. Using these concepts and taking membrane and bending effects into account, Baynham and Zienkiewicz [39] developed a Rigid-Plastic flow model for the study of multi-stage deep drawing operations with completely general tooling geometry.

Recently, the need for using a large number of elements when bending effects are taken into consideration has been overcome by Tatenami et al. [40], who presented a mixed method between FEM and FDM (Finite Difference Method) that only required a small number of (multi-layered) elements. Good agreement was obtained between

numerical and experimental strains. Gerdeen [41] has developed a FEM program for axisymmetric analyses, that could account for combinations of stretching, bending, and drawing modes of deformation, multiple stages of forming, thickness variations, strain hardening and residual stresses.

Due to the similar nature of the two processes, many FEM analyses for deep drawing have also been devoted to stretch forming, and vice-versa ([28] – [29], [32] – [33], [36,39]). Nevertheless, a number of studies have been done especially for stretch forming, with some emphasizing on the punch stretching test. Mehta and Kobayashi [42] considered a general case of non-axisymmetric stretch forming, in which displacement boundary conditions were assumed for simplicity. Excellent results were obtained for various strain distributions.

Wang and Wenner [19] analyzed axisymmetric and plane-strain stretch forming problems with the Elasto-Viscoplastic approach, that included Coulomb friction, work hardening and normal anisotropy. Their model was based on a rate-sensitive flow theory and the nonlinear membrane theory. Consideration of rate sensitivity was found to increase result accuracy, and was therefore highly recommended. The stretch forming problem was then studied by Robelo and Kobayashi [20]. They used the Rigid-Viscoplastic formulation, which took into account the effects of metal strain-rate sensitivity in conjunction with the assumption that the variational formulation for rate-insensitive materials was also valid for rate-sensitive ones. The strain distributions computed were almost identical to those of [19] and agreed well with experiments.

A more general case of sheet metal stamping with dies and punches of arbitrary shapes was investigated by Wang and Budianski [14], who assumed an Elasto-Plastic material model satisfying a rate-insensitive Mises-flow rule, that handled finite deformation, work hardening and normal anisotropy. Since the results for hemispherical punches were only in fair agreement with experiments, hardening laws based on biaxial stress-strain data were advised to be employed. The case was subsequently extended by Wennerström et al. [43] to include the friction that exists between the tools and

the sheet of metal. Alternatively, Wang [44] analyzed stretch forming of general geometries using a Rigid-Plastic rate-insensitive model with isotropic hardening and flow rules obeying Hill's new field theory.

Axisymmetric hydraulic bulging problems have also been solved in several FEM analyses [22,33,44] in parallel to deep drawing and stretch forming, with generally good solutions. The most general case of non-axisymmetric edge-clamped metal diaphragms bulged by hydraulic pressure was studied by Iseki et al. [45], with an incremental large deformation Elasto-Plastic approach. The formulation developed was then checked for the case of a circular diaphragm before it was applied to calculate the large plastic deformations of thin elliptical and rectangular diaphragms [46]. Reasonable agreements with experimental data were obtained for the central height- and polar thickness-bulge pressure relations, and also for strain distributions on the major and minor axes of the diaphragm.

In another study, Bate [47] compared, in terms of accuracy and computational efficiency, the model proposed in [45] with the ULF based on the small-strain approximation by considering the hydraulic bulging problem for the case of isotropic strain-rate insensitive materials. Little difference could be observed between the two alternatives, with the latter being a bit slower but requiring less storage. Gotoh [48] recommended a polynomial shape function for triangular elements in the analysis of general deformation of sheet metals with or without orthotropic anisotropy. Such elements were expected to be economical when used to solve Elasto-Plastic problems of hydraulically bulged sheet metals.

Unlike deep drawing, stretch forming, and hydrostatic bulging, brake bending problems solved or modelled in the literature are much more industrially oriented, especially to automobile applications, although fewer FEM studies have been undertaken. Oh and Kobayashi [49] treated sheet bending between the dies and the punch as a bulk forming process under plane-strain conditions. Utilized in the study were both the large-strain Elasto-Plastic and incremental Rigid-Plastic formulations. Excellent

agreement was obtained between the two methods in terms of springback, residual stresses in the workpiece, and detailed mechanics during bending.

A nonlinear shell element proposed by Tang et al. [50] accurately predicted the deformed shapes of automobile body panels by brake bending. With the assumption that two sides of the blank could move freely, the computation was performed by automatically selecting and progressively feeding specific increments of a proposed set of binder surface displacements as boundary conditions. Tang [51] subsequently omitted such an assumption and analyzed the resulting contact problem by means of an approximate method using a FEM program developed at Ford Research. Wang et al. [52] have recently studied the stretch flanging of V-shaped sheet metal blanks, an operation required for various automotive structural members and inner panels, and obtained reasonable agreement between numerical results and test data.

2.3 Previous Analytical Work on Pipe Bending Processes

'Pipe and tube bending' referred to in the present study is a forming process, in which a straight pipe is intentionally bent past the yield point so as to cause permanent plastic deformations. The bent pipe is then called a 'pipe bend' or 'pipe elbow'.

Nowadays, the art of pipe and tube bending is far in advance of any basic understanding of the process in terms of engineering parameters [61]. Technically oriented literature on pipe bending processes includes books by Corpet [53] and Gillanders [54], covering a variety of bending methods associated with their advantages and shortcomings as well as various standards currently adopted by manufacturers producing bends. Some detailed theory on bending has also been given in recent reviews by Winship [55], Addison [56] and Venables [57].

An early experimental study of field bending was carried out by Steffens and Barkow [58]. Its objectives were to investigate changes in wall thickness and in ovality

of the cross section resulting from bending straight pipes into arcs of different angles. Weils et al. [59] then developed formulas to predict such thickness changes, based on the assumption that the meridional natural strain was zero. However, their predictions were in poor agreement with those of [58]. In a recent study of pipe bends for outer coating design purposes, Palynchuk [60] has found that strains caused by field bending operations vary substantially from theoretical predictions.

Inoue and Mellor [61] presented strain distributions in mild steel tubes formed by radial draw bending. It was found that lubrication can have a large effect on strains and that an approximate analysis based on the assumption that bending takes place under uniaxial tension leads to good correlation with experiment. The analysis was then extended [62] to deal with stainless steel tubes and to investigate the effects of friction conditions and a booster force on the pressure die. The results were compared with simple theoretical predictions of strain to find out where improvements in straining pattern are possible. Semenov and Nikitin [63] analyzed the induction bending of thin-walled tubes to a small radius by a profiling device. Blume et al. [64] studied the material properties of pipes after bending and subsequent heat treatment while Viatour et al. [65] investigated the conditions to maintain the original properties of pipes without undergoing a post-bending heat treatment. Asao et al. [66] carried out experiments on pipe bending using high frequency induction heating, from which means were found to avoid buckling at the inside of the pipe and reduction in thickness at the outside.

So far, little work has been published concerning such aspects as final strain distributions, residual stresses due to bending, or applied forces required for bending operations. Furthermore, no studies on numerical modelling of any particular type of pipe or tube bending have appeared in the literature. It is therefore worthwhile to investigate the possibility of simulating the process using the Finite Element Method. Although attention was given to the type of Ram Bending, results obtained from the present study would generally give a better understanding of the process, and any

success achieved would lead to simulations of other types of bending as well.

2.4 Previous Work on Elbow Element

Curved pipes appear frequently and are the most flexible parts in piping systems. In general, the FEM analysis of curved pipes is carried out with three types of elements: 3-D elements, shell elements, and elbow-like elements.

Theoretically, 3-D solid elements such as tetrahedral elements or brick elements are the most general type, and can be used to model any structure. However, to obtain acceptably accurate results a large number of elements is often required. Due to the huge cost of the analysis, such elements have seldom been employed to model curved pipes. On the other hand, in less expensive analyses that usually give excellent predictions a curved pipe is treated as a toroidal shell. It is then modelled with thick-shell elements [67] or thin-shell elements [68] depending on the wall thickness of the pipe. In many cases where there is no demand for high accuracy of the results while the cost of the analysis is more crucial, a FEM analysis with shell elements is still considered to be costly even for linear problems since the analysis involves typically of the order of a thousand of equilibrium equations.

In view of the foregoing, a number of elbow-like elements have been developed for practical use. A curved pipe is considered as a chain of much shorter curved pipes (ring or elbow elements) of the same cross section. The cost of an analysis using these elements is substantially reduced while the elements still provide sufficiently accurate predictions for the overall behaviour of the pipe. In previous linear FEM analyses of pipes, a simple curved beam theory was commonly used in combination with different flexibility and stress intensification factors to account for the ovalization of the pipe cross section and the effects of internal pressure [69], in-plane loading [80], and out-of-plane loading [70]. In some special problems such as elastic or plastic bending of a curved pipe having simple geometry, closed-form element stiffness matrices were

derived for programming convenience and computational efficiency [71] – [73]. Nevertheless, curved pipes modelled by the beam theory showed greater bending flexibility and stress intensification than straight pipes did. Yet, the above analyses assumed that ovalization was constant along the pipe bend; hence, variation in ovality of cross section could not be taken into consideration.

Because of such limitations of the beam theory, different elbow element models based on a shell theory have been proposed. Ohtsubo and Watanabe [74] developed the first ring element from the general thin shell theory including shear strain. The displacement component around and along the pipe were approximated by Fourier and Hermitian polynomials, respectively. Takeda et al. [75] proposed a similar ring element. The ring has two nodal points at its ends on the center line to account for the longitudinal displacement, and the ring wall is modelled by 4-noded doubly-curved quadrilateral elements to account for the circumferential and radial displacements. The circumferential and normal displacement fields were interpolated by 2-D Hermitian functions. The longitudinal displacement field was expanded into a Fourier series in the circumferential direction with each term interpolated by a 1-D cubic function along the longitudinal direction. Later, Takeda et al. [76] modified the formulation of their ring element to take into account transverse shears and the interaction effects between straight and curved pipes. For the new element, the circumferential and radial displacements and rotations were interpolated by 2-D Lagrangian bilinear functions. The longitudinal displacement was expanded into a Fourier series in the circumferential direction, and each term was interpolated by a 1-D linear function along the longitudinal direction. The elements developed in [74] – [76] were used mainly in linear analyses.

So far, few works have been published on the plastic analysis of curved pipes. Hibbitt and Leung [77] formulated a thin-walled elbow element for nonlinear analysis involving arbitrarily large motions which involve small strains. Lazzeri [78] developed an elasto-plastic elbow element based on Vlasov's thin shell theory. The circumferen-

tial displacement was represented by a Fourier series, and the derivatives of Fourier coefficients along the azimuthal direction were evaluated using the finite difference method. A static condensation procedure was then employed to reduce the stiffness matrix to a 12×12 matrix.

Though more cost-effective than shell elements, the elbow-shell elements have a number of drawbacks, especially in nonlinear analysis. Bathe and Almeida [3] developed a new elbow element that is simple, computationally effective, and capable of accurately predicting significant deformations and stress distributions in various curved pipe segments. The elbow is a four-noded displacement-based finite element with axial, torsional, and bending displacements and the von Karman ovalization deformation, all varying cubically along the elbow length. The formulation given is basically an extension and generalization of von Karman's analysis [80]. The Ritz method is used to take the axial variation of the cross section ovality into account.

The element was then extended to include interaction effects [4] such as those between elbows and rigid flanges, curved pipes of different curvatures. The penalty procedure was used to enforce the continuity of the derivatives in the pipe skin radial displacements. Also covered were stiffening effects due to internal pressure [81], and nonlinear effects due to material and kinematic nonlinearities [5].

In the present study, the Bathe-Almeida element, that was initially developed for piping analysis, is extended to solve the ram pipe bending forming process problem. The formulation is modified to take into account changes in the curvature of the element. These changes are normally significant due to large plastic deformations. Hence the Updated Lagrangian Jaumann Stress-Rate Formulation was used, which is capable of taking into account the new, deformed configuration of the structure at the end of each time step. This formulation is different from ULF in that it deals directly with stress and strain rates, thus avoiding the transformation of stresses and strains into the new coordinate system.

Chapter 3

Finite Element Modelling

3.1 General

Pipe and tube bending can be carried out using the methods of cold or hot bending as described in Article 1.3. Regardless of the technique applied, all formed bends are subjected to such phenomena as tension at the outside of the bend and compression at the inside. As the material deforms past the yield point, thinning occurs at the outer wall and corresponding thickening occurs at the inner wall; in addition, the cross section of the bend also tends to ovalize. These major effects result from plastic flow during the bending operation.

Ram bending involves the practice and the theory of the simply supported beam, and was one of the first techniques of bending. It is often used with low-precision work, in which the effects of cross-sectional flattening and changes in the wall thickness are not of great importance. Ram bending nevertheless deserves attention because it gives an insight into the mechanics of pipe and tube bending.

Figure 3.1 shows a schematic view of Ram bending and Figure 3.2 shows the modelling using beam theory; i.e. a simply supported beam.

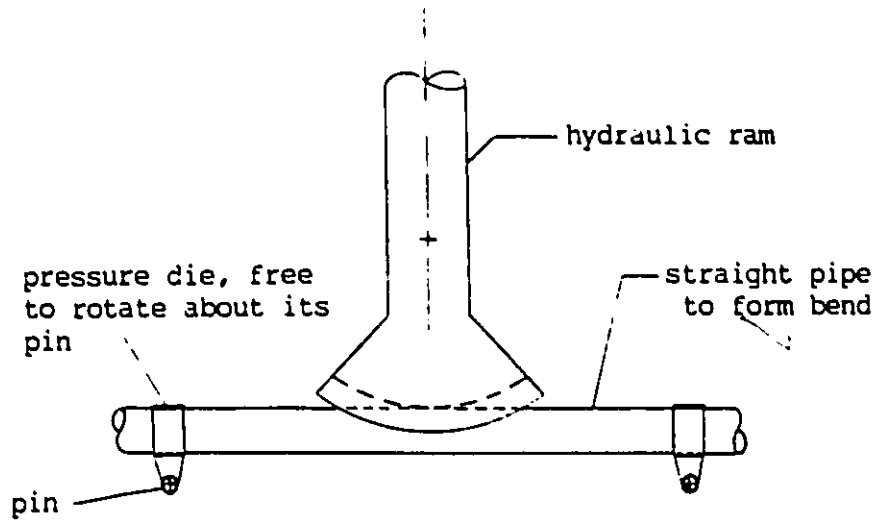


Figure 3.1: Schematic view of ram bending.

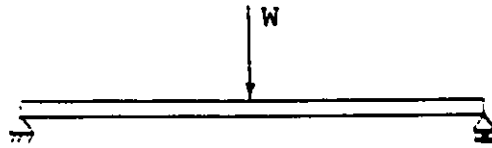


Figure 3.2: Simply supported beam.

3.2 Finite Element Method

After almost two decades of extensive development, the finite element method is now widely accepted as a powerful and general technique for the numerical solution of a variety of problems in engineering.

The basic idea behind this method is that any structure or continuous medium can be regarded as consisting of individual components or "finite elements", whose behaviour is well-defined and readily understood. These elements are interconnected at "nodal points" along their inter-element boundaries, Figure 3.3. Thus such a structure,

no matter how complex it is, can be analyzed with relative ease by studying the behaviour of its building blocks.

The finite element method is based on early work by Ritz (1909), who developed a powerful method to approximate the solution of field problems. It involved the approximation of a potential functional in terms of trial functions containing coefficients of unknown magnitudes. The minimization of the functional with respect to each unknown results in a set of linear equations that are solved for the unknowns. Accuracy could be improved by increasing the number of trial functions.

The finite element method can be applied in one of four different ways: (1) direct approach, (2) variational method, (3) weighted residual method, and (4) energy balance method. Among these, the weighted residual method is the most general approach while the variational method is the most popular one.

The variational method is the extended Ritz method in which the functional of the total potential energy of the system is to be minimized. The concept of minimum potential energy has three main forms corresponding to three variational principles: total potential energy, complementary energy, and Reissner [113].

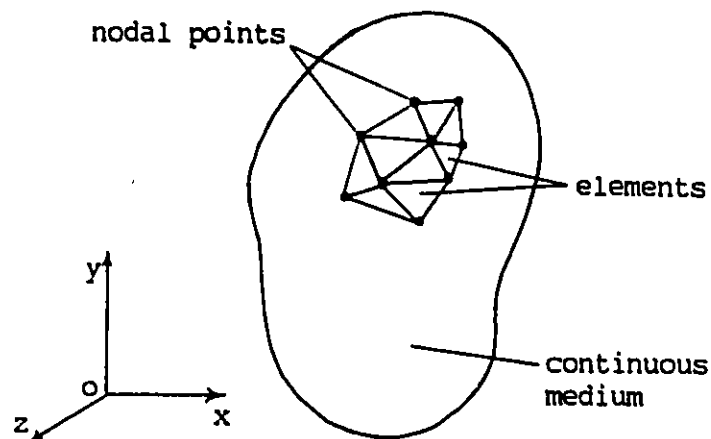


Figure 3.3: Discretization of a 3-D continuous body.

- The total potential energy principle is the cornerstone of the displacement-based finite element method. This is a most important formulation for the solution of many practical problems because of its simplicity, generality, and also numerical stability.
- In the complementary energy principle, stresses are the field variables rather than displacements; thus the use of this principle results in the stress-based equilibrium finite element method.
- A most general variational principle is that of Reissner, the primary field variables being both displacements and stresses, usually referred to as “mixed models”.

In summary, the solution to a problem using the finite element method (assumed to be displacement-based from here on) generally consists of six main steps: (1) formulation of the problem, (2) choice of the elements, (3) determination of the boundary conditions, (4) assemblage of element equilibrium equations, (5) solution of the global equations, and (6) calculation of strains, stresses, or any quantities of particular interest.

In linear analyses, the global equations can be represented by:

$$\mathbf{K}\mathbf{U} = \mathbf{R} \quad (3.1)$$

where \mathbf{K} is a constant stiffness matrix, \mathbf{U} the vector of unknown nodal point displacements and \mathbf{R} the vector of externally applied nodal forces.

In nonlinear analysis involving both geometric and material nonlinearities, the solution has to be carried out incrementally and iteratively until the desired accuracy is obtained. If the Updated Lagrangian Jaumann Stress-Rate Formulation and the Modified Newton-Raphson technique are adopted, the above equation becomes more complicated, having the form:

$$\left({}^t\mathbf{K}_L + {}^t\mathbf{K}_{NL} \right) \Delta \mathbf{U}^{(i)} = {}^{t+\Delta t}\mathbf{R} - {}^{t+\Delta t}\mathbf{F}^{(i-1)} \quad (3.2)$$

where

- ${}^t\mathbf{K}_L$: Linear strain incremental stiffness matrix.
- ${}^t\mathbf{K}_{NL}$: Nonlinear strain incremental stiffness matrix.
- ${}^{t+\Delta t}\mathbf{R}$: Vector of externally applied nodal point loads at time $t + \Delta t$.
- ${}_{t+\Delta t}^{t+\Delta t}\mathbf{F}^{(i-1)}$: Vector of nodal point forces equivalent to element stresses at time $t + \Delta t$ and in iteration $(i - 1)$
- $\Delta\mathbf{U}^{(i)}$: Vector of increments in nodal point displacements in iteration i , given by

$${}^{t+\Delta t}\mathbf{U}^{(i)} = {}^{t+\Delta t}\mathbf{U}^{(i-1)} + \Delta\mathbf{U}^{(i)}$$

In the above equation, the left superscript of a quantity represents the configuration of the body in which the quantity is calculated. Meanwhile, the left subscript indicates the configuration with respect to which the quantity is measured. When the left subscript is missing as in the case of ${}^{t+\Delta t}\mathbf{R}$, the quantity occurs in the same configuration (current) with respect to which it is measured. Detailed discussions on the applicability and various theoretical aspects, particularly those related to nonlinearities, of the Finite Element Method are given in [9]. Summaries of the Updated Lagrangian Jaumann Stress-Rate Formulation and the modified Newton-Raphson method are given in Appendix B.

3.3 Review of Elbow Element Formulation

The elbow element is a combined beam and shell finite element. The cross section of the element is assumed to be a circular annulus with constant thickness at all stages of the analysis, linear and nonlinear. The assumption about no cross-sectional change restricts the usefulness of the element to cases where ovalization is minimized

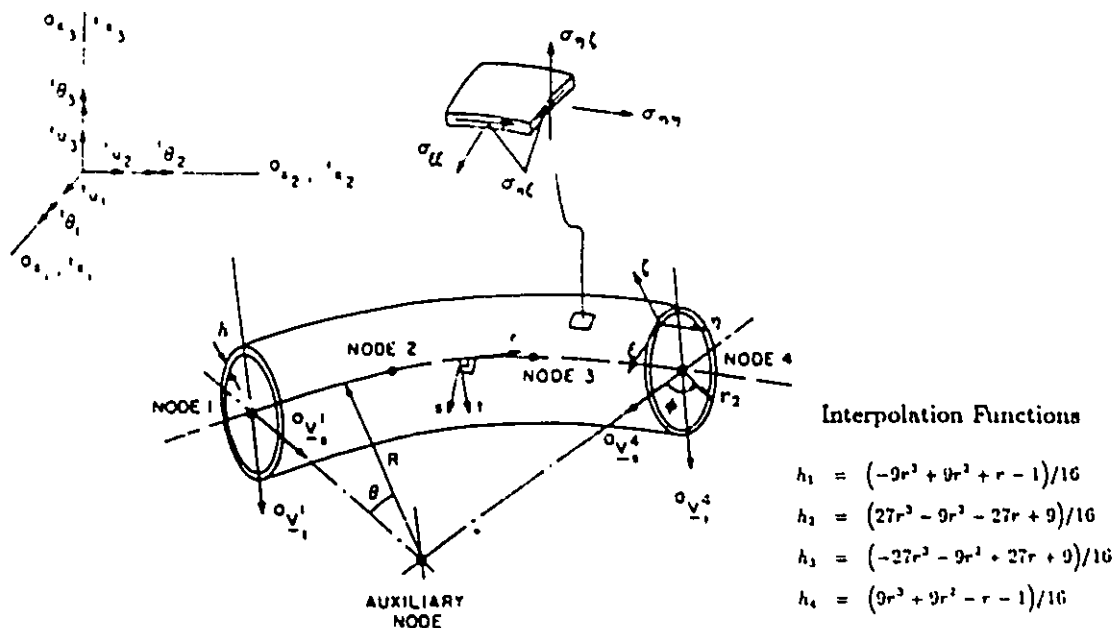


Figure 3.4: Geometry of the pipe elbow element.

using some active means. Small radial displacements are assumed to occur; these are predicted according to von Karman's hypotheses [80].

Detailed description of such an elbow element was given in [9], and the effects of ovalization have been investigated recently in [3] - [5]. For continuity of these works, a brief summary of the formulation of the elbow element is given here using the nomenclature of [3] - [5].

3.3.1 Beam Behaviour

The elbow element is an isoparametric element that has 4 nodal points equally spaced along the centerline of the element. Each nodal point has a total of 6 displacements: 3 translations and 3 rotations ($u_1, u_2, u_3, \theta_1, \theta_2, \theta_3$) with respect to the referential coordinate axes. This permits consideration of in-plane and out-of-plane loading cases. The current geometry of the element at any time t is approximated by

$${}^t x_i(r, s, t) = \sum_{k=1}^4 h_k {}^t x_i^k + s \sum_{k=1}^4 r_2^k h_k {}^t V_{si}^k + t \sum_{k=1}^4 r_2^k h_k {}^t V_{ti}^k \quad (3.3)$$

where

- $i = 1, 2, \text{ or } 3$ representing $x, y, \text{ or } z$
 $k =$ node number from 1 to 4
 $r, s, t =$ isoparametric coordinates, as shown in Figure 3.4
 $h_k(r) =$ isoparametric interpolation function for nodal point k ,
 given in Figure 3.4
 $r_2^k =$ outer radius of the element at nodal point k
 ${}^tV_{ti}^k =$ component i of unit vector ${}^tV_t^k$, in direction t
 ${}^tV_{si}^k =$ component i of unit vector ${}^tV_s^k$, in direction s .

As can be seen from Figure 3.4, Equation (3.3) is only applicable for the values of s and t satisfying

$$\left[t - \frac{h^k}{r_2^k} \right]^2 \leq s^2 + t^2 \leq 1$$

where h^k is the wall thickness of the element at nodal point k , and is assumed constant.

The displacement components, defined by $u_i = {}^{t+\Delta t}x_i - {}^tx_i$, can now be readily calculated from (3.3):

$$u_i(r, s, t) = \sum_{k=1}^4 h_k u_i^k + t \sum_{k=1}^4 r_2^k h_k V_{ti}^k + s \sum_{k=1}^4 r_2^k h_k V_{si}^k \quad (3.4)$$

with

$$V_{ti}^k = {}^{t+\Delta t}V_{ti}^k - {}^tV_{ti}^k$$

$$V_{si}^k = {}^{t+\Delta t}V_{si}^k - {}^tV_{si}^k$$

To evaluate the changes in direction cosines, V_{ti}^k and V_{si}^k , they need to be expressed in terms of nodal point rotations, namely

$$V_t^k = \theta_k \times {}^tV_t^k$$

$$V_s^k = \theta_k \times {}^tV_s^k$$

The strain components can then be determined by calculating the displacement derivatives corresponding to the global coordinate axes x_i ($i = 1, 2, 3$). Since the

displacements u_i in Equation (3.4) are being expressed in terms of the isoparametric coordinates (r, s, t) , it is impractical to differentiate (3.4) directly with respect to x_i . Instead, the computation is carried out in 2 steps.

Firstly, (3.4) is differentiated with respect to r, s , and t to yield

$$\begin{bmatrix} \frac{\partial u_i}{\partial r} \\ \frac{\partial u_i}{\partial s} \\ \frac{\partial u_i}{\partial t} \end{bmatrix} = \sum_{k=1}^4 \begin{bmatrix} \frac{\partial h_k}{\partial r} [1 \quad {}^t(g)_{1i}^k \quad {}^t(g)_{2i}^k \quad {}^t(g)_{3i}^k] \\ h_k [0 \quad {}^t(\hat{g})_{1i}^k \quad {}^t(\hat{g})_{2i}^k \quad {}^t(\hat{g})_{3i}^k] \\ h_k [0 \quad {}^t(\bar{g})_{1i}^k \quad {}^t(\bar{g})_{2i}^k \quad {}^t(\bar{g})_{3i}^k] \end{bmatrix} \begin{bmatrix} u_i^k \\ \theta_1^k \\ \theta_2^k \\ \theta_3^k \end{bmatrix} \quad (3.5)$$

where

$${}^t(\hat{g})^k = r_2^k \begin{bmatrix} 0 & -{}^tV_{s3}^k & {}^tV_{s2}^k \\ {}^tV_{s3}^k & 0 & -{}^tV_{s1}^k \\ -{}^tV_{s2}^k & {}^tV_{s1}^k & 0 \end{bmatrix}$$

$${}^t(\bar{g})^k = r_2^k \begin{bmatrix} 0 & -{}^tV_{t3}^k & {}^tV_{t2}^k \\ {}^tV_{t3}^k & 0 & -{}^tV_{t1}^k \\ -{}^tV_{t2}^k & {}^tV_{t1}^k & 0 \end{bmatrix}$$

$${}^t(g)^k = s^t(\hat{g})^k + t^t(\bar{g})^k$$

Secondly, the above derivatives are transformed into the global coordinate system by means of the Jacobian transformation that has a matrix representation:

$$\begin{bmatrix} \frac{\partial}{\partial x_1} \\ \frac{\partial}{\partial x_2} \\ \frac{\partial}{\partial x_3} \end{bmatrix} = \mathbf{J}^{-1} \begin{bmatrix} \frac{\partial}{\partial r} \\ \frac{\partial}{\partial s} \\ \frac{\partial}{\partial t} \end{bmatrix} \quad (3.6)$$

with

$$\mathbf{J} = \begin{bmatrix} \frac{\partial x_1}{\partial r} & \frac{\partial x_2}{\partial r} & \frac{\partial x_3}{\partial r} \\ \frac{\partial x_1}{\partial s} & \frac{\partial x_2}{\partial s} & \frac{\partial x_3}{\partial s} \\ \frac{\partial x_1}{\partial t} & \frac{\partial x_2}{\partial t} & \frac{\partial x_3}{\partial t} \end{bmatrix}$$

The derivatives in (3.5) can now be rewritten in terms of the global coordinates as

$$\begin{bmatrix} \frac{\partial u_i}{\partial x_1} \\ \frac{\partial u_i}{\partial x_2} \\ \frac{\partial u_i}{\partial x_3} \end{bmatrix} = \sum_{k=1}^4 \begin{bmatrix} \frac{\partial h_k}{\partial x_1} & {}^t(G1)_{i1}^k & {}^t(G2)_{i1}^k & {}^t(G3)_{i1}^k \\ \frac{\partial h_k}{\partial x_2} & {}^t(G1)_{i2}^k & {}^t(G2)_{i2}^k & {}^t(G3)_{i2}^k \\ \frac{\partial h_k}{\partial x_3} & {}^t(G1)_{i3}^k & {}^t(G2)_{i3}^k & {}^t(G3)_{i3}^k \end{bmatrix} \begin{bmatrix} u_i^k \\ \theta_1^k \\ \theta_2^k \\ \theta_3^k \end{bmatrix} \quad (3.7)$$

where

$${}^t h_{k,i} = \frac{\partial h_k}{\partial x_i} = {}^t J_{i1}^{-1} \frac{\partial h_k}{\partial r}$$

$${}^t (Gm)_{in}^k = [{}^t J_{n1}^{-1} {}^t (g)_{mi}^k] \frac{\partial h_k}{\partial r} + [{}^t J_{n2}^{-1} {}^t (\hat{g})_{mi}^k + {}^t J_{n3}^{-1} {}^t (\bar{g})_{mi}^k] h_k$$

For convenience in incremental nonlinear analyses, increments in strain components are often approximated by their linear parts,

$$\begin{bmatrix} \epsilon_{11} \\ \epsilon_{22} \\ \epsilon_{33} \\ \gamma_{12} \\ \gamma_{23} \\ \gamma_{31} \end{bmatrix} = \begin{bmatrix} \frac{\partial u_1}{\partial x_1} \\ \frac{\partial u_2}{\partial x_2} \\ \frac{\partial u_3}{\partial x_3} \\ \frac{\partial u_1}{\partial x_2} + \frac{\partial u_2}{\partial x_1} \\ \frac{\partial u_2}{\partial x_3} + \frac{\partial u_3}{\partial x_2} \\ \frac{\partial u_3}{\partial x_1} + \frac{\partial u_1}{\partial x_3} \end{bmatrix} \quad (3.8)$$

With the substitution of (3.7) into (3.8), the linear strain-displacement transformation matrix can now be obtained as

$${}^t B_L = \left[\begin{array}{ccccccc|c} | & {}^t h_{k,1} & 0 & 0 & {}^t (G1)_{11}^k & {}^t (G2)_{11}^k & {}^t (G3)_{11}^k & | \\ | & 0 & {}^t h_{k,2} & 0 & {}^t (G1)_{22}^k & {}^t (G2)_{22}^k & {}^t (G3)_{22}^k & | \\ | & 0 & 0 & {}^t h_{k,3} & {}^t (G1)_{33}^k & {}^t (G2)_{33}^k & {}^t (G3)_{33}^k & | \\ \dots & | & | & | & | & | & | & \dots \\ | & {}^t h_{k,2} & {}^t h_{k,1} & 0 & {}^t (G1)_{12}^k + {}^t (G1)_{21}^k & {}^t (G2)_{12}^k + {}^t (G2)_{21}^k & {}^t (G3)_{12}^k + {}^t (G3)_{21}^k & | \\ | & 0 & {}^t h_{k,3} & {}^t h_{k,2} & {}^t (G1)_{23}^k + {}^t (G1)_{32}^k & {}^t (G2)_{23}^k + {}^t (G2)_{32}^k & {}^t (G3)_{23}^k + {}^t (G3)_{32}^k & | \\ | & {}^t h_{k,3} & 0 & {}^t h_{k,1} & {}^t (G1)_{31}^k + {}^t (G1)_{13}^k & {}^t (G2)_{31}^k + {}^t (G2)_{13}^k & {}^t (G3)_{31}^k + {}^t (G3)_{13}^k & | \\ & & & & & & & (3.9) \end{array} \right]$$

This matrix is required to evaluate the linear stiffness matrix represented by (3.2). Similarly, the calculation of the nonlinear stiffness matrix requires a nonlinear strain-displacement transformation matrix given by:

$${}^i\mathbf{B}_{NL} = \begin{bmatrix} | & {}^i h_{k,1} & 0 & 0 & {}^i(G1)_{11}^k & {}^i(G2)_{11}^k & {}^i(G3)_{11}^k & | \\ | & {}^i h_{k,2} & 0 & 0 & {}^i(G1)_{12}^k & {}^i(G2)_{12}^k & {}^i(G3)_{12}^k & | \\ | & {}^i h_{k,3} & 0 & 0 & {}^i(G1)_{13}^k & {}^i(G2)_{13}^k & {}^i(G3)_{13}^k & | \\ | & 0 & {}^i h_{k,1} & 0 & {}^i(G1)_{21}^k & {}^i(G2)_{21}^k & {}^i(G3)_{21}^k & | \\ \cdots & | & 0 & {}^i h_{k,2} & 0 & {}^i(G1)_{22}^k & {}^i(G2)_{22}^k & {}^i(G3)_{22}^k & | & \cdots \\ | & 0 & {}^i h_{k,3} & 0 & {}^i(G1)_{23}^k & {}^i(G2)_{23}^k & {}^i(G3)_{23}^k & | \\ | & 0 & 0 & {}^i h_{k,1} & {}^i(G1)_{31}^k & {}^i(G2)_{31}^k & {}^i(G3)_{31}^k & | \\ | & 0 & 0 & {}^i h_{k,2} & {}^i(G1)_{32}^k & {}^i(G2)_{32}^k & {}^i(G3)_{32}^k & | \\ | & 0 & 0 & {}^i h_{k,3} & {}^i(G1)_{33}^k & {}^i(G2)_{33}^k & {}^i(G3)_{33}^k & | \end{bmatrix} \quad (3.10)$$

Having computed the strain-displacement matrices, the construction of element stiffness matrices and of the nodal force vector follows the usual finite element procedure, namely

$${}^i\mathbf{K}_L = \int_{iV} {}^i\mathbf{B}_L^T {}^i\mathbf{C}^{EP} {}^i\mathbf{B}_L {}^i dV \quad (3.11)$$

$${}^i\mathbf{K}_{NL} = \int_{iV} {}^i\mathbf{B}_{NL}^T {}^i\boldsymbol{\tau} {}^i\mathbf{B}_{NL} {}^i dV \quad (3.12)$$

$${}^i\mathbf{F} = \int_{iV} {}^i\mathbf{B}_L^T {}^i\hat{\boldsymbol{\tau}} {}^i dV \quad (3.13)$$

where

${}^i\mathbf{C}^{EP}$ = instantaneous elastic-plastic stress-strain matrix

${}^i\boldsymbol{\tau}$, ${}^i\hat{\boldsymbol{\tau}}$ = matrix and vector representing element residual stresses due to externally applied loads, respectively.

If the von Mises yield condition and the flow theory are utilized with the material assumed to be isothermal and isotropically hardened, ${}^i\mathbf{C}^{EP}$ is given [9,10] by:

$${}^i\mathbf{C}^{EP} = \mathbf{C}^E - \frac{\mathbf{C}^E {}^i\mathbf{q} (\mathbf{C}^E {}^i\mathbf{q})^T}{(4/9) H^* \sigma_y + {}^i\mathbf{q}^T \mathbf{C}^E {}^i\mathbf{q}} \quad (3.14)$$

where

$${}^t\mathbf{q}^T = [{}^tS_{11} \quad {}^tS_{22} \quad {}^tS_{33} \quad 2{}^tS_{12} \quad 2{}^tS_{23} \quad 2{}^tS_{31}]$$

${}^tS_{ij}$ = components of the deviatoric stress tensor

${}^t\sigma_y$ = uniaxial yield stress at time t

H^* = strain hardening constant defined by

$$H^* = \frac{E E_T}{E - E_T}$$

E_I = instantaneous tangential modulus

C^E = elastic stress-strain matrix.

Since all element stiffness matrices are finally assembled in the global coordinate system, C^E has to be recalculated as

$$C^E = \mathbf{Q}^T \left(\frac{E}{1-\nu^2} \begin{bmatrix} 1 & \nu & 0 & 0 & 0 & 0 \\ \nu & 1 & 0 & 0 & 0 & 0 \\ 0 & 0 & 0 & 0 & 0 & 0 \\ 0 & 0 & 0 & \frac{1-\nu}{2} & 0 & 0 \\ 0 & 0 & 0 & 0 & \frac{1-\nu}{2k} & 0 \\ 0 & 0 & 0 & 0 & 0 & \frac{1-\nu}{2k} \end{bmatrix} \right) \mathbf{Q} \quad (3.15)$$

where

k : shear factor, normally taken as 1.2

\mathbf{Q} : transformation matrix transforming the elastic stress-strain matrix from the local $\xi\eta\zeta$ system to the global $x_1x_2x_3$ system (see Appendix A).

As can be observed from (3.15), the normal stress in the thickness direction (σ_ζ) was assumed to be zero as in shell theory. This assumption simplifies the stress-strain relations and can be justified by the fact that σ_ζ is usually insignificant compared with other stress components except near the loaded areas.

Although closed-form integration can be carried out in some linear analyses, such an exact evaluation of (3.11) – (3.13) is not possible because of the incremental complexity of nonlinearities. Instead, integration is performed numerically. The result accuracy is greatly dependent on the integration schemes adopted. In terms of simplicity and efficiency, the most commonly used scheme is Gauss quadrature, in which the integration limits are 1 and -1. This is not a suitable choice for the current elbow element. To take into consideration full plastic behaviour of the element, especially at its two ends, the following integration scheme is employed in the present study, as suggested earlier in [5]:

- 5-point Newton-Cotes integration along the element length,
- 12- or 24-point integration using the composite trapezoidal rule in the circumferential direction,
- 5- or 7-point Newton-Cotes integration across the wall thickness.

This integration scheme implies that the integration variables are those of the cylindrical coordinates. Hence, (3.11) – (3.13) have to be evaluated appropriately. For example, (3.11) becomes

$${}^t\mathbf{K}_L = \int_{-1}^1 \int_0^{2\pi} \int_{r_2-h}^{r_2} {}^t\mathbf{B}_L^T {}^t\mathbf{C}^{EP} {}^t\mathbf{B}_L \det |\mathbf{J}| \rho \, d\rho \, d\phi \, dr$$

where $\det |\mathbf{J}|$ is the determinant of the Jacobian matrix as shown in Equation (3.6).

3.3.2 von Karman's Description of Ovalization [80]

The elbow element is an extension of von Karman's pipe elbow. For in-plane bending, von Karman analyzed the effect of ovalization of the cross section by assuming the displacement patterns:

$$w_\xi(r, \phi) = \sum_{m=1}^{N_c} \sum_{k=1}^4 h_k c_m^k \sin 2m\phi \quad (3.16)$$

where c_m^k denotes the unknown generalized ovalization displacements, ϕ is some angular position of the cross section, and N_c the number of nodal point ovalization displacements. The value of N_c ranges from 1 to 3, depending on the pipe geometric parameter $\lambda = Rh/r_m^2$ as specified in Table 3.1.

Table 3.1: Number of ovalization shape functions to be used.

Geometric range	Number of functions N_c
$0.50 \leq \lambda$	1
$0.16 \leq \lambda < 0.50$	2
$0.08 \leq \lambda < 0.16$	3

To evaluate the strains due to ovalization of the cross section, von Karman made a number of assumptions, the five major ones being

1. Plane sections originally plane and normal to the neutral axis continue to be so.
2. Longitudinal strains are of constant magnitudes through the pipe wall thickness.
3. Pipe wall thickness is small in comparison with the pipe outside radius, $h/r_2 \ll 1$.
4. Pipe outside radius is much smaller than the radius of the pipe bend, $r_2/R \ll 1$.
5. Effect of Poisson's ratio is negligible.

Due to ovalization of the cross section, the radial displacement and the circumferential displacement of the middle surface of the pipe wall are related to each other [3] by

$$w_\zeta = -\frac{dw_\xi}{d\phi} \quad (3.17)$$

where ϕ denotes a positional angle of the cross section, and (ξ, η, ζ) represent the natural coordinates in the pipe wall as shown in Figure 3.4.

A study of Novozhilov's shell theory [S2] for a curved tube indicates that in linear analysis the important strain components for the elbow are the usual beam normal and shear strains as well as the strains due to ovalization, namely

$$\epsilon_{\xi\xi} = -\frac{1}{r_m^2} \left[w_\zeta + \frac{d^2 w_\zeta}{d\phi^2} \right] \zeta \quad (3.18)$$

$$\epsilon_{\eta\eta} = \left[\frac{w_\xi \sin \phi + \frac{dw_\xi}{d\phi} \cos \phi}{R - r_m \cos \phi} \right] - \left[\left(\frac{1}{R - r_m \cos \phi} \right)^2 \frac{d^2 w_\zeta}{d\theta^2} \right] \zeta \quad (3.19)$$

$$\gamma_{\eta\xi} = \left[\frac{1}{R - r_m \cos \phi} \right] \frac{dw_\xi}{d\theta} \quad (3.20)$$

where r_m is the mean radius of the cross section, and is assumed constant throughout the analysis.

The strain components due to ovalization displacements can now be calculated using Equations (3.16) - (3.20).

$$\begin{bmatrix} \epsilon_{\xi\xi} \\ \epsilon_{\eta\eta} \\ \epsilon_{\zeta\zeta} \\ \gamma_{\xi\eta} \\ \gamma_{\eta\xi} \\ \gamma_{\zeta\xi} \end{bmatrix} = \hat{B}_{OV} \begin{bmatrix} \vdots \\ c_1^k \\ c_2^k \\ c_3^k \\ \vdots \end{bmatrix} \quad (3.21)$$

where \hat{B}_{OV} is the strain-displacement transformation matrix for ovalization given by

$$\hat{B}_{OV} = \begin{bmatrix} | & a_1 & a_2 & a_3 & | \\ | & b_1 + \hat{b}_1 & b_2 + \hat{b}_2 & b_3 + \hat{b}_3 & | \\ \dots & 0 & 0 & 0 & \dots \\ | & c_1 & c_2 & c_3 & | \\ | & 0 & 0 & 0 & | \\ | & 0 & 0 & 0 & | \end{bmatrix}$$

where

$$m = 2l$$

$$\begin{aligned}
a_l &= \left[\frac{m(1-m^2)}{r_m^2} h_k \cos m\phi \right] \zeta \\
b_l &= \frac{h_k}{(R-r_m \cos \phi)} [m \cos m\phi \cos \phi + \sin m\phi \sin \phi] \\
\hat{b}_l &= \left[\frac{2}{(R-r_m \cos \phi)\theta} \right] \frac{d^2 h_k}{dr^k} (m \cos m\phi) \zeta \\
c_l &= \left[\frac{2}{(R-r_m \cos \phi)\theta} \right] \frac{dh_k}{dr} \sin m\phi
\end{aligned}$$

Because \hat{B}_{OV} relates the ovalization displacements to the strain components in the natural coordinates (ξ, η, ζ) , it must be transformed into the global system in order to be combined with ${}^t\mathbf{B}_L$.

$$\mathbf{B}_{OV} = \mathbf{P} \hat{\mathbf{B}}_{OV} \quad (3.22)$$

where \mathbf{P} is a transformation matrix (given in Appendix A).

Thus the linear strain-displacement transformation matrix in (3.9) should be modified to incorporate (3.22),

$${}^t\mathbf{B}_L = [{}^t\mathbf{B}_L \mid \mathbf{B}_{OV}]$$

which corresponds to

$$\begin{aligned}
\mathbf{u}^T &= \left[\cdots \mid \underbrace{u_1^k \ u_2^k \ u_3^k \ \theta_1^k \ \theta_2^k \ \theta_3^k \ c_1^k}_{\text{for nodal point } k} \overbrace{c_2^k \ c_3^k}^{\text{optional}} \mid \cdots \right] \\
\boldsymbol{\epsilon}^T &= [\epsilon_{11} \ \epsilon_{22} \ \epsilon_{33} \ 2\epsilon_{12} \ 2\epsilon_{23} \ 2\epsilon_{31}]
\end{aligned}$$

3.4 Extension of Elbow Element's Capability

In FEM modelling using the elbow element, the initial curvature of an element is the same as that of the curved pipe which the element models. With regard to piping analysis where plastic deformations are usually small, the assumption that the curvatures of all elements remain constant throughout the analysis is usually made

to reduce programming efforts as well as computer time. On the other hand, large plastic deformations are normally expected in forming problems, and as a result the above assumption is no longer appropriate; the curvature of every element has to be updated to give the true picture of the deformed configuration of the pipe as bending progresses.

As far as the current FEM program and in-plane bending are concerned, an elbow element is approximated as a torus having known curvature at the time under consideration. Thus, the radius of curvature of the element at time t is given by

$${}^tR = \frac{l}{{}^t\theta}$$

where l is the length of the element measured along its center line, ${}^t\theta$ denotes the angle between the two end sections, and $t = 0$ corresponds to the time prior to bending.

At later time $t + \Delta t$, one end of the element undergoes a relative in-plane rotation $\Delta\gamma$ with respect to the other end as shown in Figure 3.5. With the same approximation, the angle between the two end sections then becomes

$${}^{t+\Delta t}\theta = {}^t\theta + \Delta\gamma$$

which implies that

$${}^{t+\Delta t}R = \frac{l}{{}^{t+\Delta t}\theta} = \frac{l}{{}^t\theta + \Delta\gamma}$$

The updating scheme presented shows that the larger the number of elements modelling the pipe, the better the deformed configuration of the pipe, and therefore the more accurate the analytical predictions. However, a larger number of elements requires a longer computing time. Thus, a compromise has to be made between the result accuracy and computer time.

Here, it is important to note that the updates of the pipe-wall thickness and the cross section are not considered in the computation process. The reasons are that first, the elbow element is formulated based on thin shell theory. One major assumption of this theory is that wall thickness remains constant. Secondly, the strain components

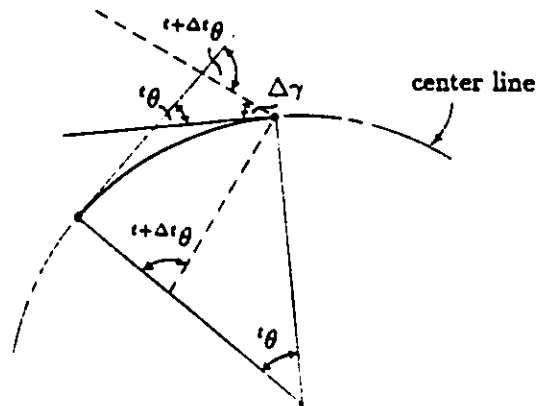


Figure 3.5: Updating of the curvature of an elbow element.

resulting from ovalizations assumed by von Karman are calculated using Novozhilov's shell theory which does not take into account variations in ovality of the cross section.

To facilitate any further reference to the current FEM program and to clarify different sources of results (Chapter 4), the program developed herein will be referred to as 'FENSA' (Finite Element Nonlinear Static Analysis). The program listing of FENSA is shown in Appendix C.3.

Chapter 4

Comparison of FENSA Results with Available Data

4.1 Introduction

In this chapter, the results from the program FENSA for five piping problems are compared with those from other methods and computer programs. The first two problems cover elastic behaviour, while the last three nonelastic behaviour. Efforts are made to assess the accuracy of the elbow element and the reliability of the program FENSA in linear and nonlinear analyses.

4.2 Elastic Bending of a Straight Pipe

The aim of this section is to study the accuracy of the displacement and rotation results produced by FENSA. The problem considered is that of a cantilever beam under a concentrated load, Figure 4.1. The beam has an annular cross section with $r_2/h = 3$ (r_2 : outside radius of the cross section, h : thickness of the pipe wall), and is subjected to bending due to a concentrated load acting on its free end. From elementary beam theory, the theoretical results for the maximum deflection and the maximum rotation

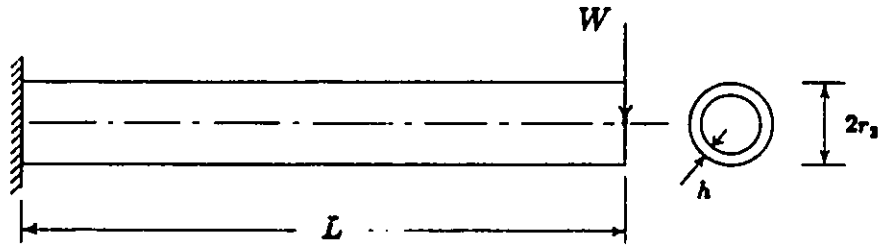


Figure 4.1: Cantilever beam under a concentrated load.

Table 4.1: Comparison of FENSA and beam-theory results for end deflection and rotation.

$\frac{L}{2r_2}$	$\frac{\delta - \delta_{th}}{\delta_{th}}$	$\frac{\gamma - \gamma_{th}}{\gamma_{th}}$
10	.005911	.00000
100	.000057	.00000
1000	.000002	.00000
10000	.000000	.00000

of the beam are

$$\delta_{th} = \frac{WL^3}{3EI}$$

$$\gamma_{th} = \frac{WL^2}{2EI}$$

where E is the Young's modulus of the material, I the second moment of the area of the cross section, L the total length of the beam, and W the concentrated load.

Table 4.1 presents a comparison of the FENSA and theoretical results when the beam is simulated by a one-element model. For $L/2r_2 = 10$, the FENSA prediction for the end deflection is only 0.6% different from the theoretical one while the two predictions for the end rotation are virtually identical. When the ratio $L/2r_2$ becomes greater, the FENSA predictions quickly approach the theoretical values because the Saint Venant effects tend to diminish. With the agreement obtained between the FENSA and beam-theory results for deflection and rotation, the elbow element looks promising in problems with more complex geometries.

4.3 Elastic In-Plane Bending of a Flanged 90°-Pipe Bend

The problem of a flanged 90° bend under a closing bending moment has been solved by Whatham [85] using thin shell theory. Whatham took into account the interaction effects due to the flanged end of the bend, and subsequently supported his theoretical work experimentally. In the present study, the bend is analyzed again as a check problem for FENSA in the linear range. Stress response, end rotations, and ovalizations for various radii of bend curvature are considered.

On considering the plane of symmetry at $\theta = 45^\circ$ with θ measured from the flanged end, only half of the 90° bend needs to be modelled. The resulting 45° bend is represented by 6 elements with a total of 19 nodal points as shown in Figure 4.2(b).

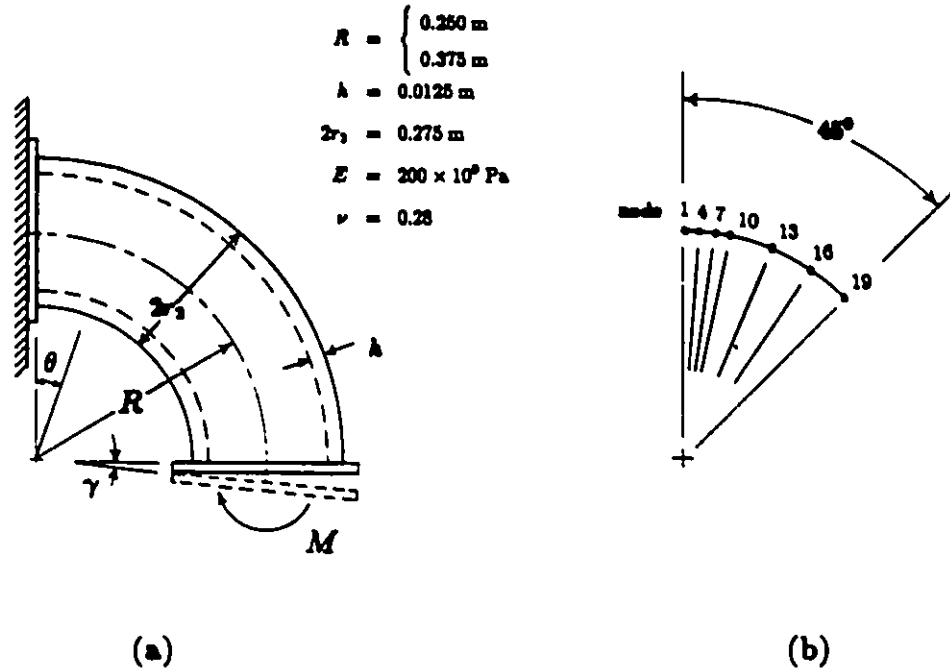


Figure 4.2: Geometry and modelling of a flanged 90° elbow.

To effectively represent the behaviour of the bend, 3 elements of 3.8° each are used to model the part near the flanged end, and 3 additional elements of 11.2° each for the remaining part of the bend. The interaction effects mainly due to the flanged end are accounted for using the penalty procedure as discussed in [4]. All geometric dimensions and material properties of the pipe bend are given in Figure 4.2(a).

The results for local stresses at $\theta = 45^\circ$ on the outside surface of the bend are given in Figures 4.3 - 4.6 for two different sizes of pipe bends, $R = 0.250\text{m}$ and $R = 0.375\text{m}$. The circumferential stress $\sigma_{\xi\xi}$ and the longitudinal stress $\sigma_{\eta\eta}$, both being expressed in a non-dimensional form

$$\sigma_{\xi\xi}^* = \frac{\sigma_{\xi\xi}}{M} \pi r_m^2 h$$

$$\sigma_{\eta\eta}^* = \frac{\sigma_{\eta\eta}}{M} \pi r_m^2 h$$

are plotted against the angle of cross section ϕ (r_m : mean radius of the cross section).

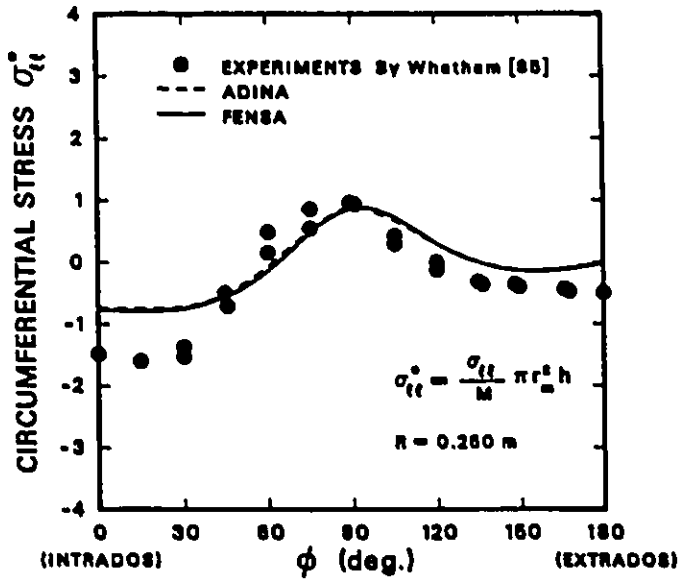


FIG. 4-3 PREDICTED CIRCUMFERENTIAL STRESSES AT $\theta=45^\circ$ AND ON OUTSIDE SURFACE FOR $R=0.260 \text{ m}$.

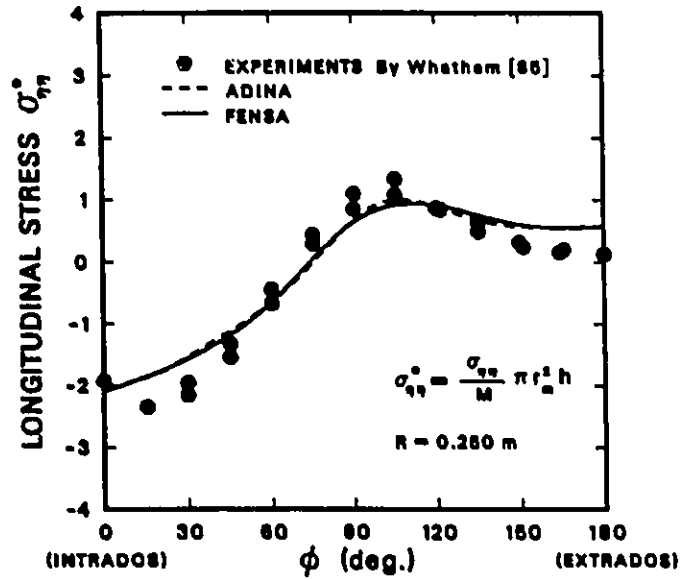


FIG. 4-4 PREDICTED LONGITUDINAL STRESSES AT $\theta=45^\circ$ AND ON OUTSIDE SURFACE FOR $R=0.260 \text{ m}$.

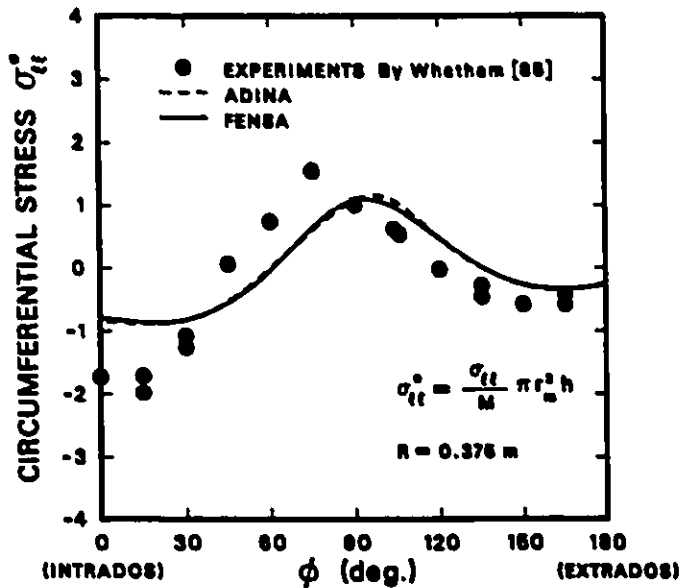


FIG. 4-5 PREDICTED CIRCUMFERENTIAL STRESSES AT $\theta=45^\circ$ AND ON OUTSIDE SURFACE FOR $R=0.376 \text{ m}$.

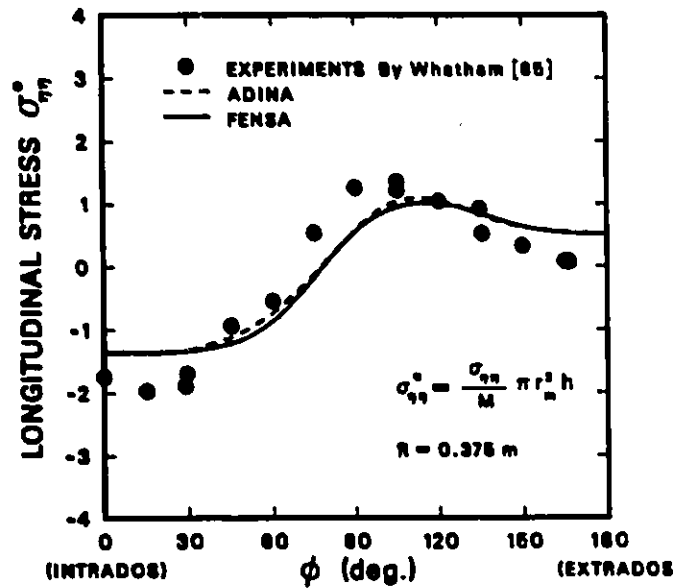


FIG. 4-6 PREDICTED LONGITUDINAL STRESSES AT $\theta=45^\circ$ AND ON OUTSIDE SURFACE FOR $R=0.376 \text{ m}$.

For $R = 0.250\text{m}$ (Figures 4.3 and 4.4), there is good agreement between the FENSA results and experimental data obtained by Whatham for $40^\circ \leq \phi < 180^\circ$. When $0^\circ \leq \phi \leq 40^\circ$, FENSA tends to underestimate $\sigma_{\xi\xi}^*$ by up to 55% at $\phi = 0^\circ$ (intrados). Discrepancies of such a magnitude in the stress results are also found in the vicinity of $\phi = 180^\circ$ (extrados). For $R = 0.375\text{m}$ (Figures 4.5 and 4.6), only qualitative agreement is obtained between the two sets of results. The FENSA predictions for $\sigma_{\xi\xi}^*$ and $\sigma_{\eta\eta}^*$ are found to deviate noticeably from the measurements when $0^\circ \leq \phi \leq 90^\circ$. A comparison between the stress results for $R = 0.250\text{m}$ and $R = 0.375\text{m}$ also shows a tendency that the differences between the FENSA predictions and the experimental measurements become larger as R increases.

It should be pointed out from these figures that due to the effects of the flanged end and of the cross-section ovalizations the $\sigma_{\eta\eta}^*$ distribution just obtained is substantially different from the one predicted by the curved-beam theory. $\sigma_{\eta\eta}^*$ is observed to be most negative at $\phi = 0^\circ$ and most positive at $\phi = 95^\circ$, approximately. Yet, $\sigma_{\xi\xi}^*$ that was previously considered to be insignificant is in fact comparable in magnitude to $\sigma_{\eta\eta}^*$.

Figure 4.7 shows the results for the flexibility factor defined by

$$f_\gamma = \frac{2\gamma}{M} \frac{r_m^3 E h}{R}$$

where γ is the end rotation, and M the applied moment. In general, there is good correspondence between the FENSA results and the experimental data. At $R = 0.375\text{m}$, the FENSA prediction is found to be only about 10% lower than the measured value.

Presented in Figure 4.8 are the results for the diameter change factor defined by

$$f_d = \frac{2\pi E h r_m}{\delta_d}$$

with δ_d being the change in the outside diameter of the cross section (at $\theta = 45^\circ$). The FENSA predictions are generally lower than measurements. The difference ranges from 33% at $R = 0.250\text{m}$ to 40% at $R = 0.375\text{m}$ for the most contracted parts of the

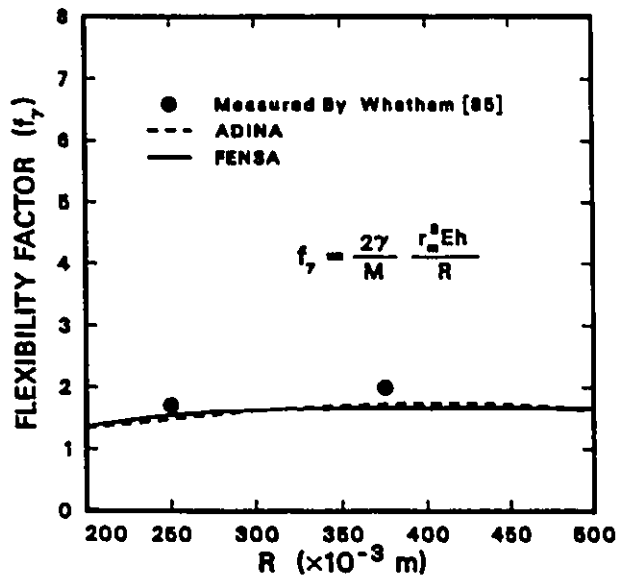


FIG. 4-7 PREDICTED FLEXIBILITY FACTORS OF FLANGED ELBOWS.

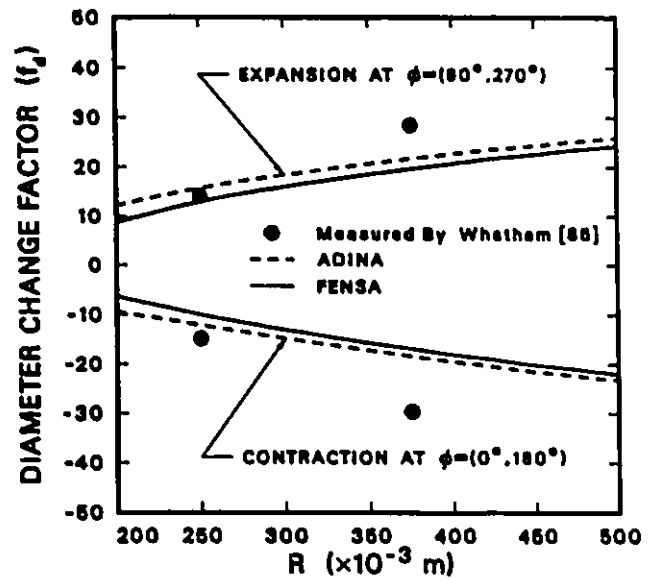


FIG. 4-8 PREDICTED DIAMETER CHANGE FACTORS OF FLANGED ELBOWS ($f_\delta = 2\pi E h r_o / \delta_o$).

Table 4.2: Convergence rate of solution.

Flexibility factor (f_γ)				
Experiment	FENSA			
	Number of elements			
	4	6	12	18
2.00	1.66433	1.66608	1.66692	1.67114
Difference (%)	16.78	16.70	16.65	16.44

cross section (intrados and extrados). This range of differences is observed to be a bit smaller for the most expanded parts ($\phi = 90^\circ$ and $\phi = 270^\circ$).

It is noted that in Figures 4.3 – 4.8 the results from the commercial finite element program ADINA are also given to indicate the validity of the program FENSA. The two sets of FEM results for $\sigma_{\xi\xi}^*$, $\sigma_{\eta\eta}^*$, f_γ , and f_d are found to be virtually identical, especially in Figures 4.3 – 4.7 where the ADINA and the FENSA curves almost coincide. This excellent agreement further validates the program FENSA. It also implies that there are limitations to the capabilities of the elbow element in predicting stresses and ovalizations.

In Table 4.2, the accuracy of the FENSA prediction for the flexibility factor f_γ with $R = 0.375\text{m}$ is monitored as the number of elbow elements is varied. This table shows that the same order of accuracy can be obtained with a mesh having as few as 4 elements. The difference between the FENSA prediction and the measurement is about 16.78% for a mesh of 4 elements, and decreases to 16.44% for a mesh of 18 elements.

4.4 Elastic-Plastic Bending of a Straight Pipe

Thin-walled tubes and pipes subjected to various loading conditions are critical components of power systems and other tubular structures. Basing their work on the Bernoulli-Euler theory, Lau et al. [86] have presented a closed-form solution for the small-deflection analysis of straight thin-walled pipes under the simultaneous actions of bending and twisting moments. Their theoretical results are a useful supplement to finite difference and finite element computer codes for preliminary design and analysis. Nevertheless, since Lau et al. have not taken changes in ovality of the cross section into consideration in the solution, their results are only good in early stages of the solution.

A straight thin-walled pipe subjected to pure bending only is considered in the

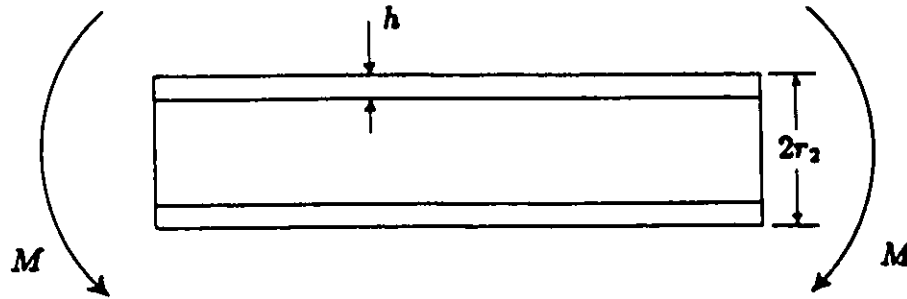


Figure 4.9: Thin-walled straight pipe under pure bending.

present study (Figure 4.9), and the FENSA solution obtained is compared with those given in Reference [S6]. Due to its geometric symmetry, the problem can be modelled as a cantilever beam as in Verification Problem 1, except that the cross section at the fixed end of the beam is now allowed to ovalize, and that a bending moment replaces the concentrated load. A total of 7 equal-sized elements and 22 nodal points are used to simulate the beam. All FENSA results presented are those on the plane of symmetry (fixed end).

The material constants of the pipe are shown in Figure 4.10. In order to make use of the results given by Lau et al., the material is assumed to have a bilinear elastic-plastic behaviour. The moment-curvature results in Figure 4.11 show that there is agreement between the FENSA solution and Lau et al.'s. Up to the elastic limit, an identical response is predicted by both solutions, and at $\kappa/\kappa_y = 8$ only a 7% difference is found in M/M_y predictions. However, these predictions are likely to be inaccurate for large plastic bending moments, especially those after collapse, since both solutions are based on beam theory which neglects effects of cross-sectional deformations.

The results for the longitudinal stress $\sigma_{\eta\eta}^*$ is shown in Figure 4.12. The two solutions show good agreement, especially for $M/M_y = 1$, although differences become slightly larger as M/M_y increases beyond 1. Due to a discontinuity in the first deriva-

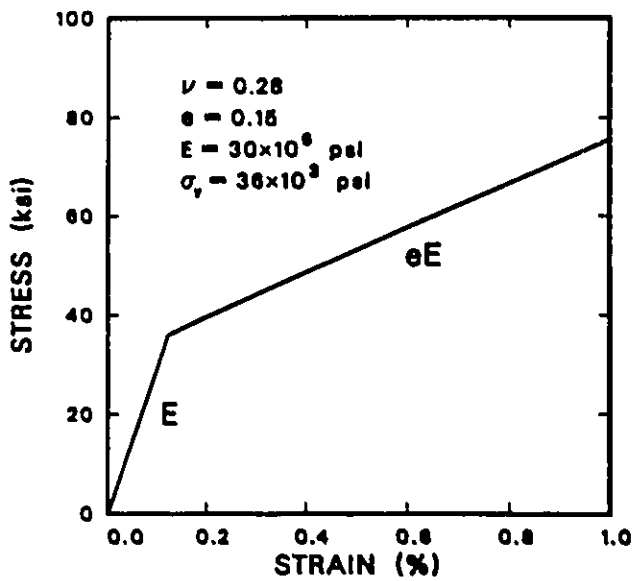


FIG. 4-10
 BILINEAR REPRESENTATION OF UNIAXIAL
 TENSILE STRESS-STRAIN CURVE.
 (1 ft = 0.3048 m, 1 psi = 6895 Pa)

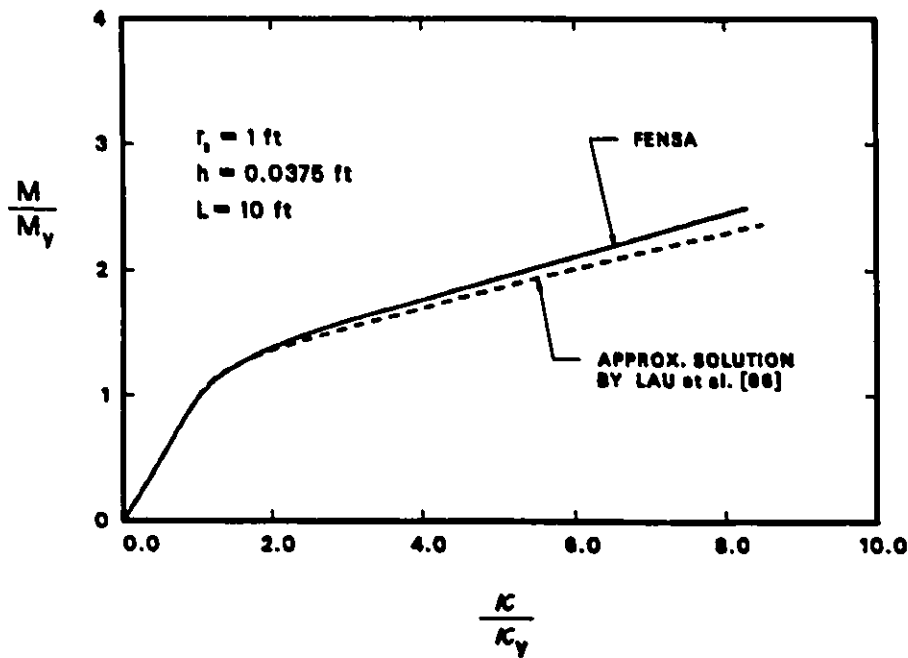
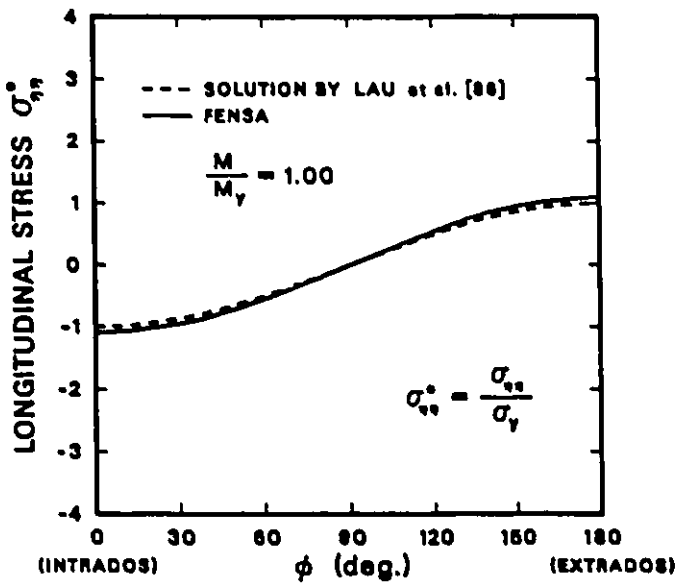
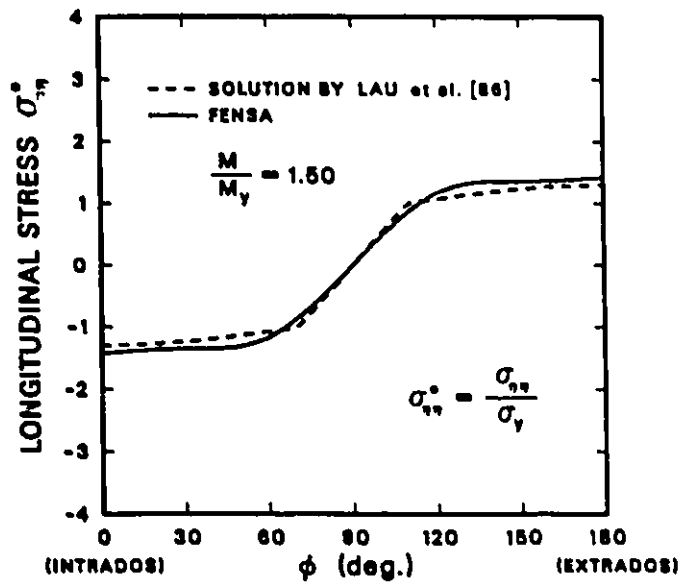


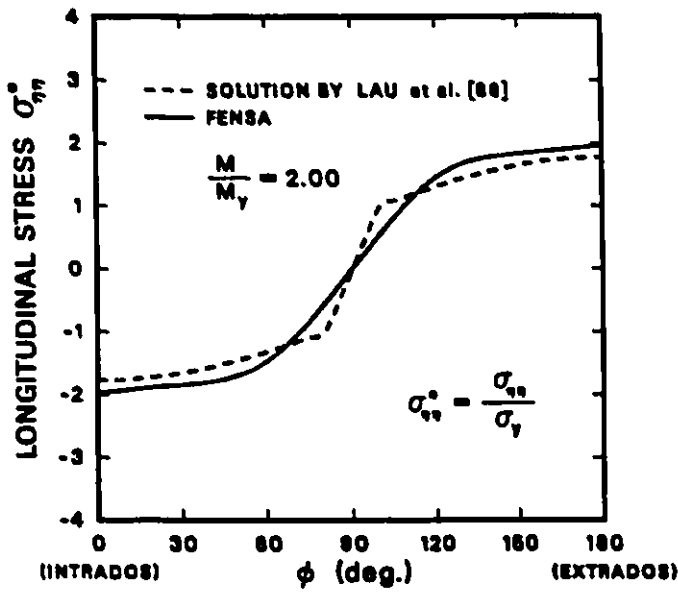
FIG. 4-11 PREDICTED MOMENT-CURVATURE RESULTS FOR STRAIGHT PIPES
 UNDER PURE BENDING (M_y : LIMIT LOAD FOR YIELD INITIATION).



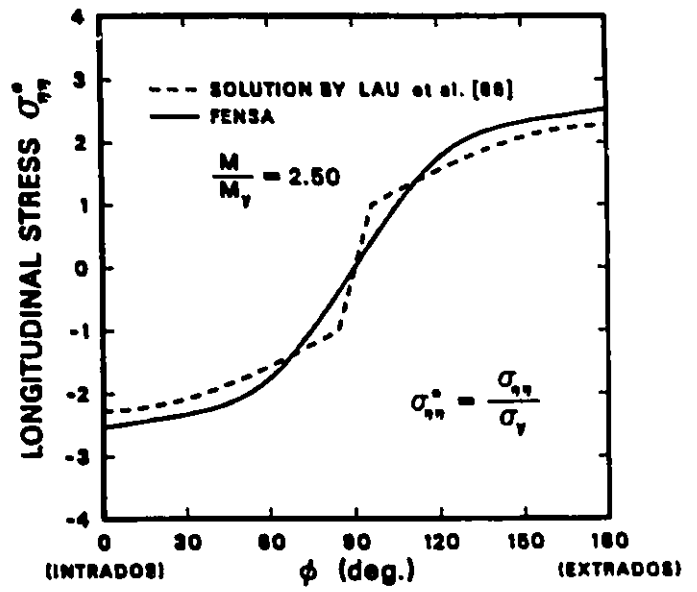
(a)



(b)



(c)



(d)

FIG. 4-12 COMPARISON OF FENSA AND THEORETICAL RESULTS FOR THE LONGITUDINAL STRESSES IN THE MIDDLE SURFACE OF THE PIPE WALL AT VARIOUS LOADINGS.

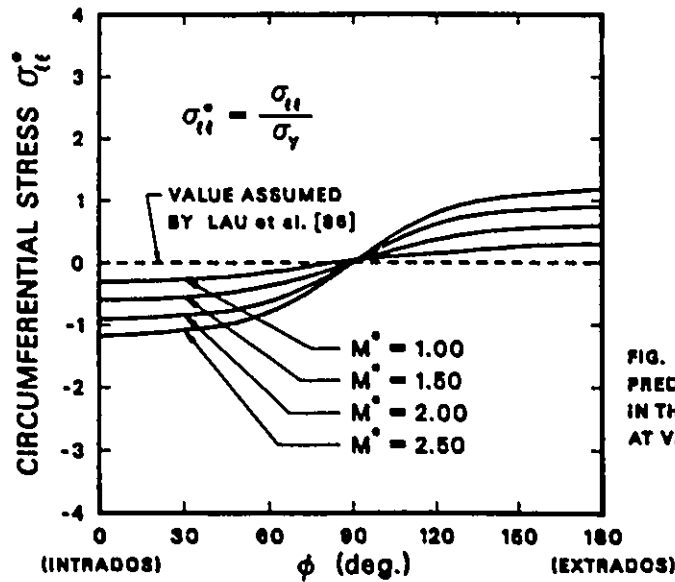


FIG. 4-13
PREDICTED CIRCUMFERENTIAL STRESSES
IN THE MIDDLE SURFACE OF PIPE WALL
AT VARIOUS LOADINGS ($M^* = M/M_y$).

tive of the theoretical solution for $\sigma_{\eta\eta}^*$, at any value of $M/M_y > 1$ two sharp bends near $\phi = 90^\circ$ are observed in the theoretical curve, creating large differences between the theoretical and the FENSA curves. At these bends and their vicinities, the solution given by Lau et al. likely overestimates the value of $\sigma_{\eta\eta}^*$. It is also found that the compressive $\sigma_{\eta\eta}^*$ at $\phi = 0^\circ$ (intrados) and the tensile $\sigma_{\eta\eta}^*$ at $\phi = 180^\circ$ (extrados) are virtually the same, and their value is proportional to the applied bending moment M/M_y .

The results for the circumferential (hoop) stress $\sigma_{\xi\xi}^*$ are presented in Figure 4.13. The values calculated by FENSA are not small nor zero as predicted by Lau et al. in their analysis. These non-zero hoop stresses are mainly due to the bending of the pipe wall as the cross section ovalizes. Figure 4.13 shows that the maximum value of $\sigma_{\xi\xi}^*$ could range from about 0.3 for $M/M_y = 1.0$ to 1.2 for $M/M_y = 2.5$. Thus, in design of piping structures where the hoop stress in the pipe usually plays a central role in causing pipe cracks, the utility of Lau et al.'s solution is doubtful.

The present comparison indicated that the solutions given by FENSA and Lau et al. for the the moment-curvature relationship and the longitudinal stresses are almost equivalent because both are formulated upon beam theory. Differences between predictions for the circumferential stresses are due to small ovalizations of the cross section according to von Karman's hypotheses.

4.5 Elastic-Plastic Bending of a 180° U-Bend

Thin-walled pressurized pipe bends are used extensively in nuclear reactors. These elbows are normally safe if only subjected to bending moments due to the designed working conditions. Under exceptional loadings such as those which arise in earthquakes, the elbows may be under excessive closing or opening moments, or a series of alternate closing and opening moments. Such loadings could lead to failure of the bends and eventually of the whole piping system.

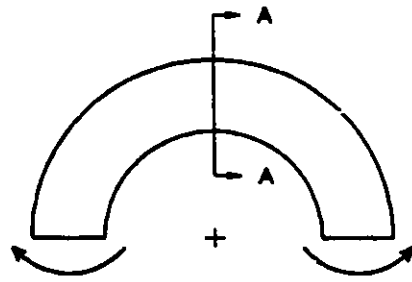
A number of investigations have been carried out on the resistance of pipe bends towards bending moments prior to collapse. Bolt et al. [87] conducted a series of tests to determine the collapse moments for 90° -pipe elbows of different sizes. Vrillon et al. [88] obtained good agreement between experimental data and numerical results from the FEM program TRICO for different U-bends. They found that FEM analysis using 3-D triangular shell elements is very quick and considerably cheaper than full-scale testing of such structures. Roche et al. [89] proposed a simplified method to carry out elastoplastic design of piping systems, with sufficient accuracy and at low cost. The proposed method was implemented in TEDEL which is also a FEM program based on a simplified nonlinear beam model. Bushnell [90] investigated failures of elbows due to the buckling of pipe wall using a modified version of the computer program BOSSOR5. This program simulates the bending of a straight or curved pipes by means of thermal loading.

In the present study, a 180° U-bend earlier tested by Vrillon et al. is analyzed for

end deflections and strains. The elbow is subjected to an in-plane opening moment as shown in Figure 4.14. Owing to symmetry of the U-bend only half of it is considered in the FEM analysis. The resulting 90° bend is modelled by a total of 8 equal-sized elements and 25 nodal points, and ovalizations of the cross section at the fixed end are also allowed. To incorporate data from the stress-strain curve of the material obtained from a tensile test into the program FENSA, the original curve is replaced by a multilinear approximation given in Figure 4.15.

In Figure 4.16, the FENSA calculations for the expansion of the bend diameter D as the applied bending moment increases are compared with experimental data and FEM results from TRICO and TEDEL. There is good agreement between all numerical results and measurements for $0 \leq M \leq 16 \times 10^4$ mN while yielding is observed to begin at about $M = 8 \times 10^4$ mN. Both TEDEL and FENSA overestimate the expansion ΔD for $M \geq 16 \times 10^4$ mN. When M is in this range, the accurate predictions given by TRICO for ΔD can be accounted for by the fact that TRICO employed 3-D triangular shell elements with a very fine mesh (shown in [88]) while TEDEL and FENSA used only pipe-like elements with a relatively small number of elements. It is further noticed that TEDEL [89] required twice as many elements as did FENSA to model the same bend; yet, the cross-sectional deformation of the elbow element implemented in FENSA was not accounted for in the computation process though it might be significant. The advantage of TEDEL may explain the observation that the TEDEL curve is closer to the experimental points than is the FENSA curve.

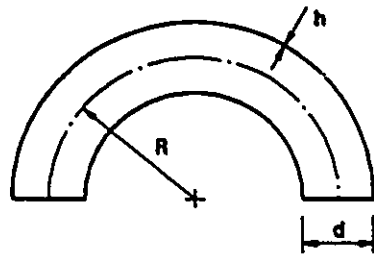
The results for axial strains and hoop strains at the plane of symmetry when $\Delta D = 76$ mm are presented in Figures 4.17 and 4.18, respectively. The experimental measurements were recorded by Bung et al. [91], and the BOSOR5 results were obtained by [90] as mentioned earlier. In general, there is good correlation between FENSA calculations, tests, and BOSOR5 results for both axial and hoop strains. The program FENSA underestimates the outer axial strain when $100^\circ \leq \phi \leq 130^\circ$ while overestimating the outer hoop strain when $80^\circ \leq \phi \leq 110^\circ$, approximately. In both



PLANE OF SYMMETRY A-A

DIMENSIONS

$R = 0.7622 \text{ m}$
 $h = 0.012 \text{ m}$
 $d = 0.512 \text{ m}$



MODELLING

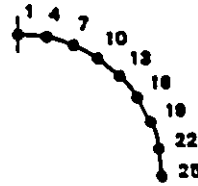


FIG. 4-14 GEOMETRY AND FINITE ELEMENT MODELLING OF A 180° U-BEND UNDER OPENING MOMENT.

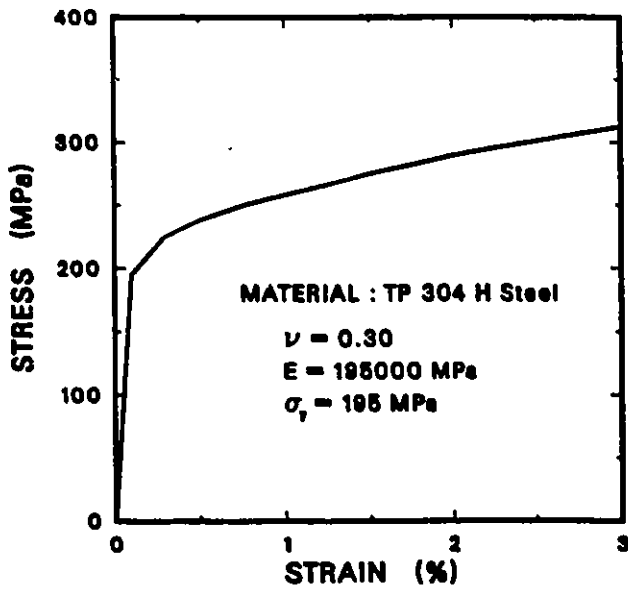


FIG. 4-15
 MULTILINEAR APPROXIMATION OF UNIAXIAL
 TENSILE STRESS-STRAIN CURVE.

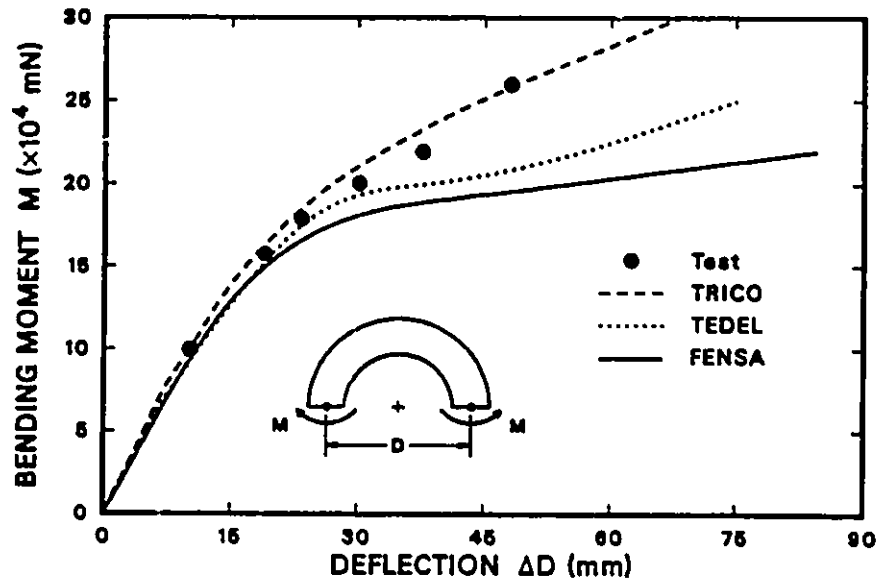


FIG. 4-16 PREDICTED MOMENT-DEFLECTION RESULTS FOR A 180° U-BEND UNDER OPENING MOMENT.

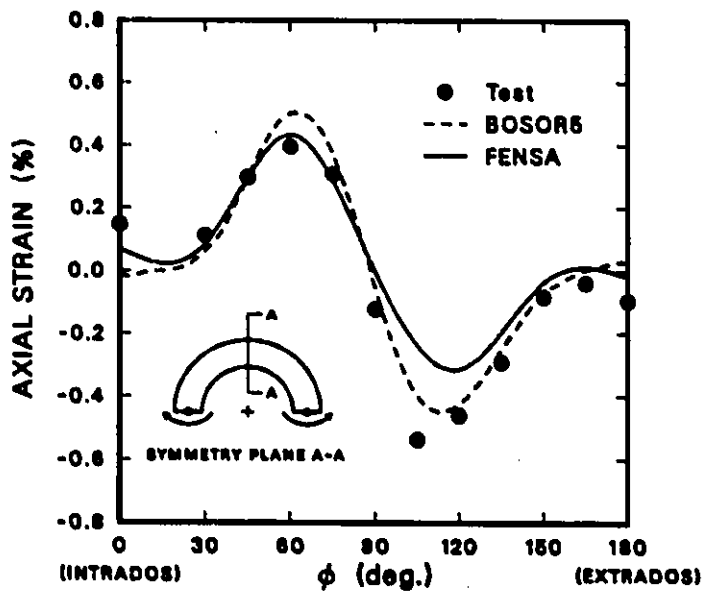


FIG. 4-17 COMPARISON OF FENSA AND EXPERIMENTAL RESULTS FOR OUTER AXIAL STRAINS AT PLANE OF SYMMETRY AND AT $\Delta D = 76$ mm.

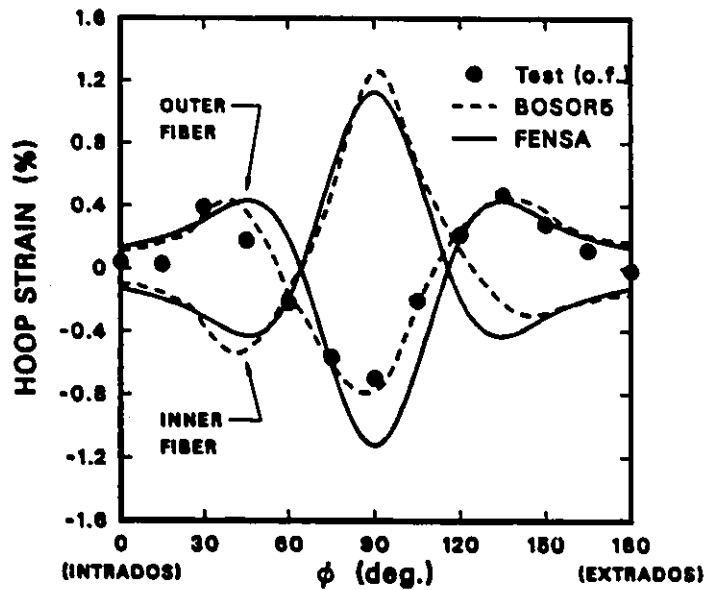


FIG. 4-18 COMPARISON OF FENSA AND EXPERIMENTAL RESULTS FOR HOOP STRAINS AT PLANE OF SYMMETRY AND AT $\Delta D = 76$ mm.

cases, the discrepancies are observed to be as high as 50%. FENSA also predicts identical magnitudes for the hoop strains on the inner and outer surfaces of the pipe as can be seen from Figure 4.18. However, a comparison between the FENSA and BOSOR5 results shows that the hoop strain on the inner surface of the bend is better predicted by FENSA than is the hoop strain on the outer surface.

4.6 Elastic-Plastic Bending of a 90⁰-Elbow with Tangent Pipes

Piping systems consist of straight and curved pipes (elbows), integrated in a complex manner in order to function properly. Those essential components were studied individually in previous sections for their elastic and elastoplastic responses resulting from in-plane bending of the structures. To further verify the program FENSA, this section is devoted to an elastic-plastic analysis of a combination of straight and curved pipes.

The structure to be analyzed is a 90⁰-pipe elbow, the two ends of which are welded to two straight pipes. These straight tangent pipes are of different lengths and thicknesses as shown in Figure 4.19(a). An in-plane closing moment is applied to the lower end of the structure whereas the upper end is fixed to a rigid wall. Sobel and Newman [92] have tested the structure, and then carried out a numerical analysis using the MARC pipe-bend element 17, with 34 intervals in the hoop direction. The MARC prediction for the collapse load is found to be 10% lower than the experimental value. Bathe et al. [5] have also considered this structure using the program ADINA in order to assess the accuracy of their newly developed elbow element in nonlinear analyses.

The whole structure is modelled with a total of 5 elements using the program FENSA. Three elements each spanning 30⁰ are used to simulate the 90⁰ elbow, and each of the two straight segments is simulated by one element, Figure 4.19(b). For

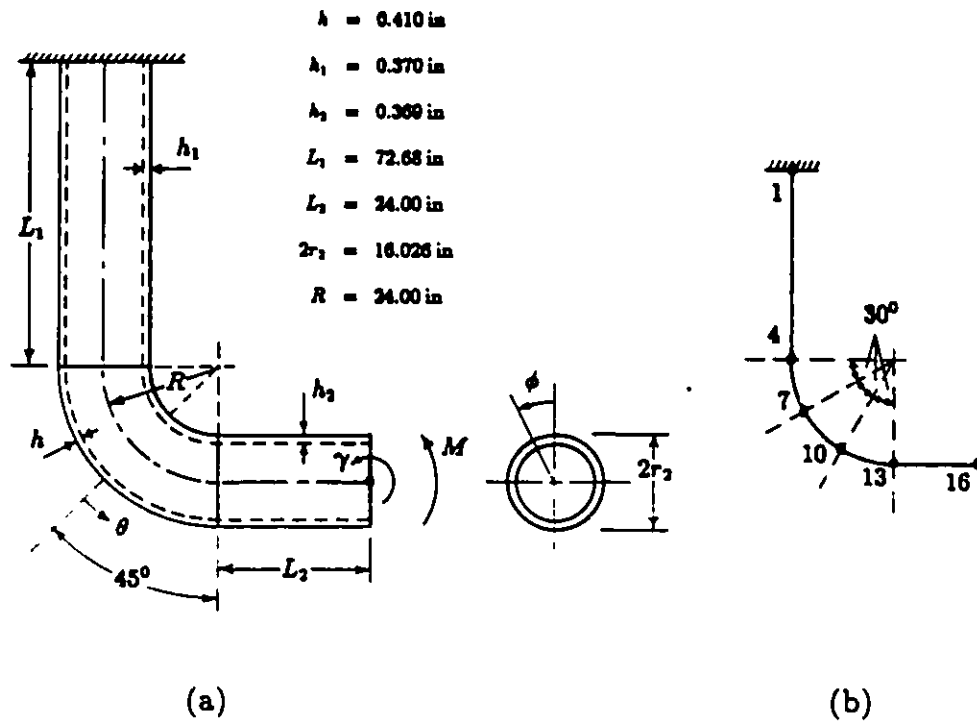


Figure 4.19: Geometry and FEM modelling of a 90°-elbow structure.

computational purposes, the stress-strain curve obtained from a uniaxial tensile test is represented by a multilinear approximation as given in Figure 4.20.

The results for the vertical displacement at the loaded end, the end rotation, and the hoop strains on the inner surface of the elbow at $\theta = 0^\circ$ and at $\phi = (90^\circ, 270^\circ)$ are presented in Figures 4.21 - 4.23, respectively. It should be noted that in this problem the angle θ is measured from the plane of symmetry of the elbow, that is perpendicular to the center line. Excellent agreement is obtained between the FENSA and the experimental results for the end displacement and the end rotation up to the collapse load ($M = 1.28 \times 10^6 \text{ in-lb}$). On the other hand, there is only a fair agreement between the FENSA results and experimental data for the hoop strains. As can be seen from Figure 4.23, FENSA overestimates the hoop strains after yielding has begun. Those discrepancies may be due to the fact that the shape of the cross section is not

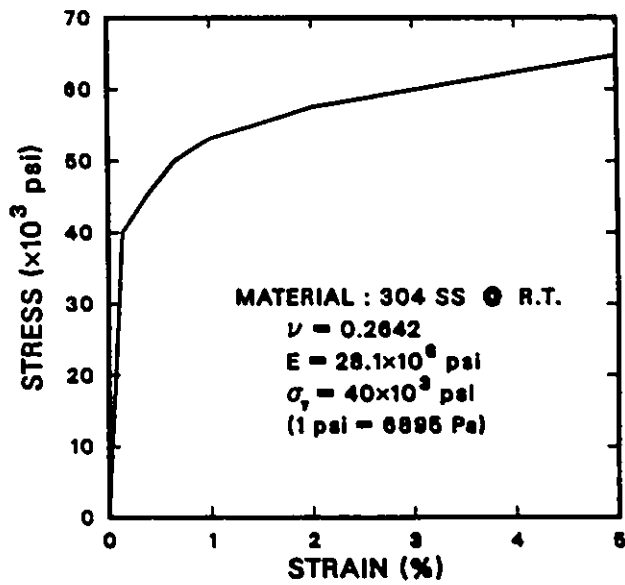


FIG. 4-20 MULTILINEAR APPROXIMATION OF UNIAxIAL TENSILE STRESS-STRAIN CURVE.

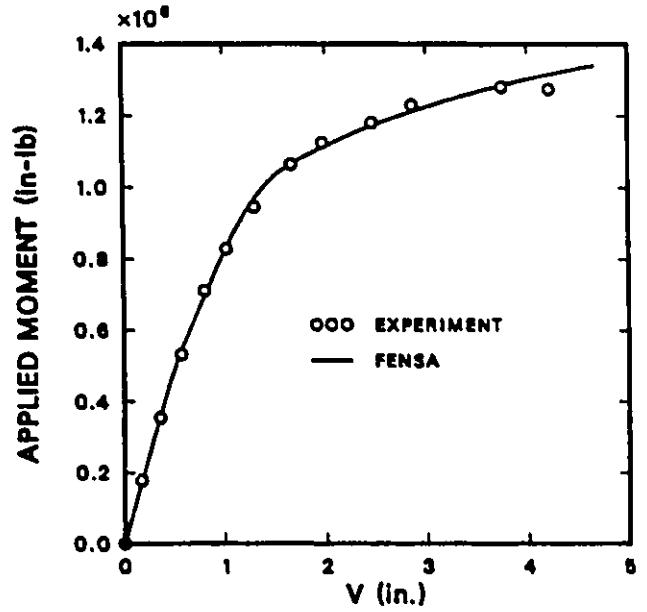


FIG. 4-21 COMPARISON OF FENSA AND EXPERIMENTAL MOMENT-END DISPLACEMENT RESULTS.

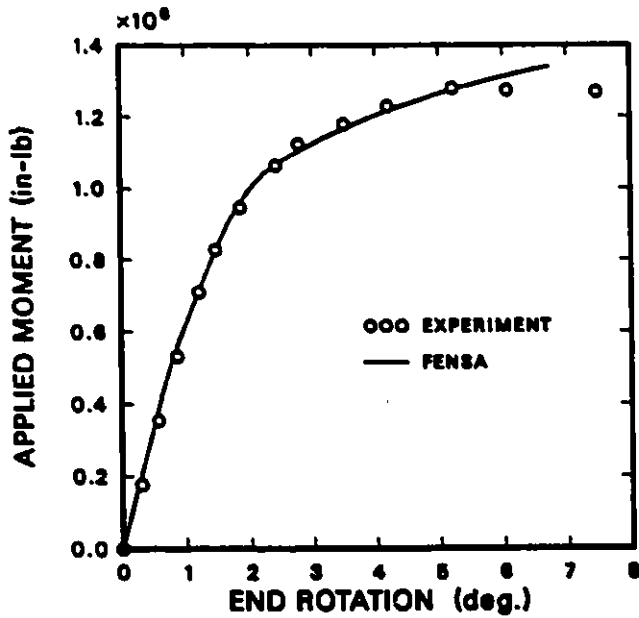


FIG. 4-22 COMPARISON OF FENSA AND EXPERIMENTAL MOMENT-END ROTATION RESULTS.

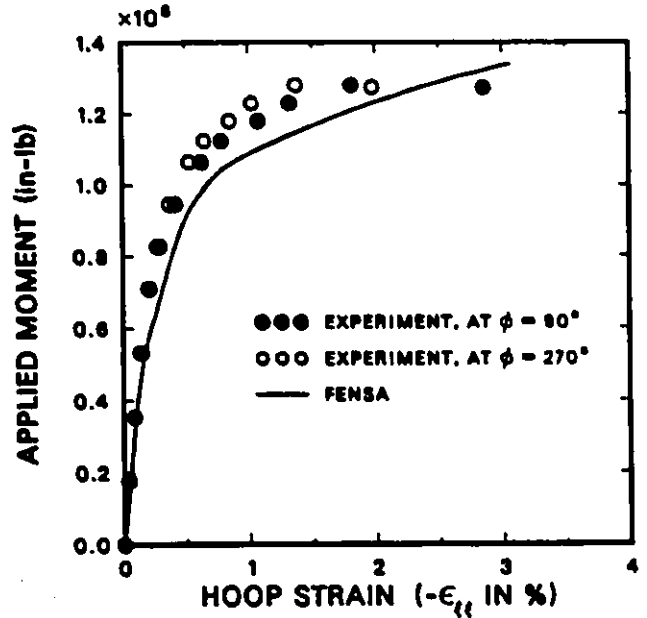
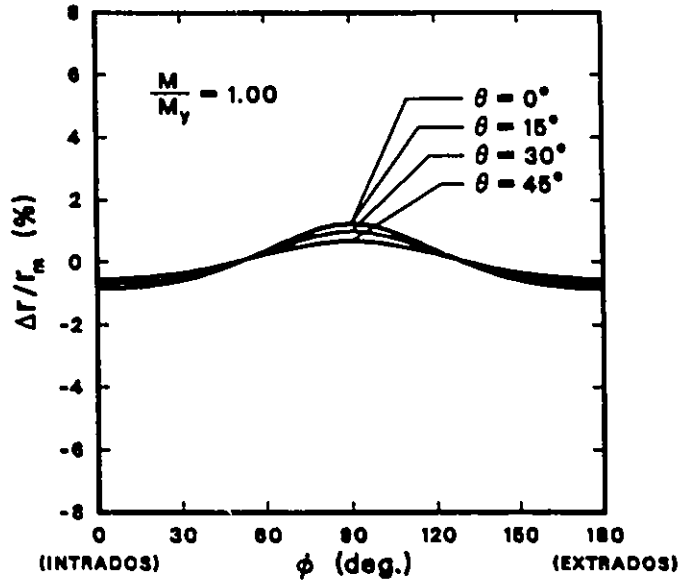


FIG. 4-23 COMPARISON OF FENSA AND EXPERIMENTAL MOMENT-HOOP STRAIN RESULTS (INNER SURFACE)

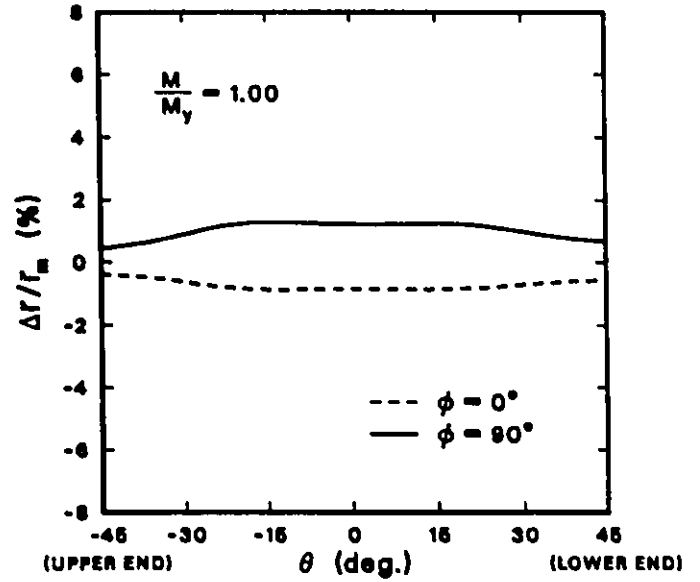
updated in the computation process.

Figures 4.24 - 4.27 give the results for ovalizations around the cross section and along the elbow length for various values of the bending moment M . Although experimental data for ovalizations are not available for comparison, the results obtained in Article 4.2 suggested that the actual radial displacements of the pipe wall could be about twice as high as the FENSA predictions. It is further noticed that while the FENSA predictions for the expansion and the corresponding contraction of a cross section of the elbow are nearly the same in elastic bending (Figure 4.24), the FENSA predictions for the expansion become much larger than those for the contraction in plastic bending. Figure 4.27 shows that for $M/M_y = 2.40$ the FENSA prediction for the maximum expansion (measured by $\Delta r/r_m$) at $\theta = 0^\circ$ is about 14% which is roughly twice that for the the maximum contraction of the same cross section. The trend that the expansion of a cross section is about twice the corresponding contraction in plastic bending was also reported by Prinja and Chitkara [93] when they carried out analyses of post-collapse plastic bending of thick pipes.

In Figures 4.28 - 4.30, the FENSA results for elastic-plastic boundaries are plotted on the inner and outer surfaces, and through the wall thickness in the plane of the pipe bend for different values of M . It is noted from these figures that no experimental results are presented for comparison, and that the FENSA predictions are obtained without the shape of the elbow cross section updated. It should also be recalled that along those boundaries the effective stress computed according to the von Mises yield criterion is equal to the yield stress of the material. At $M/M_y = 2.40$ while the FENSA curves in Figures 4.21 - 4.23 have not levelled off, Figures 4.28 - 4.30 show that the cross section at about $\theta = -15^\circ$ has completely deformed plastically (at $\theta = -15^\circ$, plastic zones cover both the inside and outside surfaces and through the wall thickness), thereby forming a plastic hinge at this position. Due to the effects of strain hardening of the material, the structure may not collapse at $M/M_y = 2.40$, or equivalently $M = 1.278 \times 10^6$ in-lb. However, the value of M/M_y at which the structure

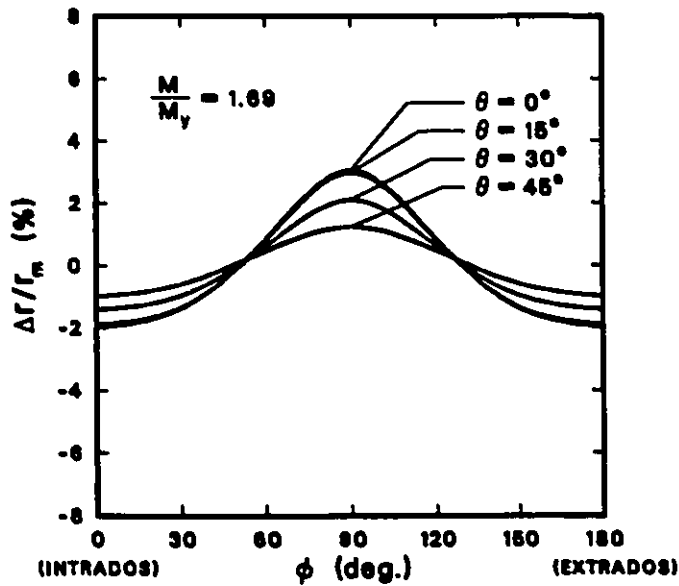


(a)

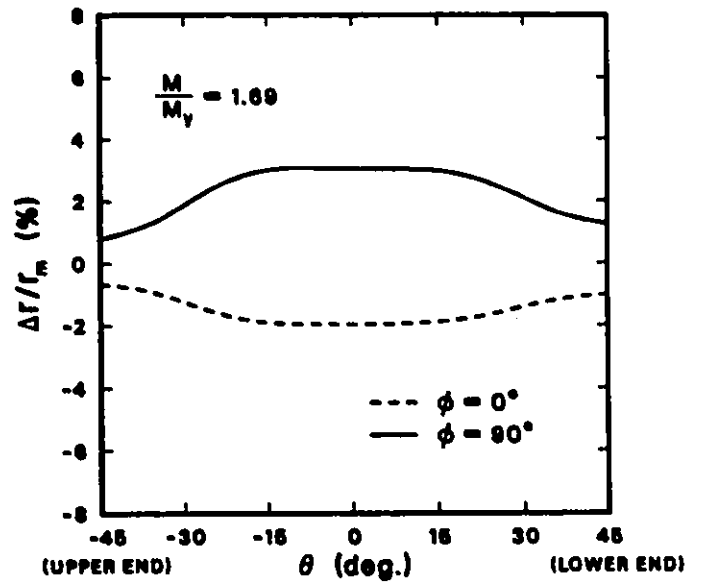


(b)

FIG. 4-24 PREDICTED CHANGES IN CROSS-SECTIONAL MEAN RADIUS (a) AROUND THE ELBOW CIRCUMFERENCE AND (b) ALONG THE ELBOW LENGTH AT $M/M_y=1.00$ (M_y : LIMIT LOAD FOR YIELD INITIATION).

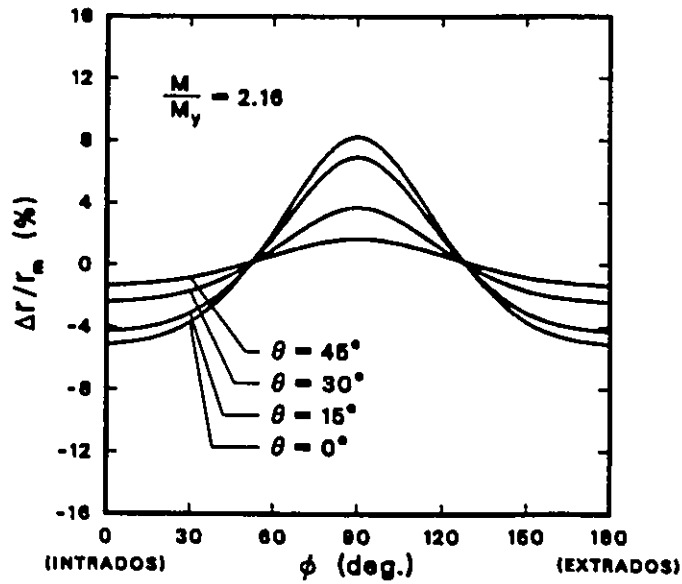


(a)

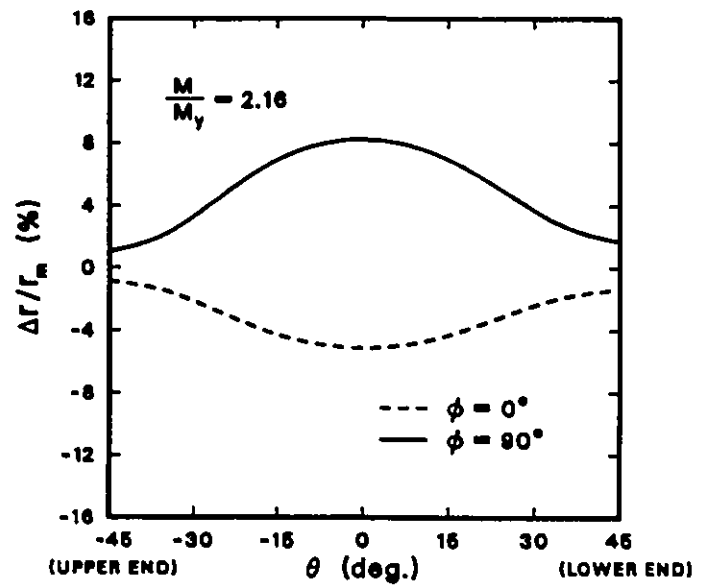


(b)

FIG. 4-25 PREDICTED CHANGES IN CROSS-SECTIONAL MEAN RADIUS (a) AROUND THE ELBOW CIRCUMFERENCE AND (b) ALONG THE ELBOW LENGTH AT $M/M_y=1.69$.

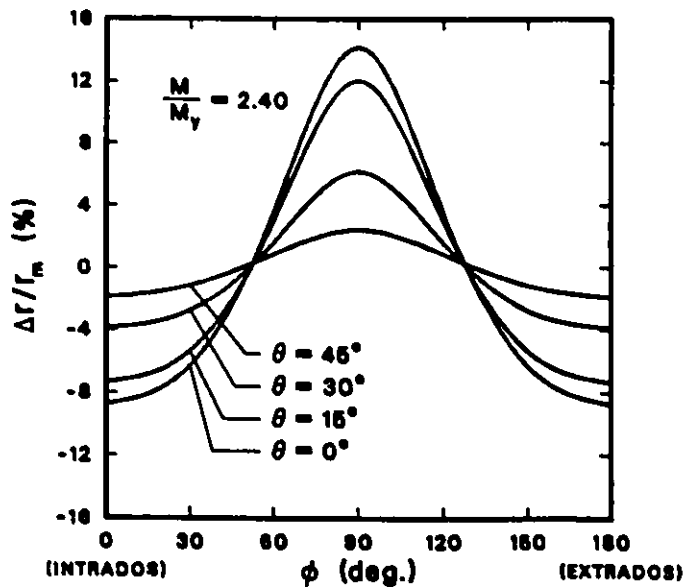


(a)

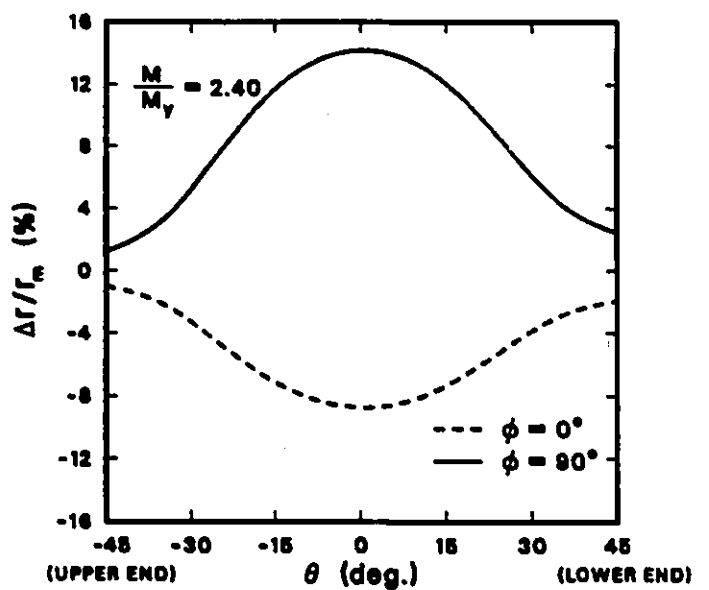


(b)

FIG. 4-26 PREDICTED CHANGES IN CROSS-SECTIONAL MEAN RADIUS (a) AROUND THE ELBOW CIRCUMFERENCE AND (b) ALONG THE ELBOW LENGTH AT $M/M_y=2.16$.



(a)



(b)

FIG. 4-27 PREDICTED CHANGES IN CROSS-SECTIONAL MEAN RADIUS (a) AROUND THE ELBOW CIRCUMFERENCE AND (b) ALONG THE ELBOW LENGTH AT $M/M_y=2.40$.

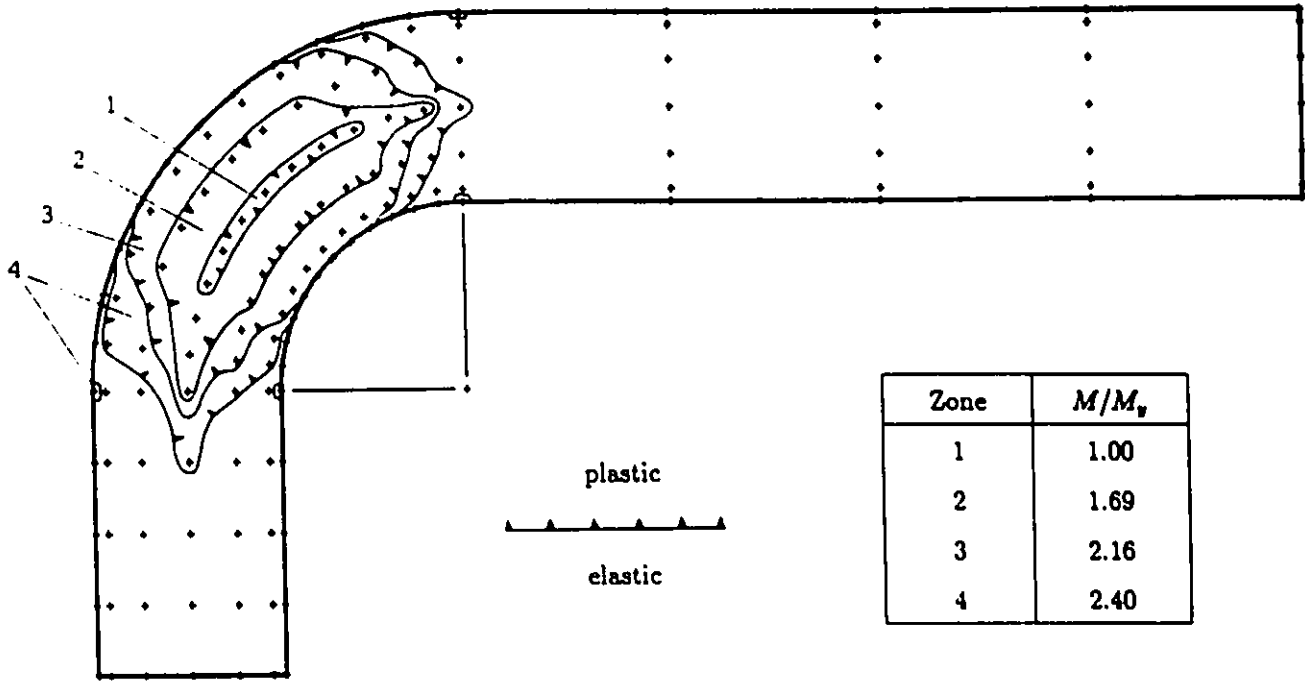


Figure 4.28: Growth of plastic zones on the outside surface.

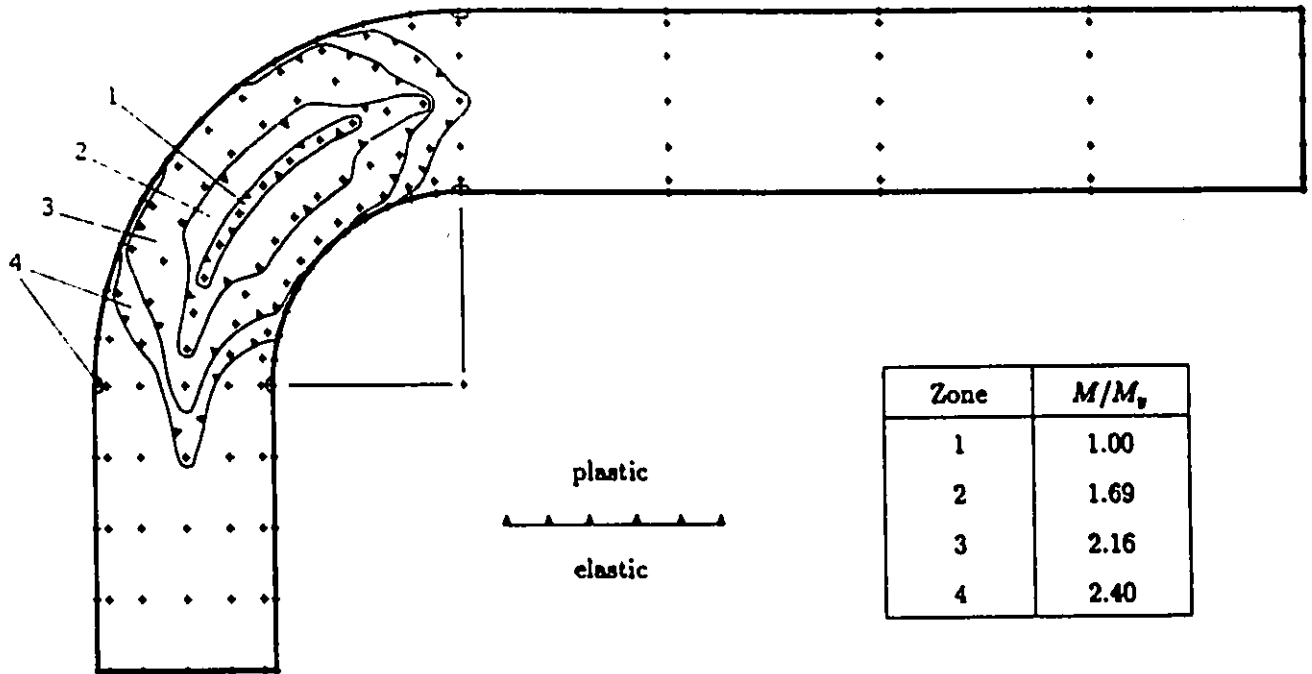


Figure 4.29: Growth of plastic zones on the inside surface.

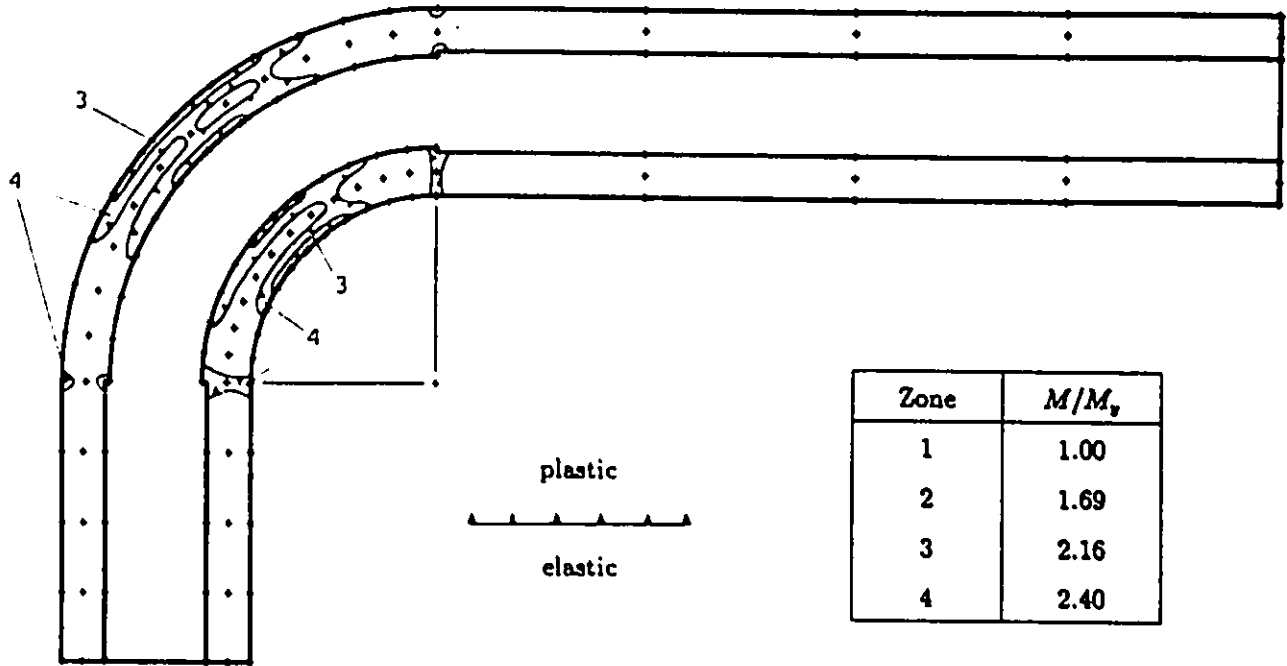


Figure 4.30: Growth of plastic zones through the wall thickness (the thickness is magnified 10 times inward).

Table 4.3: Comparison of collapse loads for a 90° elbow.

Collapse load ($\times 10^6$ in-lb)		Difference (%)
Measured	FENSA	
1.28	1.278	0.156

collapses is expected not to be far from 2.40. The fact that the collapse load measured by Sobel and Newman is 1.28×10^6 in-lb gives good agreement between the prediction given by FENSA and experimental data concerning the collapse load (Table 4.3).

Observations at $\phi = (90^\circ, 270^\circ)$ in Figures 4.28 - 4.29 reveal that yielding occurs simultaneously at those locations on both the inside and outside surfaces. This contradicts an earlier theoretical prediction given by Lang [94] based on the methods of toroidal elasticity. The prediction states that first yielding on the inside surface at $\phi = (90^\circ, 270^\circ)$ occurs just before that on the outside surface at the same locations. The contradiction stems from the fact that the hoop strain $\epsilon_{\xi\xi} = 0$ resulting from cross-section ovalizations is assumed to be zero at $\zeta = 0$. In fact, $\epsilon_{\xi\xi} = 0$ only when $\zeta > 0$ as pointed out by Munz and Mattheck [95]. If this adjustment were made in the formulation of the elbow element, such a contradiction would be eliminated.

It is also important to mention that the yielding which first occurs on the elbow at $\phi = (90^\circ, 270^\circ)$ is mainly due to circumferential bending stresses. This implies that, assuming the material to be free of irregularities, the first crack will be on the elbow along the line represented by $\phi = (90^\circ, 270^\circ)$ as has been observed experimentally by Gross [96].

It is noted that in plasticity the constitutive tensor for stresses and strains is stress-history dependent. For this reason, stresses cannot be directly calculated from experimentally recorded strains. Because of the unavailability of experimental data for stresses, the FENSA stress results in Figures 4.28 - 4.30 are presented merely as supplemental information that may be of general interest.

4.7 Summary of Comparison

In summary, the FENSA program developed herein has been applied to five typical piping problems. The main assumptions in these problems are that the thickness of the pipe (or pipe bend) is constant, and the cross section remains circular annular

throughout the analysis although small radial displacements are allowed.

- For the first two problems that dealt with elastic bending, FENSA calculations for displacements, rotations, ovalizations, and stresses were checked against beam-theory and experimental results. The FENSA predictions were good for displacements and rotations, fair for stresses, and poor for ovalizations.
- For the last three problems that involved plastic bending, the FENSA results for curvatures and stresses were compared with the solution by Lau et al. [S6]. Good correlation was obtained, but both solutions are likely to be inaccurate for large plastic bending since they are based on beam theory. The FENSA results for displacements, rotations, and strains were compared with experimental data. Good agreement was obtained between the FENSA predictions and experimental measurements for pre-collapse loads. So far, FENSA predictions for stresses in the nonlinear range have not been compared with experimental data or with those from a rigorous method.
- The curvature updating scheme presented in Article 3.4 is expected to improve the performance of the elbow element in nonlinear analyses although no comparison has been made with respect to the case where the curvature of the element is assumed to remain constant.

There are still a number of aspects that have not been touched upon in the above testing of FENSA, concerning computational difficulties and other types of loading. For instance, when a pipe is subjected to plastic bending due to a concentrated load, the resulting shear force in the pipe may cause slow convergence or even instability of the incremental solution. It is very important to point out further that due the limitations of the elbow element in modelling boundary conditions, any concentrated load applied to the pipe has to be modelled as if it were applied to the center line of the pipe. Thus, no buckling and no deformations of the pipe wall can be predicted by FENSA. These phenomena can only be studied with shell-type elements or special

elbow-shell elements [74,75]. Nevertheless, the utility of such elements raises the subject of “result accuracy and analysis cost”, that was discussed in detail and clarified in Article 2.4. Therefore, investigations of such phenomena and the utility of any shell-like element are beyond the scope of the present study.

Chapter 5

Ram Pipe Bending

5.1 Introduction

The simulation of the ram pipe bending problem is covered in this chapter. The modelling is done using two methods; beam theory, with the elastic-plastic behaviour taken into consideration [97]; and FEM using the program FENSA. It should be noted that the simulation is only possible if in the ram pipe bending process some active means are taken to ensure that cross-sectional ovalizations are minimal so that the cross section can be assumed to remain circular annular. In addition, changes in the pipe-wall thickness are assumed to be small so that the thickness can be considered as constant in the analysis.

5.2 Simulation Using Elastic-Plastic Beam Theory

The elastic-plastic beam theory method (EPBT) to be used herein was first proposed by Roderick [98] to give an estimate to the plastic deflection of rectangular cross-section beams, with the material assumed to be elastic-perfectly plastic. Roderick and Heyman [99] then extended the theory to include the effect of strain hardening, and gave good experimental support to their theoretical work, particularly for mild steels.

The method has also been used in the structural analyses of beams of other symmetric cross sections [100] – [101] and of non-symmetric cross sections [102] – [103]. It should be noted that the above references by no means represent the complete literature survey of the beam theory approach; they only give a brief background of EPBT, and show how extensively EPBT has been used in elastic-plastic beam analyses.

In the present study, a beam of annular cross section (pipe) with strain hardening material is analyzed using EPBT, Figure 5.1(b). Four major assumptions are made in the analysis:

1. There is a linear variation of longitudinal strain $\epsilon_{\eta\eta}$ across the cross section.
2. Under bending, the only stress component that is significant is the longitudinal stress $\sigma_{\eta\eta}$. Thus yielding is presumed to occur when this stress component reaches the yield stress σ_y of the material. This assumption is only valid for thin-walled pipes.
3. The material has identical bilinear elastic-plastic behaviour for both tensile and compressive parts of the cross section, Figure 5.1(a).
4. The beam is considered as straight throughout the analysis.

It is important to mention that Assumption 2 may introduce errors into the solution due to the neglect of circumferential stresses, and the magnitudes of these errors are greatly dependent on the ovalizations of the cross section. Nevertheless, the assumption can be justified by the fact that in ram pipe bending the angle of rotation per unit pipe length is relatively small compared to those in other types of pipe bending. Accordingly, the cross-section ovalizations are also small. This justification becomes more obvious when the FENSA results are presented (Article 5.4).

Taking symmetry into account, only the upper half of the cross section (Figure 5.1(b)) will be referred to in the following calculations.

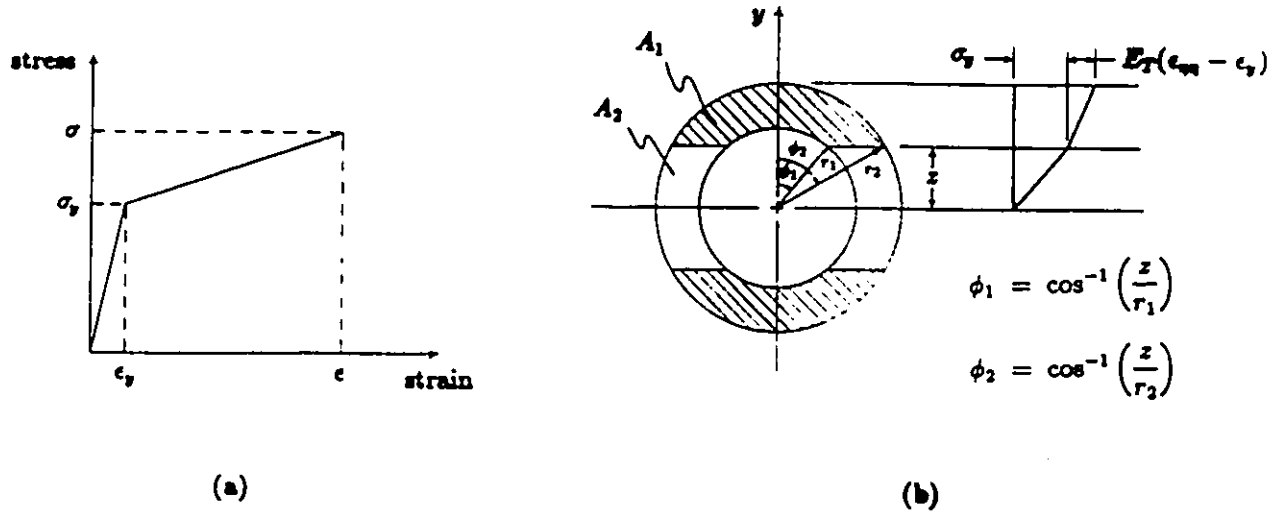


Figure 5.1: Elastic-plastic flexure of beam of annular cross section.

Bending Moment due to Stresses in Elastic Portion

In the elastic portion of the cross section, represented by A_2 of Figure 5.1(b), the longitudinal stress $\sigma_{\eta\eta}$ at any point P (not shown) is simply related to the longitudinal strain $\epsilon_{\eta\eta}$ by Hooke's law. Based on Assumption 2,

$$\sigma_{\eta\eta} = E\epsilon_{\eta\eta}$$

with E being the Young's modulus. According to Assumption 1, $\epsilon_{\eta\eta}$ can be expressed in terms of the yield strain ϵ_y as

$$\epsilon_{\eta\eta} = \epsilon_y \left(\frac{y}{z} \right) \quad (5.1)$$

where y is the vertical coordinate of the point P , and z the distance from the neutral axis to the elastic-plastic boundary.

Substituting the value of $\epsilon_{\eta\eta}$ into the expression of $\sigma_{\eta\eta}$ gives

$$\sigma_{\eta\eta} = E\epsilon_y \left(\frac{y}{z} \right) = \sigma_y \left(\frac{y}{z} \right)$$

The bending moment resulting from stresses in A_2 about the neutral axis is

derived from

$$\begin{aligned}
M_2 &= \int_{A_2} y \sigma_{\eta\eta} dA \quad \text{with } y = \rho \cos \phi \\
&= 2 \int_{\phi_1}^{\phi_2} \int_{r_1}^{z/\cos \phi} \sigma_y \left(\frac{y^2}{z} \right) \rho d\rho d\phi + 2 \int_{\phi_2}^{\pi/2} \int_{r_1}^{r_2} \sigma_y \left(\frac{y^2}{z} \right) \rho d\rho d\phi \\
&= \frac{2\sigma_y}{z} \int_{\phi_1}^{\phi_2} \int_{r_1}^{z/\cos \phi} \rho^3 \cos^2 \phi d\rho d\phi + \frac{2\sigma_y}{z} \int_{\phi_2}^{\pi/2} \int_{r_1}^{r_2} \rho^3 \cos^2 \phi d\rho d\phi \\
&= \frac{2\sigma_y}{z} \int_{\phi_1}^{\phi_2} \left[\frac{\rho^4}{4} \cos^2 \phi \right]_{r_1}^{z/\cos \phi} d\phi + \frac{2\sigma_y}{z} \int_{\phi_2}^{\pi/2} \left[\frac{\rho^4}{4} \cos^2 \phi \right]_{r_1}^{r_2} d\phi \\
&= \frac{\sigma_y}{2z} \int_{\phi_1}^{\phi_2} \left[\frac{z^4}{\cos^2 \phi} - r_1^4 \cos^2 \phi \right] d\phi + \frac{\sigma_y}{2z} (r_2^4 - r_1^4) \int_{\phi_2}^{\pi/2} \cos^2 \phi d\phi \\
&= \frac{\sigma_y}{2z} \left[z^4 \tan \phi - \frac{r_1^4}{2} \left(\phi + \frac{\sin 2\phi}{2} \right) \right]_{\phi_1}^{\phi_2} + \frac{\sigma_y}{4z} \left[(r_2^4 - r_1^4) \left(\phi + \frac{\sin 2\phi}{2} \right) \right]_{\phi_2}^{\pi/2} \\
M_2 &= \frac{\sigma_y}{8z} \left\{ 4z^4 (\tan \phi_2 - \tan \phi_1) + \pi (r_2^4 - r_1^4) + r_1^4 (2\phi_1 + \sin 2\phi_1) - r_2^4 (2\phi_2 + \sin 2\phi_2) \right\}
\end{aligned}$$

Here ϕ_1 and ϕ_2 denote the positional angles of the elastic-plastic boundaries on the inside and outside surfaces of the pipe, and r_1 and r_2 are the inside and outside radii of the cross section, respectively. It should be noted that since the pipe wall is thin, ϕ_1 is very close to ϕ_2 and therefore both ϕ_1 and ϕ_2 could have been replaced by a single ϕ . The reason that ϕ_1 and ϕ_2 are used is to clarify the mathematical derivation of the moment-curvature relationship.

Bending Moment due to Stresses in Plastic Portion

Due to the effect of strain hardening, once the material deforms past the yield point, $\sigma_{\eta\eta}$ is given by

$$\sigma_{\eta\eta} = \sigma_y + E_T (\epsilon_{\eta\eta} - \epsilon_y)$$

with E_T being the strain-hardening modulus. If $\epsilon_{\eta\eta}$ is again replaced by means of (5.1), then

$$\sigma_{\eta\eta} = \sigma_y + E_T \left[\epsilon_y \left(\frac{y}{z} \right) - \epsilon_y \right]$$

$$= \sigma_y + E_T \epsilon_y \left(\frac{y}{z} - 1 \right)$$

Like M_2 , the bending moment M_1 from stresses in the plastic portion (A_1 of Figure 5.1(b)) is determined from

$$\begin{aligned}
M_1 &= \int_{A_1} y \sigma_{\eta\eta} dA \\
&= 2 \int_0^{\phi_1} \int_{r_1}^{r_2} y \left[\sigma_y + E_T \epsilon_y \left(\frac{y}{z} - 1 \right) \right] \rho d\rho d\phi \\
&\quad + 2 \int_{\phi_1}^{\phi_2} \int_{z/\cos\phi}^{r_2} y \left[\sigma_y + E_T \epsilon_y \left(\frac{y}{z} - 1 \right) \right] \rho d\rho d\phi \\
&= 2 \int_0^{\phi_1} \int_{r_1}^{r_2} \left[(\sigma_y - E_T \epsilon_y) \rho^2 \cos\phi + \frac{E_T \epsilon_y}{z} \rho^3 \cos^2\phi \right] d\rho d\phi \\
&\quad + 2 \int_{\phi_1}^{\phi_2} \int_{z/\cos\phi}^{r_2} \left[(\sigma_y - E_T \epsilon_y) \rho^2 \cos\phi + \frac{E_T \epsilon_y}{z} \rho^3 \cos^2\phi \right] d\rho d\phi \\
&= 2 \int_0^{\phi_1} \left[(\sigma_y - E_T \epsilon_y) \frac{\rho^3}{3} \cos\phi + \frac{E_T \epsilon_y}{4z} \rho^4 \cos^2\phi \right]_{r_1}^{r_2} d\phi \\
&\quad + 2 \int_{\phi_1}^{\phi_2} \left[(\sigma_y - E_T \epsilon_y) \frac{\rho^3}{3} \cos\phi + \frac{E_T \epsilon_y}{4z} \rho^4 \cos^2\phi \right]_{z/\cos\phi}^{r_2} d\phi \\
&= 2 \int_0^{\phi_1} \left[\frac{(\sigma_y - E_T \epsilon_y)}{3} (r_2^3 - r_1^3) \cos\phi + \frac{E_T \epsilon_y}{4z} (r_2^4 - r_1^4) \cos^2\phi \right] d\phi \\
&\quad + 2 \int_{\phi_1}^{\phi_2} \left[\frac{(\sigma_y - E_T \epsilon_y)}{3} \left(r_2^3 \cos\phi - \frac{z^3}{\cos^2\phi} \right) + \frac{E_T \epsilon_y}{4z} \left(r_2^4 \cos^2\phi - \frac{z^4}{\cos^2\phi} \right) \right] d\phi \\
&= 2 \left[\frac{(\sigma_y - E_T \epsilon_y)}{3} (r_2^3 - r_1^3) + \frac{E_T \epsilon_y}{8z} (r_2^4 - r_1^4) \left(\phi + \frac{\sin 2\phi}{2} \right) \right]_0^{\phi_1} \\
&\quad + 2 \left[\frac{(\sigma_y - E_T \epsilon_y)}{3} (r_2^3 \sin\phi - z^3 \tan\phi) + \frac{E_T \epsilon_y}{8z} \left\{ r_2^4 \left(\phi + \frac{\sin 2\phi}{2} \right) - 2z^4 \tan\phi \right\} \right]_{\phi_1}^{\phi_2} \\
M_1 &= \frac{2(\sigma_y - E_T \epsilon_y)}{3} \left[(r_2^3 \sin\phi_2 - r_1^3 \sin\phi_1) - z^3 (\tan\phi_2 - \tan\phi_1) \right] \\
&\quad + \frac{E_T \epsilon_y}{8z} \left[r_2^4 (2\phi_2 + \sin 2\phi_2) - r_1^4 (2\phi_1 + \sin 2\phi_1) - 4z^4 (\tan\phi_2 - \tan\phi_1) \right]
\end{aligned}$$

Total Bending Moment

Since M_1 and M_2 have been calculated for only one half of the cross section, the total bending moment M about the neutral axis will be twice the sum of M_1 and M_2 , i.e.

$$\begin{aligned}
 M &= \frac{4(\sigma_y - E_T \epsilon_y)}{3} \left[(r_2^3 \sin \phi_2 - r_1^3 \sin \phi_1) - z^3 (\tan \phi_2 - \tan \phi_1) \right] \\
 &+ \frac{E_T \epsilon_y}{4z} \left[r_2^4 (2\phi_2 + \sin 2\phi_2) - r_1^4 (2\phi_1 + \sin 2\phi_1) - 4z^4 (\tan \phi_2 - \phi_1) \right] \\
 &+ \frac{\sigma_y}{4z} \left[4z^4 (\tan \phi_2 - \tan \phi_1) + \pi (r_2^4 - r_1^4) + r_1^4 (2\phi_1 + \sin \phi_1) - r_2^4 (2\phi_2 + \sin 2\phi_2) \right]
 \end{aligned} \tag{5.2}$$

Figure 5.1(b) indicates that yielding first occurs at $z = r_2$, $\phi_1 = \phi_2 = 0$, and for this point Equation (5.2) reduces to

$$M = M_y = \frac{\pi \sigma_y}{4r_2} (r_2^4 - r_1^4) \tag{5.3}$$

which can also be found from the familiar formula $\sigma = Mc/I$ for bending stress.

It is shown in elementary texts on the Strength of Materials that the curvature $\kappa = 1/R$ of the beam at the cross section under consideration is given by

$$\kappa = \frac{\epsilon_{\eta\eta}}{y}$$

which is valid for $0 \leq \epsilon_{\eta\eta} \leq \epsilon_y$. In extreme cases with y denoting the distance from the neutral axis to the elastic-plastic boundary,

when $y = z$

$$\kappa = \frac{\epsilon_y}{z} \tag{5.4}$$

when $y = r_2$

$$\kappa_y = \frac{\epsilon_y}{r_2} \tag{5.5}$$

where κ_y is the curvature at initial yield in the cross section.

Dividing (5.4) by (5.5), the ratio of the two curvatures is found to be

$$\frac{\kappa}{\kappa_y} = \frac{r_2}{z} \tag{5.6}$$

By introducing the non-dimensional parameters

$$r = \frac{r_1}{r_2} \quad e = \frac{E_T}{E} \quad k = \frac{\kappa}{\kappa_y} \quad m = \frac{M}{M_y} \quad (5.7)$$

the moment-curvature relationship can now be represented non-dimensionally with the substitution of (5.3), (5.6), and (5.7) into (5.2):

$$m = k + \frac{1-e}{\pi(1-r^4)} \left\{ \frac{16}{3} [\sin \phi_2 - r^3 \sin \phi_1] - k [(2\phi_2 + \sin 2\phi_2) - r^4 (2\phi_1 + \sin 2\phi_1)] - \frac{4}{3k^3} [\tan \phi_2 - \tan \phi_1] \right\} \quad (5.8)$$

where ϕ_1 and ϕ_2 become

$$\phi_1 = \cos^{-1} \left(\frac{z}{r_1} \right) = \cos^{-1} \left(\frac{r_2 z}{r_1 r_2} \right) = \cos^{-1} \left(\frac{1}{rk} \right)$$

$$\phi_2 = \cos^{-1} \left(\frac{z}{r_2} \right) = \cos^{-1} \left(\frac{1}{k} \right)$$

For thin pipes with wall thickness $h \ll r_2$, the following simplifications can be made

$$r^n = \left(\frac{r_1}{r_2} \right)^n = \left(\frac{r_2 - h}{r_2} \right)^n = \left(1 - \frac{h}{r_2} \right)^n \simeq 1 - n \left(\frac{h}{r_2} \right)$$

$$\phi_2 \simeq \phi_1 = \phi$$

which lead to

$$m = k \left\{ 1 + \frac{1-e}{\pi} (\sin 2\phi - 2\phi) \right\} \quad (5.9)$$

To visualize the moment-curvature relationship, Equation (5.8) is plotted for $r_m/h = 25$ with various values of $e = E_T/E$, and is shown in Figure 5.5. As can be seen from this figure, all curves originate from the same line for $0 \leq k \leq 1$ and then branch out to different paths because of the effect of strain hardening. For $e = 0$ that corresponds to the elastic-perfectly plastic material idealization, the curve appears as a horizontal line for $1 \leq k$ as would normally be expected.

It is also worthwhile to note that these results are almost identical to those obtained earlier by Lau et al. [86] for thin-walled pipes using an approximate method

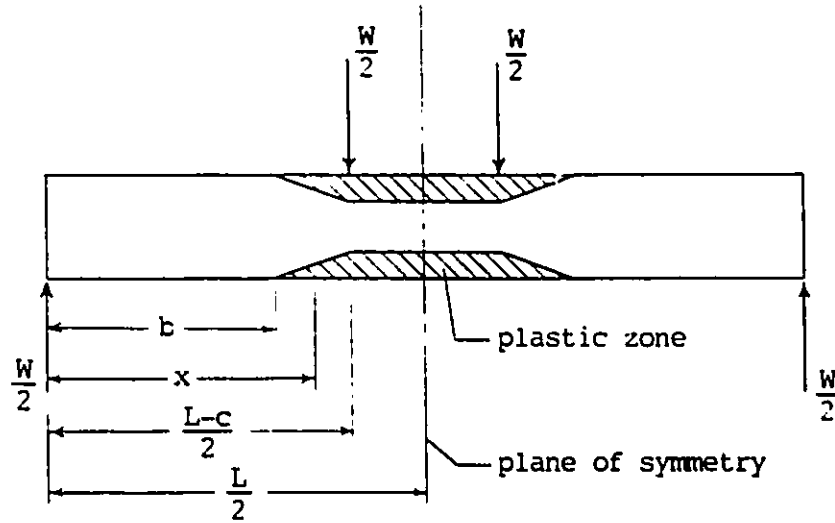


Figure 5.2: Simply supported beam under a symmetrical two-point loading.

based on the beam theory. On the other hand, larger deviations between the two results would be expected for $r_m/h < 10$ since the solution given in [86] is only good for thin pipes ($10 \leq r_m/h$). Nevertheless, the agreement just mentioned already gives some confidence in EPBT.

The moment-curvature relationship represented by (5.8) will serve as the basic equation. From it such important information as the slope and the deflection of the beam as well as the growth of the plastic zones in a particular cross section and along the length of the beam will be found, given the loading conditions. Ram bending can be modelled as a simply supported straight beam under a symmetrical two-point loading as shown in Figure 5.2.

In this figure, the bending moment in the beam is maximum and remains so at locations between the two concentrated loads. At first yielding (Figure 5.3), the bending moment is simply calculated from

$$M_y = \frac{1}{4} W_y (L - c) \quad (5.10)$$

where W_y is the yielding load, L the total length of the beam, and c the distance between the two concentrated loads. Physically, c represents the width of the ram of the bender.

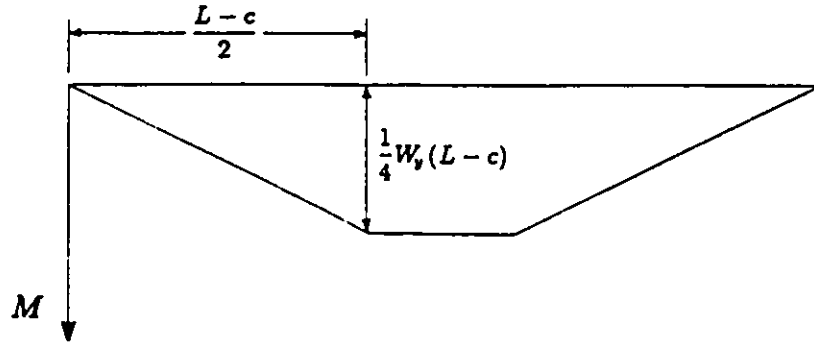


Figure 5.3: Bending moment diagram of the beam for $W = W_y$.

As the plastic zones spread sideways to the two ends of the beam, the yielding moment M_y at the cross sections separating the purely elastic and elastic-plastic parts of the beam is similarly determined by

$$M_y = \frac{1}{2}Wb \quad (5.11)$$

which infers from (5.10) that

$$b = \left(\frac{L-c}{2}\right)\frac{W_y}{W}$$

with b representing the length of the purely elastic parts of the beam. Also, the bending moment at some cross section that is partially plastic is equal to

$$M = \frac{1}{2}Wx$$

where x is the distance from the cross section to the nearer end of the beam. The above expression is combined with (5.11) to yield

$$\frac{M}{M_y} = \frac{x}{b} = \left(\frac{2x}{L-c}\right)\frac{W}{W_y} \quad (5.12)$$

By replacing k and m in (5.8) using Equations (5.6) and (5.12), respectively, and by denoting the right-hand side of (5.8) as $f(k)$, Equation (5.8) can now be rewritten in the shorter form

$$\left(\frac{2x}{L-c}\right)\frac{W}{W_y} = f\left(\frac{r_2}{z}\right)$$

or equivalently,

$$z = \frac{r_2}{f^{-1}\left\{\left(\frac{2x}{L-c}\right)\frac{W}{W_y}\right\}} \quad (5.13)$$

This last equation dictates the shape of the plastic zones for a particular value of W/W_y . Unfortunately, z cannot be explicitly expressed in terms of W/W_y as finding a closed form for $f^{-1}(k)$ in Equation (5.13) is not possible. Therefore, the determination of $f^{-1}(k)$ will be carried out numerically with a sufficiently large number of points. Once z is known, the curvature of the beam at any cross section of the beam can be readily computed from Equation (5.4).

It is well established in the Strength of Materials that the slope and the deflection of an initially straight beam may be determined from its curvature using the basic differential equation

$$k = -\frac{d^2\delta}{dx^2} \quad (5.14)$$

with δ being the deflection of the beam. Again due to the fact that no closed form of $f^{-1}(k)$ could be found, indefinite integration of (5.14) for $W/W_y \geq 1$ would have to be carried out numerically with appropriate boundary conditions from the problem. A small computer program (Appendix C) has been written to find the inverse of $f(k)$, and the slope and the deflection of the beam based on (5.14). On the other hand, for $W/W_y \leq 1$ Equation (5.14) can be integrated exactly using some elementary method [104]; thus, closed-form expressions for the slope and the deflection can be obtained. In the limiting case $W/W_y = 1$, numerical results are found to be nearly identical to the those from the closed-form solution.

Although the beam deflection is only a quantity of minor interest, it is also calculated for comparative purposes. The present study is more concerned with factors that have more practical value, such as the growth of the plastic zones in the beam with increasing loading and the final pipe rotation achievable after the removal of applied loads. These results are further discussed in Article 5.4, following the description of the FEM simulation.

5.3 Simulation Using Program FENSA

Owing to the symmetry of the ram bending problem, only half of the pipe needs to be modelled. Specifically, the problem simplifies to the analysis of a cantilever beam. Two possibilities are considered for the modelling of the loading.

One possible choice for the loading is a set of two opposite concentrated forces, one at the free end of the beam and the other near the fixed end (Figure 5.4(a)). For this choice the beam is subjected to shearing, that has been found in this study to cause slow convergence or instability in the nonlinear numerical solution. This phenomenon has been referred to as “element locking” [105,106]. The effect of “element locking” can be avoided by not integrating the shear strain ‘exactly’ [9], but this treatment would render the element unreliable. This computational difficulty with the elbow-type element has not been noted previously in the literature. Since the pipe is normally quite long compared with the other two dimensions, the deflection or rotation of the beam due to shear force is very much smaller than that due to bending moment. Using the energy method, the central deflection of the beam is found to be of the order of 10^{-10} the value due to bending moment for $L/r_m = 10$ and $r_m/h = 10$ (in the linear range). As a result, another model is considered for the FEM simulation.

The second choice for the loading is a set of concentrated moments along the beam, Figure 5.4(b). This choice is equivalent to the first in most respects because the two concentrated loads have been replaced by a series of equivalent bending moments at every nodal point to the right of the concentrated load near the fixed end. The values of the moments M'' are taken as twice those of the moments M' . Such a replacement has completely eliminated the shear effects due to the concentrated loads in the first choice.

In the numerical solution, 10 elbow elements with a total of 31 nodal points, all equally spaced, are used. In actual ram bending, the central part of the pipe is restrained by the ram, and the two ends are restrained by ring supports. Therefore, it

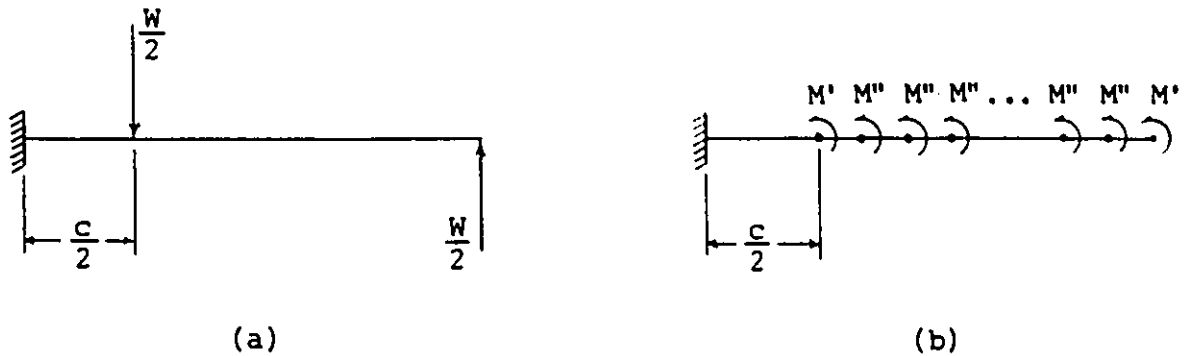


Figure 5.4: Models of ram pipe bending.

is assumed that there is no change in ovality of the cross section at these locations.

5.4 Comparison of EPBT and FENSA Results

Figures 5.6 – 5.8 show the FENSA results together with those from EPBT in the previous section for $L/r_m = 20$, $r_m/h = 25$, and $c/r_m = 2$.

Figure 5.6 gives the load-central deflection results for the pipe both in the linear range and beyond the elastic limit. Generally speaking, there is good correlation between EPBT and FENSA predictions on loading and unloading paths although some slight deviations have been observed in the unrecoverable displacements after springback. On the unloading path starting from $W/W_y = 1.5$, the permanent deflections of the central section predicted by the two methods differ by 10%. However, such a difference is quite likely to occur, and could be considered to be acceptable in view of the fact that springback accounts for about 74% of the total deflection.

The results for ovalization of the cross section for various values of W/W_y are presented in Figure 5.7. The radial displacements of the middle surface of the pipe wall are generally of the order of 10^{-5} the cross-sectional mean radius. Maximum changes in ovality of the cross section are found to be at $x/L = 0.3$ from either end of the pipe. For $0.45 \leq x/L \leq 0.5$ which represents the part of the pipe restrained by the ram, there is no ovalization ($\Delta r/r_m = 0$) as previously assumed in the FEM modelling. For

$W/W_y = 1.5$, $\Delta r/r_m$ has a maximum value of 5×10^{-5} (or $5 \times 10^{-3}\%$) which corresponds to a final beam rotation of 1.5° (or 0.25° per meter of pipe length). Assuming there is a linear variation between the pipe rotation and the radial displacement of the pipe wall, a final beam rotation of 15° would imply that $\Delta r/r_m = 5 \times 10^{-4}$ (or 0.05%) which is equivalent to 0.1% if the change in ovality is measured by $(r_m^+ - r_m^-)/r_m$. Since FENSA results are low for ovalization, the actual change in ovality which may be up to twice as much as the FENSA prediction is still well below the maximum allowed ovality of 1% according to "VGB-Dampftechnik GmbH, Essen" [54]. The magnitude of the maximum ovalization also gives support to Assumption 2 made in Article 5.2, and further implies that the pipe would be free of cracks caused by hoop stresses.

Figure 5.8 shows the shape of the plastic zones plotted for the lower left quarter of the pipe. Initially, the plastic zones develop at the plane of symmetry where the maximum bending moment takes place, and spread outward to the two ends of the pipe. Also seen from this figure is that the plastic zones predicted by FENSA are somewhat smaller than those by EPBT. The elastic-plastic boundaries for $W/W_y = 1.3$ and $W/W_y = 1.5$ given by FENSA are very close to the ones for $W/W_y = 1.2$ and $W/W_y = 1.4$ given by EPBT, respectively.

One obvious explanation for such differences is that in the FENSA solution the von Mises yield criterion was used, which takes into account all stress components. As a result, the effective stress is often smaller than the largest stress component while EPBT assumes the longitudinal stress $\sigma_{\eta\eta}$ to be the only significant stress, and uses it as the effective stress. Therefore, FENSA is more likely to give the true picture of the plastic zones than EPBT. On the other hand, predictions from EPBT tend to be on the safer side if the growth of the plastic zones is of major concern in the forming process.

It should be mentioned further that as W/W_y increases the plastic zones grow toward the neutral axis as well. It is expected that a plastic hinge would eventually form at the intersection of the neutral axis and the plane of symmetry, and then the

pipe would collapse. As implied from Equation (5.4), such a plastic hinge would require that the curvature κ approach to infinity, which is not possible from a practical point of view. Thus if the pipe fails, the failure will be due to buckling of the pipe wall (wrinkles).

Wall buckling of tubes and thin pipes subjected to bending has been studied by many researchers, for example [107] - [110]. In the present study, the program FENSA developed adopted the critical stress proposed by Brazier [107]

$$\sigma_{cr} = 0.320 \left(\frac{Eh}{r_m} \right)$$

as a means to detect buckling. This value is lower than the ones given later in [108] and [109]. In the computation process of the solution, stresses at all integration points on the middle surface of the pipe wall are checked for possible buckling. It was found that at $W/W_y = 1.5$ the maximum compressive stress calculated for these points is about $1/7$ the critical value σ_{cr} determined from the above formula. It is therefore expected that no buckling would occur if W/W_y were increased to 4 or 5 times as large. These are the highest values selected to appear in Figures 5.11 - 5.22.

For the set of data under consideration, buckling of the pipe wall is possible if $r_m/h = 25$ and $W/W_y \geq 10.5$, or $r_m/h \geq 25$ and $W/W_y = 10.5$. It should be noted that $r_m/h = 25$ chosen herein is considered as an extreme value for checking buckling. Typical values of r_m/h of pipe bends produced by ram bending or by other methods are about or below 20, thus allowing the value of W/W_y to be slightly higher than 10.5. Therefore, as far as buckling is concerned, it would theoretically be safe if Figures 5.11 - 5.22 were used because therein $r_m/h \leq 20$ and $W/W_y \leq 10$.

Presented in Figures 5.9 - 5.10 are the FENSA predictions for residual stresses in the pipe at the plane of symmetry. On both inner and outer surfaces of the pipe, the residual circumferential stress $(\sigma_{\xi\xi}^*)_{res}$ is observed to be maximum at $\phi = (0^\circ, 180^\circ)$, and is about $1/6$ the corresponding $\sigma_{\xi\xi}^*$ obtained at $W/W_y = 1.5$ on the loading path. Meanwhile, not only is the maximum longitudinal stress $\sigma_{\eta\eta}$ at $\phi = (0^\circ, 180^\circ)$ reduced in magnitude after springback, its sign is also reversed, leaving the maximum residual

$(\sigma_{\eta\eta}^*)_{res}$ at $\phi = (60^\circ, 120^\circ)$ which is found to be about $1/5$ the corresponding $\sigma_{\eta\eta}^*$ at the same locations. The sign reversal of $\sigma_{\eta\eta}^*$ in the vicinities of $\phi = (0^\circ, 180^\circ)$ is mainly due to relatively large springback of the pipe, which induces an opposite bending moment even after the removal of the applied loading. As W/W_y is increased further, springback becomes relatively smaller; hence, the $\sigma_{\eta\eta}^*$ and $(\sigma_{\eta\eta}^*)_{res}$ distributions would be expected to have similar patterns.

5.5 Computed Results for Practical Cases

In ram bending and a few other bending processes, a major concern is how to control and predict springback. The finite element program FENSA developed in the study can give an estimate of springback in addition to other aspects of pipe bends. On the other hand, with the agreement obtained in Figure 5.6 the final bend angle after springback can be calculated much less expensively using EPBT. This alternative by no means implies that the use of FENSA in the bending process has been taken over by EPBT. Rather EPBT is used as a secondary tool of analysis to save time and resources whenever possible.

In Figures 5.11 - 5.22, the applied load W/W_y has been plotted against the 'specific' final pipe rotation (rotation per unit pipe length) for different ratios of L/r_m and r_m/h . The ratios used represent typical values of pipe bends handled by most bend manufacturers [54], and the curves tabulated are expected to be of practical value. With these charts, the ram force required to form a certain bend (after springback) from a straight pipe can be determined in advance from the geometric dimensions of the pipe.

Figures 5.11 - 5.16 represent the case in which the ram width c is proportional to the pipe mean radius r_m ($c/r_m = 2$). For any particular value of L/r_m , the specific final rotation increases as the ratio r_m/h decreases. Physically, smaller values of r_m/h mean thicker pipe walls, thus allowing more plastic flow and larger plastic deformation but

less springback. As L/r_m increases, the curves representing different values of r_m/h are slowly shifted to the left, indicating a decrease in the specific final rotation. It is also noted from these figures that the specific final rotation is zero at $W/W_v \leq 1$, which represents the range of elastic loading with any deformation of the pipe completely recoverable.

Presented in the Figures 5.17 - 5.22 are the results for the case in which the ram width c is a constant, regardless of the size of the pipe cross section. The trends of the curves in these figures are observed to be the same as those in Figures 5.11 - 5.16. A comparison of the two sets of figures indicates that the specific final rotation increases with the ram width c . This observation can be explained by the fact that as c is increased, the part of the pipe with the maximum bending moment is widened and the plastic zones are enlarged, thereby permitting larger plastic deformation. From a practical viewpoint, the case with c being a constant does not seem realistic; in practice, the size of the ram chosen normally depends on the cross-section diameter of the pipe as in the case of Figures 5.11 - 5.16. The results in Figures 5.17 - 5.22 are calculated mainly to study the effect of the parameter c on the specific final rotation.

It should be mentioned that the deviation of the results presented in Figures 5.11 - 5.22 from experimental values is expected to be less than 10% as W/W_v gets higher. This expectation is based on the comparison of the EPBT and FENSA results as shown in Figure 5.6, and on the experimental work of Roderick and Heyman [99]. They showed that for $E_T/E \geq 0.08$ the deflection results calculated for a rectangular cross-section beam using EPBT are almost identical to the experimental measurements. The value of $e = E_T/E$ used in Figures 5.11 - 5.22 is 0.15 while typical values of e are expected to be slightly higher than 0.15. In the present study, the result accuracy due to higher values of e is expected to offset the error caused by the ovalizations of a bent pipe.

5.6 Remarks

The use of Brazier's formula in Article 5.4 for checking buckling of the pipe wall implicitly assumes that the pipe is free of local buckling, that may occur in the highly compressive area of contact between the ram and the pipe. In the analysis of a pipe bending process where investigation of such a buckling type is required, the present elbow element is no longer suitable because of its limitations in modelling applied loading. Therefore, other types of elements must be considered instead. In the ram pipe bending with typical values of r_m/h , the pipe cross section at the part restrained by the ram may ovalize non-symmetrically, but the local buckling is very unlikely. Hence, the elbow element developed by Bathe et al. [3] - [5] is still considered to be applicable.

The results given in Figures 5.11 - 5.22 may be greatly affected by the use of a different set of material constants (yield stress, Young's modulus, and strain-hardening modulus). In addition, for materials that are not represented by a simple bilinear elastic-plastic stress-strain curve, the program FENSA must be used instead of EPBT. The actual stress-strain curve of the material will then be replaced by a multilinear approximation as was previously done in the verification problems.

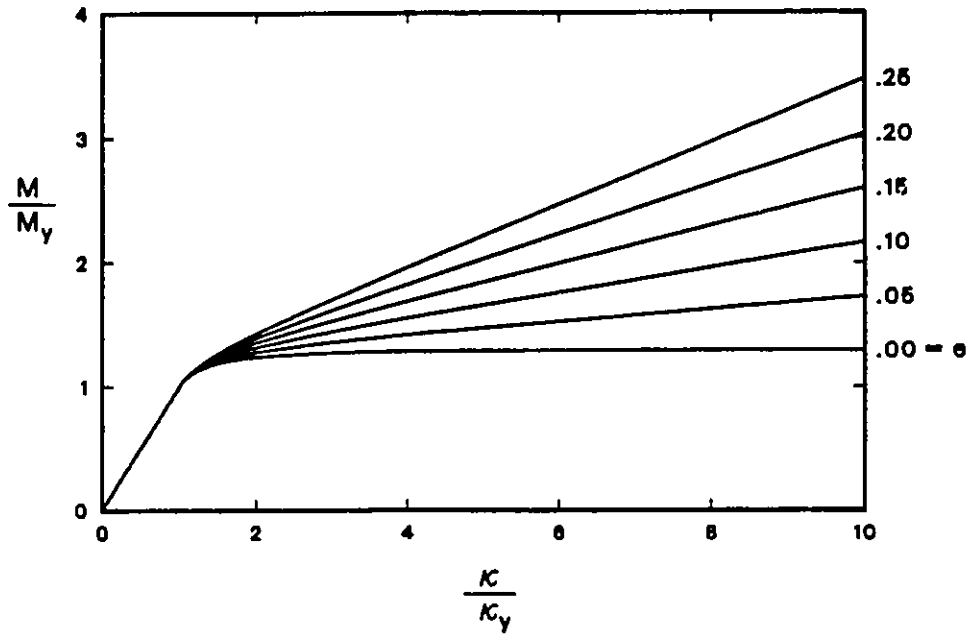


FIG. 5-5 MOMENT-CURVATURE RESULTS CALCULATED BY A BEAM-THEORY METHOD (M_y : LIMIT LOAD FOR YIELD INITIATION).

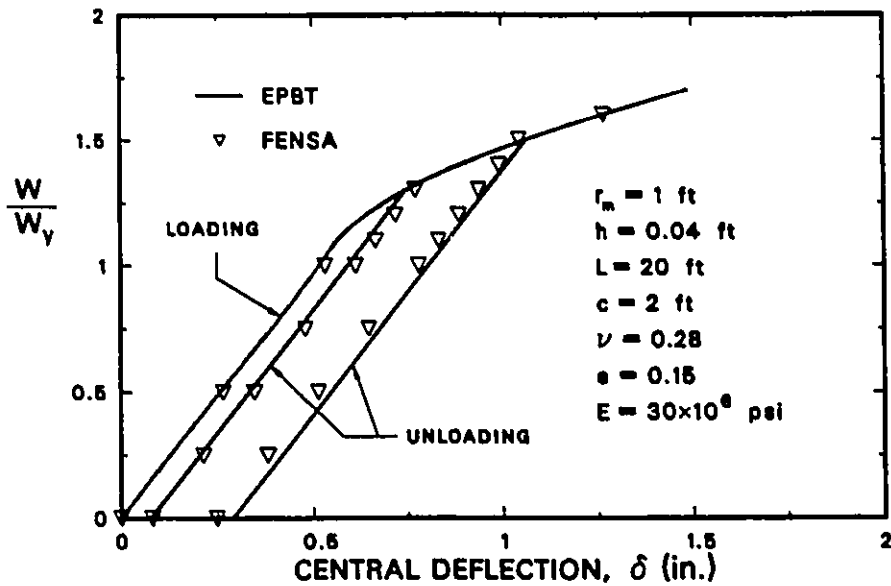


FIG. 5-6 COMPARISON OF THEORETICAL AND NUMERICAL LOAD-DEFLECTION RESULTS FOR RAM PIPE BENDING (1ft = 0.3048 m, 1psi = 6895 Pa).

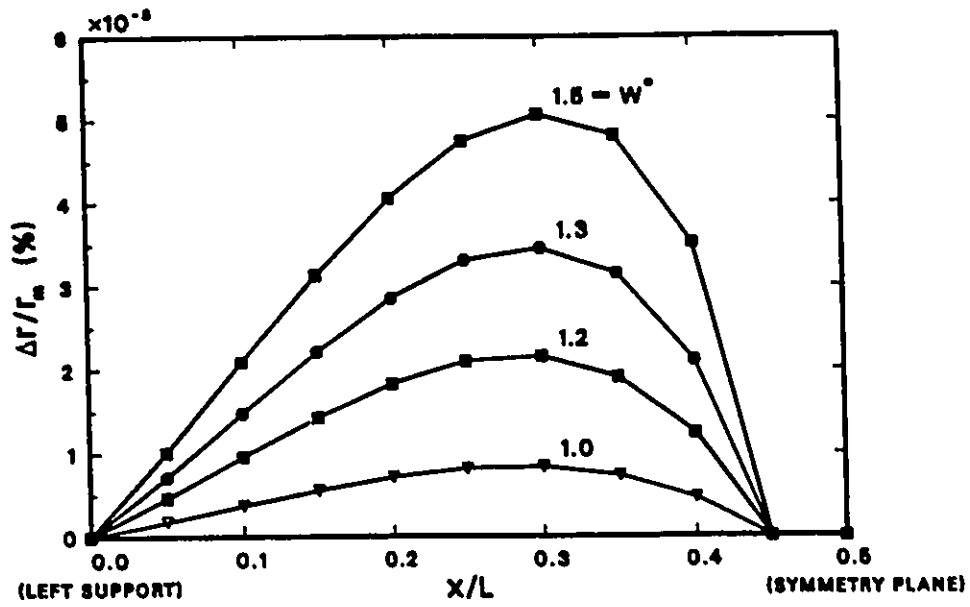


FIG. 8-7 VARIATION OF MAXIMUM CHANGES IN CROSS-SECTIONAL MEAN RADIUS ALONG PIPE LENGTH PREDICTED BY FENSA ($W^0 = W/W_0$).

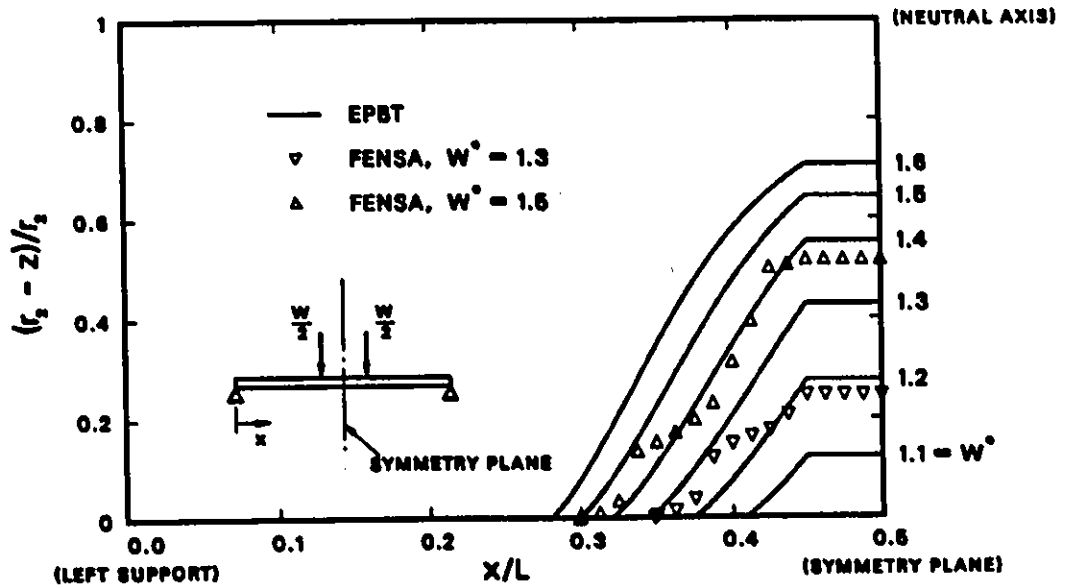
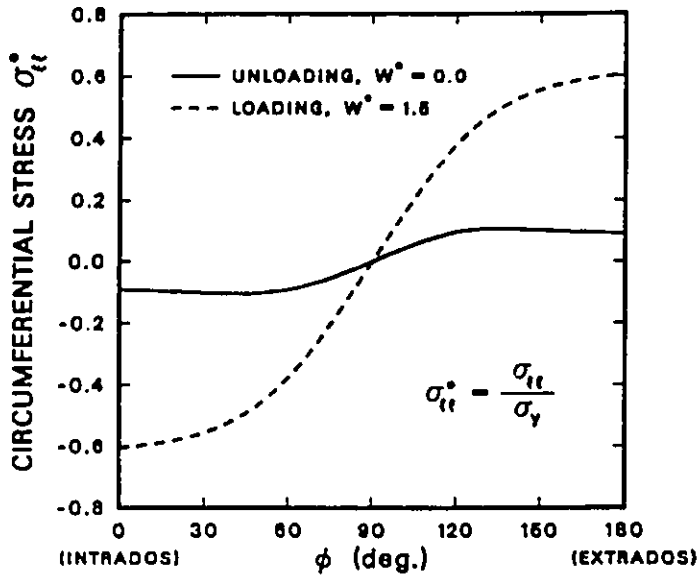
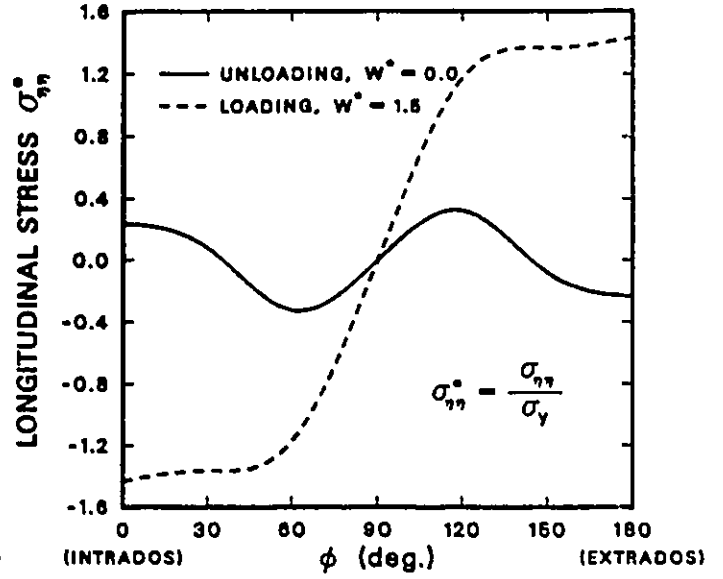


FIG. 8-8 PREDICTED GROWTH OF PLASTIC ZONES TOWARDS THE CENTRE OF PIPE DUE TO INCREASING LOADING.

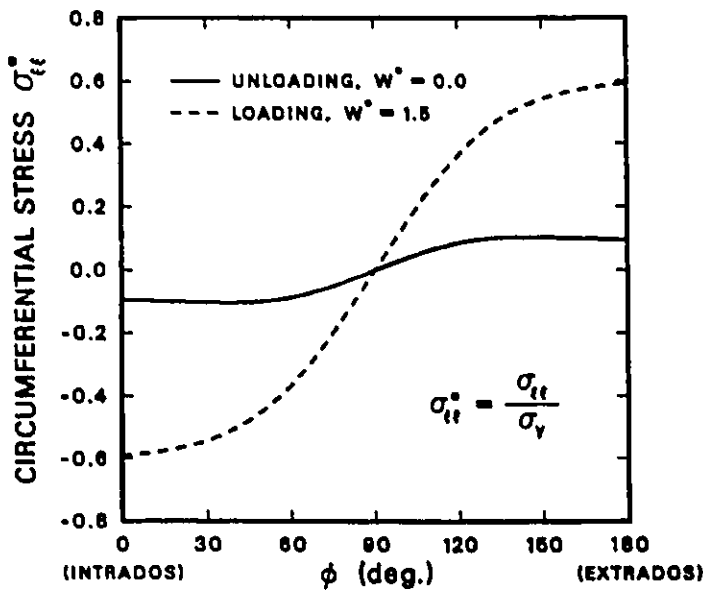


(a)

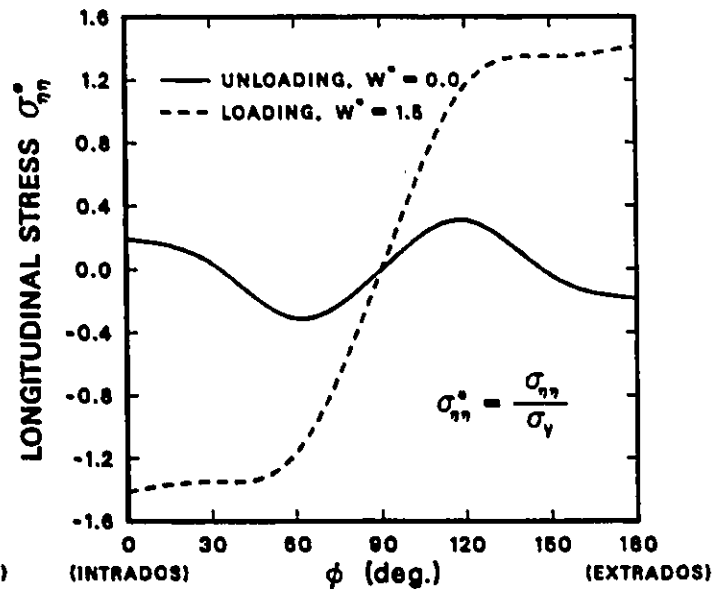


(b)

FIG. 5-9 PREDICTED RESIDUAL (a) CIRCUMFERENTIAL AND (b) LONGITUDINAL STRESSES AT THE PLANE OF SYMMETRY AND ON THE OUTSIDE SURFACE OF THE PIPE.



(a)



(b)

FIG. 5-10 PREDICTED RESIDUAL (a) CIRCUMFERENTIAL AND (b) LONGITUDINAL STRESSES AT THE PLANE OF SYMMETRY AND ON THE INSIDE SURFACE OF THE PIPE.

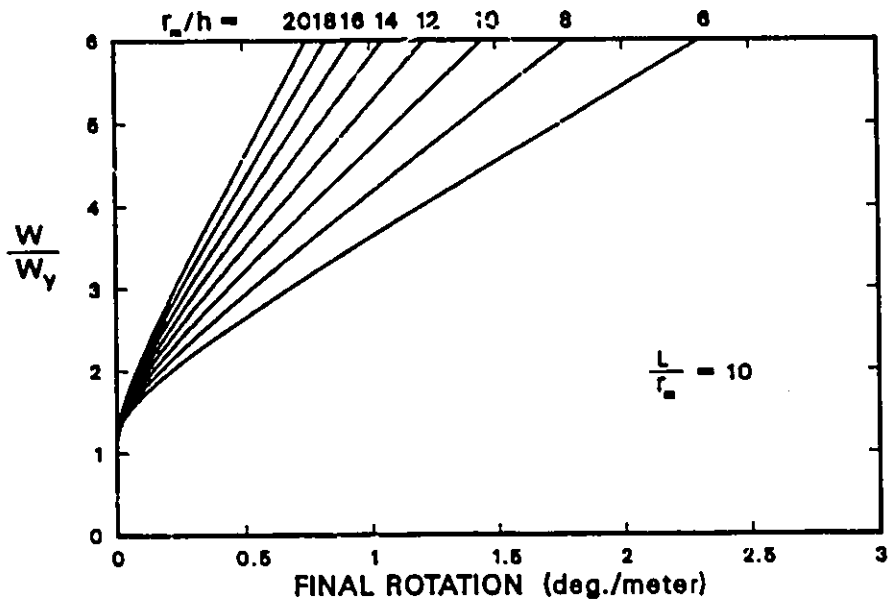


FIG. 5-11 PREDICTED FINAL ROTATION PER UNIT LENGTH OF BENT PIPE FOR $L/r_m = 10$ AND $c/r_m = 2$.

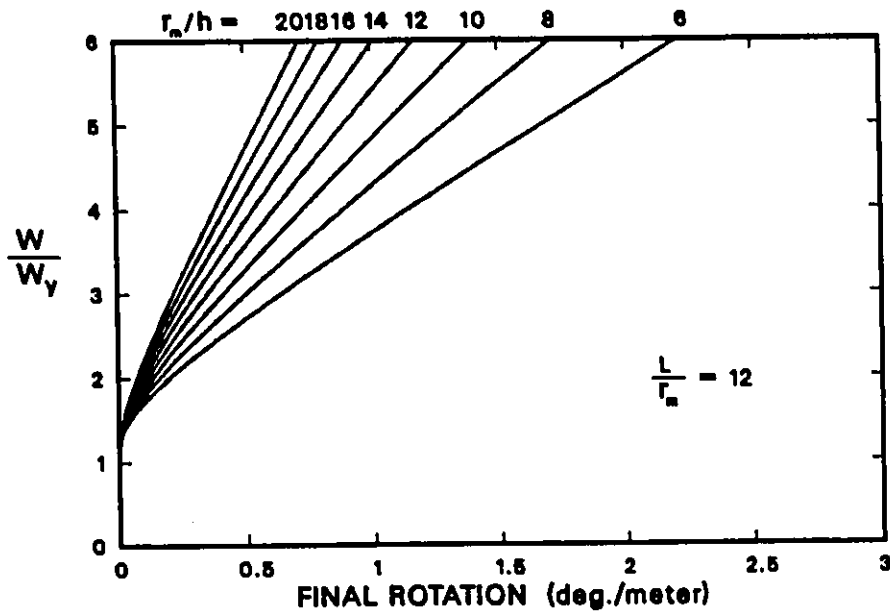


FIG. 5-12 PREDICTED FINAL ROTATION PER UNIT LENGTH OF BENT PIPE FOR $L/r_m = 12$ AND $c/r_m = 2$.

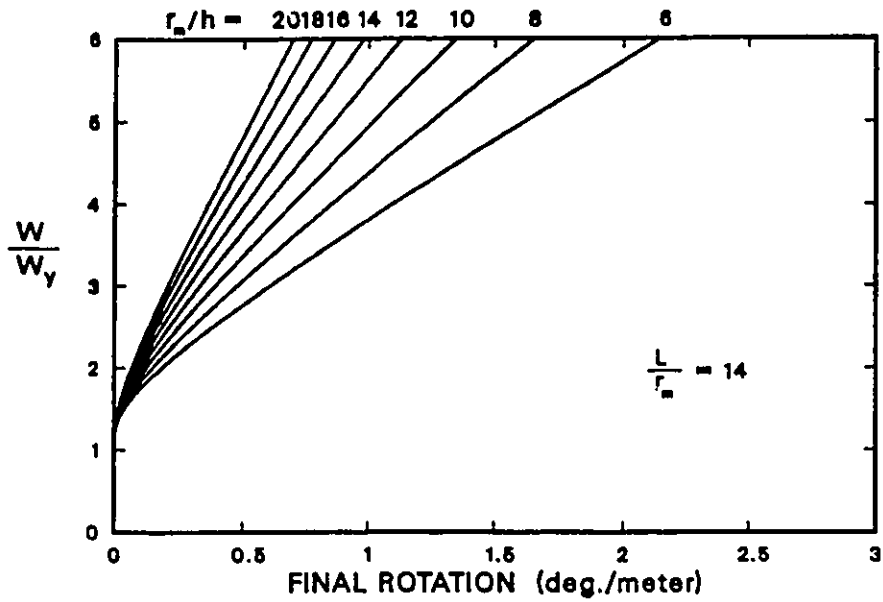


FIG. 8-13 PREDICTED FINAL ROTATION PER UNIT LENGTH OF BENT PIPE FOR $L/r_m = 14$ AND $c/r_m = 2$.

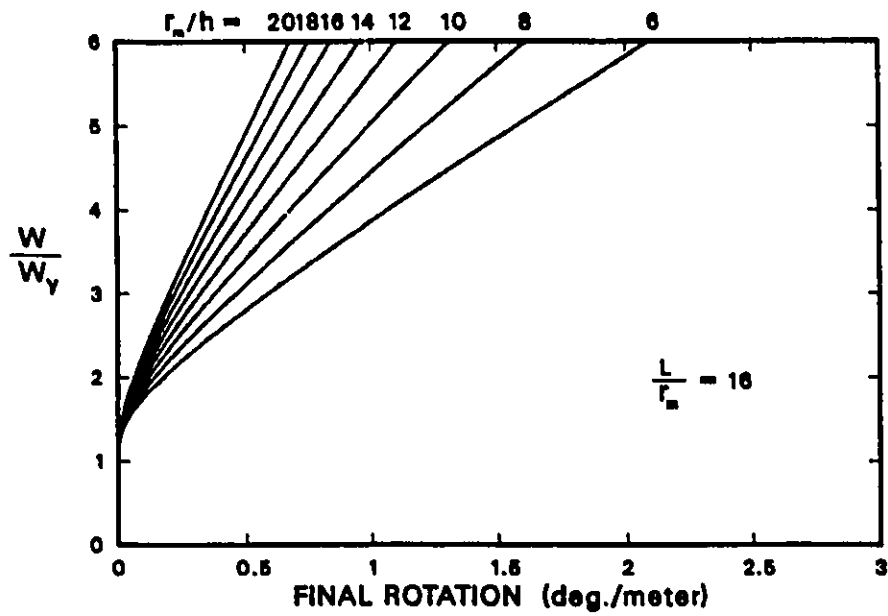


FIG. 8-14 PREDICTED FINAL ROTATION PER UNIT LENGTH OF BENT PIPE FOR $L/r_m = 16$ AND $c/r_m = 2$.

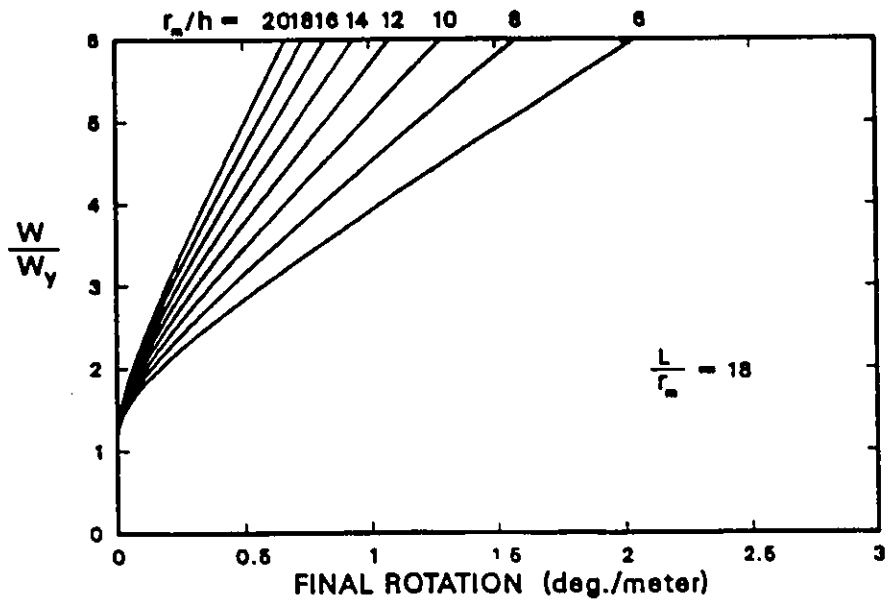


FIG. 5-16 PREDICTED FINAL ROTATION PER UNIT LENGTH OF BENT PIPE FOR $L/r_o = 18$ AND $c/r_o = 2$.

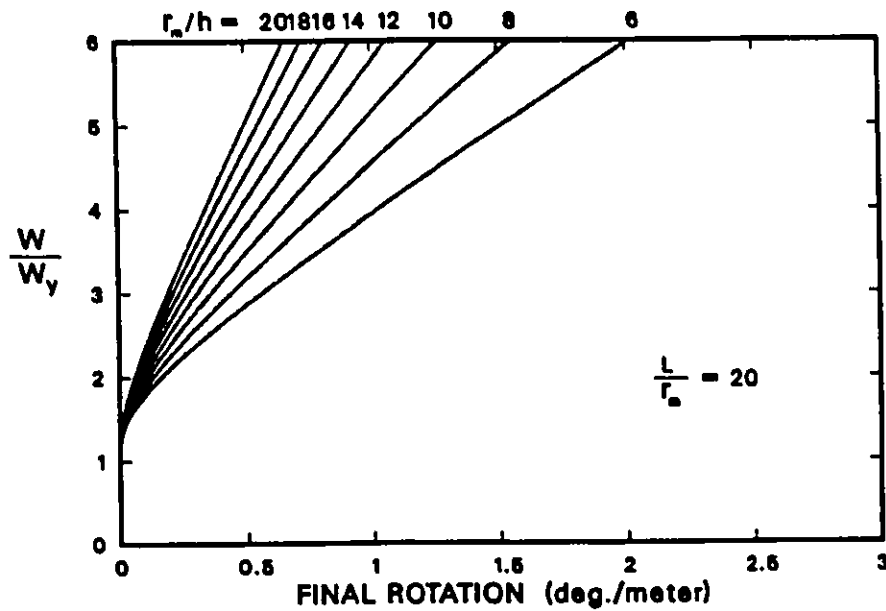


FIG. 5-18 PREDICTED FINAL ROTATION PER UNIT LENGTH OF BENT PIPE FOR $L/r_o = 20$ AND $c/r_o = 2$.

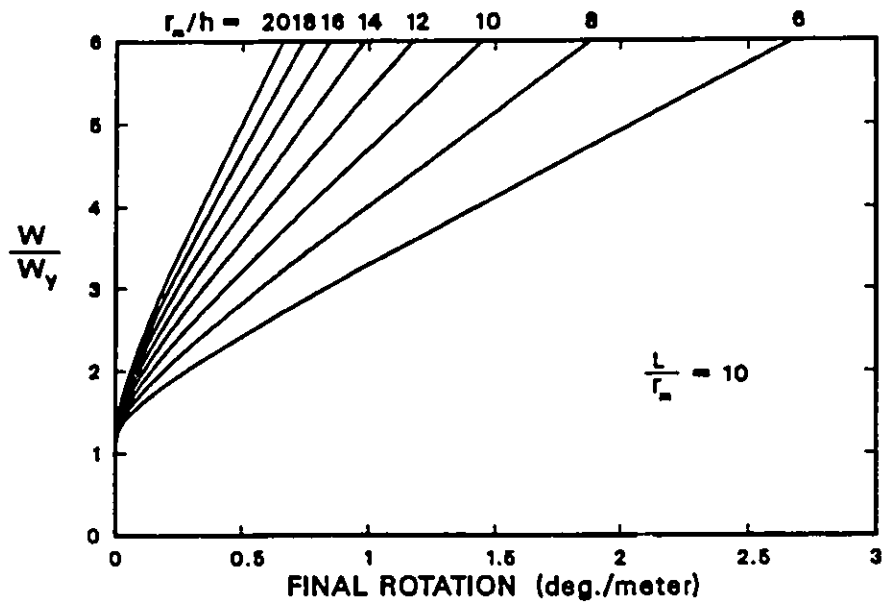


FIG. 6-17 PREDICTED FINAL ROTATION PER UNIT LENGTH OF BENT PIPE FOR $L/r_m = 10$ AND $c/h = 20$.

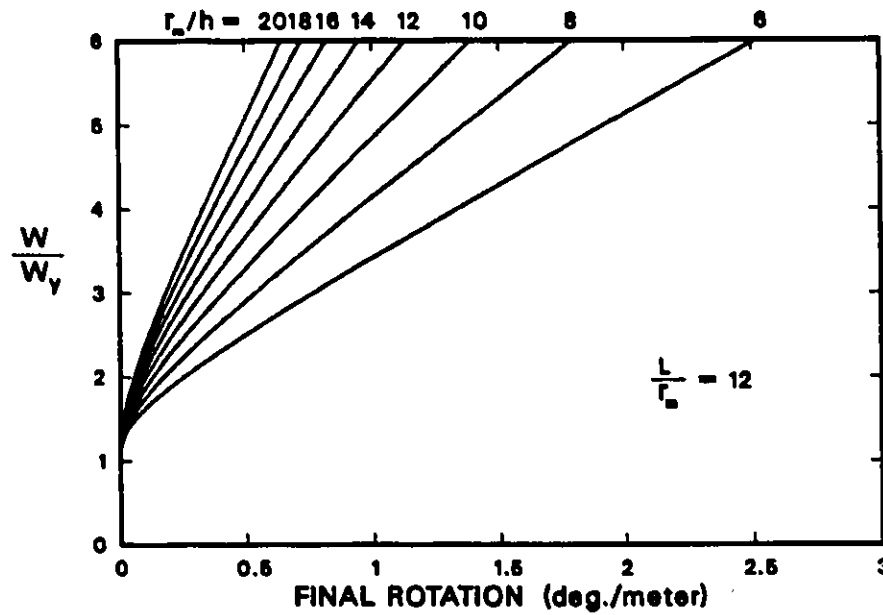


FIG. 6-18 PREDICTED FINAL ROTATION PER UNIT LENGTH OF BENT PIPE FOR $L/r_m = 12$ AND $c/h = 20$.

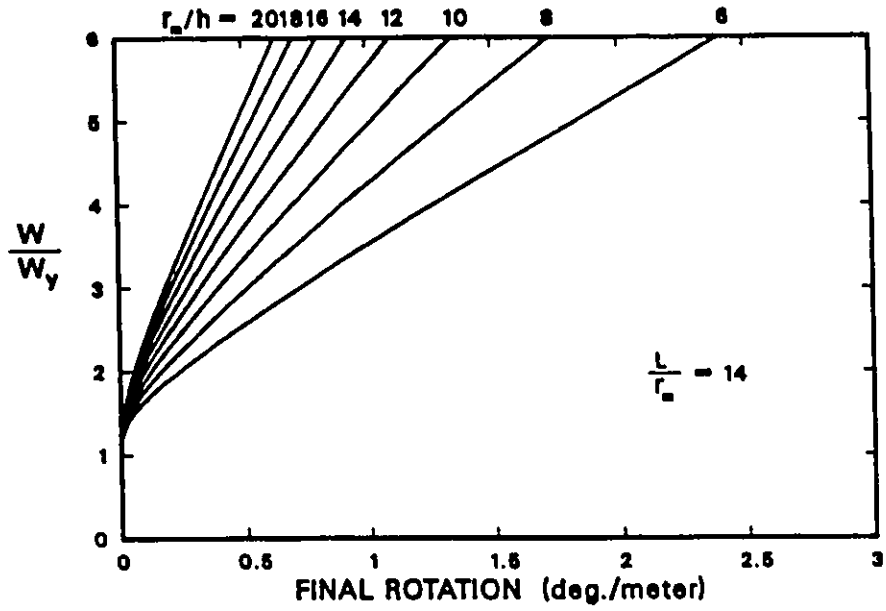


FIG. 8-18 PREDICTED FINAL ROTATION PER UNIT LENGTH OF BENT PIPE FOR $L/r_m = 14$ AND $c/h = 20$.

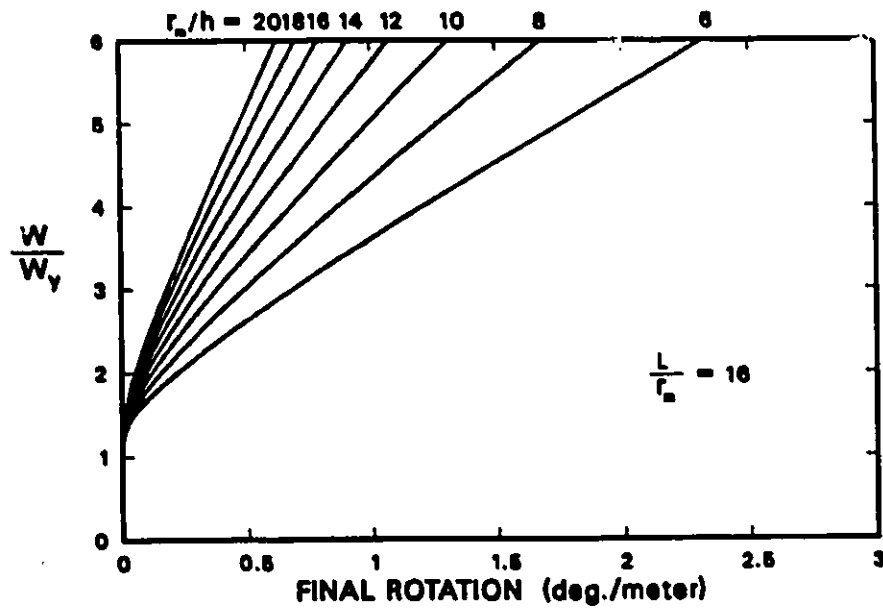


FIG. 8-20 PREDICTED FINAL ROTATION PER UNIT LENGTH OF BENT PIPE FOR $L/r_m = 16$ AND $c/h = 20$.

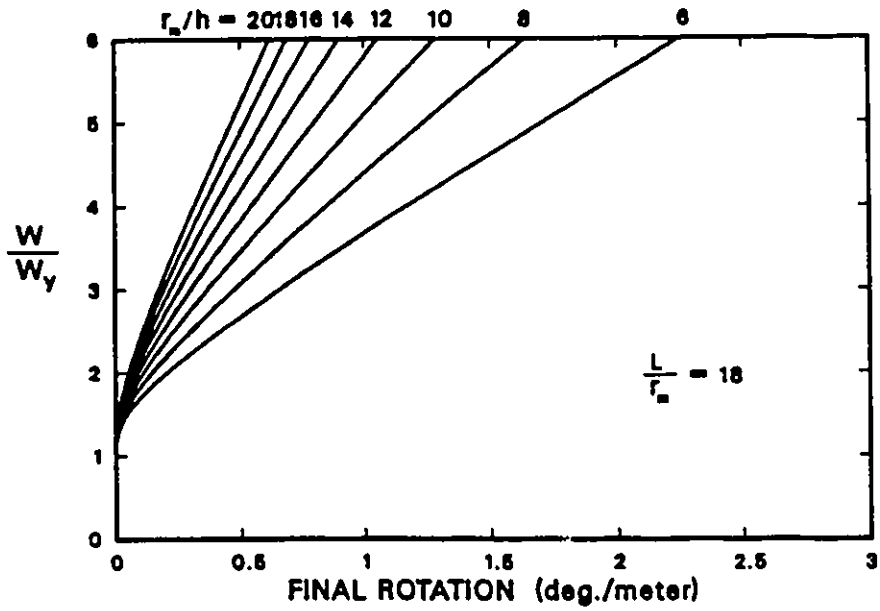


FIG. 8-21 PREDICTED FINAL ROTATION PER UNIT LENGTH OF BENT PIPE FOR $L/r_n = 18$ AND $c/h = 20$.

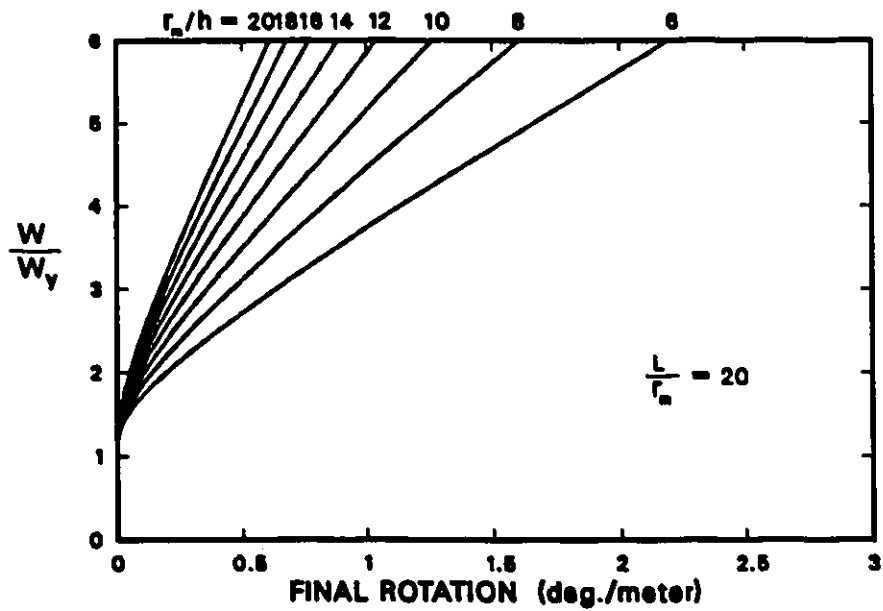


FIG. 8-22 PREDICTED FINAL ROTATION PER UNIT LENGTH OF BENT PIPE FOR $L/r_n = 20$ AND $c/h = 20$.

Chapter 6

Conclusions

From the present study, the following conclusions can be drawn regarding the use of the program FENSA to model piping problems and to simulate the ram-pipe bending process.

- Piping problems

1. In linear analyses, displacements and rotations are predicted accurately within 0.6% from the theoretical values. Due to the high order of displacement interpolation, relatively few elements are required for every day piping problems.
2. The elbow element developed in [3] – [5] underestimates the cross-section ovalizations of curved pipes. As the curvature of a pipe bend becomes larger, the predictions get closer to the experimental values. For pipe bends of $R = 0.250$ m and $R = 0.375$ m, the measurements for the maximum radial displacements of the pipe wall are found to be 1.4 and 1.7 times the FENSA predictions, respectively.
3. Although the expansion and the corresponding contraction of a cross section are nearly the same in elastic bending, the expansion is roughly twice the contraction in plastic bending. In nonlinear analyses, the use of the elbow

element should be restricted to cases where cross-sectional ovalizations are small since any change in the shape of the cross section of the element is not taken into account in the computation process.

4. Stresses and strains in straight and curved pipes are predicted closely in the linear range by the program FENSA. To determine completely their accuracy, FENSA stresses need to be checked further against other solutions.
5. The program FENSA is currently not capable of predicting exactly where first yielding occurs. However, this shortcoming could be eliminated with slight modifications in the present formulation in accordance with the theoretical work of [95].

- Ram-pipe bending process

1. For angles of bends dictated by Figures 5.11 – 5.22, the maximum value of FENSA predictions for cross-sectional ovalizations (measured by $\Delta r/r_m$) is about 0.2% in typical pipe bends produced by ram benders.
2. The pipe wall is predicted to be safe from buckling because the maximum compressive stress is below the critical value given by Brazier [107]. In the process of bending, pipe bends are free from collapse arising from the formation of a plastic hinge because plastic zones will not cover any cross section completely.
3. Predictions of final bend angles can be obtained inexpensively using EPBT while predictions for ovalizations and checking against buckling [107] are carried out with the program FENSA. The use of applied load-final pipe rotation results can save time and energy in shops producing pipe bends.
4. The present elbow element can provide preliminary information for the ram pipe bending process. For accurate simulation of the cross-section ovalization, other types of elements should be considered and more computing

time will certainly be required. Results for the maximum ovalization from a shell element using ADINA are presented in Appendix D. Friction and contact effects are ignored in the present model. The results presented thus are not applicable to practical cases where those effects are significant.

Bibliography

- [1] Altan, T., Oh, S. I., and Gegel, H. L., "Metal Forming Fundamentals and Applications". American Society for Metal, Metal Park, OH, 1983.
- [2] Oh, S. I., and Kobayashi, S.. "Finite Element Analysis of Plane Sheet Bending", Int. J. Mech. Sci., Vol. 22, pp. 538-594, 1980.
- [3] Bathe, K. J. and Almeida, C. A., "A Simple and Effective Pipe Elbow Element – Linear Analysis", J. Appl. Mech., Vol. 47, pp. 93-100, 1980.
- [4] Bathe, K. J. and Almeida, C. A., "A Simple and Effective Pipe Elbow Element – Interaction Effects", J. Appl. Mech., Vol. 49, pp. 165-171, 1982.
- [5] Bathe, K. J., Almeida, C. A., and Ho, L. W., "A Simple and Effective Pipe Elbow Element – Some Nonlinear Capabilities", Comp. Struct., Vol. 17, No. 5-6, pp. 659-667, 1983.
- [6] ADINA. Arthur D.. Little Report, 1979.
- [7] Hughes. T. J. R.. "Some Current Trends in Finite Element Research", Applied Mechanics Reviews, Vol. 33. pp. 1467-1477, 1980.
- [8] Zienkiewicz, O. C., "The Finite Element Method", McGrall-Hill, London, England, 1977.
- [9] Bathe, K. J.. "Finite Element Procedures in Engineering Analysis", Prentice-Hall, Englewood Cliffs, New Jersey, 1982.
- [10] Owen. D. R. J.. and Hinton, E., "Finite Elements in Plasticity – Theory and Practice", Pineridge Press Limited, Swansea, U.K., 1986.
- [11] Yamada, Y., Yoshimura, N. and Sukurai, T., "Plastic Stress Strain Matrix and Its Application for the Solution of Elastic-Plastic Problems by the Finite Element Method", Int. J. Mech. Sci., Vol. 10, pp. 343-354. 1968.
- [12] Zienkiewicz, O. C., Valliappan, S., and King, I. P., "Elasto-Plastic solutions of Engineering Problems. Initial Stress Finite Element Approach", Int. J. Num. Eng., Vol. 1, pp. 75-100, 1969.
- [13] Marcal, P. V., and King, I. P., "Elastic Plastic Analysis of Two Dimensional Stress System by the FEM", Int. J. Mech. Sci., Vol. 9, pp. 143-155, 1967.

- [14] Hill, R., "Some Basic Principles in the Mechanics of Solids without Natural Time", *J. Mech. Phys. Solids*, Vol. 7, pp. 209-225, 1959.
- [15] Hill, R., "Uniqueness Criteria and Extremum Principles in Self Adjoint Problems of Continuum Mechanics", *J. Mech. Phys. Solids*, Vol. 10, pp. 185-194, 1962.
- [16] Hibbitt, H. D., Marcal, P. V., and Rice, J. R., "A Finite Element Formulation for Problems of Large Strain and Large Displacement", *Int. J. Solids Structures*, Vol. 6, pp. 1069-1086, 1970.
- [17] Hofmeister, L. D., Greenbaum, G. A., and Evensen, D. A., "Large Strain Elasto-Plastic Finite Element Analysis", *AIAA Journal*, Vol. 9, pp. 1248-1254, 1971.
- [18] Zienkiewicz, O. C., Jain, P. C., and Onate, E., "Flow of Solids during Forming and Extrusion. Some Aspects of Numerical Solutions", *Int. J. Solids Structures*, Vol. 14, pp. 15-38, 1978.
- [19] Wang, N. W., and Wenner, M. L., "Elasto-Viscoplastic Analysis of Simple Stretch Forming Problems", *Mechanics of Sheet Metal Forming* (edited by D. P. Koistinen and N. M. Wang), Plenum Press, pp. 367-391, 1979.
- [20] Rebelo, N., and Kobayashi, S., "Axisymmetric Punch Stretching of Strain-Rate Sensitive Sheet Metals", *Proceedings NAMRC-VIII, Society of Manufacturing Engineers*, pp. 235-238, 1980.
- [21] Kobayashi, S., "A Review on the Finite Element Method and Metal Forming Process Modelling", *J. Appl. Metalworking*, Vol. 2, No. 3, pp. 163-169, 1982.
- [22] Wafi, A. S., "Finite Element Correction Matrices in Metal Forming Analysis (with Application to Hydrostatic Bulging of a Circular Sheet)", *Int. J. Mech. Sci.*, Vol. 24, pp. 393-406, 1982.
- [23] Gadala, M. S., and Oravas, G. A. E., "Numerical Solutions of Nonlinear Problems of Continua - I", *Comp. Struct.*, Vol. 19, pp. 865-877, 1984.
- [24] Cheng, H., and Kikuchi, N., "An Analysis of Metal Forming Processes Using Large Deformation Elastic-Plastic Formulation", *Comp. Meth. Appl. Mech. Eng.*, Vol. 49, pp. 71-108, 1985.
- [25] Woo, D.M., "Analysis of the Cup-Drawing Process", *J. of Mech. Eng. Sci.*, Vol. 6, No. 2, pp. 116-131, 1964.
- [26] Woo, D. M., "The Stretch-Forming Test", *The Engineers*, Vol. 220, pp. S76-S80, 1965.
- [27] Woo, D.M., "On the Complete Solution of the Deep-Drawing Problem", Vol. 10, pp. 83-94, 1968.
- [28] Wafi, A. S., "An Incremental Complete Solution of the Stretch Forming and Deep Drawing of a Circular Blank Using a Hemispherical Punch", *Int. J. Mech. Sci.*, Vol. 18, pp. 23-31, 1976.

- [29] Wifi, A. S., and Yamada, Y., "Finite Element Analysis of Metal Working Processes", Current Advances in Mechanical Design and Production, Proceedings of the 1st Int. Conf., Cairo University, 1979, Eds. G. Shawki and S. Metwalli.
- [30] Anderson, B. S., "A Numerical Study of the Deep-Drawing Process", Numerical Methods in Industrial Forming Processes, pp. 709-721, 1982.
- [31] Wang, N. M., and Budianski, B., "Analysis of Sheet Metal Stamping by a Finite Element Method", J. Appl. Mech., Vol. 45, pp. 73-82, 1978.
- [32] Honnor, M. E., and Wood, R. D., "A Finite Element Analysis of Deep Drawing - the Boundary Condition Problem", Numerical Methods in Industrial Forming Processes, pp. 807-808, 1982.
- [33] Kobayashi, S., and Kim, J. H., "Deformation Analysis of Axisymmetric Sheet Metal Forming Processes by the Rigid-Plastic Finite Element Method", Mechanics of Sheet Metal Forming, Michigan, pp. 341-365, 1977.
- [34] Gotoh, M., and Ishise, F., "Finite Element Analysis of Rigid-Plastic Deformation of the Flange in Deep-Drawing Processes Based on a Fourth-Degree Yield Function", Int. J. Mech. Sci., Vol. 20, pp. 423-435, 1978.
- [35] Gotoh, M., "A Finite Element Analysis of Rigid-Plastic Deformation of the Flange in Deep-Drawing Processes Based on a Fourth-Degree Yield Function - II", Int. J. Mech. Sci., Vol. 22, pp. 367-377, 1980.
- [36] Zienkiewicz, O. C., Jain, P. C., and Onate, E., "Flow of Solids during Forming and Extrusion: Some Aspects of Numerical Solutions", Int. J. Solids Structures, Vol. 14, pp. 15-38, 1978.
- [37] Onate, E., and Zienkiewicz, O. C., "Plastic Flow of Axisymmetric Thin Shells as a Non-Newtonian Flow Problem and Its Applications to Stretch Forming and Deep Drawing Problems", Sheet Metal Forming and Formability, 10th Bienial Congress, pp. 29-38, 1978.
- [38] Onate, E., and Zienkiewicz, O. C., "A Viscous Shell Formulation for the Analysis of Thin Sheet Metal Forming", Int. J. Mech. Sci., Vol. 25, pp. 305-335, 1983.
- [39] Baynham, J. M. W., and Zienkiewicz, O. C., "Development in the Finite Element Analysis of Thin Sheet Drawing and Direct Redrawing Processes, Using the Rigid-Plastic Approach", Numerical Methods in Industrial Forming Processes, pp. 697-707, 1982.
- [40] Tatenami, M., Nakamura, Y., and Saito, K., "An Analysis of Deep Drawing Process Combined with Bending", Numerical Methods in Industrial Forming Processes, pp. 687-696, 1982.
- [41] Gerdeen, J. C., "Development of a Computer Program 'AXIFORM' for the Analysis of Forming of Axisymmetric Sheet Metal Parts", NAMRC-XII, pp. 209-213, May - Jun 1984, Houghton, Michigan.
- [42] Mehta, H. S., and Kobayashi, S., "Finite Element Analysis and Experimental Investigation of Sheet Metal Stretching", J. Eng. Ind., Vol. 95, pp. 874-880, 1973.

- [43] Wennerstrom, Samuelsson, A., and Mattiasson, K., "Finite Element Method for Sheet Metal Stretching", Numerical Methods in Industrial Forming Processes, pp. 51-65, 1982.
- [44] Wang, N. M., "A Rigid-Plastic Rate-Sensitive Finite Element Method for Modelling Sheet Metal Forming Processes", Numerical Methods in Industrial Forming Processes, pp. 797-806, 1982.
- [45] Iseki, H., Jimma, T., and Murota, T., "Finite Element Method of Analysis of the Hydrostatic Bulging of a Sheet Metal (Part I)", Bull. JSME, Vol. 17, pp. 1240-1246, 1974.
- [46] Iseki, H., Murota, T., and Jimma, T., "Finite Element Method of Analysis of the Hydrostatic Bulging of a Sheet Metal (Part II)", Bull. JSME, Vol. 20, pp. 285-291, 1977.
- [47] Bate, P. S., "Finite Element Modelling of the Hydraulic Bulging of Sheet Metal", Numerical Methods in Industrial Forming Processes, pp. 669-675, 1982.
- [48] Gotoh, M., "A Finite Element Analysis of General Deformation of Sheet Metal", Int. J. Num. Meth. Eng., Vol. 8, pp. 731-741, 1974.
- [49] Oh, S. I., and Kobayashi, S., "Finite Element Analysis of Plane Sheet Bending", Int. J. Mech. Sci., Vol. 22, pp. 583-594, 1980.
- [50] Tang, S. C., Chu, E., and Samanta, S. K., "Finite Element Prediction of the Deformed Shape of an Automotive Panel During Preformed Stage", Numerical Methods in Industrial Forming Processes, pp. 629-640, 1982.
- [51] Tang, S. C., "Finite Element Prediction of the Deformed Shape of an Automobile Trunk-Deck Lid during the Binder Wrap Stage", Experimental Verification of Process Models, ASM, pp. 189-203, 1981.
- [52] Wang, N. M., Johnson, L. K., and Tang, S. C., "Stretch Flanging of 'V'-shaped Sheet Metal Blanks", J. Appl. Metalworking, Vol. 3, pp. 281-291, 1984.
- [53] Corpet, P., "Guide Pratique pour le Cintrage des Tubes", Desforges, Paris, 1977.
- [54] Gillanders, J., "Pipe and Tube Bending Manual". Gulf Publishing Company, Houston, Texas, 1984.
- [55] Winship, J. T., "Bending Tube, Pipe, and Structural", American Machinist, Vol. 127, No. 10, pp. 114-128, 1983.
- [56] Addison, H., "Developments in the Manipulation of Tube and Pipe - Advances in Pipe Bending Techniques", Sheet Metal Industries, Vol. 61, No. 6, pp. 337-342, 1984.
- [57] Venables, T., "Tube Manipulation Today", Sheet Metal Industries, Vol. 61, No. 6, pp. 340-342, 1984.
- [58] Steffens, E., and Barkow, A. G., "Study of Variations in Wall Thickness and Diameter Caused by Field Bending," Report No. NG-59-1 of the Natural Gas Pipeline Company of America, January 16, 1959, not available publicly.

- [59] Weil, N. A., Brock, J. E., and Cooper, W. E., "Stresses in a Pipe Bent into a Circular Arc", *J. Eng. Ind.*, Vol. 83, pp. 449-459, 1961.
- [60] Palynchuk, A., "Strains Caused by Field Bending of 42-Inch Pipe", *PipeLine Industry*, Vol. 58, No. 3, pp. 23-26, 1983.
- [61] Inoue, K., and Mellor, P. B., "Mechanics of the Radial-Draw Bending of Tube", *Int. Machine Tool Design and Research Conf.*, London, pp. 127-131, 1977.
- [62] Inoue, K., and Mellor, P. B., "Radial-Draw Bending of Stainless Tube", *J. of Mechanical Working Technology*, Vol. 3, pp. 151-166, 1979.
- [63] Semenov, E. I., and Nikitin, I. V., "Bending Thin-Walled Tubes to a Small Radius Using a Profiling Device and Inductive Bending", *Russian Engineering Journal*, Vol. 57, No. 10, pp. 46-48, 1977.
- [64] Blume, H., Speth, W. E., Bredenbruch, K., and Kalwa, G. "Production of Pipe Bends for Power Stations by the Induction Bending Process", *Energy Developments*, Vol. 7, pp. 9-15, Dec. 1983.
- [65] Viatour, P., Bosteels, H., and Messien, P., "Induction Bending of API-Grade Line Pipe", *PipeLine Industry*, Vol. 58, No. 5, pp. 33-40, 1983.
- [66] Asao, H., Okada, K., Watanabe, M., Yonemura, H., Matsumoto, T., and Umehara, N., "Analysis in Workability of Pipe bending Using High Frequency Induction Heating", *Int. Machine Tool Design and and Research Conf.*, London, pp. 97-104, 1983.
- [67] Ahmad, S, Irons, B. M., and Zienkiewicz, "Curved thick shell and membrane elements with particular reference to axi-symmetric problems", *Proc. 2nd Conf. Matrix Methods in Structural Mechanics*, Wright-Patterson, A. F. Base, Ohio, 1968.
- [68] Bathe, K. J., and Bolourchi, S., "A Geometric and Material Nonlinear Plate and Shell Element", *Comp. Struct.*, Vol. 11, pp. 23-48, 1980.
- [69] Dodge, W. G., and Moore, S. E., "Stress Indices and Flexibility Factors for Moment Loadings on Elbows and Curved Pipes", *Welding Research Council Bulletin* 179, Dec. 1972.
- [70] Vigness, I., "Elastic Properties of Curved Tubes", *Trans. ASME*, Vol. 55, pp. 105-120, 1943.
- [71] Palaninathan, R., and Chandrasekharan, P. S., "Curved Beam Element Stiffness Matrix Formulation", *Comp. Struct.*, Vol. 21, No. 4, pp. 663-669, 1985.
- [72] Sohal, L. S., and Chen, W. F., "Large Bending of Pipes", *Engng. Struct.*, Vol. 7, pp. 121-130, Apr. 1985.
- [73] Katori, H., Nishimura, T., and Murase, K., "Finite Bending of Curved Beam with Thin Wall Cross Section", *Bulletin of JSME*, Vol. 28, No. 243, Sept. 1985.
- [74] Ohtsubo, H., and Watanabe, O., "Stress Analysis of Pipe Bends by Ring Elements", *Trans. ASME*, Vol. 100, pp. 112-122, Feb. 1978.

- [75] Takeda, H., Asai, S., Iwata, K., and Kano, T., "A Finite Element for Detailed Analysis of Piping Systems Considering the End Effects", presented at the 56th Annual Meeting of Japan Society of Mechanical Engineers (in Japanese), 1978.
- [76] Takeda, H., Asai, S., and Iwata, K., "A New Finite Element for Structural Analysis of Piping Systems", presented in the 5th International Conference on Structural Mechanics in Reactor Technology, Paper M 5/5, Berlin, Germany, 1981.
- [77] Hibbitt, H. D., and Leung, E. K., "An Approach to Detailed Inelastic Analysis of Thin-Walled Pipelines", Hibbit, Karlson and Sorenson Inc., Rhode Island, USA.
- [78] Lazzeri, L., "An Elasto-Plastic Elbow Element - Theory and Applications", Int. J. Pres. Ves. Piping, Vol. 8, No. 3, pp. 197-213, 1980.
- [79] Sobel, L. H., "In-Plane Bending of Elbows", Comp. Struct., Vol. 7, pp. 701-715, 1977.
- [80] von Karman, T., "Über die Formänderung Dünnwandiger Rohre, Insbesondere Federnder Ausgleichrohre", Zeitschrift des Vereines deutscher Ingenieure, Vol. 55, pp. 1889-1895, 1911.
- [81] Bathe, K. J., and Almeida, C. A., "A Simple and Effective Pipe Elbow Element - Pressure Stiffening Effects", ASME J. of Appl. Mech., Vol. 49, pp. 914-916, 1982.
- [82] Novozhilov, V. V., "Thin Shell Theory" (Translated by P. E. Lowe), Noordhoff, Groningen, 1964.
- [83] Malvern, L. E., "Introduction to the Mechanics of a Continuous Medium", Prentice-Hall Inc., Englewood Cliff, N. J., 1969.
- [84] Bathe, K. J., Snyder, M. D., Cimento, A. P., and Rolph, W. D., "On some Current Procedures and Difficulties in Finite Element Analysis of Elastic-Plastic Response", Comp. Struct., Vol. 12, pp. 607-624, 1980.
- [85] Whatham, J. F., "In-Plane Bending of Flanged Elbows", Proceedings of Metal Structures Conference, the Institution of Engineers, Australia, Perth, 1978.
- [86] Lau, J. H., and Lau, T. T., "Bending and Twisting of pipes with Strain Hardening", J. Pres. Ves. Technology, Vol. 106, pp. 188-195, May 1984.
- [87] Bolt, S. E., and Greenstreet, W. L., "Experimental Determination of Plastic Collapse Loads for Pipe Elbows", ASME paper 71-PVP-37.
- [88] Vrillon, B., Montfort, C., and Beffre, J., "Experimental Analysis of Piping Components of Fast Breeder Reactors", 3rd SMIRT Conf., London, paper F3/4, 1975.
- [89] Roche, R., Hoffman, A., and Vrillon, B., "Piping Systems, Inelastic Analysis - a Simplified Numerical Method", 3rd Int. Conf. on Pressure Vessel Technology, ASME Tokyo, Japan, pp. 133-142, 1977.
- [90] Bushnell, D., "Elastic-Plastic Bending and Buckling of Pipes and Elbows", Comp. Struct., Vol. 13, pp. 241-248, 1981.

- [91] Bung, H., Clement, G., Hoffman, A., and Jakubowicz, H., "Piping Benchmark Problems—Computer Analysis with the CEASEMT finite element system", CEASEMT Ref. EMT/78/61, Oct. 1978.
- [92] Sobel, L. H., and Newman, S. Z., "Comparison of Experimental and Simplified Analytical Results for the In-Plane Plastic Bending and Buckling of an Elbow", Proc. Pressure Vessels and Piping Conf., paper 80-C2/PVP-42, ASME, San Francisco, Aug. 1980.
- [93] Prinja, N. K., and Chitkara, N. R., "Finite Element Analyses of Post-Collapse Plastic Bending of Thick Pipes", Nuclear Engineering and Design, Vol. 91, pp. 1-12, 1986.
- [94] Lang, H. A., "Plastic Hinge Formation in Elbows and Curved Tubing", Int. J. Pres. Ves. & Piping, Vol. 16, No. 6, pp. 421-429, 1982.
- [95] Munz, D., and Mattheck, C., "Cross-Sectional Flattening of Pipes Subjected to Bending", Int. J. Pres. Ves & Piping, Vol. 10, No. 6, pp. 421-429, 1982.
- [96] Gross, N., "Experiments on Short-Radius Pipe-Bends". Proc. Inst. Mech. Engrs., pp. 465-479, 1952-1953.
- [97] Neal, B. G., "The Plastic Methods of Structural Analysis", 3rd edition, Chapman and Hall Ltd., London, 1977.
- [98] Roderick, J. W., "Theory of Plasticity – Elements of Simple Theory", Philosophical Magazine, Vol. 39, Seventh Series, No. 294, pp. 529-539, 1948.
- [99] Roderick, J. W., and Heyman, J., "Extension of the Simple Plastic Theory to Take Account of the Strain-Hardening Range", Proc. Inst. Mech. Engrs., Vol. 165, pp. 189-197, 1951.
- [100] Chihenko, Y. N., "The Calculation of Plastic Deformation of I-Beam under Bending", People's Republic of China, 1956 (in Chinese).
- [101] Yu, T. X., and Johnson, W., "The Influence of Axial Force on the Elastoplastic Bending and Springback of of Beam", J. Mech. Wking. Tech., Vol. 6, pp. 5-21, 1981.
- [102] Brown, E. H., "Plastic Asymmetrical Bending of Beams", Int. J. Mech. Sci., Vol. 9, pp. 77-82, 1967.
- [103] Xu, Y., Zhang, L. C., and Yu, T. X., "The Elastic-Plastic Pure Bending and Springback of L-Shaped Beams", Int. J. Mech. Sci., Vol. 29, No. 6, pp. 425-433, 1987.
- [104] Den Hartog, J. P., "Strength of Materials", Dover Publications, Inc., New York, 1983.
- [105] Hughes, T. J. R., Taylor, R. L., and Kanoknukulchai, W., "A Simple and Efficient Finite Element for Plate Bending", Int. J. Num. Meth. Eng., Vol. 11, pp. 1529-1543, 1977.

- [106] Zienkiewicz, O. C., Bauer, J., Morgan, K., and Onate, E., "A Simple and Efficient Finite Element for Axisymmetric Shells", *Int. J. Num. Meth. Eng.*, Vol. 11, pp. 1545-1558, 1977.
- [107] Brazier, L. G., "On the Flexure of Thin Cylindrical Shells and other 'Thin' Sections", *Proc. Soc. London, Ser. A*, Vol. 116, pp. 104-114, 1927.
- [108] Flügge, W., "The Stability of Circular Cylindrical Shells", *Ing.-Archiv*, Vol. 3, pp. 463-506, 1932.
- [109] Axelrad, E. L., "Determination of the Upper Critical Bending Moment of a Pipe Considering Geometric Nonlinearity", *Izv. AN SSSR, Mechanika*, Vol. 4, pp. 133-139, 1965 (in Russian).
- [110] Emmerling, F. A., "Nonlinear Bending of Curved Tubes", *Flexible Shells* by E. L. Axelrad and F. A. Emmerling (Eds.), Springer, Berlin, 1984.
- [111] Bathe, K. J., and Cimento, A. P., "Some Practical Procedures for the Solution of Nonlinear Finite Element Equations", *Comp. Methods Appl. Mech. Eng.*, Vol. 22, pp. 59-85, 1980.
- [112] Aitken, A. C., "The Evaluation of the Latent Roots and Latent Vectors of Matrix", *Proc. Roy. Soc. Edinburgh*, Vol. 57, pp. 269-304, 1937.
- [113] Reissner, E., "On a Variational Theorem in Elasticity", *J. Math. Phys.*, Vol. 29, pp. 90-95, 1950.

Appendix A

Transformation

Physical stress and strain components belong to second-order tensors. In the finite element method, such components are converted from one system of (orthogonal) axes to another for computational purposes, and then converted back for result interpretations. These conversions are achieved with appropriate transformation matrices.

The matrices are derived from basic relations in Continuum Mechanics (for example, see [83]). If T_{pq} represents components of a second-order tensor in a first (unbarred) system of axes and \bar{T}_{rs} is its counterpart in a second (barred) system, then the following relations hold

$$T_{pq} = a_r^p a_s^q \bar{T}_{rs}$$

$$\bar{T}_{rs} = a_r^p a_s^q T_{pq}$$

where

a_r^p, a_s^q : direction cosines defined as

$$a_r^p = \cos(\bar{x}_r, x_p)$$

$$a_s^q = \cos(\bar{x}_s, x_q)$$

p, q, r, s : indices (equal to 1, 2, or 3).

With the same argument for stress and strain components, similar relations can

be obtained

$$\text{Stresses} \quad \sigma_{pq} = a_r^p a_s^q \bar{\sigma}_{rs} \quad \bar{\sigma}_{rs} = a_r^p a_s^q \sigma_{pq} \quad (a)$$

$$\text{Strains} \quad \epsilon_{pq} = a_r^p a_s^q \bar{\epsilon}_{rs} \quad \bar{\epsilon}_{rs} = a_r^p a_s^q \epsilon_{pq} \quad (b)$$

By letting

$$l_1 = \cos(e_\xi, e_{x_1}) \quad m_1 = \cos(e_\eta, e_{x_1}) \quad n_1 = \cos(e_\zeta, e_{x_1})$$

$$l_2 = \cos(e_\xi, e_{x_2}) \quad m_2 = \cos(e_\eta, e_{x_2}) \quad n_2 = \cos(e_\zeta, e_{x_2})$$

$$l_3 = \cos(e_\xi, e_{x_3}) \quad m_3 = \cos(e_\eta, e_{x_3}) \quad n_3 = \cos(e_\zeta, e_{x_3})$$

where e_ξ, e_η, e_ζ , and $e_{x_1}, e_{x_2}, e_{x_3}$ are the unit vectors in the natural coordinate system and the global system, respectively. (a) and (b) can now be represented in a matrix form as

$$\sigma = Q^T \bar{\sigma} \quad \bar{\sigma} = P^T \sigma$$

$$\epsilon = P \bar{\epsilon} \quad \bar{\epsilon} = Q \epsilon$$

where

$$Q = \begin{bmatrix} (l_1)^2 & (l_2)^2 & (l_3)^2 & l_1 l_2 & l_2 l_3 & l_3 l_1 \\ (m_1)^2 & (m_2)^2 & (m_3)^2 & m_1 m_2 & m_2 m_3 & m_3 m_1 \\ (n_1)^2 & (n_2)^2 & (n_3)^2 & n_1 n_2 & n_2 n_3 & n_3 n_1 \\ 2l_1 m_1 & 2l_2 m_2 & 2l_3 m_3 & (l_1 m_2 + l_2 m_1) & (l_2 m_3 + l_3 m_2) & (l_3 m_1 + l_1 m_3) \\ 2m_1 n_1 & 2m_2 n_2 & 2m_3 n_3 & (m_1 n_2 + m_2 n_1) & (m_2 n_3 + m_3 n_2) & (m_3 n_1 + m_1 n_3) \\ 2n_1 l_1 & 2n_2 l_2 & 2n_3 l_3 & (n_1 l_2 + n_2 l_1) & (n_2 l_3 + n_3 l_2) & (n_3 l_1 + n_1 l_3) \end{bmatrix}$$

$$P = \begin{bmatrix} (l_1)^2 & (m_1)^2 & (n_1)^2 & l_1 m_1 & m_1 n_1 & n_1 l_1 \\ (l_2)^2 & (m_2)^2 & (n_2)^2 & l_2 m_2 & m_2 n_2 & n_2 l_2 \\ (l_3)^2 & (m_3)^2 & (n_3)^2 & l_3 m_3 & m_3 n_3 & n_3 l_3 \\ 2l_1 l_2 & 2m_1 m_2 & 2n_1 n_2 & (l_1 m_2 + l_2 m_1) & (m_1 n_2 + m_2 n_1) & (n_1 l_2 + n_2 l_1) \\ 2l_2 l_3 & 2m_2 m_3 & 2n_2 n_3 & (l_2 m_3 + l_3 m_2) & (m_2 n_3 + m_3 n_2) & (n_2 l_3 + n_3 l_2) \\ 2l_3 l_1 & 2m_3 m_1 & 2n_3 n_1 & (l_3 m_1 + l_1 m_3) & (m_3 n_1 + m_1 n_3) & (n_3 l_1 + n_1 l_3) \end{bmatrix}$$

$$\sigma = [\sigma_{11} \quad \sigma_{22} \quad \sigma_{33} \quad \sigma_{12} \quad \sigma_{23} \quad \sigma_{31}]$$

$$\bar{\sigma} = [\bar{\sigma}_{11} \quad \bar{\sigma}_{22} \quad \bar{\sigma}_{33} \quad \bar{\sigma}_{12} \quad \bar{\sigma}_{23} \quad \bar{\sigma}_{31}]$$

$$\begin{aligned}\epsilon &= [\epsilon_{11} \ \epsilon_{22} \ \epsilon_{33} \ 2\epsilon_{12} \ 2\epsilon_{23} \ 2\epsilon_{31}] \\ \bar{\epsilon} &= [\bar{\epsilon}_{11} \ \bar{\epsilon}_{22} \ \bar{\epsilon}_{33} \ 2\bar{\epsilon}_{12} \ 2\bar{\epsilon}_{23} \ 2\bar{\epsilon}_{31}]\end{aligned}$$

The transformation matrices P and Q have been presented for the 3-dimensional case with all stress and strain components present. If some of these are absent, however, P and Q can be simplified by eliminating appropriate row(s) and column(s).

Appendix B

Summaries

B.1 Updated Lagrangian Formulation with Jaumann Stress Rate

The Updated Lagrangian Formulation (ULF) and the Total Lagrangian Formulation (TLF) are the two approaches developed for nonlinear analyses with the elastic-plastic material model. In small-strain small-displacement problems, there is no distinction between the two formulations because the deformed configuration of a body at any time t is not much different from the undeformed configuration at time $t = 0$. For analyses involving large displacements and/or large strains (displacement gradients), however, there is a significant difference between the two formulations. The FEM literature shows that the ULF formulation is the most appropriate for sheet metal forming. Furthermore, the most effective stress measure in the ULF formulation for these large-strain cases is the Jaumann stress rate [9,84].

The development of the Updated Lagrangian Jaumann Stress-Rate Formulation begins with Equation (3.2)

$$({}^t\mathbf{K}_L + {}^t\mathbf{K}_{NL})\Delta U^{(i)} = {}^{t+\Delta t}\mathbf{R} - \frac{{}^{t+\Delta t}\mathbf{F}^{(i-1)}}{{}^{t+\Delta t}}$$

In the above equation, all quantities are evaluated with respect to the current con-

figuration, that is, the updated configuration of the material at time t . The key ingredients in the evaluation of ${}^t\mathbf{K}_L$, ${}^t\mathbf{K}_{NL}$, and ${}^{t+\Delta t}\mathbf{F}^{(i-1)}$ are the Cauchy stresses (physical stresses).

It is known that the most crucial part in a nonlinear FEM analysis is the calculation of stresses because the stress increments from time t to time $t + \Delta t$ are determined by the constitutive relation ${}^t\mathbf{C}^{EP}$ (or the instantaneous stress-strain matrix) which is stress-history dependent. If it is assumed that all Cauchy stress components ${}^t\tau_{ij}$ at time t are known, then the stress components at time $t + \Delta t$ are determined as follows

$${}^{t+\Delta t}\boldsymbol{\tau} = {}^t\boldsymbol{\tau} + \int_{{}^t\boldsymbol{\epsilon}}^{{}^{t+\Delta t}\boldsymbol{\epsilon}} {}^t\mathbf{C}^{EP} d\boldsymbol{\epsilon} + \Delta{}^t\boldsymbol{\tau} \quad (\text{B.1})$$

The time derivative of the second term on the right-hand side of Equation (B.1) is known as the Jaumann stress rate which is solely due to straining of the material, and is therefore invariant with respect to rigid-body rotations. The third term on the right-hand side can be physically interpreted as stress corrections to be added to ${}^t\boldsymbol{\tau}$ to account for rigid-body rotations (large displacements) and material distortions (large strains). Individual components of $\Delta{}^t\boldsymbol{\tau}$ are determined from

$$\Delta{}^t\tau_{ij} = \int_t^{t+\Delta t} \{ {}^t\tau_{ip}\Omega_{pj} - \Omega_{ip}{}^t\tau_{pj} \} dt \quad (\text{B.2})$$

with Ω_{ij} being the components of the spin tensor defined by

$$\Omega_{ij} = \frac{1}{2} \left\{ \frac{\partial \dot{u}_j}{\partial x_i} - \frac{\partial \dot{u}_i}{\partial x_j} \right\}$$

The integrations in Equations (B.1) and (B.2) are usually carried out using some direct integration technique such as the Euler forward integration method with a large number of steps so as to obtain sufficient accuracy for the solution. Although the magnitude of such a number can be arbitrarily chosen, the specific value is mainly determined by the plastic-strain increments according to some rule to minimize computing time.

The accumulated strains (elastic and plastic) are also calculated in the same manner, namely

$${}^{t+\Delta t}\epsilon = {}^t\epsilon + \int_t^{t+\Delta t} {}^t\dot{\epsilon} dt + \Delta{}^t\epsilon \quad (\text{B.3})$$

The components of the second term on the right-hand side of Equation (B.3) are nothing but the strain increments, and can be calculated directly from the corresponding displacement increments.

$${}^te_{ij} = \frac{1}{2} \left\{ \frac{\partial u_i}{\partial {}^tx_j} + \frac{\partial u_j}{\partial {}^tx_i} \right\}$$

Detailed discussion of the Updated Lagrangian Formulation with Jaumann stress rate can be found in Reference [9].

B.2 Modified Newton-Raphson Method

As mentioned in Chapter 1, a nonlinear FEM analysis is most effectively carried out incrementally and iteratively using some iterative technique. The most common one is the Newton-Raphson method in which to solve a set of nonlinear equations such as Equation (3.2),

$${}^t\mathbf{K}\Delta U^{(i)} = {}^{t+\Delta t}\mathbf{R} - {}^{t+\Delta t}\mathbf{F}^{(i-1)}$$

(${}^t\mathbf{K}$ represents the total global system stiffness matrix) the coefficient matrix ${}^t\mathbf{K}$ is recalculated and factorized in every iteration until the desired accuracy of the solution is obtained, Figure B.1. Although convergence is fast and the procedure is effective in some special case, the method does not have an overall economy for general elastic-plastic analyses. It is even prohibitively expensive to use in highly nonlinear problems with all kinematic and material nonlinearities present since a large number of small-sized time steps is usually required.

An alternative to the Newton-Raphson method is the initial stiffness method. The system stiffness matrix is now calculated and factorized only once at the beginning of the analysis ($t = 0$), and then reused over and over for all subsequent time steps and iterations. This method proves to be slightly more effective than the Newton-Raphson method, but there is an extremely slow convergence because no further reformation of the system stiffness matrix is made in the analysis. Also associated with the initial stiffness method are a few other drawbacks. For example, the slow convergence often terminates the computation too early because the maximum allowable number of iterations have been met while the prescribed tolerances have not, or the iteration process may even diverge as pointed out in [8,9,111]

In the modified Newton-Raphson method (Figure B.2), the system stiffness matrix is recalculated at the beginning of every time step, and then reused for all iterations within that time step. Convergence is now faster than in the initial stiffness method but slower than in the full Newton-Raphson method. Overall, the modified Newton-

Raphson method is more economical than the other two. In cases of slow convergence, the method can be made more effective by using such an acceleration scheme as the Aitken method [112].

Experience from the present study shows that caution should be exercised when using the Aitken acceleration because of possible negative effects. For instance, instead of speeding up the convergence, it could slow it down or even lead the solution to divergence because the solutions for individual unknowns being solved for neither converge at the same rate nor all converge monotonically. For that reason, the Aitken acceleration was not implemented in the program FENSA. However, a variation of the modified Newton-Raphson was introduced; within a time step, the system stiffness matrix is allowed to be reformed a second time after a number of iterations prescribed by the user. This option is represented by the broken line in the flowchart of the program FENSA shown in Appendix C.2.

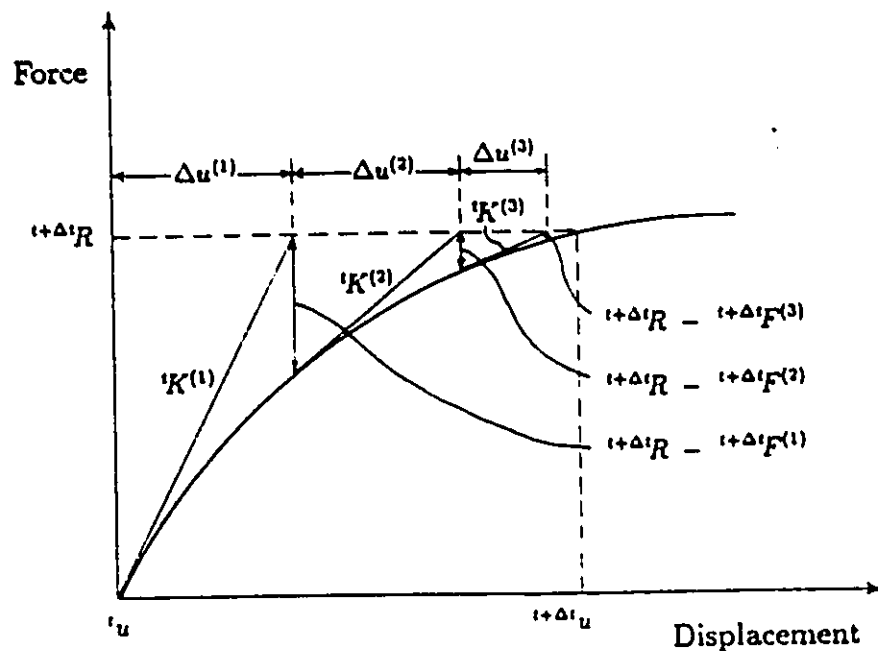


Figure B.1: Full Newton-Raphson method.

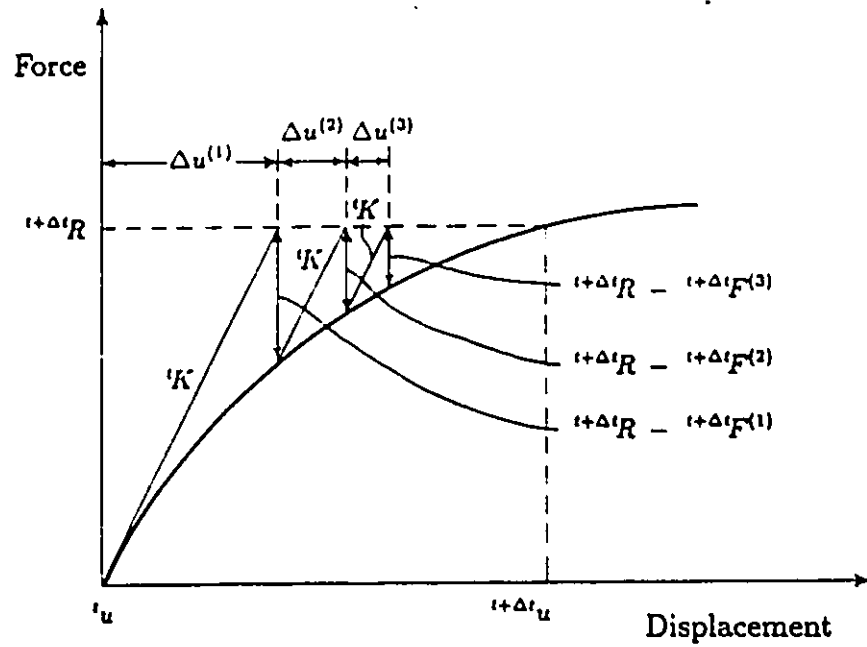


Figure B.2: Modified Newton-Raphson method.

Appendix C

Computer Software

C.1 Computer Program for EPBT

```

IMPLICIT REAL*(A-H,J-Z)
DIMENSION X(40000),Y(40000),X1(5000),Y1(5000),X2(5000),Y2(5000)
DIMENSION MBAT(26)
DATA MBAT/ 1.000, 1.200, 1.400, 1.600, 1.800,
           2.000, 2.200, 2.400, 2.600, 2.800, 3.000, 3.200,
           3.400, 3.600, 3.800, 4.000, 4.200, 4.400, 4.600,
           4.800, 5.000, 5.200, 5.400, 5.600, 5.800, 6.000 /
1 KKK= 5
DO 600 IS=1,48
READ (5,10) BI,RC,I LENG,DIST,EYLD,ELAM
WRITE (6,15) RI,RO,I LENG,DIST,EYLD,ELAM
10 FORMAT (7D15.6)
15 H= BI/RO
R2= B2/B
R3= B2/B2
R4= B2/B2
ROO= RO/BI
IO= 0.5*(I LENG - DIST)
N1= 51.940
N2= 39.940
PI= 3.14159265358979310
THICK= RO - BI
RMEAN= (RO + BI)/2.
RAT1= I LENG/EMEAN
RAT2= I LENG/EMEAN
WRITE (6,20) RAT1,RAT2
20 FORMAT (//) * RESULTS FOR RAT1 = ,D15.6,5X, RAT2 = ,D15.6)
C ... DX= 0.0200
J= 0
DO 30 I=1,N1
J= J + 1
X(J)= DX*FLOAT(I-1)
Y(J)= X(J)
30 CONTINUE
DX= 0.0100
DO 40 I=1,N2
J= J + 1
X(J)= X(J-1) + DX
XK= X(J)
TH1= 0.
TH2= DACOS(1./XK)
IF (XK.GT.ROO) TH1= DACOS(ROO/XK)
CON1= CSIN(TH2) - R3*DSIN(TH1)
CON2= (2.*TH2 + DSIN(2.*TH2)) - R4*(2.*TH1 + DSIN(2.*TH1))
CON3= DTAN(TH2) - DTAN(TH1)
CON4= (1. - ELAM)/(PI*(1. - R4))
Y(J)= XK + CON4*(16.*CON1/3. - XK*CON2 - 4.*CON3/(3.*XK*XK*XK))
40 CONTINUE
JPERM= J
PLOT THE GROWTH OF PLASTIC ZONES
DO 500 ITIME=1,26
W= WBA1(IIME)
K= 0

```

DEF00010
DEF00020
DEF00030
DEF00040
DEF00050
DEF00060
DEF00070
DEF00080
DEF00090
DEF00100
DEF00110
DEF00120
DEF00130
DEF00140
DEF00150
DEF00160
DEF00170
DEF00180
DEF00190
DEF00200
DEF00210
DEF00220
DEF00230
DEF00240
DEF00250
DEF00260
DEF00270
DEF00280
DEF00290
DEF00300
DEF00310
DEF00320
DEF00330
DEF00340
DEF00350
DEF00360
DEF00370
DEF00380
DEF00390
DEF00400
DEF00410
DEF00420
DEF00430
DEF00440
DEF00450
DEF00460
DEF00470
DEF00480
DEF00490
DEF00500
DEF00510
DEF00520
DEF00530
DEF00540
DEF00550

```

DX= 0.01D0
DO 100 I=N1,JPERM
K= K + 1
X1(K)= Y(I)*ID/W
Y1(K)= B0/X(I)
IF (X1(K)-LE.ID) GO TO 100
IX= X1(K)
IZ= Y1(K)
X1(K)= Y1(K-1) + (ID-X1(K-1))*(IZ-Y1(K-1))/(IX-X1(K-1))
GO TO 120
CONTINUE
100 WRITE (6,110) JPERM
110 FORMAT (' ***** ERBDR, MAXIMUM VALUES OF JPERM EXCEEDED ... =',IS)
STOP
N3= ( 0.5*ILENG - ID)/DX + 1
DX= ( 0.5*ILENG - ID)/FLOAT(N3)
DO 140 I=1,N3
K= K + 1
X1(K)= X1(K-1) + DX
Y1(K)= Y1(K-1)
CONTINUE
140 CONTINUE THE SLOPE CURVE
C ...
J= 1
X2(J)= X1(K)
Y2(J)= 0.
K1= K - 1
DO 200 I=K1,1,-1
J= J + 1
X2(J)= X1(I)
SLOPE= EYLD/Y1(I)
Y2(J)= Y2(J-1) - SLOPE*(X2(J-1) - X2(J))
CONTINUE
200 AA= X2(J)
N4= AA/DX + 1
DX= AA/FLOAT(N4)
DO 220 I=1,N4
J= J + 1
X2(J)= X2(J-1) - DX
SLOPE= X2(J)*EYLD/(AA*RU)
Y2(J)= Y2(J-1) - SLOPE*(X2(J-1) - X2(J))
CONTINUE
220 IF (ITIME.GT.1) GO TO 240
REF1= -(180./PI)*CATAN(Y2(J))
REF3= -(180./PI)*CATAN(Y2(J))
REF3= (REF2 - W*REF1)/ILENG
WRITE (6,280) ITIME,W,X2(J),Y2(J),REF1,REF2,REF3
280 FORMAT (' 15,6I5.6) GO TO 500
IF (KKK.EQ.5) GO TO 500
CONTINUE THE DEFLECTION CURVE
C ...
N5= J
X1(1)= 0.
Y1(1)= 0.
DO 300 I=2,N5
K= N5 - I + 2

```

DEF00560
DEF00570
DEF00580
DEF00590
DEF00600
DEF00610
DEF00620
DEF00630
DEF00640
DEF00650
DEF00660
DEF00670
DEF00680
DEF00690
DEF00700
DEF00710
DEF00720
DEF00730
DEF00740
DEF00750
DEF00760
DEF00770
DEF00780
DEF00790
DEF00800
DEF00810
DEF00820
DEF00830
DEF00840
DEF00850
DEF00860
DEF00870
DEF00880
DEF00890
DEF00900
DEF00910
DEF00920
DEF00930
DEF00940
DEF00950
DEF00960
DEF00970
DEF00980
DEF00990
DEF01000
DEF01010
DEF01020
DEF01030
DEF01040
DEF01050
DEF01060
DEF01070
DEF01080
DEF01090
DEF01100

X1(I) = X2(K-1)
Y1(I) = Y2(K) + (X1(I) - X1(I-1)) + Y1(I-1)

300 CONTINUE I=1, NS

J20 WRITE (6, 346) I, X1(I), Y1(I)

340 FORMAT (6, 346) I, X1(I), Y1(I)

500 CONTINUE

600 STOP

END

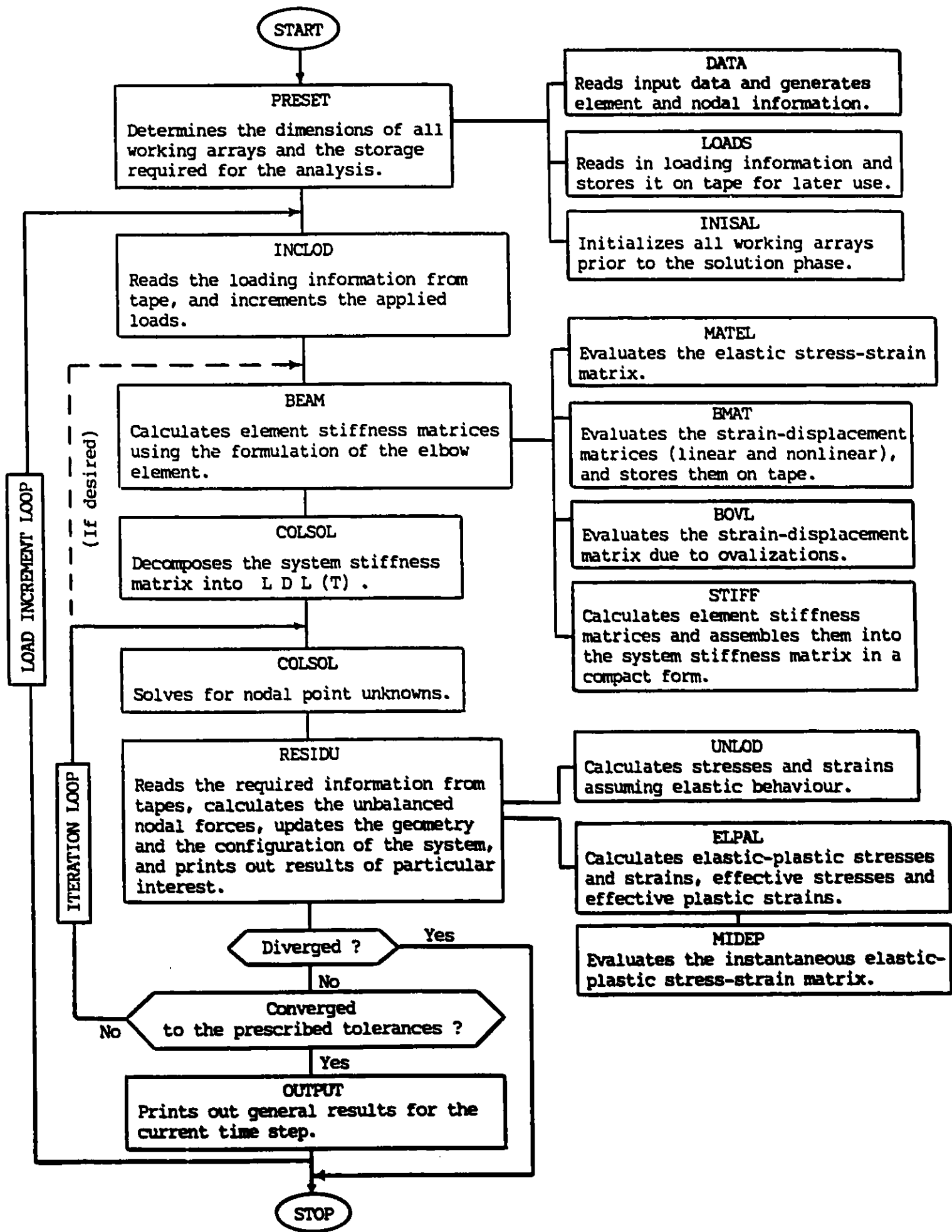
CSDATA

0.550+00	0.650+00	6.00+00	1.20+00	1.20-03	0.150+00	DEF01110
0.750+00	0.850+00	8.00+00	1.60+00	1.20-03	0.150+00	DEF01120
0.950+00	1.050+00	10.00+00	2.00+00	1.20-03	0.150+00	DEF01130
1.150+00	1.250+00	12.00+00	2.40+00	1.20-03	0.150+00	DEF01140
1.350+00	1.450+00	14.00+00	2.80+00	1.20-03	0.150+00	DEF01150
1.550+00	1.650+00	16.00+00	3.20+00	1.20-03	0.150+00	DEF01160
1.750+00	1.850+00	18.00+00	3.60+00	1.20-03	0.150+00	DEF01170
1.950+00	2.050+00	20.00+00	4.00+00	1.20-03	0.150+00	DEF01180
0.550+00	0.650+00	7.20+00	1.20+00	1.20-03	0.150+00	DEF01190
0.750+00	0.850+00	9.60+00	1.60+00	1.20-03	0.150+00	DEF01200
0.950+00	1.050+00	12.00+00	2.00+00	1.20-03	0.150+00	DEF01210
1.150+00	1.250+00	14.40+00	2.40+00	1.20-03	0.150+00	DEF01220
1.350+00	1.450+00	16.80+00	2.80+00	1.20-03	0.150+00	DEF01230
1.550+00	1.650+00	19.20+00	3.20+00	1.20-03	0.150+00	DEF01240
1.750+00	1.850+00	21.60+00	3.60+00	1.20-03	0.150+00	DEF01250
1.950+00	2.050+00	24.00+00	4.00+00	1.20-03	0.150+00	DEF01260
0.550+00	0.650+00	8.40+00	1.20+00	1.20-03	0.150+00	DEF01270
0.750+00	0.850+00	11.20+00	1.60+00	1.20-03	0.150+00	DEF01280
0.950+00	1.050+00	14.00+00	2.00+00	1.20-03	0.150+00	DEF01290
1.150+00	1.250+00	16.80+00	2.40+00	1.20-03	0.150+00	DEF01300
1.350+00	1.450+00	19.60+00	2.80+00	1.20-03	0.150+00	DEF01310
1.550+00	1.650+00	22.40+00	3.20+00	1.20-03	0.150+00	DEF01320
1.750+00	1.850+00	25.20+00	3.60+00	1.20-03	0.150+00	DEF01330
1.950+00	2.050+00	28.00+00	4.00+00	1.20-03	0.150+00	DEF01340
0.550+00	0.650+00	9.60+00	1.20+00	1.20-03	0.150+00	DEF01350
0.750+00	0.850+00	12.80+00	1.60+00	1.20-03	0.150+00	DEF01360
0.950+00	1.050+00	16.00+00	2.00+00	1.20-03	0.150+00	DEF01370
1.150+00	1.250+00	19.20+00	2.40+00	1.20-03	0.150+00	DEF01380
1.350+00	1.450+00	22.40+00	2.80+00	1.20-03	0.150+00	DEF01390
1.550+00	1.650+00	25.60+00	3.20+00	1.20-03	0.150+00	DEF01400
1.750+00	1.850+00	28.80+00	3.60+00	1.20-03	0.150+00	DEF01410
1.950+00	2.050+00	32.00+00	4.00+00	1.20-03	0.150+00	DEF01420
0.550+00	0.650+00	10.80+00	1.20+00	1.20-03	0.150+00	DEF01430
0.750+00	0.850+00	14.40+00	1.60+00	1.20-03	0.150+00	DEF01440
0.950+00	1.050+00	18.00+00	2.00+00	1.20-03	0.150+00	DEF01450
1.150+00	1.250+00	21.60+00	2.40+00	1.20-03	0.150+00	DEF01460
1.350+00	1.450+00	25.20+00	2.80+00	1.20-03	0.150+00	DEF01470
1.550+00	1.650+00	28.80+00	3.20+00	1.20-03	0.150+00	DEF01480
1.750+00	1.850+00	32.40+00	3.60+00	1.20-03	0.150+00	DEF01490
1.950+00	2.050+00	36.00+00	4.00+00	1.20-03	0.150+00	DEF01500
0.550+00	0.650+00	11.20+00	1.20+00	1.20-03	0.150+00	DEF01510
0.750+00	0.850+00	15.20+00	1.60+00	1.20-03	0.150+00	DEF01520
0.950+00	1.050+00	19.20+00	2.00+00	1.20-03	0.150+00	DEF01530
1.150+00	1.250+00	23.20+00	2.40+00	1.20-03	0.150+00	DEF01540
1.350+00	1.450+00	27.20+00	2.80+00	1.20-03	0.150+00	DEF01550
1.550+00	1.650+00	31.20+00	3.20+00	1.20-03	0.150+00	DEF01560
1.750+00	1.850+00	35.20+00	3.60+00	1.20-03	0.150+00	DEF01570
1.950+00	2.050+00	39.20+00	4.00+00	1.20-03	0.150+00	DEF01580
0.550+00	0.650+00	12.00+00	1.20+00	1.20-03	0.150+00	DEF01590
0.750+00	0.850+00	16.40+00	1.60+00	1.20-03	0.150+00	DEF01600
0.950+00	1.050+00	20.80+00	2.00+00	1.20-03	0.150+00	DEF01610
1.150+00	1.250+00	25.20+00	2.40+00	1.20-03	0.150+00	DEF01620
1.350+00	1.450+00	29.60+00	2.80+00	1.20-03	0.150+00	DEF01630
1.550+00	1.650+00	34.00+00	3.20+00	1.20-03	0.150+00	DEF01640
1.750+00	1.850+00	38.40+00	3.60+00	1.20-03	0.150+00	DEF01650

FILE: DEFL FORIHAN A UNIV. D'OF JTTAMA CMS RELEASE 4

1.350+00	1.450+00	28.00+00	2.80+00	1.20-03	0.15D+00	DEF01660
1.550+00	1.650+00	32.00+00	3.20+00	1.20-03	0.15D+00	DEF01670
1.750+00	1.850+00	36.00+00	3.60+00	1.20-03	0.15D+00	DEF01680
1.950+00	2.050+00	40.00+00	4.00+00	1.20-03	0.15D+00	DEF01690

C.2 Flowchart of Program FENSA



C.3 Listing of Program FENSA

```

C ... MAIN P80GBAM
IMPLICIT REAL*(A-H,O-Z)
COMMON/SOL/ NEQ,NEQ1,NHK,NK,NES
COMMON/VAR/ IINCS,IITER,IPEL,IREM,IND,IPT,ICHEK
COMMON/DIM/ N1,N2,N3,N4,N5,N6,N7,N8,N9,N10,N11,N12,N13,N14,N15,
1 N16,N17,N18,N19,N20,N21,N22,N23,N24,N25
COMMON/TAPE/ IT1,IT2,IT3,IT4,IT5,IT6,IT7,IT8
COMMON A(60000)
MIOI= 60000
SET UP STORAGE AND READ IN DATA
CALL PRESET (MIOI)
IF (MIOEX.EQ.0) STOP
ENTER SOLUTION PHASE
ACLOD= 0
DO 200 IINCS=1,NINCS
CALL INCLD (A(N17),A(N20),A(N21),ACLOD)
KIR= 1
HBLIE (IT6,2000) IINCS
HBLIE (IT7,2000) IINCS
DO 100 IITEB=1,MITER
IND= 1
IF (IINCS.EQ.1.AND.IITER.EQ.1) IND= 0
IF (KIR-1) 20,20,40
CALL EAM (A(N1),A(N2),A(N3),A(N4),A(N5),A(N6),A(N7),A(N9),
20 1 A(N10),A(N11),A(N12),A(N13),A(N14),A(N15),A(N23),A(N25))
COLSOL (A(N14),A(N17),A(N9),NEQ,NHK,NEQ1,KIR)
CALL KIR= 2 COLSOL (A(N14),A(N17),A(N9),:EQ,NHK,NEQ1,KIR)
40 COMPUTE RESIDUAL STRESSES
CALL RESIDU (A(N1),A(N2),A(N3),A(N4),A(N5),A(N6),A(N7),A(N10),
1 A(N11),A(N12),A(N13),A(N15),A(N16),A(N17),A(N18),A(N19),A(N20),
2 A(N21),A(N22),A(N23),A(N24),A(N25))
C ... IF SOLUTION HAS CONVERGED, STOP ITERATING AND OUTPUT RESULTS
60 IF (ICHEK) 250,80,120
C ... IF (IITEB.EQ.MITER) GO TO 250
IF (IITEBNESS IS UPDATED BEFORE CONVERGENCE, SET KTR= 1
C ... IF (IITER.NE.INTUP) GO TO 100
KTR= 1
HBLIE (IT6,2020) IITER
100 CONTINUE
120 CALL CUIPUT (A(N1),A(N6),A(N19),ACLOD)
200 CONTINUE
GO TO 300
250 CALL CUIPUT (A(N1),A(N6),A(N19),ACLOD)
300 STOP
2000 FORMAT (///50H *>*>*> CURR ENT NO. I T S F O R,
3X,38H L O A D I N C R E M E N T H O - I A //)
2020 1 FORMAT (///1CX,46H ====> SYSTEM CONFIGURATION HAS BEEN UPDATED,
1 6H AFTER,15,14H ITERATIONS //)
END
C SUBROUTINE ACDSAM (A,MAX3,S,LM,MD)
C ...
C ...

```

FEN000010
FEN000020
FEN000030
FEN000040
FEN000050
FEN000060
FEN000070
FEN000080
FEN000090
FEN000100
FEN000110
FEN000120
FEN000130
FEN000140
FEN000150
FEN000160
FEN000170
FEN000180
FEN000190
FEN000200
FEN000210
FEN000220
FEN000230
FEN000240
FEN000250
FEN00G260
FEN000270
FEN000280
FEN000290
FEN000300
FEN000310
FEN000320
FEN000330
FEN000340
FEN000350
FEN000360
FEN000370
FEN000380
FEN000390
FEN000400
FEN000410
FEN000420
FEN000430
FEN000440
FEN000450
FEN000460
FEN000470
FEN000480
FEN000490
FEN000500
FEN000510
FEN000520
FEN000530
FEN000540
FEN000550


```

C ... CLEAR ABBAY MAXA
DO 20 I=1,NEC1
20 MAXA(I)=0.
MAXA(1)=1
MAXA(2)=2
MK=0
IF (NEG.EQ.1) GO TO 100
DO 10 I=2,NEC
IF (MHI(I).GT.MK) MK= MHI(I)
10 MAXA(I+1)= MAXA(I) + MHT(I) + 1
100 MK= MK + 1
MK= MAXA(NEC+1) -- MAXA(1)
RETURN
END

C BLOCK DATA
IMPLICIT REAL*8(A-H,O-Z)
COMMON/INTG/ ELXY(3,4),VS(3,4),VT(3,4),WGR(5),WGP(2),MGH(5)
DATA WGB/ 7.00, 32.00, 12.00, 32.00, 7.00 /
DATA WGP/ 1.00, 1.00 /
DATA WGH/ 7.00, 32.00, 12.00, 32.00, 7.00 /
END

C SUBROUTINE EEAM (ID,NEL,XYZ,VSP,VTP,BDS,ELG,MAXA,LX,BL,BN,SE,AG,
ASIG,IUP,ISTATE)
IMPLICIT REAL*8(A-H,O-Z)
COMMON/GEN/ NUMNP,NUMEL,MPE,NDF,NDE,NDS,NIPS,IPL,IPP,IPW,IPH
COMMON/MAI/ STRESS(6),SIRAIN(6),C(6,6),YLD,HPRIME,IST,ISR
COMMON/PRO/ GEOM(8),PROP(6),EMOD(3,10),FLOD(JO),NPAR(6)
COMMON/VAR/ IINCS,LITER,IPEL,IREM,IND,IPT,ICHEK
COMMON/SOL/ NEJ,NE21,NMK,MK,MES
COMMON/LOCA/ B,S,I,TH,THIC,ZI,FI,CS,SN,RD,EG,IP1,IP2,N,NC,NTC
COMMON/INTG/ ELXY(3,4),VS(3,4),Vf(3,4),WGR(5),MGP(2),MGH(5)
COMMON/INTG/ IT1,IT2,IT3,IT4,IT5,IT6,IT7,IT8
COMMON/INTG/ IC(NDF,1),NEL(NPE,1),LM(NDC,1),BL(6,NDE),BN(9,NDE),SE(1),
ELG(1),MAXA(1),
DIMENSION IC(NDF,1),NEL(NPE,1),IUP(IPH,1),EXA(324)
1 ELG(1),ASIG(1),
2 AG(7),CI(6,6),J2(6,6),EXA(37),Q2(1,1)
1 EQUIVALENCE
{GEOM(2),RA},(NPAR(3),INTEF),(NPAR(4),IFIX),
{EXA(1),J1(1,1)},(EXA(37),Q2(1,1))
REWIND IT2
REWIND IT3
INITIALIZE GLOBAL STIFFNESS ABBAY
CALL CLEAR (AG,NMK)
NTC= NDF-6
PI= 3.14159265358979320
KP= IPP/6
IP1= 1 + IPP/4
IP2= IP1 + IPP/4
IMW= (IPW + 1)/2
DIA= 2.*PI/LFLOAT(IPP)
DIF= DFLOAT(IPW-1)
IF (INC.GT.0) GO TO 40
DC 10 I=1, IPL

```

FEN01110
FEN01120
FEN01130
FEN01140
FEN01150
FEN01160
FEN01170
FEN01180
FEN01190
FEN01200
FEN01210
FEN01220
FEN01230
FEN01240
FEN01250
FEN01260
FEN01270
FEN01280
FEN01290
FEN01300
FEN01310
FEN01320
FEN01330
FEN01340
FEN01350
FEN01360
FEN01370
FEN01380
FEN01390
FEN01400
FEN01410
FEN01420
FEN01430
FEN01440
FEN01450
FEN01460
FEN01470
FEN01480
FEN01490
FEN01500
FEN01510
FEN01520
FEN01530
FEN01540
FEN01550
FEN01560
FEN01570
FEN01580
FEN01590
FEN01600
FEN01610
FEN01620
FEN01630
FEN01640
FEN01650

```

10 WGR(I) = WGR(I)/45.
20 MGP(I) = PI*WGP(I)/12.
80 IPT = 0
CALL MATEL (P8OP,C)
DO 200 N=1,NUMEL
M1 = NEL(M,N)
DO 60 L=1,3
ELXY(L,M) = XYZ(L,M1)
VS(L,M) = VSP(L,M1)
VT(L,M) = VTP(L,M1)
60 BD = BDS(N)
EG = ELG(N)
CALL CLEAR (SE,NE5)
ENTER INTEGRATION LOOP WITH NEWTON-COTES FORMULAS
DO 160 IB=1,IP1
B = -1.5 + 0.5*DFLOAT(IR)
ITHIC = (N-1)*IP1 + IR
DO 160 IA=1,IPH
FAC1 = 2.
FAC2 = 2.
IF (IA.EQ.1.CB.IA.EQ.IPH) FAC2 = 1.
FI = DIA*DFLOAT(IA-1)
CS = DCCS(FI)
SN = DSIN(FI)
IF (IA.EQ.IP1) CS = 0.
IF (IA.EQ.IP2) SN = 0.
ITHIC = IUP(IA,ITHIC)
RAT = THIC/RA
ZIN = THIC/DI
DO 80 I=1,IPW
WH(I) = BAI*WGM(I)/90.
80 DO 160 IT=1,IPH
IH = 1. - BAI*DFLOAT(IPW-IT)/DI
ZI = -2. IN*DFLOAT(IM-IT)
S = IH*CS
I = IH*SN
IPT = IPT + 1
IPEL = ISTATE(IPT)
CALCULATE STRAIN-DISPLACEMENT TRANSFORMATION MATRICES
IF (INC.EQ.-1) CALL LOCAT (ELXY,VS,VT,R,S,I,RA,N,IR,IA,IT,IPT)
CALL SHAPE (ELXY,VS,VT,J1,J2,BL,BH,DET)
IH = FAC1*FAC2*TH*CGR(IN)*WGP(I)*WH(IT)
IF (INC.EQ.0.OR.IREM.EQ.1) GO TO 120
DETERMINE CURRENT STRESSES
DO 100 I=1,IST
STRESS(I) = ASIG(I,IPT)
100 CALL STIFF (EL,BN,J1,J2,C,SE,STRESS,EXA,EXA,WT)
160 CONTINUE
CALL ALDDBAN (AG,MAXA,SE,LM(1,N),NDE)
CGN INUE
IF (INC.EQ.0.CB.(INIEF.EQ.0.AND.IFIX.EQ.0)) RETURN
CALL PENAL (ID,AG,MAXA,NJHNP,MUF,ALFA)
CALL RPCI (RCS,ELJ,LM,SE,ALFA)

```

- FEN01660
- FEN01670
- FEN01680
- FEN01690
- FEN01700
- FEN01710
- FEN01720
- FEN01730
- FEN01740
- FEN01750
- FEN01760
- FEN01770
- FEN01780
- FEN01790
- FEN01800
- FEN01810
- FEN01820
- FEN01830
- FEN01840
- FEN01850
- FEN01860
- FEN01870
- FEN01890
- FEN01890
- FEN01900
- FEN01910
- FEN01920
- FEN01930
- FEN01940
- FEN01950
- FEN01960
- FEN01970
- FEN01980
- FEN01990
- FEN02000
- FEN02010
- FEN02020
- FEN02030
- FEN02040
- FEN02050
- FEN02060
- FEN02070
- FEN02080
- FEN02090
- FEN02100
- FEN02110
- FEN02120
- FEN02130
- FEN02140
- FEN02150
- FEN02160
- FEN02170
- FEN02180
- FEN02190
- FEN02200

FEN02210
 FEN02220
 FEN02230
 FEN02240
 FEN02250
 FEN02260
 FEN02270
 FEN02280
 FEN02290
 FEN02300
 FEN02310
 FEN02320
 FEN02330
 FEN02340
 FEN02350
 FEN02360
 FEN02370
 FEN02380
 FEN02390
 FEN02400
 FEN02410
 FEN02420
 FEN02430
 FEN02440
 FEN02450
 FEN02460
 FEN02470
 FEN02480
 FEN02490
 FEN02500
 FEN02510
 FEN02520
 FEN02530
 FEN02540
 FEN02550
 FEN02560
 FEN02570
 FEN02580
 FEN02590
 FEN02600
 FEN02610
 FEN02620
 FEN02630
 FEN02640
 FEN02650
 FEN02660
 FEN02670
 FEN02680
 FEN02690
 FEN02700
 FEN02710
 FEN02720
 FEN02730
 FEN02740
 FEN02750

```

RETURN
END
C
SUBROUTINE BMAT (JL,UN,VS,VT,XJI,H,DH,S,T,THLC,HA,NPE,NDF)
C
IMPLICIT REAL*8(A-Z)
DIMENSION BL(6,1),UN(9,1),VS(3,1),VT(3,1),XJI(3,1),H(1),DH(1)
DIMENSION G1(3,3),G2(3,3),G3(3,3),GS2(3,3),GS3(3,3),
1 DHXY(3)
DO 120 K=1,NPE
DO 10 I=1,3
GS1(I,I)=0.
GS1(I,1)= -VS(3,K)*RA
GS1(1,2)= -VS(2,K)*RA
GS1(2,3)= -VS(1,K)*RA
GS2(1,2)= -VT(1,K)*RA
GS2(2,3)= -VT(2,K)*RA
DO 20 I=1,3
I1= I - 1
DO 20 J=1,I1
GS1(I,J)= -GS1(J,I)
GS2(I,J)= -GS2(J,I)
20 DO 30 I=1,3
DO 30 J=1,3
GS3(I,J)= S*GS1(I,J) + T*GS2(I,J)
DO 40 I=1,3
DHXY(I)= XJI(I,1)*DH(K)
DO 40 N=1,3
G1(I,N)= XJI(N,1)*SSJ(1,I)*DH(K) + H(K)*XJI(N,2)*GS1(1,I)
1 G2(I,N)= XJI(N,1)*SSJ(2,I)*DH(K) + H(K)*XJI(N,2)*GS1(2,I)
1 G3(I,N)= XJI(N,1)*SSJ(3,I)*DH(K) + H(K)*XJI(N,2)*GS1(3,I)
1 IF (DABS(G1(I,N)).LT.1.D-35) G1(I,N)= 0.
IF (DABS(G2(I,N)).LT.1.D-35) G2(I,N)= 0.
IF (DABS(G3(I,N)).LT.1.D-35) G3(I,N)= 0.
CONTINUE
40 KM= (K-1)*NDF
KM1= KM + 1
KM2= KM + NDF
CALCULATE LINEAR STRAIN-DISPLACEMENT TRANSFORMATION MATRIX
C ...
DO 50 I=1,6
DC 50 J=KM1,KM2
DO 60 I=1,3
BL(I,KM+I)= DHXY(I)
BL(I,KM+4)= G1(I,I)
BL(I,KM+5)= G2(I,I)
BL(I,KM+6)= G3(I,I)
H= 1 + MOD(I,3)
BL(I+3,KM+I)= DHXY(H)
BL(I+3,KM+M)= DHXY(I)
50
    
```

```

60  BL(I+3,KM+4) = G1(I,M) + G1(M,I)
    BL(I+3,KM+5) = G2(I,M) + G2(M,I)
    BL(I+3,KM+6) = G3(I,M) + G3(M,I)
C ... CALCULATE NON-LINEAR STRAIN-DISPLACEMENT TRANSFORMATION MATRIX
DO 70 I=1,9
DC 70 J=KM1,KM2
BN(I,J) = 0.
DO 80 I=1,3
DC 80 J=1,3
IJ = (I-1)*3 + J
BN(IJ,KM+J) = CHXY(I)
BN(IJ,KM+4) = G1(J,I)
BN(IJ,KM+5) = G2(J,I)
BN(IJ,KM+6) = G3(J,I)
120 CONTINUE
END

C
C
SUBROUTINE BCVL ( H,DH,Q2,BL,IA,IA,IT)
IMPLICIT REAL*(A-H,I-J-Z)
COMMON/PRO/ GEOM(8),PROP(6),EMOD(3,10),FLOD(30),NPAR(6)
COMMON/GEN/ NUMNP,NUMEL,NPE,NDF,NDS,NIPS,IPL,IPP,IPW,IPH
COMMON/LOCA/ R,S,I,TU,I,HIC,ZI,FI,CS,SM,RD,EG,IPI,IP2,N,NC,NTC
COMMON/VAR/ IINCS,IIFSR,IPEL,IEM,IAD,IPT,ICHEK
DIMENSION H(1),DH(4),J2(6,1),BL(6,1),D6(6,12),DB(6,12)
EQUIVALENCE (GEOM(1),I AVG), (GEOM(2),BA), (NPAR(3),INIEF)

A = BA - 0.5*IAVG
DO 30 K=1,NPE
KK = (K-1)*NC
DO 30 J=1,NC
DO 10 I=1,6
BM(I,KK+J) = 0.
FM = DFL0AT(2*J)
C1 = DCC5(FM*FI)
C2 = CS
C3 = DSIN(FM*FI)
C4 = SN
VR1 = FM*(1. - FM*E4)*H(K)*C1*ZT/(A*A)
VR2 = H(K)*(FM*C1*C2 + C3*C4)/(RD - A*C2)
IF (INIEF.EQ.0) GJ TJ 20
IEI = EG/RD
C5 = 2./((RD-A*C2)*IEI)
VR2 = VB2 + C5*C5*D.I(K,2)*FM*C1*ZT
VR3 = C5*C3*CH(K,1)
IF (DABS(VR3).GE.1.D-35) DO(4, KK+J) = VR3
IF (DABS(VR2).GE.1.D-35) DO(2, KK+J) = VR2
IF (DABS(VR1).GE.1.D-35) DO(1, KK+J) = VR1
20 CONTINUE
30 CONTINUE

DO 50 I=1,6
DC 50 J=1,NC
SUM = 0.
DO 40 K=1,6

```

FEN02760
FEN02770
FEN02780
FEN02790
FEN02800
FEN02810
FEN02820
FEN02830
FEN02840
FEN02850
FEN02860
FEN02870
FEN02880
FEN02890
FEN02900
FEN02910
FEN02920
FEN02930
FEN02940
FEN02950
FEN02960
FEN02970
FEN02980
FEN02990
FEN03000
FEN03010
FEN03020
FEN03030
FEN03040
FEN03050
FEN03060
FEN03070
FEN03080
FEN03090
FEN03100
FEN03110
FEN03120
FEN03130
FEN03140
FEN03150
FEN03160
FEN03170
FEN03180
FEN03190
FEN03200
FEN03210
FEN03220
FEN03230
FEN03240
FEN03250
FEN03260
FEN03270
FEN03280
FEN03290
FEN03300

```

40 SUM = SUM + G2(I,K)*BU(K,J) SUM = 0.
50 DB(I,J) = SUM
DO 60 K=1,NPE
K1 = (K-1)*NDF + 6
K2 = (K-1)*NC
DO 60 I=1,6
DO 60 J=1,NC DB(I,K2+J)
60 RETURN
END
C
SUBROUTINE CLEAR (L,L2)
C
IMPLICIT REAL*8(A-J,O-Z)
DIMENSION Z(L2)
DO 10 I=1,L2
10 Z(I) = 0.
RETURN
END
C
SUBROUTINE COLLT (MHI,LM,ND)
C
IMPLICIT REAL*8(A-J,O-Z)
DIMENSION MHI(1),LM(1)
LS = 100000
DO 100 I=1,NC
IF (LM(I)) 110,100,110
110 IF (LM(I)-LS) 120,100,100
120 LS = LM(I)
100 CONTINUE
C
DO 200 I=1,NC
II = LM(I)
IF (II.EQ.0) GO TO 200
ME = II - LS
IF (ME.GT.MHI(II)) MHI(II) = ME
200 CONTINUE
RETURN
END
C
SUBROUTINE CCLSOL (A,V,MAXA,NN,MHK,NNM,KKK)
C
P R O C E S S
TO SOLVE FINITE ELEMENT STATIC EQUILIBRIUM EQUATIONS IN
CORE, USING COMPACTED STORAGE AND COLUMN REDUCTION SCHEME
C
** INPUT VARIABLES
A(NMK) = STIFFNESS MATRIX STORED IN COMPACTED FORM
V(NN) = RIGHT-HAND-SIDE LOAD VECTOR
MAXA(NNM) = VECTOR CONTAINING ADDRESSES OF DIAGONAL
ELEMENTS OF STIFFNESS MATRIX IN A
NN = NUMBER OF EQUATIONS
NMK = NUMBER OF ELEMENTS BELOW SKYLINE OF MATRIX
C

```

FEN03310
FEN03320
FEN03330
FEN03340
FEN03350
FEN03360
FEN03370
FEN03380
FEN03390
FEN03400
FEN03410
FEN03420
FEN03430
FEN03440
FEN03450
FEN03460
FEN03470
FEN03480
FEN03490
FEN03500
FEN03510
FEN03520
FEN03530
FEN03540
FEN03550
FEN03560
FEN03570
FEN03580
FEN03590
FEN03600
FEN03610
FEN03620
FEN03630
FEN03640
FEN03650
FEN03660
FEN03670
FEN03680
FEN03690
FEN03700
FEN03710
FEN03720
FEN03730
FEN03740
FEN03750
FEN03760
FEN03770
FEN03780
FEN03790
FEN03800
FEN03810
FEN03820
FEN03830
FEN03840
FEN03850


```

160 K = N
    C = 0
    DO 170 KK=KL,KU
    K = K - 1
    C = C + A(KK)*V(K)
170 V(N) = V(N) - C
180 CONTINUE
    C ... BACK-SUBSTITUTE
    DO 200 N=1,NN
    K = MAXA(N)
200 V(N) = V(N)/A(K)
    IF (NN.EQ.1) RETURN
    N = NN
    DO 230 L=2,NN
    KL = MAXA(N) + 1
    KU = MAXA(N+1) - 1
    IF (KU-RL) 230,210,210
210 K = N
    DO 220 KK=KL,KU
    K = K - 1
220 V(K) = V(K) - A(KK)*V(N)
230 N = N - 1
    RETURN
2000 1 FORMAT(//48H STOP - STIFFNESS MATRIX NOT POSITIVE DEFINITE //
      2 32H NONPOSITIVE PIVOT FOR EQUATION ,I4//
      10H PIVOT = ,D20.12 )
      2 END
C
C SUBROUTINE CCSET (ID,NEL,MHT,MAXA,LM)
C IMPLICIT REAL*8(A-H,O-Z)
COMMON/GEN/ NUMNP, NUMEL, NPE, NDF, NDE, NDS, NIPS, IPL, IPP, IPH, IPH
COMMON/PRO/ GEOM(8), PROP(6), EMOD(3,10), FLOD(30), NPAR(6)
COMMON/SOL/ NEL, NEL1, NPK, MK, NES
COMMON/TAPE/ I1, I2, I3, I4, I5, I6, I7, I8
DIMENSION I1(NDE,1), I2(NPE,1), I3(NPE,1), MHT(1), MAXA(1), LM(NDE,1)
EQUIVALENCE (NPAR(3), INIEF)
CALCULATE COLUMN HEIGHTS
C ... DO 10 I=1,NEC
10 MHT(I) = 0.
    DO 40 I=1,NUMEL
    IJ = 0
    DO 20 J=1,NPE
    IK = NEL(J,I)
    DO 20 K=1,NDF
    IJ = IJ + 1
    LM(IJ,I) = ID(K,IK)
20 CALL CCLHT (MHT,LM(1,I),NDE)
40 CONTINUE
C ... IF (INIEF.EQ.0.OR.:NUMEL.EQ.1.OR.NDF.EQ.6) GC TO 150
    RECALCULATE COLUMN HEIGHTS IF INTEFF'S ARE TAKEN INTO ACCOUNT
    NPE1 = NPE - 1
    NUM = NUMEL - 1
    DO 120 I=1,NUM
    LOW = 10000

```

FEN04410
FEN04420
FEN04430
FEN04440
FEN04450
FEN04460
FEN04470
FEN04480
FEN04490
FEN04500
FEN04510
FEN04520
FEN04530
FEN04540
FEN04550
FEN04560
FEN04570
FEN04580
FEN04590
FEN04600
FEN04610
FEN04620
FEN04630
FEN04640
FEN04650
FEN04660
FEN04670
FEN04680
FEN04690
FEN04700
FEN04710
FEN04720
FEN04730
FEN04740
FEN04750
FEN04760
FEN04770
FEN04780
FEN04790
FEN04800
FEN04810
FEN04820
FEN04830
FEN04840
FEN04850
FEN04860
FEN04870
FEN04880
FEN04890
FEN04900
FEN04910
FEN04920
FEN04930
FEN04940
FEN04950

```

DO 80 J=1,NPE1
J1=(J-1)*NDE
DO 80 K=7,NCF
NEW=LP(J1+K,I)
IF (NEW) 80,80,60
IF (NEW.LT.LCH) LJM=NEA
60 CGNTINCE
80 DO 100 J=2,NPE
J1=(J-1)*NDF
DO 100 K=7,NDF
KK=LH(J1+K,I+1)
IF (KK.EQ.0) GO TO 100
KK=KK-LOW
IF (KH.GI.MHI(KK)) M.II(KK)=KM
100 CONTINUE
120 CALCULATE ADDRESS OF DIAGONAL ELEMENTS OF STIFFNESS MATRIX
C ... CALL ACCRES (MAXA,MHI)
150 MM=NHK/NEQ
WRITE (IT6,2000) NEQ,NHK,MK,MM
RETURN
2000 FORMAT (// 40H T O I A L S Y S T E M D A T A //5X,
1 40H NUMBER OF EQUATIONS (NEQ) =,I6/5X,
2 40H NUMBER OF MATRIX ELEMENTS (NHK) =,I6/5X,
3 40H MAXIMUM HALF BANDWIDTH (MK) =,I6/5X,
4 40H MEAN HALF BANDWIDTH (M4) =,I6)
END
C SUBROUTINE DATA (ID,NEL,XYZ,VSP,VIP,BDS,ELG,NRN)
C
IMPLICIT REAL*8(A-Z)
COMMON/GEN/ NUMNP,NUMEL,NPE,NDF,NDE,NDS,NIPS,IPL,IPP,IPW,IPH
COMMON/MAT/ STRESS(6),SIVALN(6),C(6,6),YLD,HPRIME,ISF,ISR
COMMON/PRO/ GEOM(8),PROP(6),EMOD(3,10),FLOD,HPRIME,ISF,ISR
COMMON/MAX/ NMODS,NINCS,MIFER,MODEX,INITUP
COMMON/SOL/ FIOLE,TOLFO,TOLER,CURVY
COMMON/TAPE/ I1,I2,I3,I4,I5,I6,IT7,IT8
COMMON/ION/ ID(NDF,1),NEL(NPE,1),XYZ(3,1),VSP(3,1),VIP(3,1),RDS(1),
1 EQUIVALENCE (GEOM(3),RMAX),(PROP(1),YM),(NPAR(1),ITYPE)
WRITE (IT6,2000)
READ (IT5,1000) {JEOH(I),I=1,6},{PBOH(I),I=1,6},{NPAR(I),I=1,6}
WRITE (IT6,2020) {JEOH(I),I=1,4},{PBOH(I),I=1,4},{NPAR(I),I=1,4}
NDE=NPE*NDF
IPH=1+IPP/2
NIPS=NUMEL*IPL*IPH
NES=NDE*(NDE+1)/2
ISR=6
C ... DATA ABE REAC IN
DO 20 I=1,NUMEL
RDS(I)=RMAX
READ (IT5,1010) J,ELJ(J)
C ... ELEMENT CONNECTIVITY IS GENERATED

```

FEN04960
FEN04970
FEN04980
FEN04990
FEN05000
FEN05010
FEN05020
FEN05030
FEN05040
FEN05050
FEN05060
FEN05070
FEN05080
FEN05090
FEN05100
FEN05110
FEN05120
FEN05130
FEN05140
FEN05150
FEN05160
FEN05170
FEN05180
FEN05190
FEN05200
FEN05210
FEN05220
FEN05230
FEN05240
FEN05250
FEN05260
FEN05270
FEN05280
FEN05290
FEN05300
FEN05310
FEN05320
FEN05330
FEN05340
FEN05350
FEN05360
FEN05370
FEN05380
FEN05390
FEN05400
FEN05410
FEN05420
FEN05430
FEN05440
FEN05450
FEN05460
FEN05470
FEN05480
FEN05490
FEN05500

```

I=1
DO 40 N=1, NUMEL
I=I+1
DO 40 K=1, NPE
I=I+1
40 NEL(K,N)=I
C ... COORDINATES AND UNIT VECTORS ARE GENERATED
DO 60 I=1, NUMPN
XYZ(2,I)=0.
XYZ(3,I)=0.
VSP(1,I)=0.
VSP(2,I)=1.
VIP(1,I)=0.
VIP(2,I)=0.
VIP(3,I)=1.
60 CONTINUE
XYZ(1,1)=0.
JJ=1
DO 80 I=1, NUMEL
XINC=ELG(I)/3.
DO 70 J=2, NPE
JI=NEL(J,I)
JJ=JJ+1
70 XYZ(1,JI)=XYZ(1, JJ) + XINC*DFLOAT(J-1)
80 WRITE (IT6, 2040)
C 120 WRITE (IT6, 2060)
C ... READ IN RESTRAINT NODE INFORMATION
DO 140 I=1, NUMNP
DO 140 J=1, NLF
IC(J,I)=0.
DO 160 IRN=1, NRN
READ (IT5, 1020) NRN, (ID(IDE, NORN), IDF=1, NDF)
WRITE (IT6, 2100) NRN, (ID(IDE, NORN), IDF=1, NDF)
CALL NLMUN (ID, NDF, NEJ, NUMNP)
NEQI=NEJ+1
C ... READ IN LOAD FACTORS
READ (IT5, 1040) (FLOJ(I), I=1, NINCS)
WRITE (IT6, 2120)
WRITE (IT6, 2140) (FLOJ(I), I=1, NINCS)
IF (IYPE.EC.0) RETURN
WRITE (IT6, 2160)
C ... READ IN DATA FROM INUS STRESS-STRAIN CURVE OF MATERIAL -- A MAXIMUM
DO 180 I=1, NMJDS
DO 180 IMODS=1, NMJDS
WRITE (IT5, 1060) I, (EMOD(J,I), J=1, 2)
DO 220 I=1, NMODS
IF (I.EC.1) GO TO 200
EI=(EPCD(2,I)-EMCJ(2,I-1))/(EMOD(1,I)-EMOD(1,I-1))
EMOD(3,I)=EM+EI/(YH-EI)
GO TO 220
200 EMOD(3,I)=0.
220 CONTINUE

```

FEN05510
FEN05520
FEN05530
FEN05540
FEN05550
FEN05560
FEN05570
FEN05580
FEN05590
FEN05600
FEN05610
FEN05620
FEN05630
FEN05640
FEN05650
FEN05660
FEN05670
FEN05680
FEN05690
FEN05700
FEN05710
FEN05720
FEN05730
FEN05740
FEN05750
FEN05760
FEN05770
FEN05780
FEN05790
FEN05800
FEN05810
FEN05820
FEN05830
FEN05840
FEN05850
FEN05860
FEN05870
FEN05880
FEN05890
FEN05900
FEN05910
FEN05920
FEN05930
FEN05940
FEN05950
FEN05960
FEN05970
FEN05980
FEN05990
FEN06000
FEN06010
FEN06020
FEN06030
FEN06040
FEN06050

```

C ... CALCULATE THE ACCUMULATIVE EFFECTIVE PLASTIC STRAIN FOR EACH
C LINEAR RANGE
DO 260 I=1, NMODS
IF (I.EQ.1) GO TO C 240
EMOD(I,I)= EMOD(1,I) - EMOD(2,I)/YM
GO TO 260

240 EMOD(I,I)= 0.
260 WRITE (I16,2180) L(EMOD(J,I) J=1,3)
C ... READ IN CONVERGENCE CRITERIA FOR NON-LINEAR ANALYSIS
READ (I15,1080) FTOL,ETOL
WRITE (I16,2200) FTOL,ETOL
TOLFO = 0.
RETURN
(6D10.4/6D10.4/,6I5)
1000 FORMAT (I5,D15.5)
1010 FORMAT (I5,5X,9I5)
1020 FORMAT (7F10.5)
1040 FORMAT (I5,2E15.5)
1060 FORMAT (2U10.4)
1080 FORMAT (//48H I N F O R M A T I O N O F S T R U C T U R E )
2000 FORMAT (//5X,40H * * * * * )
2020 FORMAT (
1 50H PIPE WALL THICKNESS (GEOM(1)) =,D15.5//5X,
2 50H INITIAL OUTSIDE RADIUS OF X-SECTION (GEOM(2)) =,D15.5//5X,
3 50H INITIAL RADIUS OF CURVATURE (GEOM(3)) =,D15.5//5X,
4 50H INITIAL LENGTH OF THE PIPE (GEOM(4)) =,D15.5//5X,
1 50H * * * * * (PROP(1)) =,D15.5//5X,
2 50H YOUNG'S MODULUS (YM) (PROP(2)) =,D15.5//5X,
3 50H POISSON RATIO (NU) (PROP(3)) =,D15.5//5X,
4 50H SHEAR FACTOR (K) (PROP(4)) =,D15.5//5X,
5 50H UNIAxIAL YIELD STRENGTH (UNIAX) (NP(1)) =,IS//5X,
1 50H * * * * * TYPE OF ANALYSIS (NP(2)) =,IS//5X,
2 50H EQ.0 : LINEAR, EQ.1 : NON-LINEAR (NP(3)) =,IS//5X,
3 50H EQ.0 : DATA INPUT (NP(4)) =,IS//5X,
4 50H EQ.0 : GENERATED, EQ.1 : READ-IN (NP(5)) =,IS//5X,
5 50H OPTION CF INTERACTION EFFECTS (NP(6)) =,IS//5X,
6 50H EQ.0 : IGNORED, EQ.1 : CONSIDERED (NP(7)) =,IS//5X,
7 50H OPTION CF FIXITY CONDITION (NP(8)) =,IS//5X,
8 50H EQ.C : IGNORED, EQ.J : CONSIDERED AT J (NP(9)) =,IS//5X,
9 52H EQ.C : ELEMENT I N F O R M A T I O N //
2040 6X,7HELEMENT,7X,12HCONNECTIVITY,9X,8HRADIUS-C,7X,6HLENGTH)
2060 FORMAT (//I10,9X,4I1,10X,D10.4,5X,D10.4)
2080 18HDEGREES OF FREEDOM)
2100 FORMAT (//8X,15,10X,9I5)
2120 FORMAT (//50H * * * * * ORDER OF INCREMENTAL LOAD FACTORS APPLIED )
2140 FORMAT (//10F10.4) *
2160 16H-LINEAR ANALYSIS //16X,3HSET,12X,9HP-EPSILON,10X,5HSIGMA,13X,
2HET)
2180 FORMAT (//16X,12,7X,10I5.5)
2200 1 //5X,40H CONVERGENCE CONDITIONS FOR NONLINEAR ANALYSIS
2 //5X,40H CONVERGENCE (FTOL) =,D12.3
//5X,40H ENERGY TOLERANCE (ETOL) =,D12.3)
END

```

FEN06060
FEN06070
FEN06080
FEN06090
FEN06100
FEN06110
FEN06120
FEN06130
FEN06140
FEN06150
FEN06160
FEN06170
FEN06180
FEN06190
FEN06200
FEN06210
FEN06220
FEN06230
FEN06240
FEN06250
FEN06260
FEN06270
FEN06280
FEN06290
FEN06300
FEN06310
FEN06320
FEN06330
FEN06340
FEN06350
FEN06360
FEN06370
FEN06380
FEN06390
FEN06400
FEN06410
FEN06420
FEN06430
FEN06440
FEN06450
FEN06460
FEN06470
FEN06480
FEN06490
FEN06500
FEN06510
FEN06520
FEN06530
FEN06540
FEN06550
FEN06560
FEN06570
FEN06580
FEN06590
FEN06600

```

C
C
SUBROUTINE ELPAL (SI, EPS, OHM, EFSI)
IMPLICIT REAL*8(A-H, O-Z)
COMMON/MAT/ STRES(6), STRAIN(6), C(6,6), YLD, HPRIME, IST, ISR
COMMON/MAX/ NMODS, VINCS, MITER, MODEX, INTUP
COMMON/PRO/ GEOM(8), PROP(6), EMOD(3,10), FLOD(30), NPAR(6)
COMMON/VAR/ IINCS, IFRH, IPEL, IREM, IIND, IPT, ICHEK
COMMON/TAPE/ IT1, IT2, IT3, IT4, IT5, IT6, IT7, IT8
DIMENSION SIG(1), EPS(1), OHM(J,1)
DIMENSION TAU(6), DELSIG(6), DELEPS(6), CEP(6,6), RS(3,6),
1 EQUIVALENCE RN(3,6), (CEP(1,1), RS(1,1)), (CEP(1,4), RN(1,1)), (DELEPS, DEPS)
YN= PRCP(1)
UNIAX= PROP(4)
IMODS= 2
IF (IPEL.EQ.1) GO TO 60
DO 20 IMODS=2, NMODS
IF (EFSI.LI.EMOD(1, IMODS)) GO TO 40
20 CONTINUE
WRITE (IT6, 2000) EFSI
STOP
40 W= (EMOD(2, IMODS)-EMOD(2, IMODS-1))/(EMOD(1, IMODS)-EMOD(1, IMODS-1))
YLD= EMOD(2, IMODS-1) + W*(EFSI - EMOD(1, IMODS-1))
YLDMAX= EMOD(2, IMODS)
NEULER= 20
GO TO 80
60 YLD= UNIAX
YLDMAX= EMOD(2,2)
NEULER= 5
IF (INC.EQ.0) GO TO 240
XNEU= CFLOA(I, NEULER)
OHM(1,2)= OHM(1,2)/XNEU
OHM(2,3)= OHM(2,3)/XNEU
OHM(1,3)= OHM(1,3)/XNEU
OHM(2,1)= -OHM(1,2)
OHM(3,2)= -OHM(2,3)
OHM(3,1)= -OHM(1,3)
MAKE CORRECTIONS FOR STRESSES AND STRAINS DUE TO R.U. ROTATIONS
DO 100 I=1,3
RS(I,1)= SIG(I)
RN(1,1)= EPS(I)
RS(1,2)= SIG(4)
RS(2,3)= SIG(5)
RS(2,1)= SIG(6)
RN(1,2)= 0.5*EPS(4)
RN(2,3)= 0.5*EPS(5)
RN(1,3)= 0.5*EPS(6)
DO 120 I=1,3
I1= I-1
DO 120 J=1, I1
RS(I, J)= RS(J, I)
RN(I, J)= RN(J, I)
120 STARI= PERFORMING EULER FORWARD INTEGRATION WITH NEULER INTERVALS
C ... DO 140 I=1,3

```

FEN06610
FEN06620
FEN06630
FEN06640
FEN06650
FEN06660
FEN06670
FEN06680
FEN06690
FEN06700
FEN06710
FEN06720
FEN06730
FEN06740
FEN06750
FEN06760
FEN06770
FEN06780
FEN06790
FEN06800
FEN06810
FEN06820
FEN06830
FEN06840
FEN06850
FEN06860
FEN06870
FEN06880
FEN06890
FEN06900
FEN06910
FEN06920
FEN06930
FEN06940
FEN06950
FEN06960
FEN06970
FEN06980
FEN06990
FEN07000
FEN07010
FEN07020
FEN07030
FEN07040
FEN07050
FEN07060
FEN07070
FEN07080
FEN07090
FEN07100
FEN07110
FEN07120
FEN07130
FEN07140
FEN07150

```

140 DO 140 J=1 3
    RS(I,J+3)=RS(I,J)
    RN(I,J+3)=RN(I,J)
160 DO 200 IE=1,3
    DO 160 J=1,3
    DO 160 K=1,3
    RS(I,J+3)=RS(I,J+J)+RH(I,K)*OHM(K,J)-OHM(I,K)*RN(K,J)
    RN(I,J+3)=RN(I,J+J)+RH(I,K)*OHM(K,J)-OHM(I,K)*RN(K,J)
180 DO 180 J=1,3
    RS(I,J)=RS(I,J+3)
    RN(I,J)=RN(I,J+3)
200 CONTINUE
220 DO 220 I=1,3
    SIG(I)=RS(I,I)
    EPS(I)=RN(I,I)
    SIG(4)=RS(1,2)
    SIG(5)=RS(2,3)
    SIG(6)=RS(1,3)
    EPS(4)=2.*RN(1,2)
    EPS(5)=2.*RN(2,3)
    EPS(6)=2.*RN(1,3)
1. CALCULATE INCREMENTAL STRAINS
C ... UPDATE STRAIN COMPONENTS AND TOTAL EFFECTIVE STRAIN
240 DO 260 I=1,3
    EPS(I)=EPS(I)+STRAIN(I)
    DELEPS(I)=SIG(I)-STRAIN(I)
260 2. CALCULATE STRESS INCREMENT, ASSUMING ELASTIC BEHAVIOUR
C ...
    DC 240 IS=1,ISI
    DELSIG(IS)=0.
    DO 280 IR=1,ISR
    DELSIG(IS)=DELSIG(IS)+C(IS,IR)*DELEPS(IR)
280 3. CALCULATE TOTAL STRESSES, ASSUMING ELASTIC BEHAVIOUR
C ...
    DO 300 I=1,ISI
    SUM=SIG(I)+DELSIG(I)
    IF (DABS(SUM).LT.1.D-35) SUM=0.
300 TAU(I)=SUM
C ... 4. CHECK WHETHER *TAU* STATE OF STRESS FALLS OUTSIDE THE LOADING
    JM= (TAU(1)+TAU(2)+TAU(3))/3.
    SX= TAU(1) - SM
    SY= TAU(2) - SM
    SZ= TAU(3) - SM
    SXY= TAU(4)
    SYZ= TAU(5)
    SZX= TAU(6)
    FT= 0.5*(SX*SY+SY*SZ+SZ*SX+SY*SZ+SZ*SY+SZ*SY)-YLD*YLD/3.
    IF (FI) 620,620,340
    STATE CF STRESS WITHIN LOADING SURFACE - ELASTIC BEHAVIOUR
C ... STATE CF STRESS OUTSIDE LOADING SURFACE - PLASTIC BEHAVIOUR
620 IPEL= 1
C ... STATE CF STRESS OUTSIDE LOADING SURFACE - PLASTIC BEHAVIOUR
340 IF (IPEL.EQ.1) GO TO 380
C ... MATERIAL WAS PREVIOUSLY PLASTIC
    RATIO= 0.

```

FEN07160
FEN07170
FEN07180
FEN07190
FEN07200
FEN07210
FEN07220
FEN07230
FEN07240
FEN07250
FEN07260
FEN07270
FEN07280
FEN07290
FEN07300
FEN07310
FEN07320
FEN07330
FEN07340
FEN07350
FEN07360
FEN07370
FEN07380
FEN07390
FEN07400
FEN07410
FEN07420
FEN07430
FEN07440
FEN07450
FEN07460
FEN07470
FEN07480
FEN07490
FEN07500
FEN07510
FEN07520
FEN07530
FEN07540
FEN07550
FEN07560
FEN07570
FEN07580
FEN07590
FEN07600
FEN07610
FEN07620
FEN07630
FEN07640
FEN07650
FEN07660
FEN07670
FEN07680
FEN07690
FEN07700

```

360 DO 360 I=1,IST
    TAU(I)=SIG(I)
GO TO 420
C 380 MATERIAL WAS PREVIOUSLY ELASTIC
    IPEL=2
    SM=(SIG(1)+SIG(2)+SIG(J))/3.
    SX=SIG(1)-SM
    SY=SIG(2)-SM
    SZ=SIG(3)-SM
    SXY=SIG(4)
    SYZ=SIG(5)
    SZX=SIG(6)
    DM=(DELSIG(1)+DELSIG(2)+DELSIG(3))/3.
    DX=DELSIG(1)-DM
    DY=DELSIG(2)-DM
    DZ=DELSIG(3)-DM
    DXY=DELSIG(4)
    DYZ=DELSIG(5)
    DZX=DELSIG(6)
    A=(DX*DX+LY*DY+DZ*DZ)+2.*(DX*DX+DY*DY+DZ*DZ)
    B=(SX*DX+SY*SY+SZ*SZ)+2.*(SX*SY+SY*SZ+SZ*SX)-2.*YLD*YLD/3.
    RATIO=(-B+CSQRT(B*B-A*B))/A
DO 400 I=1,IST
    TAU(I)=SIG(I)+RATIO*DELSIG(I)
C 400 TAU NOW CONTAINS (PREVIOUS STRESSES + STRESSES DUE TO ELASTIC
C 400 STRAIN INCREMENTS)
C 420
    S=CALCULATE PLASTIC STRESSES
    DETERMINE INCREMENT INTERVAL
    M=30.*DSQRT(FI)/YLD+1.
    IF (M.GT.30) M=30
    XM=(1.-RATIO)/DELOAD(M)
DO 440 I=1,ISR
    DEPS(I)=XM*CELEPS(I)
DO 460 I=1,IST
    STRES(I)=XM*DELSIG(I)
C 460 DETERMINE CURRENT VALUE OF STRAIN HARDENING
    HPRIME=EMOD(3,IMCDS)
C 480 CALCULATION OF ELASTO-PLASTIC STRESSES (STARI...)
    EBAR=C.
DO 600 IM=1,M
    CALL MIDEP(TAU,CEP,DEJAR,1)
DO 520 I=1,IST
    DO 520 J=1,ISH
    TAU(I,J)=TAU(I)+CEP(I,J)*DEPS(J)
C 520 SCALE COMPONENTIAL EFFECTIVE STRESS TO YIELD SURFACE IF REQUIRED
    EBAR=EBAR+CEBAR
    YLD=YLD+HPRIME*DEJAR
    IF (YLD.LE.YLDMAX) GO TO 560
C 540 RECALCULATE YLD AND YLD' IF YLD' ENTERS A NEW LINEAR RANGE
    IMODS=IMODS+1
    IF (IMCDS.LE.AMODS) GO TO 530
    WRITE (IT6,2CC0)
STOP
C 530 EPEX=(YLD-YLDMAX)/HPRIME

```

FEN07710
FEN07720
FEN07730
FEN07740
FEN07750
FEN07760
FEN07770
FEN07780
FEN07790
FEN07800
FEN07810
FEN07820
FEN07830
FEN07840
FEN07850
FEN07860
FEN07870
FEN07880
FEN07890
FEN07900
FEN07910
FEN07920
FEN07930
FEN07940
FEN07950
FEN07960
FEN07970
FEN07980
FEN07990
FEN08000
FEN08010
FEN08020
FEN08030
FEN08040
FEN08050
FEN08060
FEN08070
FEN08080
FEN08090
FEN08100
FEN08110
FEN08120
FEN08130
FEN08140
FEN08150
FEN08160
FEN08170
FEN08180
FEN08190
FEN08200
FEN08210
FEN08220
FEN08230
FEN08240
FEN08250

```

560 HPRIME= EMOD(3,IMCJS)
      YLD= YLCMAX + EPEX*HPRIME
      YLDMAX= EMOD(2,IMCJS)
      IF (YLLC.GT.YLCMAX) GJ TJ 540
      DM= (IAU(1) + IAU(2) + IAU(3))/3.
      DX= IAU(1) - DM
      DY= IAU(2) - DM
      DZ= IAU(3) - DM
      DXY= IAU(4)
      DYZ= IAU(5)
      DZX= IAU(6)
      SBAR= LSORT(1.5*(DX*DX+DY*DY+DZ*DZ)+3.*(DXY*DXY+DYZ*YZ+DZX*DZX))
      IF (YLD.GT.SBAR) GJ TO 600
      SCALE= YLD/SBAR
      DO 580 I=1,ISI
      IAU(I)= SCALE*I*IAU(I)
580 CONTINUE
600 *** CALCULATION OF ELASTO-PLASTIC STRESSES (END...*)
      C ... UPDATE EFFECTIVE PLASTIC STRAIN AND FORM NEW MATERIAL LAW
      C ... EFST= EFST + EBAR
      DO 620 I=1,ISI
      SIG(I)= IAU(I)
620 IF (IPEL.GT.1.AND.ICHEK.GI.0) GO TO 660
      RETURN
      CALL MIDEP (IAU,CEP,DEBAR,0)
      DO 680 I=1,6
      DO 680 J=1,6
      C(I,J)= CEP(I,J)
680 RETURN
2000 FORMAT (///50H *** CALCULATED PLASTIC STRAIN HAS EXCEEDED DATA,
      1 30H PROVIDED, PROGRAM STOPPED...*,5X,D15.6)
      END
C SUBROUTINE EPSLON (UL,BN,EDIS,STRAIN,OHM,NDE)
C IMPLICIT REAL*(A-I,J-Z)
      DIMENSION BL(6,1),BN(9,1),EDIS(1),SIRAIN(1),OHM(3,1),SIR(9)
      CALCULATE INCREMENTAL LINEAR STRAINS
      DO 20 I=1,6
      SUM= 0.
      DO 10 J=1,NDE
      SUM= SUM + BL(I,J)*EDIS(J)
      IF (DABS(SUM).LT.1.0-35) SUM= 0.
      SIRAIN(I)= SUM
      CALCULATE INCREMENTAL NON-LINEAR STRAINS
      CALL CLEAR (SIR,9)
      DO 60 I=1,9
      SUM= 0.
      DO 40 J=1,NDE
      SUM= SUM + BN(I,J)*EDIS(J)
      IF (DABS(SUM).LT.1.0-35) SUM= 0.
      SIR(I)= SUM
      CALCULATE COMPONENTS OF SPIN TENSOR
      DO 160 I=1,3
      OHM(I,I)= 0.

```

FEN08260
FEN08270
FEN08280
FEN08290
FEN08300
FEN08310
FEN08320
FEN08330
FEN08340
FEN08350
FEN08360
FEN08370
FEN08380
FEN08390
FEN08400
FEN08410
FEN08420
FEN08430
FEN08440
FEN08450
FEN08460
FEN08470
FEN08480
FEN08490
FEN08500
FEN08510
FEN08520
FEN08530
FEN08540
FEN08550
FEN08560
FEN08570
FEN08580
FEN08590
FEN08600
FEN08610
FEN08620
FEN08630
FEN08640
FEN08650
FEN08660
FEN08670
FEN08680
FEN08690
FEN08700
FEN08710
FEN08720
FEN08730
FEN08740
FEN08750
FEN08760
FEN08770
FEN08780
FEN08790
FEN08800

```

OHM(1,2) = 0.5*(STR(2) - SIR(4))
OHM(1,3) = 0.5*(STR(3) - SIR(7))
OHM(2,3) = 0.5*(STR(6) - SIR(8))
RETURN
END

C SUBROUTINE EBRCH (N,I)
C COMMON/TAPE/ II,IF2,IF3,IF4,IF5,IF6,IF7,IF8
GO TO (1,2,3,4),I
1 WRITE (IF6,2000)
GO TO 10
2 WRITE (IF6,2010)
GO TO 10
3 WRITE (IF6,2020)
GO TO 10
4 WRITE (IF6,2030)

C 10 WRITE (IF6,2090) N
STOP
2000 FORMAT (// * 7H NOT ENOUGH STORAGE FOR HEAD-IN OF ID ARRAY AND,
2010 2 * H NODAL POINT COORDINATES)
2020 FORMAT (// * 50H NOT ENOUGH STORAGE FOR DEFINITION OF LOAD VECTORS)
2030 FORMAT (// * 2H NOT ENOUGH STORAGE FOR ELEMENT DATA INPUT)
1 58H STRUCTURE STIFFNESS, AND DISPLACEMENT AND STRESS SOLUTION,
2 10H PHASE
2090 FORMAT (// 35H *** ERROR... STORAGE EXCEEDED BY, I10)
END

C SUBROUTINE INCLUD (U,ALOD,SLOD,ACLOD)
C IMPLICIT REAL*8(A-H,O-Z)
COMMON/PRO/ GEOM(8),PROP(6),EMOD(3,10),FLOOD(30),NPAR(6)
COMMON/VAR/ IINCS,IITER,IPEL,IREM,IND,IPT,ICHEK
COMMON/SOL/ NEQ,NE1,NK,MK,NE5
COMMON/TAPE/ II,IF2,IF3,IF4,IF5,IF6,IF7,IF8
DIMENSION U(NEQ),ALOD(NEQ),SLOD(NEQ)
CALL CLEAR (ALOD,NEQ)
BEHIND II
ACNEW= ACLOD + FLOJ(IINCS)
IF (ACNEW-ACLOD) 20,20,40
SET IREM = 1 UPON ENCOUNTERING UNLOADING
C ** 20 IF (IREM.EQ.0) WRITE (IF6,2000) IREM
IREM = 1
GO TO 60
40 IREM = 0
60 ACLOD = ACNEW
BEAD (II) ALOD
DO 80 I=1,NEQ
ALOD(I) = ALOD(I) + ALOD
80 U(I) = ALOD(I) - SLOD(I)
RETURN
2000 1 40H ENCCUNTERED >>> UNLOADING HAS (IREM=,I2,2H) )

```

FEN08810
FEN08820
FEN08830
FEN08840
FEN08850
FEN08860
FEN08870
FEN08880
FEN08890
FEN08900
FEN08910
FEN08920
FEN08930
FEN08940
FEN08950
FEN08960
FEN08970
FEN08980
FEN08990
FEN09000
FEN09010
FEN09020
FEN09030
FEN09040
FEN09050
FEN09060
FEN09070
FEN09080
FEN09090
FEN09100
FEN09110
FEN09120
FEN09130
FEN09140
FEN09150
FEN09160
FEN09170
FEN09180
FEN09190
FEN09200
FEN09210
FEN09220
FEN09230
FEN09240
FEN09250
FEN09260
FEN09270
FEN09280
FEN09290
FEN09300
FEN09310
FEN09320
FEN09330
FEN09340
FEN09350

B E E N


```

C
C
SUBROUTINE LOADS (ID,R,NOD,DIRN,FLOAD,NLOAD)
IMPLICIT REAL*(A-I,O-Z)
COMMON/GEN/ NUMNP,NUMEL,NPE,NDF,NDE,NDS,NIPS,IPL,IPP,IPW,IPH
COMMON/MAX/ NMODS,INCS,MITER,MODEX,INTOP
COMMON/SOL/ NEX,NEJ,NEK,MK,RES
COMMON/IAPE/ I1,I2,I3,I4,I5,IT6,IT7,IT8
DIMENSION IC(NDF,1),R(NEJ,1),DIRN(I),FLOAD(1)
WRITE (II6,2C00)
DO 20 I=1,NLCAD
  READ (II5,1C00)
  WRITE (II6,2010)
CONTINUE
IF (MOLEX.EQ.0) RETURN
REWIND III
CALL CLEAR (B,NEQ)
DO 60 L=1,NLCAD
  LN= NOL(L)
  LI= IDIRN(L)
  IF (LI) 60,60,40
  IF (LI) = R(II) * FLOAD(L)
60 CONTINUE
WRITE (II1) R
RETURN
FORMAT (2I5,3D15.8)
2000 FORMAT (//4H * * * LOCATION: OF CONCENTRATED LOADS APPLIED //4X,
1 4HNODE 7X,9HCIRECTION,9X,4HLOAD /3X,6HNUMBER,21X,9HMAGNITUDE )
2010 FORMAT (//I,9X,I4,3X,J12.5)

C
C
SUBROUTINE LCCAT (ELXY,VS,VT,H,S,I,RA,N,IR,IA,II,IPT)
IMPLICIT REAL*(A-I,O-Z)
COMMON/GEN/ NUMNP,NUMEL,NPE,NDF,NDE,NDS,NIPS,IPL,IPP,IPW,IPH
DIMENSION ELXY(3,1),VS(3,1),VT(3,1),H(4),XYZ(3)
COMMON/IAPE/ I1,I2,II3,II4,II5,II6,II7,II8
JA= MOD(IA-1,IPH-1)
JI= MOD(II-1,IPW-1)
IF (JA) 10,30,10
IF (JI) 20,30,20
10 RETURN
20 R2= H*5
30 R3= R*52
H(1) = 0.0625*( -9.*R3 + 9.*R2 + R - 1.)
H(2) = 0.0625*( 27.*R3 - 9.*R2 - 27.*R + 9.)
H(3) = 0.0625*( -27.*R3 - 9.*R2 + 27.*R + 9.)
H(4) = 0.0625*( 9.*R3 + 9.*R2 - R - 1.)
DO 60 I=1,3
SUM= 0.
DO 40 J=1,NPE
SUM= SUM + H(J)*(ELXY(I,J) + RA*(S*VS(I,J) + I*VT(I,J)))
60 XYZ(I) = SUM
WRITE (II8,2C00) I,I3,IA,II,IPT,(XYZ(I),I=1,3)

```

FEN09910
FEN09920
FEN09930
FEN09940
FEN09950
FEN09960
FEN09970
FEN09980
FEN09990
FEN10000
FEN10010
FEN10020
FEN10030
FEN10040
FEN10050
FEN10060
FEN10070
FEN10080
FEN10090
FEN10100
FEN10110
FEN10120
FEN10130
FEN10140
FEN10150
FEN10160
FEN10170
FEN10180
FEN10190
FEN10200
FEN10210
FEN10220
FEN10230
FEN10240
FEN10250
FEN10260
FEN10270
FEN10280
FEN10290
FEN10300
FEN10310
FEN10320
FEN10330
FEN10340
FEN10350
FEN10360
FEN10370
FEN10380
FEN10390
FEN10400
FEN10410
FEN10420
FEN10430
FEN10440
FEN10450

```

2000 RETURN
      ECBMAY ( IS, SX, JIS, JX, IS, SX, JUIS, J6 )
      END
C
C
      SUBROUTINE MAIEL ( PROP, C )
      IMPLICIT REAL*8 ( A-H, O-Z )
      DIMENSION PRCPP( 1 ), C( 6, 1 )
      YM= PRCPP( 1 )
      PV= PRCPP( 2 )
      FT= PRCPP( 3 )
      A1= YM/( 1. - PV*PV )
      A2= A1*PV
      A3= 0.5*A1*( 1. - PV )
      A4= A3/FT
      CALL CLEAR ( C, 36 )
      C( 1, 1 )= A1
      C( 1, 2 )= A2
      C( 2, 1 )= A1
      C( 2, 2 )= A1
      C( 4, 4 )= A3
      C( 5, 5 )= A4
      RETURN
      END
C
      SUBROUTINE MIDEP ( IAV, CEP, DEBAR, IFLAG )
      IMPLICIT REAL*8 ( A-H, O-Z )
      COMMON/MAT/ STRESS( 6 ), STRAIN( 6 ), C( 6, 6 ), YLD, HPRIME, IST, ISR
      DIMENSION TAU( 1 ), CEP( 6, 1 ), CJ( 6 ), Q( 6 )
      SM= ( TAU( 1 )+IAU( 2 )+IAU( 3 ) )/3.
      DO 20 I=1, 3
      Q( I )= TAU( I ) - SM
      Q( I+3 )= 2.*IAU( I+3 )
      CALCULATE THE INSTANTANEOUS ELASTIC-PLASTIC STRESS-STRAIN MATRIX
      CONT= 4.*HPRIME*YLD*YLD/3.
      DO 60 I=1, 6
      CQ( I )= 0.
      DO 60 J=1, 6
      CQ( I, J )= CQ( I ) + C( I, J )*Q( J )
      CON2= 0.
      DO 80 I=1, 6
      CON2= CON2 + Q( I )*Q( I )
      CON3= 1./ ( CON1 + CON2 )
      CALL CLEAR ( CEP, 36 )
      DO 120 K=1, 6
      CEP( K, J )= C( K, J ) - CON3*Q( K )*Q( J )
      DO 140 I=1, 6
      K= I-1
      DO 140 J=1, K
      CEP( I, J )= CEP( J, I )
      IF ( IFLAG.EQ.0 ) RETURN
      CALCULATE EFFECTIVE PLASTIC-STRAIN INCREMENT
      SUM= 0.

```

FEN10460
FEN10470
FEN10480
FEN10490
FEN10500
FEN10510
FEN10520
FEN10530
FEN10540
FEN10550
FEN10560
FEN10570
FEN10580
FEN10590
FEN10600
FEN10610
FEN10620
FEN10630
FEN10640
FEN10650
FEN10660
FEN10670
FEN10680
FEN10690
FEN10700
FEN10710
FEN10720
FEN10730
FEN10740
FEN10750
FEN10760
FEN10770
FEN10780
FEN10790
FEN10800
FEN10810
FEN10820
FEN10830
FEN10840
FEN10850
FEN10860
FEN10870
FEN10880
FEN10890
FEN10900
FEN10910
FEN10920
FEN10930
FEN10940
FEN10950
FEN10960
FEN10970
FEN10980
FEN10990
FEN11000

```

DO 200 I=1,6
SUM=SUM+Q(I)*STRESJ(I)
DLAM=CONJ*SUM
IF (DLAM-LI.0.) DLAM=0.
DEBAR=2.*DLAM*YLC/J.
RETURN
END

C
SUBROUTINE NUMUN (ID,NDF,NE2,NUMNP)
C
IMPLICIT REAL*8(A-H,O-Z)
DIMENSION ID(NDF,1)
CALCULATE THE NUMBER OF UNKNOWN5
NE2=0
DO 40 N=1,NUMNP
DO 40 I=1,NEF
IF (ID(I,N)) 30,20,30
20 NE2=NE2+1
GO TO 40
30 ID(I,N)=0.
40 CONTINUE
RETURN
END

C
SUBROUTINE OUTPUT (IJ,RD5,ADIS,ACL0D)
C
IMPLICIT REAL*8(A-H,O-Z)
COMMON/GEN/ NUMNP,NUMEL,NPS,NDF,NDE,NDS,NIPS,IPL,IPP,IPH,IPH
COMMON/PRO/ GEOM(8),PROP(6),EMOD(3,10),FLOD(10),NPAR(6)
COMMON/VAR/ IINCS,IITER,IPEL,IHEM,IND,IPT,ICHEK
COMMON/MAE/ NMODS,MITER,MODEX,INTUP
COMMON/TAPE/ I1,I2,I3,I4,I5,I6,I7,I8
DIMENSION IC(NDF,1),KDS(1),ADIS(1),D(9),O(9)
EQUIVALENCE (GEOM(1),ICHK),(GEOM(2),RA),(PROP(1),YM)
WRITE (II6,200) ICHEK
IF (ICHEK) 1,2,3
1 WRITE (II6,202) IITER
2 WRITE (II6,204) MITER
3 WRITE (II6,206) IITER
10 WRITE (II6,208) ACL0D
DO 60 N=1,NUMNP
DO 20 M=1,NEF
D(M)=0.
I1=ID(M,N)
IF (I1.NE.0) D(M)=ADIS(I1)
20 CONTINUE
60 WRITE (II6,210) N,D(I),I=1,NDF)
WRITE (II6,212)
DO 100 N=1,NUMEL
100 WRITE (II6,214) 1,RD5(N)
RETURN
2000 FORMAT (//5X,36H * * CONVERGENCE MODE OF SOLUTION, I10)

```

FEN11010
FEN11020
FEN11030
FEN11040
FEN11050
FEN11060
FEN11070
FEN11080
FEN11090
FEN11100
FEN11110
FEN11120
FEN11130
FEN11140
FEN11150
FEN11160
FEN11170
FEN11180
FEN11190
FEN11200
FEN11210
FEN11220
FEN11230
FEN11240
FEN11250
FEN11260
FEN11270
FEN11280
FEN11290
FEN11300
FEN11310
FEN11320
FEN11330
FEN11340
FEN11350
FEN11360
FEN11370
FEN11380
FEN11390
FEN11400
FEN11410
FEN11420
FEN11430
FEN11440
FEN11450
FEN11460
FEN11470
FEN11480
FEN11490
FEN11500
FEN11510
FEN11520
FEN11530
FEN11540
FEN11550

```

2020 FORMAT (//5X,49H * * * PROGRAM STOPPED... SOLUTION DIVERGING AT, FEN11560
10H ITER = I4 ) FEN11570
2000 FORMAT (//5X,45H * * * NO CONVERGENCE ACHIEVED WITH MAXIMUM, FEN11580
25H NUMBER OF ITERATIONS ( I3,2H ) ) FEN11590
2000 FORMAT (//5X,41H * * * CONVERGENCE ACHIEVED AT ITER = I4 ) FEN11600
2080 FORMAT (//5X,43H * * * DISPLACEMENTS : TRANSLATIONS C, I4 ) FEN11610
1 50ROTATIONS C JVALIZATIONS ( LOAD ACCUMULATION = F8.4,2H )// FEN11620
2 6H NGDE,7X 7HX-DISPL,6X,7HY-DISPL,6X,7HZ-DISPL,6X,5HX-ROI,8X, FEN11630
3 5HY-ROI,8X,5HZ-ROI,8X,8H1 5T-OVAL,5X,8H2ND-OVAL,5X,8H3RD-OVAL, FEN11640
2100 FORMAT (//5X,45H * * * UPDATED (RADI I OF CURVATURE OF ELEMENTS, // FEN11650
2120 FORMAT (//5X,45H * * * RADIUS-C/) FEN11660
1 10X,8H ELEMENT,17X,3H RADIUS-C/) FEN11670
2140 FORMAT (13X,12,16X,15.6) FEN11680
END FEN11690
C FEN11700
C SUBROUTINE PENAL (ID,A3,MAXA,NUMNP,NDF,ALPHA) FEN11710
C FEN11720
C IMPLICIT REAL*8(A-H,O-Z) FEN11730
C COMMON/TAPE/ IT1,IT2,IT3,IT4,IT5,IT6,IT7,IT8 FEN11740
C DIMENSION IC(NDF,1),AG(I),MAXR(I) FEN11750
C ALPHA= 0. FEN11760
C DO 20 N=1,NUMNP FEN11770
C DO 20 M=7,NCF FEN11780
C IF (I.EQ.0) GO TO 20 FEN11790
C K= MAXA(I) FEN11800
C IF (AG(K).GT.ALPHA) ALPHA= AG(K) FEN11810
C CONTINUE FEN11820
C WRITE (I16,2C00) ALP,IA FEN11830
C RETURN FEN11840
C 2000 FORMAT (42H * * * FOR INTERACTION EFFECTS ALPHA = ,D15.5) FEN11850
C FEN11860
C FEN11870
C FEN11880
C SUBROUTINE PRESET (MFOI) FEN11890
C FEN11900
C IMPLICIT REAL*8(A-H,O-Z) FEN11910
C COMMON/GEN/ NUMNP,UA,IL,NPE,NDF,NDE,MDS,NIPS,IPL,IPP,IPW,IPH FEN11920
C COMMON/MAX/ NMODS,NINCS,MITER,MODEX,INTUP FEN11930
C COMMON/SOL/ NEQ,NEJ,1,CHK,MK,NE5 FEN11940
C COMMON/MAT/ STRESS(6),STRAIN(6),C(6,6),YLD,HPRIME,IST,ISR FEN11950
C COMMON/DIM/ N1,N2,N3,N4,N5,N6,N7,N8,N9,N10,N11,N12,N13,N14,N15, FEN11960
C N16,N17,N18,N19,N20,N21,N22,N23,N24,N25 FEN11970
1 COMMON/TAPE/ IT1,IT2,IT3,IT4,IT5,IT6,IT7,IT8 FEN11980
COMMON A(1) FEN11990
DIMENSION HEC(18) FEN12000
IT1= 1 FEN12010
IT2= 2 FEN12020
IT3= 3 FEN12030
IT4= 4 FEN12040
IT5= 5 FEN12050
IT6= 6 FEN12060
IT7= 7 FEN12070
IT8= 8 FEN12080
HEAD ( IT5,1000) HED,NUMNP,NUMEL,NDF,NPE,IPL,IPP,IPW,NRN,NLOAD, FEN12090
NMODS,NINCS,MITER,INTUP,MODEX FEN12100
1 FEN12100

```



```

1 50H NUMBER OF CONCENTRATED LOADS
2 50H NUMBER OF STRESS-STRAIN POINTS
3 50H NUMBER OF LOAD INCREMENTS
4 50H MAXIMUM NUMBER OF ITERATIONS
5 50H STIFFNESS UPDATING OPTION
6 50H EQ. N : UPDATING EVERY N ITERATIONS
7 50H EQ. 0 : UPDATING NOT REQUIRED
8 50H SCLUTION MODE
9 50H
1 50H
2020 FORMAT (5X,40H STORAGE OF COMMON ARRAY OCCUPIED =,I6)
END

C
C SUBROUTINE RACII (RDS,EL3,LM,SE,ALPHA)
IMPLICIT REAL*8(A-Z)
COMMON/GEN/ NUMNP,NUM3L,NPE,NJF,NDE,NDS,NIPS,IPL,IPP,IPH,IPW,IPH
COMMON/PRO/ GEOM(8),PROP(6),EMOD(3,10),FLCD(30),NPAR(6)
COMMON/INTG/ ELX(3,4),VJ(3,4),VT(3,4),W3R(5),WGP(2),WGM(5)
COMMON/LOCA/ B,S,I,TH,FHIC,ZT,FI,CS,SH,RD,EG,IP1,IP2,N,NC,NTC
COMMON/DIM/ N1,N2,N3,N4,N5,N6,N7,N8,N9,N10,N11,N12,N13,N14,N15,
N16,N17,N18,N19,N20,N21,N22,N23,N24,N25
COMMON/TAPE/ I11,I12,I13,I14,I15,I16,I17,I18
COMMON A(1)
DIMENSION RDS(1),EL3(1),LM(NJF,1),SE(1),DH(4,2),G(21),LL(21)
EQUIVALENCE (GEOM(1),I1VG),(GEOM(2),RA),(NPAR(3),INTEF),
(NPAR(4),IFIX)
C ... VALUES FOR FIRST DERIVATIVES OF EL# I AT H=+1 AND EL#II AT R=-1
DATA LH/-0.500,2.250,-4.500,2.750,0,-2.750,0,4.500,0.500/
C ... ENFORCE CONTINUITY BETWEEN ADJACENT ELEMENTS
MEAN = RA - I1VG/2.
PI = 3.141592653589793J0
DIA = 2.*PI/DFLOAT(IPP)
IF (INTEF.EQ.0) GJ TO 140
NPE1 = 2*NPE - 1
KI = NPE1*NC
KS = KI*(KI + 1)/2
NEM = NUMEL - 1
DO 160 N=1,NEM
BD1 = RCS(N)
BD2 = RCS(N+1)
CALL CLEAR (SE,KS)
CO 120 KI=1,IPH
FAC1 = 2.
FAC2 = 2.
IF (KI.EQ.1.CR.KI.EQ.IPH) FAC2 = 1.
PHI = DIAN*DFLOAT(KI-1)
AC = AMEAN*DCOS(PHI)
IF (KI.EQ.1) AC = 0.
IET = ELG(N)/BD1
C1 = 2./((RD1-AC)*IET)
IET = ELG(N+1)/BD2
C2 = 2./((RD2-AC)*IET)
DO 100 I=1,NPE1
II = (I-1)*NC
(NLOAD) =,I5/5X,
{NMCDS) =,I5/5X,
{NINCS) =,I5/5X,
{MIER) =,I5/5X,
{INTUP) =,I5/5X,
(MOEX) =,I5/5X,
}
FEN1 2660
FEN1 2670
FEN1 2680
FEN1 2690
FEN1 2700
FEN1 2710
FEN1 2720
FEN1 2730
FEN1 2740
FEN1 2750
FEN1 2760
FEN1 2770
FEN1 2780
FEN1 2790
FEN1 2800
FEN1 2810
FEN1 2820
FEN1 2830
FEN1 2840
FEN1 2850
FEN1 2860
FEN1 2870
FEN1 2880
FEN1 2890
FEN1 2900
FEN1 2910
FEN1 2920
FEN1 2930
FEN1 2940
FEN1 2950
FEN1 2960
FEN1 2970
FEN1 2980
FEN1 2990
FEN1 3000
FEN1 3010
FEN1 3020
FEN1 3030
FEN1 3040
FEN1 3050
FEN1 3060
FEN1 3070
FEN1 3080
FEN1 3090
FEN1 3100
FEN1 3110
FEN1 3120
FEN1 3130
FEN1 3140
FEN1 3150
FEN1 3160
FEN1 3170
FEN1 3180
FEN1 3190
FEN1 3200

```

```

GO 100 J=1,NC
FM= DFLOAT(2*J)
C3= FM*CCOS(FM*PHI)
IF (I-4) 70 80 90
G(I+J)= -C1*C3*DH(I,1)
70 GO TO 100
80 G(I+J)= (C2*EH(1,2) - C1*DH(4,1))*C3
90 GO TO 100
90 G(I+J)= C2*C3*DH(1-3,2)
100 CONTINUE
IK= 0
DO 110 I=1, KI
J=I, KI
IK= IK + 1
110 SE(IK)= SE(IK) + FAC1*FAC2*WGP(1)*G(I)*G(J)
120 CONTINUE
DO 130 I=1, KS
SE(I)= ALPHA*SE(I)
130 IK= 0
DO 140 I=1, NPE
J=I, NPE
II= (I-1)*NDF + 6
DO 140 J=1, NC
IK= IK + 1
140 LL(IK)= LM(I+J,N)
DO 150 I=2, NPE
J=I, NPE
II= (I-1)*NDF + 6
DO 150 J=1, NC
IK= IK + 1
150 LL(IK)= LM(I+J,N+1)
WHITE (I2) (SE(I), I=1, KS), (LL(I), I=1, KI)
CALL ACDBAN (A(N14),A(N1),J2,LL,KI)
CONTINUE
IF (IFIX.EQ.0) RETURN
ENFORCE FIXITY CONDITION AT FIXED END
160 KS= NTC*(NTC+1)/2
CALL CLEAR (SE,KS)
RD= RDS(IFIX)
EG= ELC(IFIX)
DO 100 KI=1, IPH
FAC1= 2.
FAC2= 2.
IF (KI.EQ.1) GR= KI*EQ, IPH) FAC2= 1.
PHI= DIAN*DFLOAT(KI-1)
AC= AMEAN*DCOS(PHI)
IF (KI.EQ.1) AC= 0.
TET= EG/RD
CI= 2./((RD-AC)*TET)
DO 260 I=1, NPE
II= (I-1)*NC
DO 260 J=1, NC
FM= DFLOAT(2*J)
C2= FM*CCOS(FM*PHI)
G(I+J)= -C1*C2*DH(1,2)
260 CONTINUE
IK= 0

```

FEN13210
FEN13220
FEN13230
FEN13240
FEN13250
FEN13260
FEN13270
FEN13280
FEN13290
FEN13300
FEN13310
FEN13320
FEN13330
FEN13340
FEN13350
FEN13360
FEN13370
FEN13380
FEN13390
FEN13400
FEN13410
FEN13420
FEN13430
FEN13440
FEN13450
FEN13460
FEN13470
FEN13480
FEN13490
FEN13500
FEN13510
FEN13520
FEN13530
FEN13540
FEN13550
FEN13560
FEN13570
FEN13580
FEN13590
FEN13600
FEN13610
FEN13620
FEN13630
FEN13640
FEN13650
FEN13660
FEN13670
FEN13680
FEN13690
FEN13700
FEN13710
FEN13720
FEN13730
FEN13740
FEN13750

```

DO 280 I=1,NTC
DO 290 J=1,NIC
IK= IK * 1
SE(IK)= SE(IK) * FAC1*FAC2*WGP(1)*J(I)*G(J)
300 CONTINUE
DO 320 I=1,KS
SE(I)= ALPHA*SE(I)
IK= 0
DO 340 I=1,NPE
II= (I-1)*NDF * 6
DO 340 J=1,NC
IK= IK * 1
LL(IK)= LM(II+J,IFIX)
WRITE (IT2) (SE(I),I=1,KS),(LL(I),I=1,NTC)
CALL ACOBAN (A(N1+),A(N9),SE,LL,NIC)
C
CALL CLEAR (SE,KS)
RD= RDS(NUMEL)
EG= ELG(NUMEL)
DO 500 KI=1,IPH
FAC1= 2.
FAC2= 2.
IF (KI.EQ.1.CH.KI..2).IPH) FAC2= 1.
PHI= DTA*DFLCAT(KI-1)
AC= AHEAN*DCOS(PHI)
IF (KI.EQ.1PI) AC= 0.
TET= EG/RD
CI= 2./((RD-AC)*TET)
DO 60 I=1,NPE
II= (I-1)*NC
CO 60 J=1,NC
FM= DFLCAT(2*J)
C2= FM*CCOS(FM*PHI)
G(II+J)= -C1*C2*DH(I,1)
60 CONTINUE
IK= 0
DO 480 I=1,NTC
DO 480 J=1,NIC
IK= IK * 1
SE(IK)= SE(IK) * FAC1*FAC2*WGP(1)*J(I)*G(J)
500 CONTINUE
DO 520 I=1,KS
SE(I)= ALPHA*SE(I)
IK= 0
DO 540 I=1,NPE
II= (I-1)*NDF * 6
DO 540 J=1,NC
IK= IK * 1
LL(IK)= LM(II+J,NUMEL)
WRITE (IT2) (SE(I),I=1,KS),(LL(I),I=1,NTC)
CALL ACOBAN (A(N1+),A(N9),SE,LL,NIC)
RETURN
END
C
SUBROUTINE RESIDU (LD,HEL,XY,VSP,VIP,RDS,ELJ,LM,BL,BN,SE,ASIG,

```

```

FEN13760
FEN13770
FEN13780
FEN13790
FEN13800
FEN13810
FEN13820
FEN13830
FEN13840
FEN13850
FEN13860
FEN13870
FEN13880
FEN13890
FEN13900
FEN13910
FEN13920
FEN13930
FEN13940
FEN13950
FEN13960
FEN13970
FEN13980
FEN13990
FEN14000
FEN14010
FEN14020
FEN14030
FEN14040
FEN14050
FEN14060
FEN14070
FEN14080
FEN14090
FEN14100
FEN14110
FEN14120
FEN14130
FEN14140
FEN14150
FEN14160
FEN14170
FEN14180
FEN14190
FEN14200
FEN14210
FEN14220
FEN14230
FEN14240
FEN14250
FEN14260
FEN14270
FEN14280
FEN14290
FEN14300

```

```

1      AEPS, U, UDIS, ADIS, ALOD, SLOD, PLOD, TUP, EFSTN, ISTATE)
C
1      IMPLICIT REAL*(A-F, O-Z)
COMMON/GEN/  NUMNP, JUMEL, NPE, NDF, NDE, NDS, NIPS, IPL, IPP, IPH, IPH
COMMON/MAT/  STRES(6), STRAIN(6), C(6,6), YLD, HPRIME, ISF, ISR
COMMON/PRO/  GEOM(8), PROP(6), EMOD(3,10), FLOD(30), NPAR(6)
COMMON/VAR/  INCS, ITER, IPEL, IKUM, IND, IPT, ICHK
COMMON/MAX/  NMODS, HINCS, MITER, HODEX, INTUP
COMMON/CON/  FIOL, ETOL, TOLFO, TOLFN, CURVY
COMMON/SOL/  NEQ, NEJ, NWK, MK, NES
COMMON/TAPE/ I11, I12, I13, I14, I15, I16, I17, I18
DIMENSION  IC(NDF,1), NUL(NPC,1), XYZ(3,1), VSP(3,1), VTP(3,1), RDS(1),
1          ELG(1), LM(NDE,1), UL(2,NDE), DN(9,NDE), SE(1), ASIG(1),
2          AEPS(1), U(1), UDIS(1), ADIS(1), ALOD(1), SLOD(1),
3          PLOD(1), TUP(1), IPH(1), EFSTN(1), ISTATE(1)
1          DIMENSION  DISP(36), ELOD(36), Q1(6,6), Q2(6,6), OHM(3,3), SIG(6),
1          EQUIVALENCE  EP(5(6)), AA(3), VV(3)
1          (GEOM(1), THICK), (GEOM(2), RA), (PROP(1), YH),
1          (PROP(4), UNIAX)
1          REMIND I12
1          REMIND I13
1          PREPARE FOR CONVERGENCE CHECKS
1          IF (ITER.NE.1) GO TO 40
1          CALL CLEAR (UDIS, NEJ)
1          DO 10 I=1, NEQ
1          SLOD(I)=ALOD(I) - SLJD(I)
1          CALCULATE NORM OF INITIAL LOAD INCREMENT
1          SUM=0
1          DO 20 I=1, NEQ
1          SUM=SUM+SLJD(I)*SLJD(I)
1          TOLFO=DSORT(SUM)
1          CALCULATE INITIAL ENERGY INCREMENT
1          SUM=0
1          DO 30 I=1, NEQ
1          SUM=SUM+U(I)*SLJD(I)
1          TOLEN=SUM
1          ICHK=0
1          GO TO 80
1          CALCULATE FORCE AND ENERGY FOR CONVERGENCE CHECKS
40          UO 50 I=1, NEQ
50          SLOD(I)=ALOD(I) - SLJD(I)
1          SUM=0
60          DO 60 I=1, NEQ
1          SUM=SUM+SLJD(I)*SLJD(I)
1          FORCE=DSORT(SUM)
1          FRATE=FORCE/TOLFO
1          ENERGY=0
70          DO 70 I=1, NEQ
1          ENERGY=ENERGY+U(I)*SLJD(I)
1          ERATE=ENERGY/TOLEN
1          WRITE (I16,2000) I11EN, FRATE, ERAT
1          IF (ERAT.LE.FIOL.AND.ERAT.LE.ETOL) ICHK=999
1          IF (ERAT.GT.1) ICHK=-999
80          UDIS(I)=UDIS(I)+U(I)

```

FEN14310
FEN14320
FEN14330
FEN14340
FEN14350
FEN14360
FEN14370
FEN14380
FEN14390
FEN14400
FEN14410
FEN14420
FEN14430
FEN14440
FEN14450
FEN14460
FEN14470
FEN14480
FEN14490
FEN14500
FEN14510
FEN14520
FEN14530
FEN14540
FEN14550
FEN14560
FEN14570
FEN14580
FEN14590
FEN14600
FEN14610
FEN14620
FEN14630
FEN14640
FEN14650
FEN14660
FEN14670
FEN14680
FEN14690
FEN14700
FEN14710
FEN14720
FEN14730
FEN14740
FEN14750
FEN14760
FEN14770
FEN14780
FEN14790
FEN14800
FEN14810
FEN14820
FEN14830
FEN14840
FEN14850

```

90 ADIS(I) = ADIS(I) + U(I)
C ... DETERMINE LOCATION: OF IUP AND BOTTOM OF PLANE OF SYMMETRY
      LTOP = IPH*IPH
C ... DETERMINE ACCUMULATIVE LOAD FACTOR
      APLOD = 0.
      DO 100 I=1, IINCS
      APLOD = APLOD + FLCJ(I)
      CONTINUE
100 IF (APLOD.LT.1.) CURVY = 1.
C ... CALCULATE THE CRITICAL VALUE: OF BUCKLING STRESS
      SCRIT = -0.32*YM*THICK/RA
      IF (INC.EQ.0) WRITE (I15,201 J) SCRIT
C ... CALCULATION OF STRESSES, STRAINS AND NODAL FORCES (START...)
      CALL CLEAR (SLOD,NE2)
      IPT = 0
      DO 400 N=1, NUMEL
      CALCULATE LOCAL DISPLACEMENTS
      DO 140 M=1, NDE
      M1 = LM(M,N)
      DISP(M) = 0.
      IF (M1.NE.0) DISP(M) = U(M1)
140 CONTINUE
      CALL CLEAR (ELOD,NJE)
      ENTER INTEGRATION LOOP
      DO 360 IR=1,IPL
      ITHIC = (N-1)*IPL + IR
      DO 360 IA=1,IPH
      THIC = IUP(IA,ITHIC)
      ESUM = 0.
      DO 350 IT=1,IPH
      IPT = IPT + 1
      BL = BN + 1, 2, C MF
      CALCULATE INCREMENTAL STRAINS
      CALL EPSLON (BL, BN, DISP, STRAIN, OIM, NDE)
      DO 150 I=1, IST
      SIG(I) = ASIG(I, IPT)
150 DO 160 I=1, ISR
      EPS(I) = AEPS(I, IPT)
160 EPST = EFSTN(IPT)
      IPEL = ISTATE(IPT)
      CALCULATE INCREMENTAL STRESSES
      IF (IBEM) 1, 1, 2
      CALL ELPAL (SIG, EPJ, OIM, EPST)
C ... WRITE NONLINEAR MATERIAL LAW ON TAPE IF YIELDING HAS OCCURRED
      IF (IPEL.GT.1. AND .ICHEK.GI.0) WRITE (IT3) C
      IF (.ICHEK.NE.0. OR .IITER.EQ. IITER) GO TO 170
      GO TO 190
170 DM = (SIG(1) + SIG(2) + SIG(3))/3.
      DX = SIG(1) - DM
      DY = SIG(2) - DM
      DZ = SIG(3) - DM
      DXY = SIG(4)
      DYX = SIG(5)
      DZX = SIG(6)

```

FEN14860
FEN14870
FEN14880
FEN14890
FEN14900
FEN14910
FEN14920
FEN14930
FEN14940
FEN14950
FEN14960
FEN14970
FEN14980
FEN14990
FEN15000
FEN15010
FEN15020
FEN15030
FEN15040
FEN15050
FEN15060
FEN15070
FEN15080
FEN15090
FEN15100
FEN15110
FEN15120
FEN15130
FEN15140
FEN15150
FEN15160
FEN15170
FEN15180
FEN15190
FEN15200
FEN15210
FEN15220
FEN15230
FEN15240
FEN15250
FEN15260
FEN15270
FEN15280
FEN15290
FEN15300
FEN15310
FEN15320
FEN15330
FEN15340
FEN15350
FEN15360
FEN15370
FEN15380
FEN15390
FEN15400

```

190 SBAR= CSQRT(1.5*(DX*DX+DY*DY+DZ*DZ))+3.*(OXY*OXY+OYZ*OYZ+OZX*OZX))
      WRITE (I17,2C20) N,IR,IA,II,IPT,SBAR,EFSI
      ISTATE(IPT)= IPEL
      EFSIN(IPT)= EFSI
      GO TO 200
C     2 CALL UNL0D (SIG,EP3,U,IM)
      200 UPDATE TOTAL STRESSES AND STRAINS
      210 DO 210 I=1, ISI
      210 ASIG(I, IPT)= SIG(I)
      220 DO 220 I=1, ISR
      220 AEPS(I, IPT)= EPS(I)
      230 UPDATE THICKNESS USING AVERAGE STRAIN FROM INTEGRATION POINTS
      230 ETHIC= 0.
      230 DO 230 J=1, ISR
      230 ETHIC= ETHIC + Q1(J,J)*SIRAIN(J)
      230 ESUM= ESUM + ETHIC
      240 CALCULATE ELEMENT NODAL FORCES
      240 DO 240 I=1, NDE
      240 SUM= 0.
      240 DO 240 J=1, ISI
      240 SUM= SUM + BL(J, I)*SIG(J)
      260 ELOD(I)= ELOD(I) + WT*SUM
      260 IF (ICHECK.EQ.0.AND.LITER.NE.MITER) GO TO 300
      DO 270 I=1, 6
      270 SS= 0.
      270 DO 270 J=1, 6
      270 SSI= SS + Q2(J, I)*SIG(J)
      270 STRESS(I)= SSI/UNIAK
      270 WRITE (I16,31) N,IA,II,IPT, (STRESS(K),K=1,6)
      330 FORMAT (I5,5X,3I5,5X,6D15.6)
      330 ... CALCULATE NON-DIMENSIONAL LOCAL STRESSES AT PLANE OF SYMMETRY
      330 ... IF (N.NE.1.OR.IR.NE.1.OR.(I*NE.1.AND.II.NE.IPW)) GO TO 300
      DO 270 I=1, 3
      270 SUM= 0.
      270 DO 265 J=1, ISI
      265 SUM= SUM + Q2(J, I)*SIJ(J)
      270 STRESS(I)= SUM/UNIAK
      330 WRITE (I16,2080) IA, II, (STRESS(I),I=1,3)
      330 ... CALCULATE CURVAIUGS AT PLANE OF SYMMETRY
      330 ... IF (IPT.NE.LBCT.AND.IPT.NE.LTOP) GO TO 300
      280 EPHI= 0.
      280 DO 280 I=1, ISR
      280 EPHI= EPHI + Q1(2,I)*EPS(I)
      330 IF (IPT.LTOP) 3,3,4
      330 ETOP= EPHI
      330 GO TO 300
      330 EBOT= EPHI
      330 CURVA= 0.5*DABS(EBOT-LTOP)/RA
      330 IF (APL0D.EQ.1.) CURVY= CURVA
      330 CURRAI= CURVA/CURVY
      330 WRITE (I16,2C40) CURVY,CURRAI,APL0D
      330 ... CHECK NORMAL STRESSES FOR POSSIBLE BUCKLING IN ELEMENTS 1 AND 2
      330 ... IF (N.GI.2) I=1, 3
      330 ... IF (N.GI.2) I=1, 3
      330 ... SUM= 0.

```

FEN15410
FEN15420
FEN15430
FEN15440
FEN15450
FEN15460
FEN15470
FEN15480
FEN15490
FEN15500
FEN15510
FEN15520
FEN15530
FEN15540
FEN15550
FEN15560
FEN15570
FEN15580
FEN15590
FEN15600
FEN15610
FEN15620
FEN15630
FEN15640
FEN15650
FEN15660
FEN15670
FEN15680
FEN15690
FEN15700
FEN15710
FEN15720
FEN15730
FEN15740
FEN15750
FEN15760
FEN15770
FEN15780
FEN15790
FEN15800
FEN15810
FEN15820
FEN15830
FEN15840
FEN15850
FEN15860
FEN15870
FEN15880
FEN15890
FEN15900
FEN15910
FEN15920
FEN15930
FEN15940
FEN15950

```

310 DO 310 J=1,6
SUM = SUM + C2(J,I)*SIG(J)
IF (SUM.LT.SCRIT) WRITE (IT6,2060) IPT,SUM
320 CONTINUE
350 CONTINUE
EAVG= ESUM/DFLOAT(IP,J)
TUP(IA,ITHIC)= (1. + EAV)*ITHIC
360 CONTINUE
C ... ASSEMBLE ELEMENT NODAL FORCES INTO GLOBAL NODAL FORCE VECTOR
DO 380 I=1,N
J= LM(I,N)
IF (J) = 380,380,37J
370 SLOC(J) = ELOD(I)
380 CONTINUE
400 CONTINUE
C ... CALCULATE NODAL FORCES CORRESPONDING TO PENALTY MATRICES
IF (NDF.GT.6) CALL RESINT (SLOC,PL0D,ELOD,U,DISP,SE,NEQ)
C ... UPDATE NODAL COORDINATES AND NODAL VECTOR COMPONENTS
DO 520 I=1,NUMNP
DO 520 J=1,3
IJ= ID(J,I)
IF (IJ.NE.0) XYZ(J,I)= XYZ(J,I) + Y(IJ)
IJ= ID(J+3,I)
AA(J)= 0.
IF (IJ.NE.0) AA(J)= J(IJ)
CONTINUE
420 PERFORM EULER FORWARD INTEGRATION WITH NEULER INTERVALS
C ...
COM1= CABS(AA(1))
COM2= CABS(AA(2))
COM3= CABS(AA(3))
BIGGY= DMAX1(COM1,COM2,COM3)
NEULER= 1. + 1000.*BIGGY
DO 430 K=1,3
AA(K)= AA(K)/DFLOAT(NEULER)
DO 500 IE=1,NEULER
VV(1)= AA(2)*VSP(3,I) - AA(3)*VSP(2,I)
VV(2)= AA(3)*VSP(1,I) - AA(1)*VSP(3,I)
VV(3)= AA(1)*VSP(2,I) - AA(2)*VSP(1,I)
DO 440 K=1,3
VSP(K,I) = VV(K)
VV(1)= AA(2)*VIP(3,I) - AA(3)*VTP(2,I)
VV(2)= AA(3)*VIP(1,I) - AA(1)*VIP(3,I)
VV(3)= AA(1)*VIP(2,I) - AA(2)*VTP(1,I)
DO 450 K=1,3
VTP(K,I) = VV(K)
H= 1./DSQRT(VSP(1,I)*VSP(1,I)+VSP(2,I)*VSP(2,I)+VSP(3,I)*VSP(3,I))
Z= 1./DSQRT(VIP(1,I)*VIP(1,I)+VIP(2,I)*VIP(2,I)+VIP(3,I)*VIP(3,I))
DO 460 K=1,3
VSP(K,I) = H*VSP(K,I)
VIP(K,I) = Z*VIP(K,I)
460 CONTINUE
500 CONTINUE
520 IF (ICHECK.LT.999.AND.IITER.NE.HITER.AND.IITER.NE.INTUP) GO TO 580
C ... UPDATE ELEMENT RADII OF CURVATURE ASSUMING Z-ROTATIONS
DO 560 N=1,NUMEL

```

FEN15960
FEN15970
FEN15980
FEN15990
FEN16000
FEN16010
FEN16020
FEN16030
FEN16040
FEN16050
FEN16060
FEN16070
FEN16080
FEN16090
FEN16100
FEN16110
FEN16120
FEN16130
FEN16140
FEN16150
FEN16160
FEN16170
FEN16180
FEN16190
FEN16200
FEN16210
FEN16220
FEN16230
FEN16240
FEN16250
FEN16260
FEN16270
FEN16280
FEN16290
FEN16300
FEN16310
FEN16320
FEN16330
FEN16340
FEN16350
FEN16360
FEN16370
FEN16380
FEN16390
FEN16400
FEN16410
FEN16420
FEN16430
FEN16440
FEN16450
FEN16460
FEN16470
FEN16480
FEN16490
FEN16500

```

N1= NEL(1,N)
N2= NEL(NPE,N)
I1= IC(6,N1)
I2= IC(6,N2)
A1= 0.
A2= 0.
IF (I1.NE.0) A1= JDIS(I1)
IF (I2.NE.0) A2= JDIS(I2)
C ... ASSUME ELEMENTS OF CIRCULAR ARC, UNDERGOING CLOSING MOMENTS
TETOLD= ELG(N)/RDS(N)
TETUPC= TETOLD + TABS(A2 - A1)
BDS(N)= ELG(N)/TETUPD
CONTINUE
560 IF (ITER.EQ.INTUP) CALL CLEAR (JDIS,NEQ)
C ... CALCULATE UNBALANCED FORCES FOR NEXT ITERATION
DO 600 I=1,NEQ
600 U(I)= ALOD(I) - SLOD(I)
RETURN
2000 FORMAT (//39H * * CONVERGENCE CHECKS AT ITER =,I4,4H :.5X,
1 8H FBAT =,D10.3,3X,9H ERAT =,D10.3)
2010 FORMAT (//46H ** CRITICAL VALUE OF BUCKLING STRESS =,D15.6)
2020 FORMAT (15,5X,315,5X,15,5X,2015.6)
2040 FORMAT (/53H ** CURVATURE AT PLANE OF SYMMETRY : KY KRAT KRAT,
1 JD15.6)
2060 FORMAT (//52H *** POSSIBLE BUCKLING HAS BEEN DETECTED AT IPT =,
1 15,28H WITH COMPRESSIVE STRESS =,D15.6)
2080 FORMAT (41H >>> LOCAL NORMAL STRESSES AT IA IT =,2I4,2H :,
1 JD15.6)
END
C
C SUBROUTINE RESINT (SLOD,PLOD,ELOD,U,DISP,SE,NEQ)
IMPLICIT REAL*8(A-J,O-Z)
COMMON/GEN/ NUMNP,NUMEL,NPE,NDF,NDE,NDS,NIPS,IPL,IPP,IPH,IPH,IPH
COMMON/PRO/ GEOM(8),PROP(6),EMOD(3,10),FLCD(30),NPAR(6)
COMMON/LOCA/ B,S,I,H,THIC,ZI,FI,CS,SN,BD,EG,IP1,IP2,N,NC,NTC
COMMON/TAPE/ I1,I2,IT3,I4,IT5,IT6,IT7,IT8
DIMENSION SLOD(1),PLOD(1),ELOD(1),U(1),DISP(1),SE(21,1),LL(21)
EQUIVALENCE (NPAR(3),INIEF),(NPAR(4),IFIX)
IF (INIEF.EQ.0.AND.FIX.EQ.0) RETURN
IF (INIEF.EQ.0) GO TO 200
KI= (2*NPE - 1)*HC
KS= KI*(KI + 1)/2
NEM= NUMEL - 1
READ PENALTY STIFFNES: MATRIX AND JOF ADDRESSES FROM TAPE
DO 100 N=1,NEM
READ (IT2),((SE(I,J),J=1,KI),I=1,KI),(LL(I),I=1,KI)
DO 20 I=2,KI
I= I - 1
DO 20 J=1,II
SE(I,J)= SE(J,I)
DO 40 I=1,KI
J= LL(I)
DISP(I)= 0.
IF (J.NE.0) DISP(I)= U(J)

```

FEN16510
FEN16520
FEN16530
FEN16540
FEN16550
FEN16560
FEN16570
FEN16580
FEN16590
FEN16600
FEN16610
FEN16620
FEN16630
FEN16640
FEN16650
FEN16660
FEN16670
FEN16680
FEN16690
FEN16700
FEN16710
FEN16720
FEN16730
FEN16740
FEN16750
FEN16760
FEN16770
FEN16780
FEN16790
FEN16800
FEN16810
FEN16820
FEN16830
FEN16840
FEN16850
FEN16860
FEN16870
FEN16880
FEN16890
FEN16900
FEN16910
FEN16920
FEN16930
FEN16940
FEN16950
FEN16960
FEN16970
FEN16980
FEN16990
FEN17000
FEN17010
FEN17020
FEN17030
FEN17040
FEN17050

```

40 CONTINUE
C ... CALCULATE LOCAL FORCES
DO 80 I=1,KI
SUM= 0.
DO 60 J=1,KI
SUM= SUM + SE(I,J)*DISP(J)
80 ELOC(I)= SUM
DO 120 I=1,KI
J= LL(I)
IF (J) 120,120,100
100 PLOC(J)= PLOC(J) + ELJJ(I)
120 CONTINUE
140 CONTINUE
IF (IFIX.EQ.0) GO TO 400

C 200 KS= NTC*(NTC + 1)/2
DO 340 JFIX=1,2
BEAD (IT2) ((SE(I,J),J=1,NTC),I=1,NTC),(LL(I),I=1,NTC)
DO 220 I=2,NTC
II= I - 1
DO 220 J=1,II
SE(I,J)= SE(J,I)
DO 240 I=1,NTC
J= LL(I)
DISP(I)= 0. DISP(I)= U(J)
IF (J.NE.0)
CONTINUE I=1,NTC
DO 280 I=1,NTC
SUM= 0.
DO 260 J=1,NTC
SUM= SUM + SE(I,J)*DISP(J)
280 ELOC(I)= SUM
DO 320 I=1,NTC
J= LL(I)
320,320,300
IF (J)
PLOC(J)= PLOC(J) + ELJJ(I)
CONTINUE
340 CONTINUE

C 400 DO 420 I=1,NEQ
420 SLOC(I)= SLOC(I) + PLJJ(I)
RETURN
END

C SUBROUTINE SHAPE (ELXY,V5,VI,J1,Q2,BL,BN,DET)
C
C IMPLICIT REAL*8(A-J,O-Z)
COMMON/PRO/ GEOM(8),PROP(6),EMOD(J,10),FLOD(30),NPAR(6)
COMMON/GEN/ NUMNP,NUMEL,NPE,NDF,NDE,NDS,NIPS,IPL,IPP,IPH,IPH
COMMON/LOCA/ R,S,I,TH,THIC,ZT,FI,C5,SN,RU,EG,IP1,IP2,N,NC,NTC
DIMENSION ELXY(3,1),V5(3,1),VI(3,1),Q1(1),Q2(1),BL(1),BN(1)
DIMENSION H(4,2),XJ(3,3),XJI(3,3)
EQUIVALENCE (GEOM(2),H)
I2= H#6

```

FEN17060
FEN17070
FEN17080
FEN17090
FEN17100
FEN17110
FEN17120
FEN17130
FEN17140
FEN17150
FEN17160
FEN17170
FEN17180
FEN17190
FEN17200
FEN17210
FEN17220
FEN17230
FEN17240
FEN17250
FEN17260
FEN17270
FEN17280
FEN17290
FEN17300
FEN17310
FEN17320
FEN17330
FEN17340
FEN17350
FEN17360
FEN17370
FEN17380
FEN17390
FEN17400
FEN17410
FEN17420
FEN17430
FEN17440
FEN17450
FEN17460
FEN17470
FEN17480
FEN17490
FEN17500
FEN17510
FEN17520
FEN17530
FEN17540
FEN17550
FEN17560
FEN17570
FEN17580
FEN17590
FEN17600

```

C ...      R3= R#E2
INTERPOLATION FUNCTIONS
H(1) = 0.0625*( -9.*R3 + 9.*R2 + R - 1.)
H(2) = 0.0625*( -27.*R3 - 9.*R2 - 27.*R + 3.)
H(3) = 0.0625*( -27.*R3 + 9.*R2 + 27.*R + 9.)
H(4) = 0.0625*( 9.*R3 + 9.*R2 - R - 1.)
C ...      THEIR DERIVATIVES W.R.T. K
DH(1,1) = 0.0625*( -27.*R2 + 18.*R + 1.)
DH(2,1) = 0.0625*( -91.*R2 - 18.*R - 27.)
DH(3,1) = 0.0625*( -91.*R2 - 18.*R + 27.)
DH(4,1) = 0.0625*( 27.*R2 + 18.*R - 1.)
DH(1,2) = 0.0625*( -54.*R + 18.)
DH(2,2) = 0.0625*( 162.*R - 18.)
DH(3,2) = 0.0625*( -162.*R - 18.)
DH(4,2) = 0.0625*( 54.*R + 18.)
C ...      JACOBIAN MATRIX AT NODE (R,S,T)
DO 40 I=1,3
DO 40 J=1,3
XJ(I,J) = 0.
GO TO (1,2,3) I
10  DO 10 K=1,NPE
XJ(I,J) = XJ(I,J) + D.I(K,I)*(ELXY(J,K)+RA*(S*VS(J,K)+T*VT(J,K)))
20  DO 20 K=1,NFE
XJ(I,J) = XJ(I,J) + RA*H(K)*VS(J,K)
30  DO 30 K=1,NPE
XJ(I,J) = XJ(I,J) + RA*H(K)*VT(J,K)
40  CONTINUE
C
CALL JACOB (XJ,XJI,DEI,N)
CALL TRANS (XJ,JI,JI2)
CALL BMAT (BL,UN,V3,VI,XJI,d,DH,S,T,THIC,RA,NPE,NDF)
IF (NC.GT.0) CALL BDVL (H,UN,Q2,BL)
RETURN
END
C
SUBROUTINE STIFF (BL,UN,JI,JI2,C,S,SIG,OM,DEL,WI)
C
IMPLICIT REAL*(A-J,2)
COMMON/GEN/ IUMCP,NUMEL,NPE,NDF,NDE,IND,IPT,IPM,IPH
COMMON/VAR/ I11,I12,I13,I14,I15,I16,I17,I18
COMMON/TAPE/ I11,I12,I13,I14,I15,I16,I17,I18
DIMENSION BL(6,6),D(6,6),I1(6,6),I2(6,6),I3(6,6),I4(6,6),I5(6,6),I6(6,6),I7(6,6),I8(6,6),C(6,6),S(1),SIG(1),
EQUVALENCE D(6,6),I1(6,6),I2(6,6),I3(6,6),I4(6,6),I5(6,6),I6(6,6),I7(6,6),I8(6,6),C(6,6),S(1),SIG(1),
FORM LINEAR MATERIAL LAW IN GLOBAL COORDINATES
DO 20 I=1,6
DO 20 J=1,6
CV(I,J) = 0.
DO 20 K=1,6
CY(I,J) = CV(I,J) + C(I,K)*J(K,J)
DO 50 I=1,6
DO 50 J=1,6
SUM = J.

```

FEN17610
FEN17620
FEN17630
FEN17640
FEN17650
FEN17660
FEN17670
FEN17680
FEN17690
FEN17700
FEN17710
FEN17720
FEN17730
FEN17740
FEN17750
FEN17760
FEN17770
FEN17780
FEN17790
FEN17800
FEN17810
FEN17820
FEN17830
FEN17840
FEN17850
FEN17860
FEN17870
FEN17880
FEN17890
FEN17900
FEN17910
FEN17920
FEN17930
FEN17940
FEN17950
FEN17960
FEN17970
FEN17980
FEN17990
FEN18000
FEN18010
FEN18020
FEN18030
FEN18040
FEN18050
FEN18060
FEN18070
FEN18080
FEN18090
FEN18100
FEN18110
FEN18120
FEN18130
FEN18140
FEN18150

```

DO 40 K=1,6
40 SUM=SUM+C1(K,I)*CJ(K,J)
50 D(I,J)=SUM
DO 60 I=2,6
I=I-1
DO 60 J=1,I
D(I,J)=D(J,I)
60 WRITE TRANSFORMATION MATRICES ON TAPE IT2
C ... WRITE (IT2) BL,BH,J1,J2,U,WT
IF (IPEL.EQ.1.OR.ICM.EQ.1) GO TO 80
C ... BETHIEVE *NONLINEAR* MATERIAL LAW FROM TAPE IT3
CALL CLEAR (L,J6)
C ... HEAD (IT3)
CALCULATE LINEAR STIFFNESS CONTRIBUTION
80 DO 110 I=1,6
DO 110 J=1,NCE
DUM=0
DO 100 K=1,6
100 DUM=DUM+C(I,K)*JL(K,J)
110 IF (DABS(DUM).LT.1.0-35) DUM=0.
IF (DUM) DBL(I,J)=DUM
IJ=0
DO 140 I=1,NCE
DO 140 J=1,NCE
DUM=0
DO 120 K=1,6
120 DUM=DUM+BL(K,I)*JDL(K,J)
IJ=IJ+1
140 S(I,J)=S(I,J)+DUM*WT
IF (INC.EQ.0.OR.IRDM.EQ.1) RETURN
C ... FORM STRESS TENSOR
DO 160 I=1,3
160 TAU(I,I)=SIG(I)
TAU(1,2)=SIG(4)
TAU(2,1)=SIG(4)
TAU(2,3)=SIG(5)
TAU(3,2)=SIG(5)
TAU(1,3)=SIG(6)
TAU(3,1)=SIG(6)
CALL CLEAR (SBAR,81)
DO 180 I=1,3
I=(I-1)*3
DO 180 J=1,3
J=(J-1)*3
180 SBAR(I+K,J+K)=TAU(I,J)
C ... CALCULATE NONLINEAR STIFFNESS CONTRIBUTION
DO 200 I=1,9
DO 200 J=1,NCE
DUM=0
DO 190 K=1,9
190 DUM=DUM+SBAR(I,K)*JL(K,J)
200 IF (DABS(DUM).LT.1.0-35) DUM=0.
IF (DUM) DBN(I,J)=DUM

```

FEN18160
FEN18170
FEN18180
FEN18190
FEN18200
FEN18210
FEN18220
FEN18230
FEN18240
FEN18250
FEN18260
FEN18270
FEN18280
FEN18290
FEN18300
FEN18310
FEN18320
FEN18330
FEN18340
FEN18350
FEN18360
FEN18370
FEN18380
FEN18390
FEN18400
FEN18410
FEN18420
FEN18430
FEN18440
FEN18450
FEN18460
FEN18470
FEN18480
FEN18490
FEN18500
FEN18510
FEN18520
FEN18530
FEN18540
FEN18550
FEN18560
FEN18570
FEN18580
FEN18590
FEN18600
FEN18610
FEN18620
FEN18630
FEN18640
FEN18650
FEN18660
FEN18670
FEN18680
FEN18690
FEN18700

```

DO 240 I=1,NOE
DO 240 J=1,NDE
DUM=0.
DC 220 K=1 9
220 DUM = DUM + BK(K,I)*DUH(K,J)
IJ= IJ + 1
240 S(IJ)= S(IJ) + DUM*WT
RETURN
END

C
SUBROUTINE T6ANS (KJ,J1,J2)
C
IMPLICIT REAL*8(A-H,O-Z)
COMMON/LOC/ E,S,I,TH,IHLG,ZI,FI,CS,SN,RD,EG,IPI,IP2,N,NC,NTC
DIMENSION XJ(3,1),U1(6,1),E2(3),E1(3),EJ(3)
CALCULATE ORTHOGONAL VECTORS AT INTEGRATION POINT (H,S,I)
DUMS= 1./DSQRT(XJ(2,1)*XJ(2,2)+XJ(3,2)*XJ(3,3))
DUMT= 1./DSQRT(XJ(3,1)*XJ(3,2)+XJ(3,2)*XJ(3,3))
DO 20 I=1,3
E2(I) = XJ(2,I)*DUMS
E1(I) = XJ(3,I)*DUMT
CALL VEX (E2,E3,E1)
DO 30 I=1,3
Y1(I,1) = E1(I)
Y1(I,2) = E2(I)
Y1(I,3) = E3(I)
DO 30 J=1,3
Y1(I,J+3) = 0.
Y1(5,4) = -SN
Y1(6,4) = 1-CS
Y1(4,5) = 1-CS
Y1(5,6) = CS
Y1(6,5) = SN
DO 40 J=1,3
DO 40 K=1,3
Y1(I,J+3) = Y1(I,K+3,J+3)
DO 60 I=1,3
E1(I) = Y1(I,4)
E2(I) = Y1(I,5)
E3(I) = Y1(I,6)
C ...
ELEMENTS OF MATRIX Q FOR EPSBAR = Q*EPS
Y1(1,1) = E1(1)*E1(1)
Y1(2,1) = E2(1)*E2(1)
Y1(3,1) = E3(1)*E3(1)
Y1(4,1) = 2.*E1(1)*E2(1)
Y1(5,1) = 2.*E1(1)*E3(1)
Y1(6,1) = 2.*E2(1)*E3(1)
C
Y1(1,2) = E1(2)*E1(2)
Y1(2,2) = E2(2)*E2(2)
Y1(3,2) = E3(2)*E3(2)
Y1(4,2) = 2.*E1(2)*E2(2)
Y1(5,2) = 2.*E1(2)*E3(2)

```

FEN18710
FEN18720
FEN18730
FEN18740
FEN18750
FEN18760
FEN18770
FEN18780
FEN18790
FEN18800
FEN18810
FEN18820
FEN18830
FEN18840
FEN18850
FEN18860
FEN18870
FEN18880
FEN18890
FEN18900
FEN18910
FEN18920
FEN18930
FEN18940
FEN18950
FEN18960
FEN18970
FEN18980
FEN18990
FEN19000
FEN19010
FEN19020
FEN19030
FEN19040
FEN19050
FEN19060
FEN19070
FEN19080
FEN19090
FEN19100
FEN19110
FEN19120
FEN19130
FEN19140
FEN19150
FEN19160
FEN19170
FEN19180
FEN19190
FEN19200
FEN19210
FEN19220
FEN19230
FEN19240
FEN19250

```

C
U1(6,2) = 2.*E3(2)*E1(2)
U1(1,3) = E1(3)*E1(J)
U1(2,3) = E2(3)*E2(J)
U1(3,3) = E3(3)*E3(J)
U1(4,3) = 2.*E1(3)*E2(J)
U1(5,3) = 2.*E2(3)*E3(J)
U1(6,3) = 2.*E3(3)*E1(J)

C
U1(1,4) = E1(1)*E1(2)
U1(2,4) = E2(1)*E2(2)
U1(3,4) = E3(1)*E3(2)
U1(4,4) = E1(1)*E2(2)
U1(5,4) = E2(1)*E3(2)
U1(6,4) = E3(1)*E1(2)

C
U1(1,5) = E1(2)*E1(3)
U1(2,5) = E2(2)*E2(3)
U1(3,5) = E3(2)*E3(3)
U1(4,5) = E1(2)*E2(3)
U1(5,5) = E2(2)*E3(3)
U1(6,5) = E3(2)*E1(3)

C
U1(1,6) = E1(3)*E1(1)
U1(2,6) = E2(3)*E2(1)
U1(3,6) = E3(3)*E3(1)
U1(4,6) = E1(3)*E2(1)
U1(5,6) = E2(3)*E3(1)
U1(6,6) = E3(3)*E1(1)

ELEMENTS OF MATRIX U FOR EPS = U*EPSBAR
U2(1,1) = E1(1)*E1(1)
U2(2,1) = E1(2)*E1(2)
U2(3,1) = E1(3)*E1(3)
U2(4,1) = 2.*E1(1)*E1(2)
U2(5,1) = 2.*E1(2)*E1(3)
U2(6,1) = 2.*E1(3)*E1(1)

C
U2(1,2) = E2(1)*E2(1)
U2(2,2) = E2(2)*E2(2)
U2(3,2) = E2(3)*E2(3)
U2(4,2) = 2.*E2(1)*E2(2)
U2(5,2) = 2.*E2(2)*E2(3)
U2(6,2) = 2.*E2(3)*E2(1)

C
U2(1,3) = E3(1)*E3(1)
U2(2,3) = E3(2)*E3(2)
U2(3,3) = E3(3)*E3(3)
U2(4,3) = 2.*E3(1)*E3(2)
U2(5,3) = 2.*E3(2)*E3(3)
U2(6,3) = 2.*E3(3)*E3(1)

C
U2(1,4) = E1(1)*E2(1)
U2(2,4) = E1(2)*E2(2)
U2(3,4) = E1(3)*E2(3)
U2(4,4) = E1(1)*E2(2)
U2(5,4) = E1(2)*E2(3)
U2(6,4) = E1(3)*E2(1)

```

FEN19260
FEN19270
FEN19280
FEN19290
FEN19300
FEN19310
FEN19320
FEN19330
FEN19340
FEN19350
FEN19360
FEN19370
FEN19380
FEN19390
FEN19400
FEN19410
FEN19420
FEN19430
FEN19440
FEN19450
FEN19460
FEN19470
FEN19480
FEN19490
FEN19500
FEN19510
FEN19520
FEN19530
FEN19540
FEN19550
FEN19560
FEN19570
FEN19580
FEN19590
FEN19600
FEN19610
FEN19620
FEN19630
FEN19640
FEN19650
FEN19660
FEN19670
FEN19680
FEN19690
FEN19700
FEN19710
FEN19720
FEN19730
FEN19740
FEN19750
FEN19760
FEN19770
FEN19780
FEN19790
FEN19800

```

C
Q2(5,4) = E1(2)*E2(J) + E2(2)*E1(3)
Q2(6,4) = E1(3)*E2(1) + E2(3)*E1(1)

J2(1,3) = E2(1)*E3(1)
J2(2,3) = E2(2)*E3(2)
J2(3,3) = E2(3)*E3(3)
J2(4,3) = E2(1)*E3(2) + E3(1)*E2(2)
J2(5,3) = E2(2)*E3(3) + E3(2)*E2(3)
J2(6,3) = E2(3)*E3(1) + E3(3)*E2(1)

C
J2(1,6) = E3(1)*E1(1)
J2(2,6) = E3(2)*E1(2)
J2(3,6) = E3(3)*E1(3)
J2(4,6) = E3(1)*E1(2) + E1(1)*E3(2)
J2(5,6) = E3(2)*E1(3) + E1(2)*E3(3)
J2(6,6) = E3(3)*E1(1) + E1(3)*E3(1)
DO 80 I=1,6
DO 80 J=1,6
IF (DABS(Q2(I,J)).LT.1.D-35) Q1(I,J) = 0.
IF (DABS(Q2(I,J)).LT.1.D-35) Q2(I,J) = 0.
80 CONTINUE
END
RETURN

C
SUBROUTINE LNLOD (SIG, EPS, OHM)
C
IMPLICIT REAL*8(A-H,O-Z)
COMMON/MAT/ STRESS(6), STRAIN(6), C(6,6), YLD, HPRIME, IST, ISR
DIMENSION SIG(1), EPS(1), OHM(3,1), RS(3,6), RN(3,6)
NEULER = 10
DO 20 I=1,3
DO 20 J=1,3
OHM(I,J) = OHM(I,J)/DFLOAT(NEULER)
C ... MAKE CORRECTIONS FOR STRESSES AND STRAINS DUE TO R.B. ROTATIONS
40 DO 40 I=1,3
RS(I,I) = SIG(I)
RN(I,I) = EPS(I)
RS(1,2) = SIG(4)
RS(2,3) = SIG(5)
RN(1,2) = 0.5*EPS(4)
RN(2,3) = 0.5*EPS(5)
RN(1,3) = 0.5*EPS(6)
DO 60 I=2,3
I1 = I-1
DO 60 J=1, I1
RS(I,J) = RS(J,I)
RN(I,J) = RN(J,I)
60 START PERFORMING EULER FORWARD INTEGRATION WITH NEULER INTERVALS
80 DO 80 I=1,3
RS(I,J+3) = RS(I,J)
RN(I,J+3) = RN(I,J)
DO 100 I=1,3

```

FEN19810
FEN19820
FEN19830
FEN19840
FEN19850
FEN19860
FEN19870
FEN19880
FEN19890
FEN19900
FEN19910
FEN19920
FEN19930
FEN19940
FEN19950
FEN19960
FEN19970
FEN19980
FEN19990
FEN20000
FEN20010
FEN20020
FEN20030
FEN20040
FEN20050
FEN20060
FEN20070
FEN20080
FEN20090
FEN20100
FEN20110
FEN20120
FEN20130
FEN20140
FEN20150
FEN20160
FEN20170
FEN20180
FEN20190
FEN20200
FEN20210
FEN20220
FEN20230
FEN20240
FEN20250
FEN20260
FEN20270
FEN20280
FEN20290
FEN20300
FEN20310
FEN20320
FEN20330
FEN20340
FEN20350

```

DO 100 J=1,3
DC 100 K=1,3
RS(I,J+3)=RS(I,J+3) + HJ(I,K)*OHM(K,J) - OHM(I,K)*RN(K,J)
RN(I,J+3)=RN(I,J+3) + RN(I,K)*OHM(K,J) - OHM(I,K)*RN(K,J)
100 DO 110 I=1,3
DO 110 J=1,3
RS(I,J)=RS(I,J+3)
RN(I,J)=RN(I,J+3)
110 CONTINUE
DO 140 I=1,3
SIG(I)=RS(I,1)
EPS(I)=RN(I,1)
SIG(4)=RS(1,2)
SIG(5)=RS(2,3)
SIG(6)=RS(1,3)
EPS(4)=2.*RN(1,2)
EPS(5)=2.*RN(2,3)
EPS(6)=2.*RN(1,3)
C ... CALCULATE TOTAL STRESSES, ASSUMING PURELY ELASTIC BEHAVIOUR
DO 180 IS=1,1ST
DELSIG=0.
DO 160 IR=1,ISR
DELSIG=DELSIG + C(IS,IR)*STRAIN(IR)
160 SIG(IS)=DELSIG + DELSIG
180 DO 200 IR=1,ISR
EPS(IR)=EPS(IR) + STRAIN(IR)
200 RETURN
END
C SUBROUTINE VEX (W1,W2,W3)
C IMPLICIT REAL*8(A-H,O-Z)
DIMENSION W1(1),W2(1),W3(1)
GENERATE A UNIT VECTOR ORTHOGONAL TO TWO GIVEN VECTORS
WJ(1)=W1(2)*W2(3) - W1(3)*W2(2)
WJ(2)=W1(3)*W2(1) - W1(1)*W2(3)
WJ(3)=W1(1)*W2(2) - W1(2)*W2(1)
WH=1./SQRT(WJ(1)*WJ(1)+WJ(2)*WJ(2)+WJ(3)*WJ(3))
DO 30 I=1,3
WJ(I)=WJ(I)*WH
30 RETURN
END
C$DATA
PROBLEM : SIMULATION OF PIPE BENDING
31 7 4 5 12 31 28 2 9 25 0 1
0.48D+00 12.24D+00 1.0D+31 1.20D+02
30.0D+06 0.28D+00 1.2D+00 16.0D+03
1 1 0.12D+02
2 2 0.12D+02
3 3 0.12D+02
4 4 0.12D+02
5 5 0.12D+02
6 6 0.12D+02
7 7 0.12D+02

```

FEN20360
FEN20370
FEN20380
FEN20390
FEN20400
FEN20410
FEN20420
FEN20430
FEN20440
FEN20450
FEN20460
FEN20470
FEN20480
FEN20490
FEN20500
FEN20510
FEN20520
FEN20530
FEN20540
FEN20550
FEN20560
FEN20570
FEN20580
FEN20590
FEN20600
FEN20610
FEN20620
FEN20630
FEN20640
FEN20650
FEN20660
FEN20670
FEN20680
FEN20690
FEN20700
FEN20710
FEN20720
FEN20730
FEN20740
FEN20750
FEN20760
FEN20770
FEN20780
FEN20790
FEN20800
FEN20810
FEN20820
FEN20830
FEN20840
FEN20850
FEN20860
FEN20870
FEN20880
FEN20890
FEN20900

FILE: FENSA FORIBAN # UNIV. D'OF OTIAMA CMS RELEASE: 4

20	6	317802-220+00
21	6	317802-220+00
22	6	317802-220+00
23	6	317802-220+00
24	6	317802-220+00
25	6	317802-220+00
26	6	317802-220+00
27	5	317802-220+00
28	6	317802-220+00
29	6	317802-220+00
30	6	317802-270+00
31	6	158901-110+00

FEN21460
FEN21470
FEN21480
FEN21490
FEN21500
FEN21510
FEN21520
FEN21530
FEN21540
FEN21550
FEN21560
FEN21570

Appendix D

ADINA Shell-Element Results

In this Appendix, cross-section ovalization of a pipe bent by a ram bender will be calculated using an ADINA shell element, and the results obtained will be compared to those by FENSA as were presented in Chapter 5.

Taking into account the symmetry of the pipe (Figure 5.2), only a quarter of it needs to be considered. This portion is modelled by a mesh of 48 unequal-sized 9-noded shell elements and a total of 221 nodal points, Figure D.1. However, all elements each span 15° in the circumferential direction of the cross section. The dimensions of the pipe and the size of the ram used are those shown in Figure 5.6. To simulate the ram force exerting on the pipe wall, a concentrated load is applied to each nodal point that happens to be in the area of contact between the ram and the pipe wall. The ratios of the magnitudes of these concentrated loads are the same as those of the vertical distances from the corresponding nodes to the horizontal plane (zx -plane). The Gaussian integration scheme employed is $3 \times 3 \times 2$ (r - s - t), and a total of 1011 equilibrium equations are solved in the numerical solution.

Figure D-2 shows the ovalization results obtained for the cross section in the plane of symmetry. A number of important observations have been made from this figure.

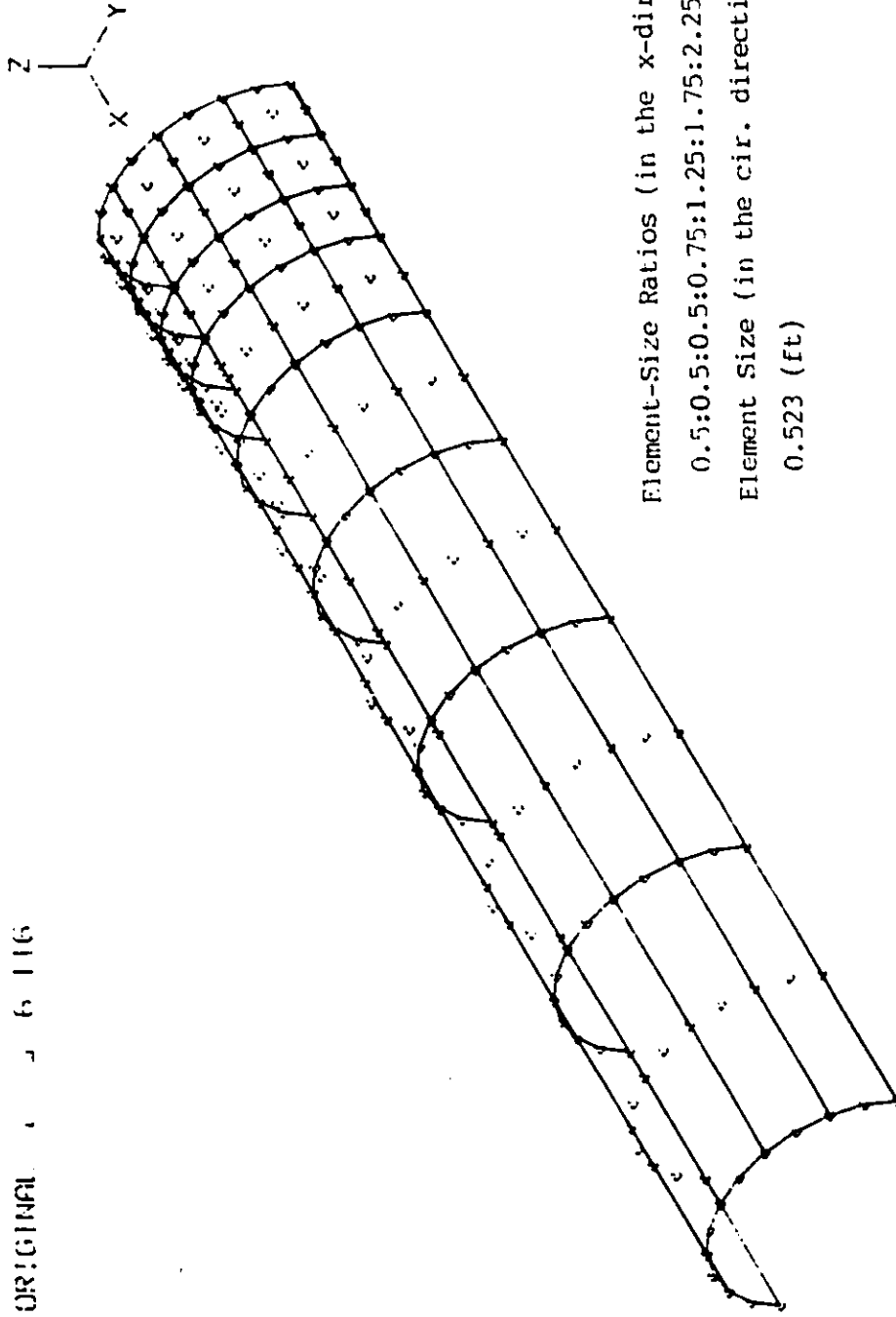
- The fact that the curves representing expansion and contraction are almost

straight lines supports the assumption made earlier that ovalization increases linearly with the applied load (even beyond the yielding point).

- At the plane of symmetry, the cross-sectional expansion is smaller than the corresponding contraction. The shell prediction is attributed to the local deformation of the pipe wall at the ram. Thus the prediction by no means contradicts the fact that the expansion is larger than the contraction in most pipe bending problems with no local deformations.
- At $W/W_y = 1.5$, the maximum change (contraction) in the mean diameter of the cross section (measured by $\Delta r/r_m$) is observed to be about 1%. This value is of the order of 200 times that given by FENSA using the elbow element (Figure 5.7). The prediction also implies that local cross-sectional deformation at the ram might be much larger than that predicted by the elbow element although the magnitude of the shell prediction may vary somewhat, depending on how the ram force exerting on the pipe wall is modelled.

Thus, as far as local deformation and cross-section ovalization are concerned, details of the pipe can be obtained using a shell-element approach.

ORIGINAL . . . 6 116



Element-Size Ratios (in the x-direction)
0.5:0.5:0.5:0.75:1.25:1.75:2.25:2.50 (ft)
Element Size (in the cir. direction)
0.523 (ft)

Fig. D-1 Undeformed mesh of 9-noded shell elements generated by ADINA.

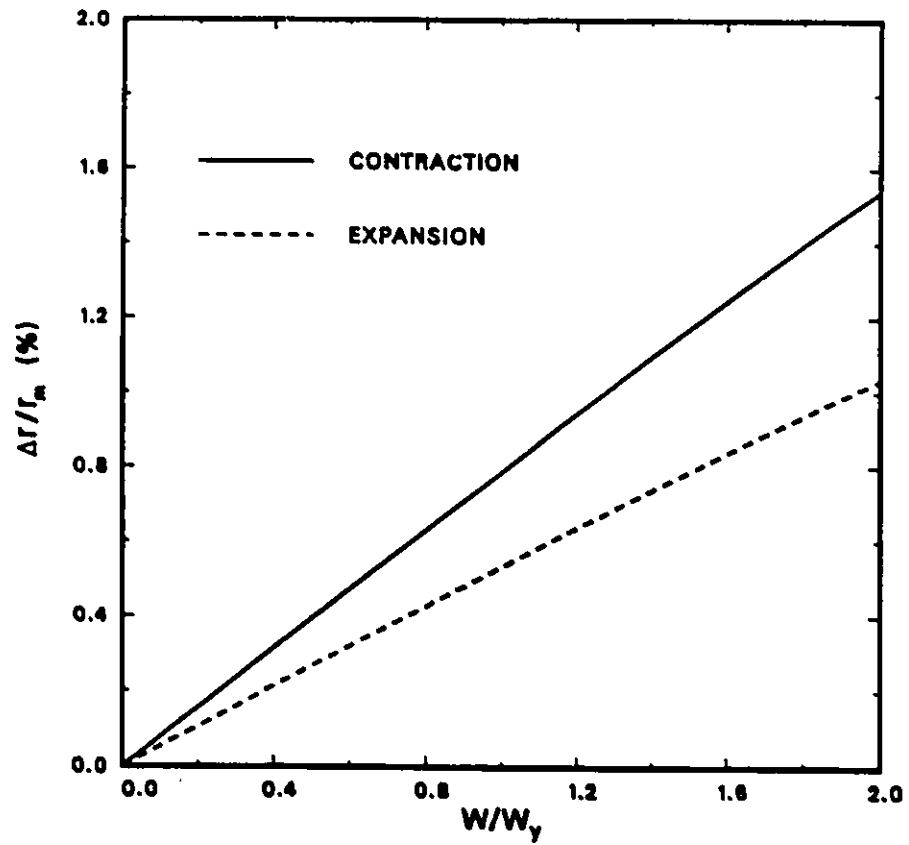


FIG. D-2 MAXIMUM CHANGES IN CROSS-SECTIONAL MEAN RADIUS PREDICTED BY ADINA.